EXPERIMENTAL AND NUMERICAL ANALYSIS OF PEM FUEL CELL PERFORMANCE USING BIO-INSPIRED FLOW FIELDS

A Thesis Submitted in partial fulfillment of the requirements for the award of the Degree of

DOCTOR OF PHILOSOPHY

in

MECHANICAL ENGINEERING

by

Srinivasa Reddy Badduri
(Roll No.: 714129)

Supervisor

Dr. G. Naga Srinivasulu
(Associate Professor)

Co-Supervisor

Dr. S. Srinivasa Rao
(Professor)

DEPARTEMENT OF MECHANICAL ENGINEERING
NATIONAL INSTITUTE OF TECHNOLOGY,
WARANGAL (TS), INDIA 506004
MARCH 2020

NATIONAL INSTITUTE OF TECHNOLOGY
WARANGAL (T.S) INDIA 506 004

CERTIFICATE

This is to certify that the dissertation work entitled **EXPERIMENTAL AND NUMERICAL ANALYSIS OF PEM FUEL CELL PERFORMANCE USING BIO-INSPIRED FLOW FIELDS**, which is being submitted by **Mr. Srinivasa Reddy Badduri**(Roll No. 714129), is a bonafide work submitted to the Department of Mechanical Engineering, National Institute of Technology, Warangal in partial fulfillment of the requirement for the award of the degree of **Doctor of Philosophy in Mechanical Engineering.**

To the best of our knowledge, the work incorporated in this thesis has not been submitted elsewhere for the award of any degree.

Dr. G. Naga Srinivasulu
Supervisor
Department of Mechanical Engineering
National Institute of Technology
Warangal-506004

Prof. S. Srinivasa Rao
Co-Supervisor
Department of Mechanical Engineering
National Institute of Technology
Warangal-506004

Prof. A. Kumar
Head,
Department of Mechanical Engineering
National Institute of Technology
Warangal-506004

Dedicated

to

- **My beloved grandparents, parents &All my family members**

- **All my Teachers and Professors who taught and encouraged me with positive thoughts.**

THESIS APPROVAL FOR Ph.D

This Thesis entitled "**EXPERIMENTAL AND NUMERICAL ANALYSIS OF PEM FUEL CELL PERFORMANCE USING BIO-INSPIRED FLOW FIELDS"** by **Srinivasa Reddy Badduri** is approved for the Degree of Doctor of Philosophy.

Examiners

_____

_____

_____

Supervisor(s)

Dr. G. Naga Srinivasulu
(Supervisor)
Associate Professor, Mechanical Engineering Department, NIT Warangal

Dr. S Srinivasa Rao
(Co-Supervisor)
Professor, Mechanical Engineering Department, NIT Warangal

Chairman

Prof. A. Kumar

Head, Mechanical Engineering Department, NIT Warangal

NATIONAL INSTITUTE OF TECHNOLOGY

WARANGAL (T.S) INDIA 506 004

DECLARATION

This is to certify that the work presented in the thesis entitled **"EXPERIMENTAL AND NUMERICAL ANALYSIS OF PEM FUEL CELL PERFORMANCE USING BIO-INSPIRED FLOW FIELDS"**is a bonafide work done by me under the supervision of **Dr. G. Naga Srinivasulu and Dr. S. Srinivasa Rao**, and was not submitted elsewhere for the award of any degree. I declare that this written submission represents my ideas in my own words and where others' ideas or words have been included, I adequately cited and referenced the original sources. I also declare that I have adhered to all principles of academic honesty and integrity and have not misrepresented or fabricated or falsified any idea / data / fact / source in my submission. I understand that any violation of the above will be a cause for disciplinary action by the Institute and can also evoke penal action from the sources which have thus not been properly cited or from whom proper permission has not been taken when needed.

(Srinivasa Reddy Badduri)

Research Scholar,
Roll No.714129

Date:
Place: Warangal

ACKNOWLEDGEMENTS

I would like to express my sincere gratitude and it gives me an immense pleasure to acknowledge the people who were the part of this research work in plenty ways. It would not have been possible without close association with many people. I take this opportunity to extend my sincere gratitude and appreciation to all those who made this research work possible. First and foremost, I would like to express my sincere gratitude to my research supervisors Dr. G. Naga Srinivasulu for his continuous guidance, advice, inspiration, encouragement and continuous support, throughout my research work. His enthusiasm, integral view on research and mission for providing high-quality work, has made a deep impression on me. I indebted to him for his persistence in moulding me as a researcher with his methodical supervision that enabled me to complete the research work in the present form. I will never forget his association and encouragement and whole hearted support during my entire tenure of research. During our course of interaction, I have learnt many things, like how to explore new possibilities and how to approach a problem by systematic thinking. I owe him with lots of gratitude for showing me this way of research.

I would like to express special words of thanks to my research co-supervisor Prof. S Srinivasa Rao for his continuous support, guidance, cooperation, encouragement and for facilitating all the requirements, going out of his way. He taught me another aspect of life, that, "goodness can never be defied and good human beings can never be denied". His constant motivation and support have always kept me going ahead. I owe a lot of gratitude to him for always being there for me in spite of his busy schedule and I feel privileged to be associated with him.

I am grateful to Prof. N.V. Ramana Rao, Director-NIT Warangal who has been constant source of inspiration for me. I thank Prof. R. Narasimha Rao, Head of the Department of Mechanical Engineering for providing the necessary facilities to carry out the research. I would like to express my sincere thanks to Prof. Amba Prasad Rao, Dr. V. R. K. Raju, Dr. Karthik Balasubramanian and Dr. P. V. Suresh (Chemical Engineering Department), learned members of my Doctoral Scrutiny Committee for being helpful and generous during the entire course of this work.

I am always grateful to my institute NITW, where I learn many things along with the research. I express my heart-felt gratitude to Dr. M Raja Vishwanathan, Humanities & Social Science Department and other faculty members of the institute during the stay. They are very kind enough to extend their help at various phases of this research, whenever I approached them, and I do hereby acknowledge all of them.

My heartfelt thanks to fellow-scholars for their consistent help, moral support and encouragement. My special thanks to Venkateswarlu Velisala, Sheikh Abdulla, G Venkatesh, M Kameswara Reddy, K V Koteswara Rao, Murali Krishna Boni, Ganesh R Gawale, Satish M, Ramesh M, T N Suri, P Pratap Naidu, B Rama Krishna, N Siva Prasad, Chandra Sekhar Reddy, D Naresh Yadav, Chirra Suman and many others for always standing by my side and sharing a great relationship as compassionate friends. I will always cherish the warmth shown by them.

In this auspicious moment, I owe my deepest regards to my family members and well-wishers for their eternal support and understanding of my goals and aspirations. My heartfelt regards goes to my parents, Sri Venkata Reddy and Smt. Venkayamma. My special regards to my brother Mr. Brahmananda Reddy, sisters Smt. Venkata Ramana and Santha Kumari, and brother-in-laws Sri Hanimi Reddy and Rami Reddy. My special thanks to my well-wishers Smt D Sridevi, Assistant Professor, VR siddartha engineering college, Smt M. Sailaja Madhuri, and many other friends for their patience and understanding during the entire period of the research work. I also must thank all my hostel mates for making my stay at NIT Warangal become more memorable.

As always it is impossible to mention everybody who had an impact to this work, however, there are those whose spiritual support is even more important. I feel a deep sense of gratitude to each and every one who directly or indirectly extended their support to fulfill my research. Finally, I am thankful to library staff and administrative staff of NITW for their cooperation.

NIT Warangal (**Srinivasa Reddy Badduri**)

March 2020

ABSTRACT

Fuel cell is an electro-chemical energy conversion system, which converts chemical energy of fuel directly into electrical energy. The ever-increasing demand for energy, non-polluting energy generation, and other environmental issues have persuaded many researchers to look for new efficient energy conversion technologies. Proton exchange membrane fuel cells (PEMFC) have many unique features compared with other types of fuel cell, such as relatively low operating temperature (around 80 ^{o}C), high power density, quick start, rapid response, and high modularity. This makes PEM fuel cell as most promising system for automotive sector, distributed power generation sector and in portable electronic devices.

In this study, a three-dimensional fuel cell model was developed using ANSYS FLUENT-15.0 to study the effect of serpentine flow channel with different rib thickness and channel width on the performance of PEMFC under 100% humidity. Further, the influence of operating temperature and flow rates on the performance of fuel cell fitted with different rib thickness configurations are analyzed. From the results it is observed that fuel cell performance enhanced with increase in operating temperature from 313 K to 343 K while the performance deteriorated beyond 343 K. The fuel cell with 0.5 mm rib thickness gives the best performance in comparison with 1 mm, 1.5 mm and 2 mm, when operated with high flow rates. The fuel cell with 1 mm rib thickness gives the best performance when parasitic losses are considered. Further, examined the influence of operating pressure on the performance of fuel cell fitted with different channel width configurations. The fuel cell with 1 mm channel width gives the best performance when parasitic losses are considered. The simulation results of serpentine flow field with optimum design parameters was compared with experimental results and it is observed that the results were in good agreement.

Experimental study was carried out to analyse the performance of PEMFC with four different flow field configurations on cathode side, viz., single serpentine flow channel, Lung channel, bio-channel and leaf channel designs, under different operating conditions. In this study the influence of operating parameters such as operating temperature, relative humidity (RH) of the reactants, flow rates in terms of stoichiometric ratios, operating pressure and back pressures on the performance of the fuel cell fitted with different channel designs were analyzed. From the results it is observed that fuel cell performance enhanced, when the operating temperature increases from 40 ^{o}C to 70 ^{o}C. The fuel cell power output is maximum at 70 ^{o}C. However, the performance of the cell deteriorated beyond 70^{o}C operating temperature. Relative Humidity (RH) had considerable influence on the cell performance. Greater values of RH caused

greater power output of the fuel cell. The performance of the fuel cell enhanced as the stoichiometric ratio was increased from λ_c=1 to λ_c=3; any further increase of stoichiometric ratio gives the same performance or slightly decreased performance. With the increase in cell operating pressure, the cell performance improved. Back pressure had a positive effect on fuel cell performance, i.e., PEMFC performance enhanced with increase in back pressure. The above parameters are investigated with respect to each flow channel design fitted on cathode side of the fuel cell and observed that the fuel cell with leaf channel design performed better among four channel designs.

Further, experimental study was carried out to analyse the performance of PEMFC with four different design modifications of a leaf channel, viz., non-interdigitated leaf channel design (NILCD), interdigitated leaf channel design (ILCD), interdigitated leaf channel design with curved edges (ILCDWCE) and Murray's design, under optimum operating conditions. It is observed from the results that the fuel cell with ILCD is 7.01 % more efficient than the fuel cell with NILCD. Similarly, the fuel cell with ILCDWCE is 15.7 % more efficient than the PEMFC with the NILCD and the fuel cell with the Murray's design is 19.29 % more efficient than the fuel cell with NILCD. Thus, the fuel cell with Murray's design channel gave the best performance compared with other designs.

In general, the graphite bipolar plates are used for the supply of reactants to the reaction area. In the present work besides the graphite plates, an attempt is made to study the performance of PEMFC with titanium (Ti) metal bipolar plate of Murray's design with different coatings, viz., graphite, graphene oxide and graphene. This plate acts as both flow field and current collector. From the results it is observed that the PEMFC with graphite coated Ti bipolar plate generated 5.17 % more power density compared to non-coated Ti bipolar plate. The performance of PEMFC with graphene oxide coated Ti bipolar plate generated 12.06 % more power density when compared with non-coated Ti bipolar plate. The performance of PEMFC with reduced graphene oxide (graphene) coated Ti bipolar plate generated 18.96 % more power density when compared with non-coated Ti bipolar plate. Thus, the Fuel cell with graphene coated metal (Ti) bipolar plate of Murray's design gave the best performance among three coatings.

CONTENTS

List of Figures

List of tables

Nomenclature

V_{cell}	Cell output voltage
E_r	Reversible cell voltage
η_{act}	Activation losses
η_{ohmic}	Ohmic losses
η_{conc}	Concentration losses
T	Fuel cell operating temperature
R	Universal gas constant
α	Transfer constant
n	Number of electrons participated in the reaction
F	Faraday's constant
i	Cell current density
i_0	Exchange current density
R_{ohmic}	Resistivity of membrane
λ_{mem}	Membrane water content
t_{mem}	Thickness of the membrane
σ_{mem}	Conductivity of the membrane
σ_{mem}	Membrane conductivity
P_{sat}	water saturation pressure
P_{O_2}	Partial pressure of oxygen
T_{fc}	cell temperature
S_m	Species source term
$\vec{v}$	Fluid velocity vector
ρ	Density
μ	Viscosity
p	pressure
k	Permeability of CL and GDL
E	Total energy

k_{eff}	Effective conductivity
$\vec{J}_i$	Flux diffusion for the species
y_i	Mass fraction of each species
D_i	Diffusion coefficient
σ	Ionic conductivity
ϕ	cell voltage (V)
R_{mem}	Transfer current in the membrane
γ	Concentration coefficient
r_w	Condensation rate
W_p	Parasitic losses
ΔP	Pressure drop
$\mathbf{W_g}$	**G**ross power density
W_{net}	Net power density

Abbreviations

PEMFC	Proton Exchange Membrane Fuel Cell
PEM	Proton Exchange Membrane
FC	Fuel Cell
MEA	Membrane electrode assembly
CL	Catalyst Layer
GDL	Gas Diffusion Layer
CFD	computational Fluid Dynamic
FFP	Flow Field Plate
SSFCD	single serpentine flow channel design
NILCD	Non-Interdigitated leaf channel design
ILCD	Interdigitated Leaf Channel Design
ILCDWCE	Interdigitated Leaf Channel Design with Curved Edges
WFTS	Workflow based File Tracking System
FCTS	Fuel cell Test Station

Chapter-1
Introduction

1.1 Introduction

The international energy outlook in 2018 (IEO 2018) estimated that the global energy consumption may increase around 35% by 2040 from its present utilization of 89 million barrels in a day. It is predicted that 70 % of this increase may come from developing nations, led by India and China. The current energy demand of the world is largely met by conventional fuel sources. However, the uses of fossil fuel pose unsolicited side effects such as emission of toxic and greenhouse gases to the environment. Moreover, the existing world energy situation reveals that within a few decades, the world would face severe shortage of conventional fuel resources. Therefore, the scientists and the technologists are in search of non-conventional energy sources and the efficient energy conversion devices because of the possible shortage in the availability of the conventional fuels. There are various non-conventional energy sources and a lot of research work has been carried out throughout the world to make the technologies economically feasible. Consequently, it is observed that fuel cell is one of the most capable power conversion devices in the near future[1].

Fuel cell is an electro chemical device which can transform chemical energy of supplied fuel into electrical energy. The ever increase in energy demand, pollution-free energy generation, and other environmental issues have persuaded many researchers to look for new efficient energy conversion technologies [2]. With that perception, fuel cell systems may be measured as the best alternative because of the practical advantages like quick startup, low harm to the environment, good dynamic response, high efficiency, high power density, low emissions, light weight and low noise. Depending on the type of electrolyte material used, fuel cells are categorized as alkaline fuel cells, polymer exchange membrane fuel cells or Proton exchange membrane fuel cells (PEMFCs), phosphoric acid fuel cells, molten carbonate fuel cells, direct methanol fuel cell and solid oxide fuel cells [3]. Table 1 represents the classification of most common type of fuel cells along with their operating temperature ranges and other details. Among different kinds of fuel cells available, proton exchange membrane (PEM) fuel cell among the available different kind of cells possesses unique features such as relatively low operating temperature (around 80^{o}C), high power density, quick start, rapid response, and high modularity which makes it the best promising

system for generating power in the applications like automotive sector, distributed power generation an portable electronic devices [3,4]. However, PEMFCs must overcome various challenges related to performance, cost and durability, before they can be used as commercial feasible alternatives for transportation [5–8] and portable applications.

Fuel cell type	**PEMFC**	**DMFC**	**HT-PEMFC**	**AFC**	**PAFC**	**MCFC**	**SOFC**
Operating temperature (^oC)	40-80	25-80	100-200	60-220	170-220	600-650	600-1000
Fuel	H_2	CH_3OH	H_2	H_2	H_2	H_2 and CH_4	H_2, CH_4 and CO
Catalyst	Pt	Pt and/or Pt-Ru	Pt	Pt	Pt	Ni	Ni
Carrier ion	H^+	H^+	H^+	OH^-	H^+	CO_3^{2-}	O^{2-}
Electrolyte	Solid polymer	Solid polymer	Solid polymer	Aqueous KOH	Aqueous H3PO4	Molten carbonate	Ceramic
Output power range	Watts/ Kilowatts	Watts	Watts/ Kilowatts	Watts/ Kilowatts	Kilowatts	Kilowatts/megawatts	Megawatts
limitations	High catalyst cost, Water management and catalyst poisoning	Low efficiency and methanol crossover	Solid polymer electrolyte and composite bipolar plate	Expensive catalyst, sensitive to poisoning, and water management	Expensive catalyst, corrosive electrolyte, and electrolyte management	Corrosive electrolyte, high cost materials, and degradation	Expensive materials and degradation
Applications	Portable devices, electrical equipment, automotive and domestic	Vehicles and appliances	Portable devices, electrical equipment, automotive and domestic	Space, military	Electrical equipment, Transportation and stationary application	Stationary and distributed power generator	Power plants, combine heat and power, and stationary
advantages	High power density, short start-up time, and low temperature	Short start-up time and low temperature	High CO tolerance, separate water management is not required	Low cost materials and high performance	Low cost electrolyte, long time performance and reliable	High quality waste heat and high efficiency	High quality waste heat, fuel flexibility and high efficiency

1.2 The History of Fuel Cell

The basic operating principle of the fuel cell was introduced for the first time by Sir William grove in the year 1839. Later in 1842, Grove produced a 50-cell stack and named it "gaseous voltaic battery". After Grove's invention, it took almost a century to re-introduce the fuel cells to the scientific community. In 1937, F.T. Bacon began to work on practical fuel cell and he successfully built a 6 kW output stack by the end of the 1950s. In the early 1960s Grubb and Niedrach assembled a fuel cell by using solid ion-exchange membrane electrolyte. Primarily, sulfonated polystyrene based membranes were employed as the electrolytes; thereafter Nafion membranes substituted sulfonated polystyrene based membranes. Membranes made of Nafion has proved itself in durability and performance, and it is the most common used membrane. Fuel cell having membrane as electrolyte is generally called polymer electrolyte membrane fuel cell or proton exchange membrane fuel cell.

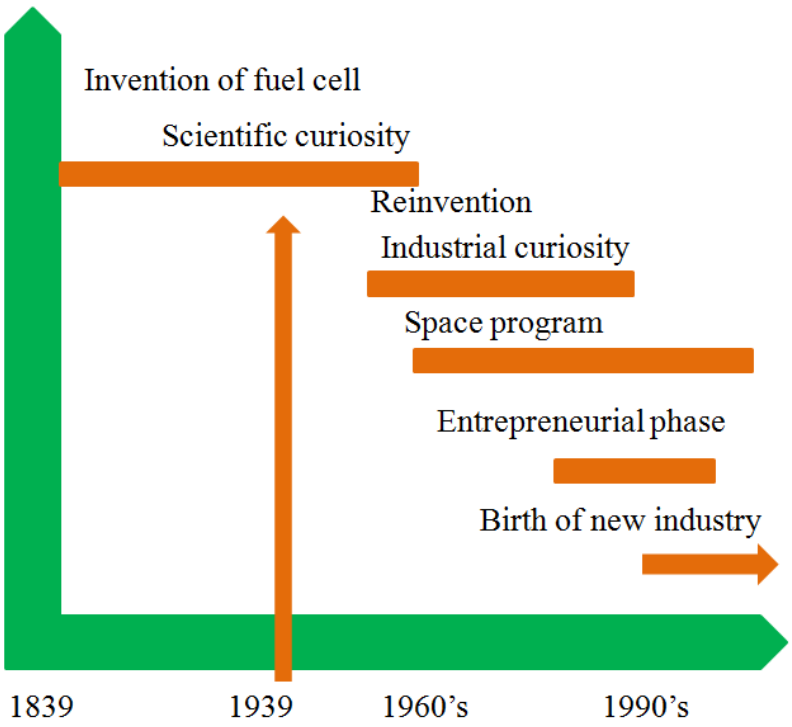

Fig. 1.1 History of the fuel cells

In the early 1960s, General Electric has developed a PEM fuel cell (PEMFC) Electric by depending on Grubb and Niedrach's work, which was used in Gemini space program for the

first time. FC were also used in the other space programs like Apollo program, where it was used for production of electricity for life support and communications. Due to the high cost of the fuel cells, they were limitedly used in some distinctive applications like space programs. Ballard Power systems started developing the PEMFC systems in the year 1990. Ballard's strategy was to decrease the charge of the fuel cell by consuming low cost fabrication techniques and materials; fuel cell then turned out to be an apt option for many applications. In 1993, Ballard Power Systems manufactured buses powered by fuel cell. In 1993, Energy Partners demonstrated the first passenger car operating on PEMFCs. By the end of the century, majority of the car manufacturers followed this concept and manifested and built a vehicle powered by fuel cell. The timeline of FC development history is demonstrated in Fig. 1.1.

1.3 Principle of operation of PEM fuel cell and its components

The schematic diagram of PEMFC is shown in Fig. 1.2. The fuel cell comprises an anode, a cathode, and an electrolyte (membrane) that consents ions, regularly positively charged hydrogen ions (protons), to move between the two sides of the fuel cell. Membrane electrode assembly (MEA) comprising 5 layers, namely catalyst layers placed on either side of the membrane and it is sandwiched between two gas diffusion layers (GDL). The prepared MEA is placed between two bipolar plates which supply reactants to reaction area for electrochemical reaction. The GDLs act as electrodes which are fabricated using carbon paper or carbon cloth. Platinum is used as a catalyst which is placed between membrane and GDL [4]. Hydrogen (H_2) comes into anode flow channel and disperses into anode gas diffusion layer (GDL) whereas oxygen (O_2) enters the cathode flow channel and disperses into cathode gas diffusion layer (GDL). The hydrogen side which is negative is named as the anode, while the oxygen side of the fuel cell is positive which is considered cathode. The membrane comprises a catalyst, usually platinum, on both sides and it is made from a material that permits only hydrogen ions and offers resistance to the flow of electrons. When hydrogen and oxygen reach the catalyst layers (CLs) through GDLs on the PEM, the following reaction takes place.

Anode: $H_2 \rightarrow 2H^+ + 2e^-$ (**1.1**)

Cathode: $½\ O_2 + 2e^- + 2H^+ \rightarrow H_2O$ **(1.2)**

At anode catalyst layer hydrogen splits into hydrogen ions and electrons. Hydrogen ions pass from anode to cathode, through the Nafion membrane and electrons flow out of the cell through an electrical circuit. At the cathode CL, oxygen reacts with hydrogen ions and electrons flow into the cathode, completing an electrical circuit. The overall reaction in a hydrogen and oxygen fuel cell is given in Equation 1.3.

Overall: $H_2 + 1/2\ O_2 \rightarrow H_2O$ **(1.3)**

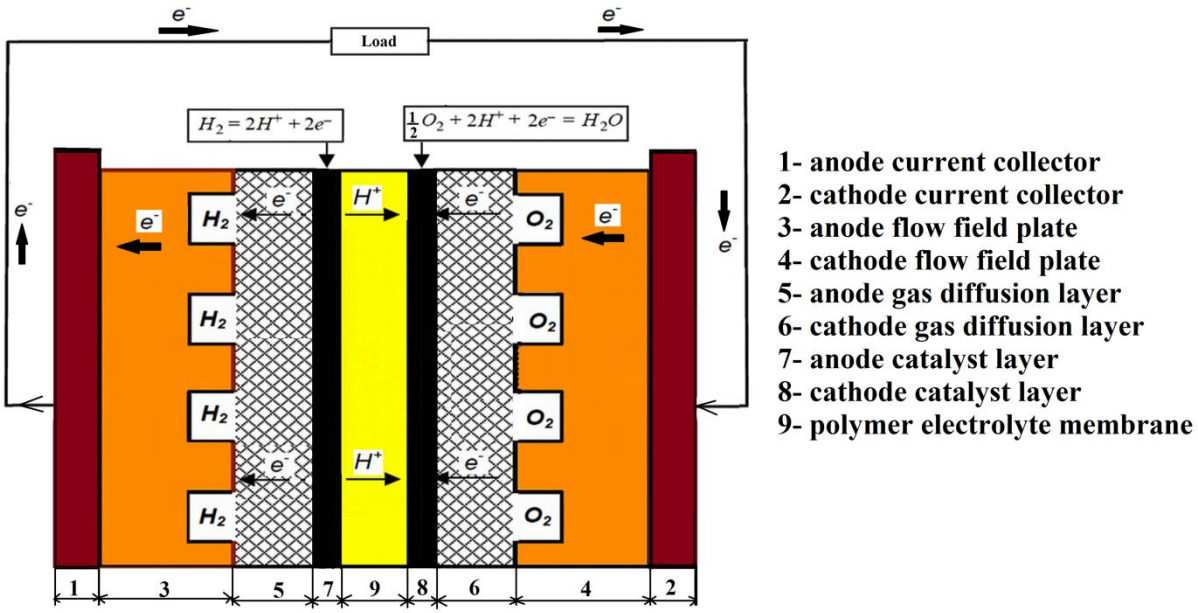

Fig. 1.2 Schematic of a PEM fuel cell along with parts

1.3.1 Membrane (PEM)

PEM stands for proton exchange membrane or polymer electrolyte membrane. A proton-exchange membrane, or polymer-electrolyte membrane (PEM) which is a semipermeable membrane generally formed from ionomers and designed to conduct protons while working as an electronic insulator and reactant barrier, e.g. to oxygen and hydrogen gas. A polymer membrane exists in the fuel cell because of which it is named polymer electrolyte membrane fuel cell (PEMFC). The membrane is considered the heart of PEMFC, in which hydrogen ions flow from anode CL to cathode CL. The function of the membrane is to separate the fuel (H_2) and oxygen (O_2). The hydrogen ions/protons transfer from anode to

cathode through the membrane, the membrane needs to possess relatively high proton conductivity. Also the membrane should be stable at mechanical and chemical environment present in the fuel cell. Perfluorocarbon-sulfonic acid ionomer (PSA) membrane is usually used in PEMFCs. Dupont developed the membranes based on a sulfonated tetrafluoroethylene-based fluoropolymer-copolymer (Nafion family) and are considered the best material for the membrane. A fully humidified membrane conducts the protons effectively, therefore it is essential to keep membrane hydrated. Sometimes the water produced in the electrochemical reactions is inadequate to keep the enough humidification level in the membrane. Also, use of dry reactant gases and the electro-osmotic drag results in under-humidified state. Therefore, it is desirable to humidify the inlet reactant gases before they enter the cell to achieve the required humidification range in the membrane [10].

1.3.2 Catalyst Layers (CLs)

In a PEMFC, there are two CLs on both sides of the membrane. These CLs are placed between the membrane and GDLs at anode and cathode respectively. All the electrochemical reactions take place at the catalyst layer. The catalyst layer must have high intrinsic activity, large active surface area, high ionic and electric conductivity, high porosity for reactants entry as well as product removal.

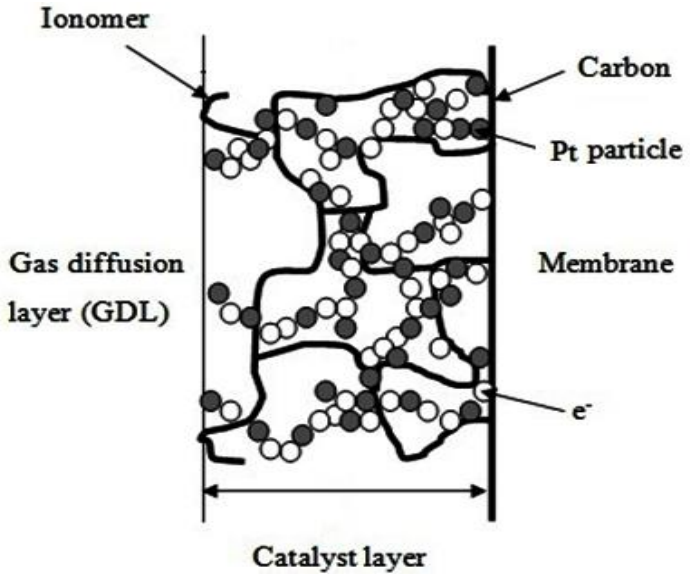

Fig. 1.3 Catalyst layer [11]

Usually Platinum (Pt) is preferred as the catalyst in PEMFCs because of its great stability and reactivity. Sometimes Pt alloys also can be chosen as catalysts to further improve kinetic activity, stability, and tolerance to impurities when reformate gas is used on the anode side. Pt is generally in the form of tiny particles and these small Pt particles are reinforced on carbon particles to generate high surface area. A catalyst layer with Pt supported on carbon is depicted in Fig. 1.3.

1.3.3 Gas Diffusion Layers (GDLs)

Two GDLs are bonded to anode and cathode catalyst layers. Usually hydrophobic carbon cloth or carbon paper is used as GDL and it is called substrate. A micro porous layer (MPL) with hydrophobic property is applied to the catalyst side of the substrate. The hydrophobicity is usually attained through application of Poly Tetra Fluoro Ethylene (PTFE). SEM images of carbon fiber paper and cloth are shown in Fig. 1.4. The following are some key functions of GDL

- It works as a passageway to carrying reactant gasses from the flow channels to the reaction site.
- It works as a passageway for evacuation of product (water) from reaction site to flow channels.
- It works as a heat conductor.
- It conducts the electrons from CL to the current collector via bipolar plate.

The membrane electrode assembly (MEA) is the combination of membrane, CLs and GDLs.

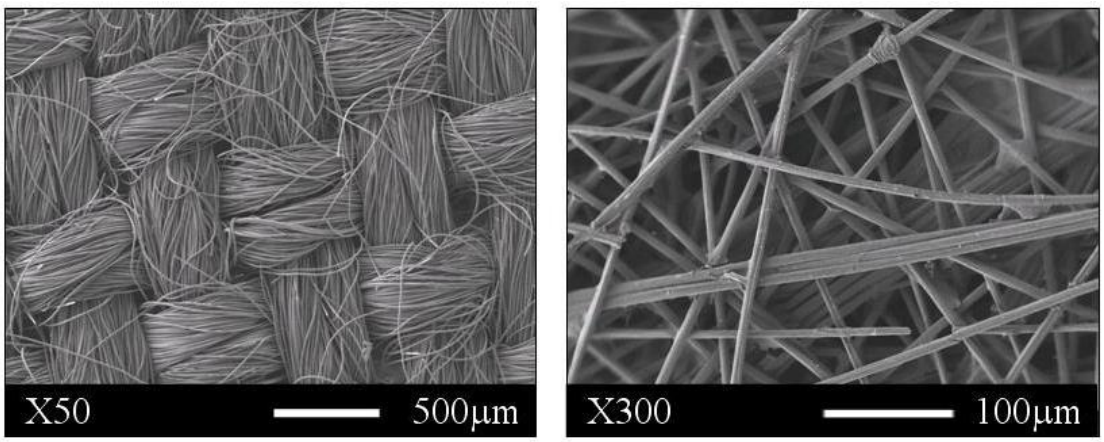

Fig. 1.4 GDL material: carbon cloth (left) and carbon paper (right) [12]

1.3.4 Flow Field Plates(FFP)

Every single PEM fuel cell has two flow field plates (FFPs) and MEA is kept between these two flow fields and assembled with the help of bolts and nuts. These FFPs are in direct contact with GDLs. These FF plates are generally fabricated with graphite material or metals. The key purposes of the FFPs are:

- To distribute the reactants to the GDLs, and evacuate the unused gases and water from the cell.
- To transfer electrons and heat.
- To give mechanical strength.

To serve these purposes FFPs need to be chemically stable, electrically and thermally conductive, mechanically strong and contamination free. Fig. 1.5 shows the commonly used flow field designs in PEM fuel cells.

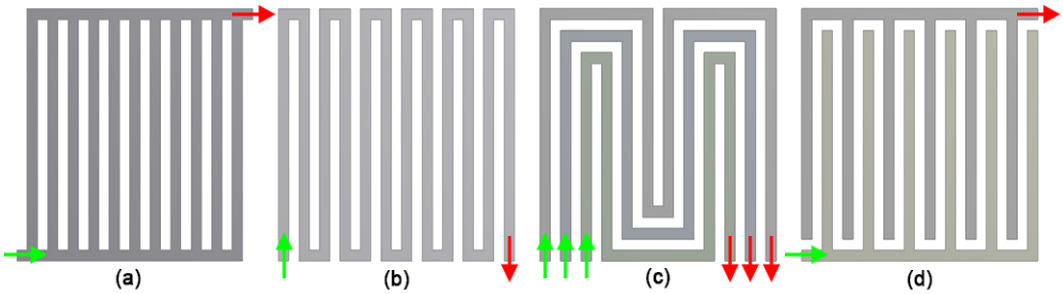

Fig. 1.5 Common flow-fields: (a) Parallel (b) 1-pass serpentine (c) 3-pass serpentine and (d) Interdigitated [13].

With the help of above components a complete fuel cell can be assembled with the help of bolts and nuts and the exploded view of a complete PEM fuel cell can be seen in Fig. 1.6.

1.4 Performance of PEMFC

The performance of PEM fuel cell can be briefly explained with a graph of its current-voltage characteristic features. The line graph shown in Fig. 1.7 is called *i*–V curve (solid line), which displays the voltage output of FC for a given current output. An ideal FC will generate any quantity of current at a constant voltage when there is enough supply of reactant gases. In practice, the real output voltage of a fuel cell is less than the ideal thermodynamically predicted voltage. Besides that, a further increase in the current drawn results drop in FC

output voltage and limits the total power output. The power (*P*) output of a fuel cell is given by the product of current and voltage *Power density curve of a fuel cell* can be drawn from the data obtained from fuel cell *i*-V curve, which gives the power output of an FC. Power density curves (dotted line) are shown in Fig. 1.7. FC voltage is rendered on the primary *y*-axis (left), while power density is demonstrated on the secondary *y*-axis (right).

$$P = V * \mathrm{I} \tag{1.4}$$

The current generated in an FC is unswervingly proportional to the quantity of consumed fuel. It is difficult to keep the fuel cell at high voltage under the current load. Due to irreversible losses the output voltage of a practical fuel cell is lower than the thermodynamically expected output voltage. These losses which are irreversible are greater while more current is drawn from the FC. Three foremost types of FC losses given below are shown in *i–V* curve of a FC and its characteristic shape.

1. Activation losses
2. Ohmic losses
3. Concentration losses

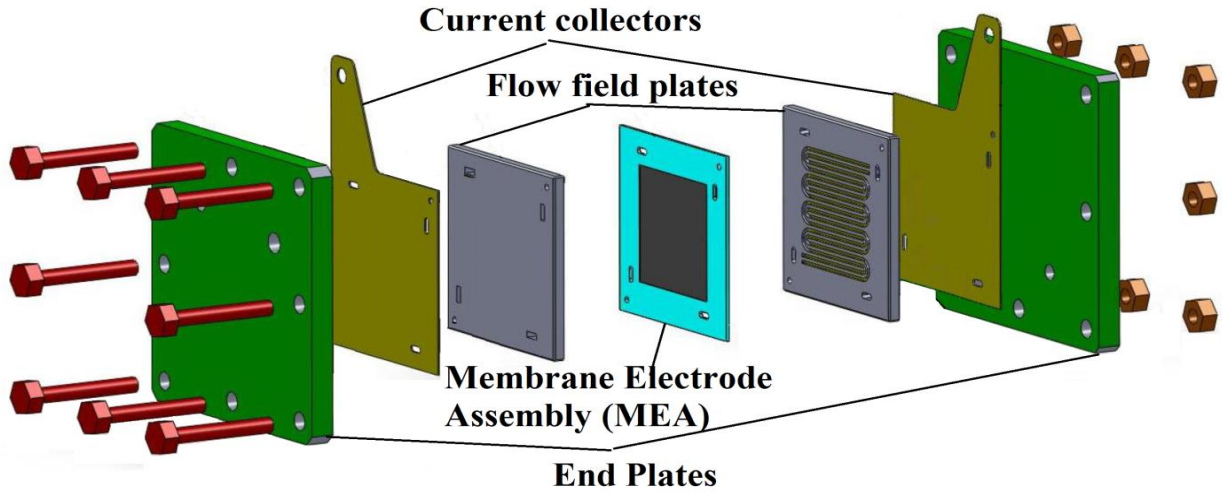

Fig. 1.6 Exploded view of a PEM fuel cell

The real output voltage of a FC can be composed by beginning with the thermodynamically expected voltage output and then deducting the voltage drops due to three losses mentioned above:

$$V_{cell} = E_r - \eta_{act} - \eta_{ohmic} - \eta_{conc} \tag{1.5}$$

$$E_{nernst} = 1.229 - 0.85 * 10^{-3}(T - 298.15) + 4.3085 * 10^{-5}\, T[\ln(P_{H_2}) + \ln 0.5\,(P_{O_2})\textbf{(1.6)}$$

Where V_{cell} is cell output voltage, $E_r$is reversible cell voltage, η_{act} is activation losses, η_{ohmic} is ohmic losses, η_{conc} is concentration losses.

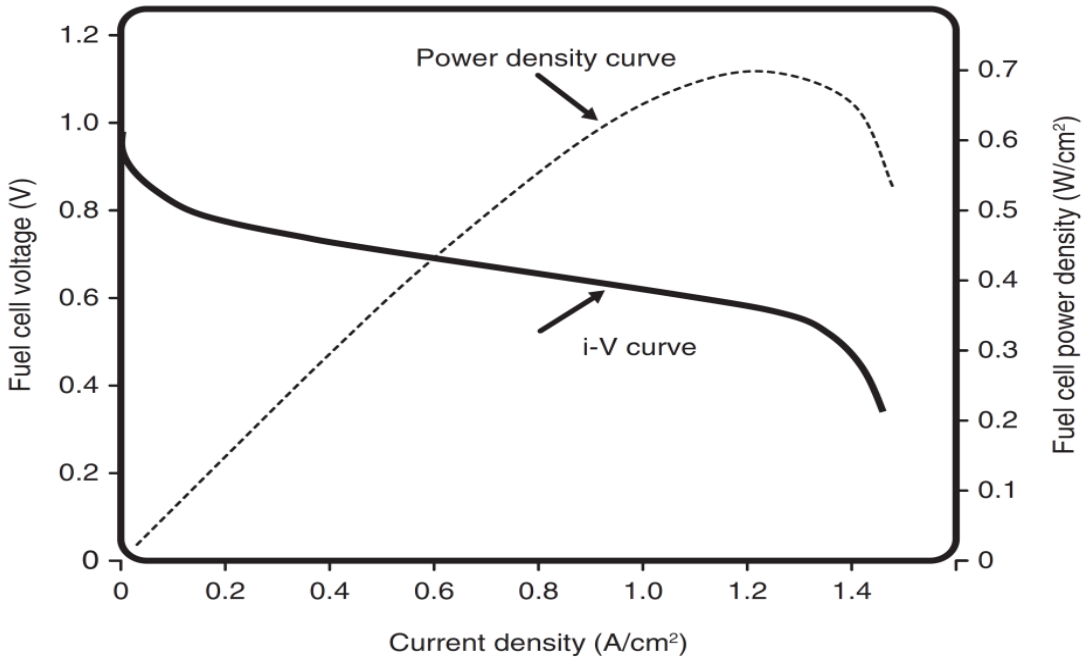

Fig. 1.7 Polarization and performance characteristics of a fuel cell [14]

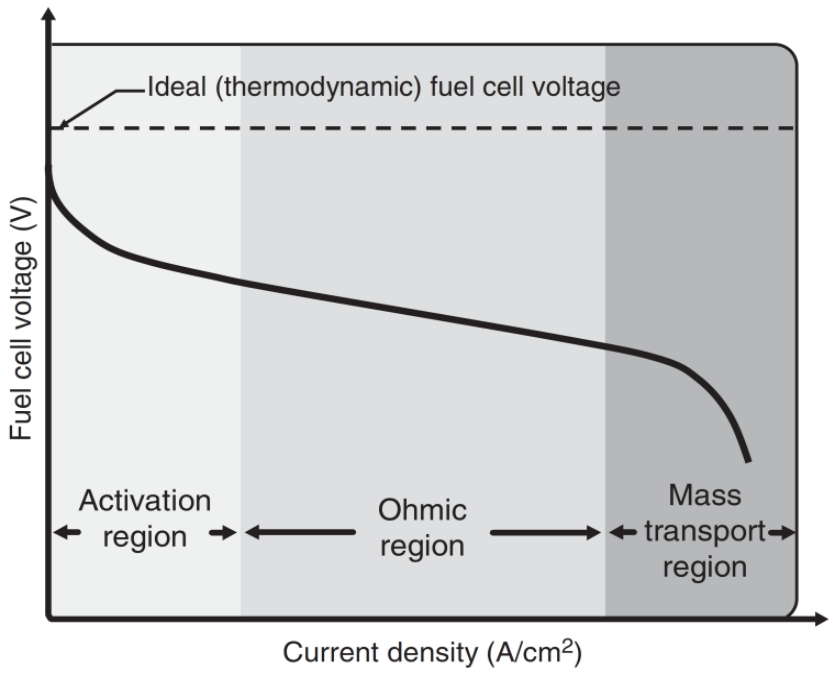

Fig. 1.8 Polarization curve with irreversible losses of a fuel cell

These three irreversible losses each add to the characteristic shape of the fuel cell *i–V* curve. As illustrated in Fig. 1.8, the activation losses majorly influence the first part of the curve, ohmic losses are most ostensible in the middle part of the curve, and the concentration losses are most significant in the tail part of the *i–V* curve. Equation 1.5 helps to characterize and model the performance of fuel cells used in daily life.

Activation losses

Activation loss is associated with energy barrier which needs to be overcome to start a chemical reaction. At low current density, the electron transfer rate is sluggish and a bit of the cell voltage is lost to be able to compensate for low electro-catalytic activity. The activation voltage drop can be described as

$$V_{act} = \frac{RT}{\alpha nF}\, ln\left(\frac{i}{i_0}\right) \quad \textbf{(1.7)}$$

Where T is Fuel cell operating temperature (kelvin), R is Universal gas constant, α is the transfer constant, n is number of electrons participated in the reaction, F is Faraday's constant, *i* is cell current density, and i_0 is the exchange current density.

Ohmic losses

Every material comes with an inherent amount of resistance to charge flow. The material's usual resistance to charge-flow triggers ohmic polarization, which in turn causes drop in FC voltage. Resistive losses take place in the electrolyte (ionic), electrodes (electronic and ionic), and terminal connections of the cell (electronic). The ohmic losses (ohmic voltage drop) can be described as:

$$V_{ohmic} = i * R_{ohmic} \quad \textbf{(1.8)}$$

Where i is the current density and R_{ohmic} resistivity of membrane. The cell resistance relies upon membrane water content $\lambda_{\ mem}$ and cell temperature. On the other hand, the cell resistance is proportional to thickness of the membrane (t_{mem}) and inversely proportional to the conductivity of the membrane (σ_{mem}). Thus resistivity of membrane can be described as follows

$$R_{ohmic} = \frac{t_{mem}}{\sigma_{mem}} \quad \textbf{(1.9)}$$

The membrane conductivity greatly depends on membrane water content λ_{mem} and cell temperature T_c. The membrane conductivity can be determined using the following formula

$$\sigma_{mem} = (0.005139 * \lambda_{mem} - 0.00326)\, exp\left[1268 * \left(\frac{1}{303} - \frac{1}{T_c}\right)\right] \quad \textbf{(1.10)}$$

Concentration losses

Concentration losses are associated with mass transport limitations (reactants / products)**.** In this region, the reactants turn out to be consumed at higher rates than the supplied rate whereas the product amasses at a larger rate than it could be cleared. Eventually, this will influence the reaction completely and the FC voltage drops to zero

$$V_{conc} = i(\beta_1 * \frac{i}{i_{max}})^{\beta_2} \quad \textbf{(1.11)}$$

Where β_1 and β_2 are constants which are based on the temperature of cell and partial pressure of reactants. β_2 is taken as 2, and β_1 is defined by Pukrushpan et al.[15]as follows

$$\beta_1 = \begin{cases} (7.16 * 10^{-4} * T_c - 0.622)\left(\frac{P_{O_2}}{0.1173} + P_{sat}\right) + (-1.45 * 10^{-3} * T_c + 1.68) \\ if\ \frac{P_{O_2}}{0.1173} P_{sat} \leq 2\ atm \\ else \\ \left(8.66 * 10^{-5} * T_{fc} - 0.068\right)\left(\frac{P_{O_2}}{0.1173} + P_{sat}\right) + \left(-1.6 * 10^{-3} * T_{fc} + 0.54\right) \\ if\ \frac{P_{O_2}}{0.1173} P_{sat} \geq 2\ atm \end{cases} \quad \textbf{(1.12)}$$

Where P_{sat} is water saturation pressure, P_{O_2} is Partial pressure of oxygen and T_{fc} cell temperature.

1.5 Thesis Organization

The present thesis comprises 8 chapters, chapter 1 outlines the introduction of PEM Fuel Cell (PEMFC). The literature review on PEMFC is provided in chapter 2. The gaps identified in the literature review and thesis objectives are also presented in chapter 2. Both experimental methodology and computational methodology for PEMFC have been presented in chapter 3. In this chapter the fundamental concepts of electrochemistry modelling, current and mass conservation, liquid water formation and transport phenomena have been presented. In chapter 4 the simulation results of PEM fuel cell fitted with different channel and land widths of a single serpentine flow channel configuration is demonstrated. The experimental results of the fuel cell fitted with different channel configurations viz. single serpentine channel, lung channel, bio-channel and non-interdigitated leaf channel configuration under different operating conditions is described in the chapter 5. Chapter 6 depicts the experimental results of the PEMFC with four different design modifications of a leaf channel configuration, viz., NILCD, ILCD, ILCDWCE and Murray's design. The experimental results of the PEMFC with Ti metal bipolar plate with different types of coatings, viz., graphite, graphene oxide and graphene under optimum operating conditionshave been described in the chapter 7. Finally, the overall conclusions drawn from this research work and some recommendations for future research are given in chapter 8.

Chapter – 2

Literature Review

2.1 General

A significant number of theoretical and experimental studies has been carried out by many researchers on proton exchange membrane fuel cells (PEMFCs). Experimental tests are the commonly used approaches for understanding and predicting PEMFC performance. Some empirical and mathematical models have also been proposed in the literature to comprehend and analyze the performance of PEMFCs. These models are usually acceptable to experimental data by means of a single equation but they are less precise and trustworthy in envisaging fuel cell performance. To understand basic transport processes, more fundamental PEMFC models were developed and investigated for fuel cell performance. The objective of the current literature review is to present overview of PEM fuel cell development.

For the first time in 1839, Sir William Grove demonstrated the working principle of a fuel cell. After his demonstration, it took almost one decade to re-introduce the fuel cell to the scientific community. Being enthralled with Grove's invention, Bacon began experimenting on fuel cells in 1939 and was successful in constructing a fuel cell stack of 6 kW output power 1959 [16]. Based on Bacon's patents, Pratt and Whitney made fuel cells. General Motors made trials with a fuel cell operated van by the mid-1960s; in the meantime the U.S. Space Program continued to effectively make use of fuel cells today. In the 1960s, many industries recognised that fuel cells can be used in different applications, but because of their high manufacturing cost and technical difficulties, fuel cells did not have the capacity to work in tandem with other energy conversion devices. In the 1980s, the Canadian Government sponsored the preliminary development work of fuel cells which was supported by Ballard Power Systems. Later in 1989, the company decided to concentrate on fuel cell systems for transportation and stationary applications.

2.2 Simulation Studies on PEMFC models

Bernardi & Verbrugge [17]presented a mathematical model of the solid polymer electrolyte fuel cell to examine the causes limiting the performance of fuel cell and also explain the species transport mechanism in the intricate network of gas, liquid, and solid phases of the fuel cell. Kim et al. [18]presented an empirical fuel cell model which fits into the whole IV curve. The authors found that addition of an exponential term be responsible for

compensation for the mass-transport region at high current densities. Kazim et al. [19]presented a 2-D steady state PEMFC model with conventional and interdigitated flow fields. It is observed from the results that the limiting current density of interdigitated flow field fuel cell is about three times the limiting current density of the conventional flow field. Mann et al.[20] established a generalised steady-state electrochemical model (GSSEM) which is more extensive in practice than previously reported steady state electrochemical models (SSEM) of Amphlett et al. It now has the ability to deal with PEMFCs of any active area and Nafion membrane thickness.

Gurau et al. [21] developed a mathematical PEMFC model and obtained strenuous analytical results of the model. Their modeling domain comprises cathode flow channel, catalyst layer (CL), membrane and gas diffusion layer (GDL). Beginning with oxygen transport equations and Ohm's law for proton movement, expressions for oxygen distribution in the flow field, GDL, CL, current density in the CL and membrane phase potential have been derived. Fowler et al.[22] modified the generalised steady-state electrochemical model (GSSEM) of Mann et al. [20]with the incorporation of voltage degradation term to estimate the durability of fuel cells and named this model generalised steady-state electrochemical degradation model (GSSEDM). Berning et al. [23] established a non-isothermal, single-phase 3-Dimentional model using CFX-4.3 (AEA Technology). This model consist of the gas flow channels, GDLs, and membrane; the CLs were treated as interfaces. Kumar & Reddy [24]developed a computational 3-D half-cell PEMFC model to study the impact of different channels sizes and shapes in the flow-field. Their channel sizes study results showed that high fuel consumptions (≈80%) were obtained with optimum channel depth and width as well as land width, close to values of 1.5, 0.5 and 1.5 mm, respectively. The channel shape study results revealed that channel cross-section in triangular and hemispherical shape caused an improvement in hydrogen consumption around 9% at the anode. Wang et al. [25]developed a spherical flooded-agglomerate model for the cathode catalyst layer of a PEMFC. This model incorporates the kinetics of oxygen reduction at the interface of catalyst-membrane, proton transportation through the membrane, oxygen diffusion through pores, and dissolved oxygen diffusion through membrane. The studies (1-D and 2-D models) presented so far require a number of simplifications due to limitations of the numerical techniques.

Nguyen et al. [26] developed a 3-D CFD fuel cell model fitted with serpentine flow field using CFX-4.3. A distinctive feature of this model is the implementation of VTC (voltage-to-current) algorithm, which allows more accurate three-dimensional variation of electrochemical kinetics. Furthermore, the 3-D activity of the catalyst layer was also considered in this model. Lum & McGuirk [27] build a steady-state, 3-D fuel cell model and to analyse the influence of different parameters i.e. electrode thickness, oxidant concentration, degree of permeability and shoulder width on fuel cell performance. Lin & Beale [28] developed a 3-D full model and a hybrid model for an industrial PEM fuel cell to predict water transport distribution within the cell and also the impact of oversaturation and dehydration on either side of the membrane, on overall cell performance.Yan et al. [29] developed a three dimensional fuel cell model to study the performance of PEMFC with several flow field designs, viz., parallel channel design, Z-type channel design, serpentine channel design, parallel channel design with baffles and Z-type channel design with baffles. The results revealed that the parallel channel design with baffles offered less pressure drop and gave the best performance. Sun et al. [30] prepared 1 3-D PEMFC model with 3-pass serpentine channel with trapezoidal design and studied the pressure variation along the flow channel and the fuel cross-over over GDL. The results revealed that the fuel crossover increases with increase of channel size ratio (R=B/A) and the pressure drop across the channel decreases with decrease in flow cross-over. Shimpalee et al. [31] developed a 3-D PEMFC model with 200 cm2 active area and studied the effect of different configurations such as 3-channel serpentine, 6-channel serpentine and 13-channel serpentine flow fields on fuel cell performance. Their investigations concluded that the fuel cell with smaller path lengths or more number of channels helps to achieve more uniform local temperature and current density distribution.

Liu et al. [32] presented an isothermal, steady-state, 3-D multicomponent transport model for PEMFC with straight gas channels and their findings revealed that the distribution patterns are moderately uniform at low current densities and are non-uniform at high current densities because of the mass transfer limitation. Yan et al. [33] developed a 3-D PEMFC model with a novel straight channel tapered in height or width, to increase the fuel utilization efficiency. The results revealed that tapered channel designs enhance fuel velocity, fuel transport through porous gas diffusion layers, fuel utilization, and water removal capability. Duan et al. [34]

developed three dimensional computational fuel cell model to investigate the impact of various variables on the working of bipolar plate on a fuel cell, such as the number of bends in the flow channels and quantity of flow channels. The predictions show that single serpentine flow field performance enhances with increase in number of channel bends. It also shows that the performance of the single serpentine channel is most beneficial when compared to multi serpentine channel designs. Jang et al. [35] developed 3-D numerical PEMFC models with parallel flow field, Z-type flow field, and serpentine flow fields to investigate the performance as well as transport phenomena of PEMFCs. The authors reported that PEMFC with serpentine flow field offered the best performance, followed by Z-type flow field and then parallel flow field. Sadiq Al-Baghdadi [36] also developed a full 3-D, non-isothermal CFD model of a tubular in shape PEMFC to study the transport phenomena.

Wang et al. [37] developed a 3-D numerical PEMFC model and investigated the local transport phenomena and power output of the cell using parallel and interdigitated flow fields. The results of the studies have shown that the performance of PEMFC with interdigitated flow field is superior to PEMFC with parallel flow field.Yan et al. [38] introduced a 3-D flow model with conventional type flow fields by taking finite volume method (FVM) into consideration to study the impact of flow channel design on the reactant utilization, fuel cell performance and rate of water removal. It was observed that the conventional flow field performance is enhanced because of an increase in channel length and a simultaneous decrease in the quantity of channels. Akbari et al. [39] numerically investigated the steady state 3-D PEMFC performance by varying the clamping pressure on the output of PEMFC. From the results it is observed that, a clamping pressure of 1 Mpa will give the optimum cell performance. Weng et al. [40] presented a 3-D PEMFC model with contracted outlet flow channels to analyze the performance of FC and local transport phenomena. The authors reported that the contracted channel design ameliorate reactant velocities, which enhances liquid water evacuation and increases reactant utilization. Rismanchi& Akbar [41] also presented a 3-D PEMFC model with square cross section straight flow channels to study the flow structure, species concentrations and current distribution inside the cell.

Iranzo et al. [42] conducted experiments on PEMFC to study the effect of different working parameters and various channel designs on the performance of PEMFC. The authors

reported that PEMFC with serpentine channel design performance is superior compared to the PEMFC with parallel channel design. The performance of the fuel cell was enhanced with supply of pure oxygen and humidified reactants. Bansode et al. [43] carried out computational and experimental studies on PEMFC using 3 different channel designs such as serpentine, mixed and parallel channels, and examined the influence of working temperature and flow rate of reactants on the power output of the PEMFC. From the results it was noted that, the mixed channel design offered the best performance and also maintained uniform pressure from inlet to exit of the channel when compared with other two designs.

Xiao-Dong wang et. al. [44] made a two phase 3-D model to evaluate the influence of channel size (varied from 0.307mm to 1.533 mm) on the performance of PEMFC. It is observed from their results that, power density of PEMFC increased with decrease of channel size from 1.533 mm to 0.535 mm. On further decreasing the channel size, the performance decreased due to more pressure drop. Wang et al. [45] presented a full 3-D, two-phase transport model for PEMFCs based on the two-fluid method to examine the influence of gas channel aspect ratio on the performance of FCs with one pass and three pass serpentine flow field. The results revealed that enhancement in the cell performance can be obtained with decrease in the aspect ratio and the aspect ratio has less influence on the performance for three-pass serpentine flow field PEMFC than one pass serpentine flow field PEMFC because of the weaker under-rib convection. Manso et al. [46] presented a 3-D CFD model for PEMFC with serpentine flow field to examine the influence of the flow channel's aspect ratios, varying between 0.07 and 15. The study concluded that the channel with high aspect ratio displayed more uniform current distribution, moderate temperature distribution gradients, and higher water content in the membrane than channel with low aspect ratio.

Robles et al. [47] developed a single phase 3-D PEMFC model with a flow field path in the shape of 1, 2, 3, 4, 6, and 8 concentric spirals. The authors found that the model with 4 spirals had the best geometry due to more uniform current density distribution, uniform water distribution, and relatively small pressure drop. Choi et al. [48] presented a 3-D PEMFC with serpentine flow field having five flow passes to examine the influence of flow channel height and width on pressure drop and liquid water removal. The authors noticed reduction in pressure drop with increase in channel height and width. The authors also noticed that the

increase in the channel width caused quicker liquid water removal than when the channel height increases. Fontana et al [49] carried out numerical analysis by introducing three dimensional flow model in order to investigate the influence of uneven flow area of the channels on the working of fuel cell. From this study it is manifest that the current density increases with an increase of flow channel inclination and it gives more power density. Fatemeh Hashemi et. al. [50] established the non-isothermal, 3-dimentional model and investigated the effect of straight and serpentine flow channels on the performance of PEM fuel. The model findings revealed that the serpentine flow channel shows better distribution of current density and temperature. Modeling predictions were compared with the experimental data reported in the literature for different values of current densities and showed good agreement with the experimental data. Khazaee &Ghazikhani[51] built a duct-shaped PEMFC numerical model and investigated the influence of the number of connections between bipolar plate (BP) and GDL on the cell power output and species distribution. Their study concluded that, the increase in the number of connections between BP and GDL increased fuel cell performance, utilization of hydrogen, oxygen and water generation.

Sierra et al. [52] conducted a 3-D numerical analysis on a PEMFC model using serpentine, interdigitated and straight channels adapted to tubular plates. The authors compared the numerical results with literature data described for analogous designs and the results revealed that conventional flow channel designs have several benefits such as uniform pressure along the channel and also maintain uniform current density distributions. Performance and flow characteristics of bigger-size PEMFC (cell active area 300 cm^2) with branch channels were studied by Han et al. [53] through simulation and experiments. The branch channel (f=0.5) performance was compared with serpentine channel performance and it was found that the performance of branch channel was analogous to serpentine channel performance. Also it was found that the pressure drop in the branch channel was less by 52.5% than that of serpentine channel. Limjeerajarus &Amornkitt [54] numerically studied the effect of six flow field designs, namely, 1-S, 3-S, 5-S, parallel, 3-PIS and 5-PIS as well as a number of channels on performance of a small PEMFC (5 cm^2 active area). The authors reported that: i) 1-S flow field gave the highest performance and uniformity whereas the parallel flow field gave the least performance, ii) with the same number of channels, the parallel in series (PIS) flow fields performance was superior to that of multi-channel

serpentine flow field design. Rostami et al. [55] created a single phase model of PEMFC with serpentine flow field and studied the effect of bend size (from 0.8 mm to 1.2 mm) on the cell performance. The study concluded that bend size of 1.2 mm has an improved performance when matched with the other bend sizes.

Karvelas et al. [56] generated three dimensional numerical model to examine the influence of laminar and turbulent flows on pressure drop, distribution of reactants in the anode channels and residence time of the reactants inside the PEMFC. From the results, it was observed that with increase of Reynolds number, the residence time, pressure drop and non-uniformity in flow rate increased. Saco et al. [57] numerically analyzed the performance of 225 cm2 active area PEMFC with the straight parallel, serpentine parallel, straight zig-zag, and serpentine zig-zag paths. The study revealed that, straight zig- zag design had better reactant consumption with uniform distribution of water on the electrolyte improving the proton conductivity. This design also offered less pressure drop compared to other designs used in their study. Monsaf et al. [58] studied the geometrical factors to analyze their effect on the performance of a PEMFC with spiral flow filed. From the analysis, they reached to a conclusion that, reactant distribution was better in wider channels. The obtained results showed that the performance of PEMFC was enhanced due to induced centrifugal motion of the reactants in a spiral design. Paulino et al. [59] presented a CFD based 3-D PEMFC model with single channel and studied the effect of channel cross section (rectangular, trapezoidal and hybrid stepped geometries) on the performance and water management of the cell. The results revealed that the performance of rectangular channel FC was slightly higher than that of stepped and trapezoidal channel FCs while water management behavior of stepped and trapezoidal channel FCs was superior thanthat of rectangular channel FC. Damian-Ascencio et al. [60] computationally developed four different tree-like channel design configurations based on the veins of the leaves of various trees for PEM fuel cell. Their results showed that the configuration having two levels of bifurcation at an angle of 37o was more efficient at removing water and resulted in improved current density. It was also observed that with the increase in the number of bifurcations, the PEM fuel cell performance improved. Mohammad Ziauddin Chowdhury et al. [61] developed a 3-D isothermal single phage model for investigating the influence of land width on fuel cell performance. From their numerical study results, it was shown that the pressure drop is dependent more on channel width compared to

land width, and the anode pressure drop is less significant than cathode pressure drop. However, both channel and land width have equal importance on fuel cell current density. Moosa et al. [62] developed 3-D two phase model to investigate the effect of cathode stoichiometry on cell performance. From the results it is observed that the output power and efficiency of the fuel cell is stable at high cathode stoichiometric ratios. Wan et al. [63] designed an M-like channel for cathode bipolar plate in a PEM fuel cell and compared its performance with wave-like channel computationally. The results showed that the maximum power density of the cell with M-like channel was 21.3 % higher compared to that of cell with wave-like channel.

Hybrid serpentine channel [57]

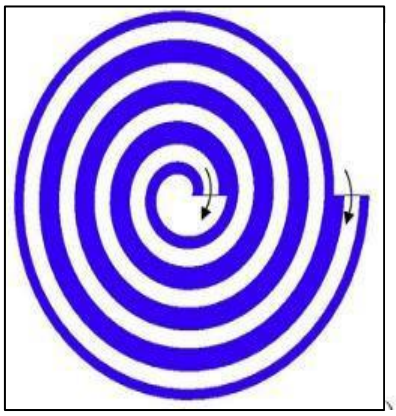

spiral channel [58]

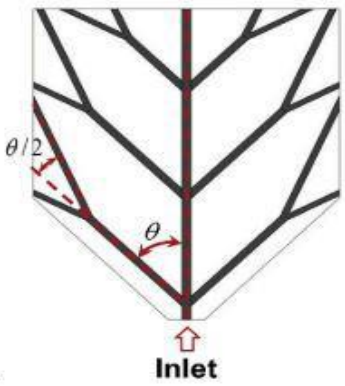

Tree like channel [60]

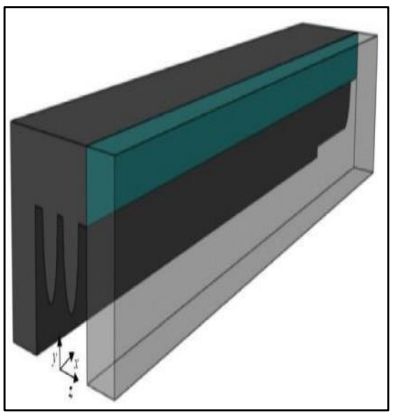

M-like channel [63]

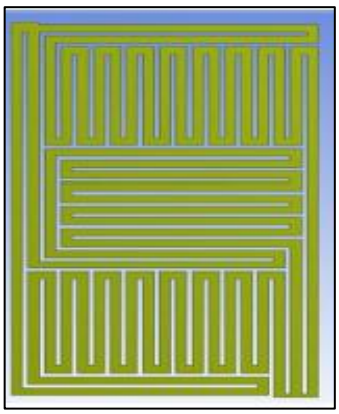

ECSSFF design [65]

staggered Trepezoidal baffle channel [66]

Abdulla et al. [64] developed a three dimensional multiphase computational fluid dynamics model to study the effect of enhanced cross-flow split serpentine flow field (ECSSFF) design on the performance of PEMFC. The results showed that ECSSFF design

gives better performance than triple serpentine channel design. **Abdulla et. al.** [65] studied the effect of rib width-to-channel width ratio on the cell performance for the two flow field designs (i.e. enhanced cross-flow split serpentine flow field (ECSSFF) and single serpentine flow field). The results showed that the fuel cell with enhanced cross-flow split serpentine flow field exhibited superior performance in terms of offering high currents and low pressure drops compared to single serpentine flow field. Wang et al. [66] studied a 3-D multiphase fuel cell model with Forchheimer's inertial effect in the porous electrode to better simulate the convective flow induced due to baffle plates. They analysed conventional parallel flow field, staggered trapezoid baffle plate and parallel trapezoid baffle plate in this study. The staggered trapezoid baffle plate and parallel trapezoid baffle plate designs resulted in the peak net power enhancements of 6.39% and 2.54%, respectively compared to the parallel flow design.

2.3 Studies on PEMFC flow field designs

Nguyen [67] developed a non-conventional flow channel to enhance the mass-transport of reactants from flow channels to porous electrodes and to decrease cathode electrode water flooding**.** Kazim et al. [68] inspected the effect of cathode operating conditions on the output power of fuel cell fitted with an interdigitated flow channel configuration. The operating conditions include working temperature, working pressure; oxygen mole fraction and cathode porosity. The results demonstrate that, the overall power output of the PEMFC enhanced with increasing the GDL porosity as well as mole fraction. Guilin et al [69] developed a 3-D mathematical model and studied the influence of conventional flow channel and inter digitated flow field configurations on fuel cell performance. The inter-digitated design gave high performance compared to conventional flow field design for its mass transport capabilities of fuel cell. Kumar & Reddy [70] studied the effect of different flow channel configurations, viz. parallal. Discontinuous, Serpentine and multi parallel configurations on the performance of PEMFC at the steady state and transient state simulations. The study concluded that multi-parallel design steady state and transient state performance were better than other three designs. Su et al. [71] generated 3-D PEMFC model with straight and serpentine flow field plates to study the influence of step depth on pressure drop and mass transfer phenomena. The authors observed i) an improvement in the performance and drop in pressure with the number of step-depths in the straight flow pattern, ii) no increase in the

performance and pressure drop with the number of step-depths in the serpentine flow pattern. Hongthong et al. [72] created a isothermal, single phase three dimensional PEMFC models of 5 cm^2 active area and examined the impact of geometry and pattern of flow channel on the performance of the FC. The results demonstrate that the change in channel geometry has no impact on FC performance and interdigitated flow channel pattern offers higher limiting current density and performance than conventional flow channel pattern on cathode.

Al-baghdadi & Al-janabi [73] developed a full 3-D, non-isothermal CFD model of fuel cell with straight flow channels to analyse the species transport, heat transfer, electrochemical kinetics, and water transport through the membrane. Ferng & Su [74] developed a 3-D CFD model of PEMFC with different types of flow field channels, namely, parallel and serpentine flow channels, single-path and multi-path flow channels, and uniform depth and step-wise depth flow channels to study their effect of cell performance. The results confirmed that parallel flow channel with the step-wise depth design significantly promotes fuel cell performance. Jeon et al. [75] presented experimental and computational studies of a PEMFC using various types of serpentine flow fields, where the effect of relative humidity on the power output of fuel cell was investigated. The outcomes of the work predicted that, the double serpentine flow channel gives superior performance among all flow fields at high inlet relative humidity. However, there were small performance variances among four serpentine flow-fields at low inlet humidity. Yan et al. [76] showed a 3-D full scale fuel cell model with serpentine flow channel to analyze the effects of channel height and length contraction ratios on cell performance. The authors concluded that i) when the power losses because of pressure drops are neglected, the performance of the cell with contracted outlet channel keeps increasing, ii) when the pressure losses are considered, the optimum performance is attained at a height contraction ratio of 0.4 and a length contraction ratio of 0.4. Min [77] presented a 3-D model of PEMFC with stepped flow field channel and carried out simulations. The results reported that stepped flow field increases local current density generation, reactant distribution, water vapor concentration distribution and performance of the FC.

Carton &Olabi [78] conducted DOE study on a 14.45 cm^2 PEMFC fitted with serpentine, parallel and maze type flow plate designs under different operating conditions (H_2 flow rate, O_2 flow rate and the inlet H_2 pressure). The results show that the serpentine channel

configuration is more effective than maze or parallel channel configuration and the parallel channel configuration performed fairly well at high inlet pressures but over-all, statistically the serpentine channel configuration achieved better performance. Wang et al. [79] presented two phase 3-D PEMFC model with serpentine flow field and analyzed the effect of cathode channel size on fuel cell performance. The numerical predictions revealed that smaller cross-sectional area channels enhanced liquid water removal and optimal performance was obtained with 0.535x0.535 mm^2 cross-sectional area flow channel when pressure drop losses are considered. Yan et al. [80] fabricated a 256 cm^2 active area PEMFC with serpentine flow field and conducted experiments with two membranes, namely, PRIMEA 5621 and PRIMEA 57. The authors found that PRIMEA 57 membrane performance was better than that of PRIMEA 5621 membrane. Suresh et al. [81] developed split serpentine flow channel configuration based on the enhancement of local cross-flow conditions and concluded that split serpentine flow field enhances cross flow, reduces total pressure drop, increases stoichiometric ratio and provides higher current as well as power.

A variation of serpentine design named as Enhanced Cross-flow Split Serpentine Flow Field (ECSSFF) was proposed by Suresh et al.[82] This field design was developed based on the splitting of the channel with enhanced cross-flow in selected regions that are more prone to localized flooding. The layout was designed in such a way that all the U-bends of the split serpentine channels were taken care by the nearest feeder channels. Its principal hydrodynamic features were demonstrated using CFD analysis in their study. It showed lower pressure drop, enhanced cross-flow along with better reactant distribution. However, the full scale fuel cell performance simulation study with the ECSSFF design was not performed. Saco et al. [69] numerically analyzed the performance of 225 cm2 active area PEMFC with the straight parallel, serpentine parallel, straight zig-zag, and serpentine zig-zag paths. The study revealed that, straight zig- zag design had better reactant consumption with uniform distribution of water on the electrolyte improving the proton conductivity. This design also offered less pressure drop compared to other designs used in their study. Chowdhury and Timurkutluk [70] modified the conventional single serpentine flow field into convergent and divergent design and investigated numerically. The modified convergent serpentine design was found to be superior compared to the divergent serpentine and conventional serpentine due to its ability to offer uniformity in current density, pressure distribution & oxygen

transport and also showed reduced water concentration in the CL. Their study indicated an increase of 2% better oxygen mass fraction and 3.3% reduction of water content at CL for the modified convergent serpentine flow field compared to conventional single serpentine. Manso et al [83] studied the influence of channel aspect ratio on the performance of fuel cell with serpentine flow designs. The results revealed that at low voltages it is insignificant while at high voltages the performance improved due to high mass transport velocity.

Chiu et al. [84] generated a 3-D numerical fuel cell model with parallel, interdigitated and serpentine flow fields to examine performance and transport phenomena. The authors also examined the influence of channel geometry and size on cell performance and water activity in the channels. The outcomes of the work revealed that decrease in channel height caused increase in water removal rate and decrease in cell performance and parallel flow channel width increase resulted drop in the cell performance due to low gas velocity with low water removal. Jang et al. [85] proposed spiral channels for PEM fuel cells and conducted both simulations and experiments to evaluate the performance of PEMFC using spiral and serpentine flow channels. The authors compared the spiral and serpentine channels results and found that the cell with spiral channel performs better than the cell with serpentine channel because of increased heat and mass transfer and reduced pressure drop in the channels. Sreenivasulu et al. [86] conducted experimental study on PEMFC with three types of flow fields (4-Serpentine, interdigitated and dual inlet and single outlet flow channel) to explore the effect of back-pressures on FC performance. The results indicated that highest PEMFC performance can be obtained using 4-Serpentine flow channel and with and without back-pressure. Additionally, the performance of twin inlet and single outlet flow channel PEMFC is better than interdigitated channel PEMFC at higher back pressures.

Liu et al. [87] conducted experimental study on single cell PEMFC and PEMFC stack to examine the influence of different flow field designs on performance. The study found that PEMFC with serpentine flow fields exhibited far better performance than other designs, while PEMFC with spiral flow field design exhibited the poor performance. Khazaee [88] conducted numerical and experimental investigations on 25 cm^2 active area PEM fuel cell to study the effect of rectangular, triangular and elliptical channel geometries on cell performance. Both numerical and experimental results reveal that PEMFC with rectangular geometry channel

performed better than cells with triangular and elliptical geometry channel. Torkavannejad et al. [89] developed circular, square and octagonal duct-shaped PEMFCs and analyzed their performance numerically. The results indicated that the performance of square duct shaped PEMFC is better than circular and octagonal duct shaped PEMFCs. Performance and flow characteristics of large-sized PEMFC (active area 300 cm^2) having branch channel were studied by Han et al. [53] through simulation and experiments. They compared the performance of branch channel (f=0.5) with serpentine channel and found that the performance of branch channel was similar to serpentine channel performance. In addition, they found that the pressure generated inside the branch channel was lower by 52.5% than serpentine channel.

Iranzo et al. [90] conducted experiments on PEMFC with multi-pass serpentine channel designs and examined the influence of channel orientation (horizontal and vertical) on liquid water distribution and cell performance. The results revealed that the fuel cell with horizontal channel orientation gives superior performance and prevents the blocking of flow channels with liquid water. Nguyen and Hyung [91] studied experimentally and numerically the influence of forced convection under the rib on fuel cell performance with two types of channel designs, viz., serpentine channel design with sub channel configuration and serpentine channel design with bypass configuration. It is observed from the results that serpentine channel configuration with sub channel and serpentine channel design with bypass channel permits more effective catalyst area utilization and also enhances the fuel cell power output. Li et al. [92] considered waved serpentine flow field (WSFF) channels for PEM fuel cells and studied numerically and experimentally the effect of WSFF on the performance of PEMFC. The results revealed that WSFF channel offered less pressure drop and exhibited better performance than conventional serpentine flow field (CSFF) channel. WSFF channel also enhanced the oxygen transport and liquid water removal.

Mahmoudimehr and Daryadel [93] numerically studied the rectangular cross sectional area of the cathode GFC of a PEM fuel cell to find the optimal dimensions. It was found that there are multiple optimal cross sectional dimensions for various operating conditions. They showed that the polarization curves for two different cross sections can intersect meaning that although one cross section may have higher maximum power, but it also may have lower average power compared to the other case. Furthermore, the most significant parameter

affecting the optimal cross section was found to be the relative humidity of the inlet gasses. Furthermore, Ahmadi et al. [94] investigated the effect of changing cross sectional area of the PEMFC (i.e. circular and elliptical cross sections) using analytical solution based on the perturbation method. They found that by changing the circular cross section to an elliptical one (i.e., increasing the value of perturbation parameter), the axial velocity increases and as a result, the penetration of species into the reaction areas decreases. They concluded that by converting the circular cross section to the elliptical one, while other conditions are fixed, the PEMFC produces less current density. The cathode flow-field design of a polymer electrolyte membrane(PEM) fuel cell is crucial to its performance, because it determines the distribution of reactants and the removal of liquid water from the fuel cell. Peng Liang et al. [95] developed 3-D finite element model to examine the result of coating, weld and dimensional error on contact resistance of a metal bipolar plate. From the results it is observed that 47% contact resistance led to reduction in case of dense weld arrangement and it was also observed that there was 14.5% increment in contact resistance when the dimensional error exceeds 30μm. In order to improve the efficiency of PEM Fuel cell

Sadeghifar et al. [96] presented a novel, net-shaped flat architecture with unique capabilities of PEM fuel cell. They showed that netlike design of PEMFC increases the active area significantly. The netlike design was constructed by bringing each channel that is in contact with electrodes. The new design was provided more uniform distribution of oxygen,water, temperature and current with lower size and the bipolar plate cost. **Wen et al.** [97] proposed an intersectant flow field on metal bipolar plate. To do this, optimization of the flow channel geometry using computational fluid ynamics (CFD) method was performed. They used the single serpentine flow field as the reference to evaluate the efficiency. They reported that optimal porosity and flow channel depth of intersectant flow field are 0.5 and 0.3 mm, respectively. **Ebrahimzadeh et. al.** [98] numerically and experimentally investigate the effect of obstacles along the gas flow field on the efficiency of the fuel cell. It has been observed that in cylindrical and trapezoidal obstacles in some areas of the flow field, the concentration of species has increased due to the formation of a stop area, which shows its impact on the produced current density. The obtained results show that the triangular obstacle has the lowest pressure drop and highest species consumption rate and current density and therefore, it has been selected as the best type of obstacle. **Elif Eker Kahveci and Imdat**

Taymaz [99] experimentally studied the effect of PTFE and Sio2 coatings on flow channels of a bipolar plates on the water management inside the fuel cell. Experiments were performed with single cell and stack with these materials and uncoated polymer composite bipolar plates at same operating conditions. The results showed that PEM fuel cell stack given the highest current and power density values when the fuel cell with the hydrophobic PTFE coated plates. But in hydrophilic fuel cell stack, no voltage and current values could be measured due to the sudden decreases due to excessive flooding of the flow channels.

Venkateswarlu et al [100] developed 3-D PEMFC model to investigate effect of operating temperature and relative humidity of reactants on the performance of the fuel cell with single serpentine flow fields configuration. It was observed from the results that the fuel cell power output increased with increase in cell operating temperature and relative humidity. The simulation results of fuel cell were compared with experimental results, and it was found that numerical results are in good agreement with the experimental results. **Liang He et al.** [101] designed and analysed the effect of S-shaped flow channels on the performance of PEM fuel cells. The results indicated that the small radius and large length are beneficial to the promotion of cell performance owing to the increased turbulence and decreased liquid water content in the cell, which is also proved by the electrochemical impedance spectroscopy (EIS).

2.4 Studies on PEMFC operating parameters

The performance of fuel cells is known to be affected by various cell operating and design parameters, for example, fuel cell operating temperature, operating pressure, humidification temperature of the reactant gases, fuel cell components dimensions, and shape. It is essential to be acquainted with the impact of these parameters on fuel cell operation to enhance the performance of the fuel cell. In this regard, it is helpful to recognize the operating conditions that offer the maximum possible power output with respect to the chosen current density. With regard to the current density, the operating conditions to attain the maximum power are different, and thus it is useful to know the complete operation map of the PEMFC. Fig. 2.1 shows the various design and operating parameters which affect fuel cell power output.

For safe and efficient operation of PEM fuel cells, the influence of operating parameters such cell temperature, gas humidification temperature, pressure, gas flow rate need to be studied and optimized in addition to design parameters such as dimensions of flow channel, membrane, catalyst loading, and gas diffusion layers. It is well known that both membrane dehydration and flooding can limit the cell performance, and hence it is very important to know the water and thermal management in a PEMFC and their effect on the cell's power output. Zhigang et al. [102] presented the process for membrane electrode assembly (MEA) activation of a PEMFC. Activation was done at elevated temperature and pressure to achieve improved cell performance. Berning &Djilali [103] developed a 3-D single-phase model of a PEMFC and studied the influence of operating and cell material parameters on the fuel cell performance. The study found that both cell operating temperature and pressure has positive influence on cell performance. Lin Wang et. al. [104] studied the effect of operating conditions on the power output of PEM fuel cell numerically and experimentally. Their results has shown that PEMFC performance improved with increase in working temperature of PEMFC. The performance of PEMFC decreased, whenever the RH temperature of the reactants crossed the fuel cell operating temperature.

Wang & Liu [105] conducted both experimental and numerical studies on a interdigitated flow field PEM fuel cell (50 cm^2) to investigate the influence of different cell temperatures, humidification temperatures, backpressures and mass flow rates on cell performance. The authors concluded that increase in cell temperature showed positive influence on cell performance when sufficient humidification was provided and negative influence when sufficient humidification is not provided. The authors also concluded that with the increase in the anode and cathode humidification temperature, operation pressure and reactant flow rate, the cell performance improves.

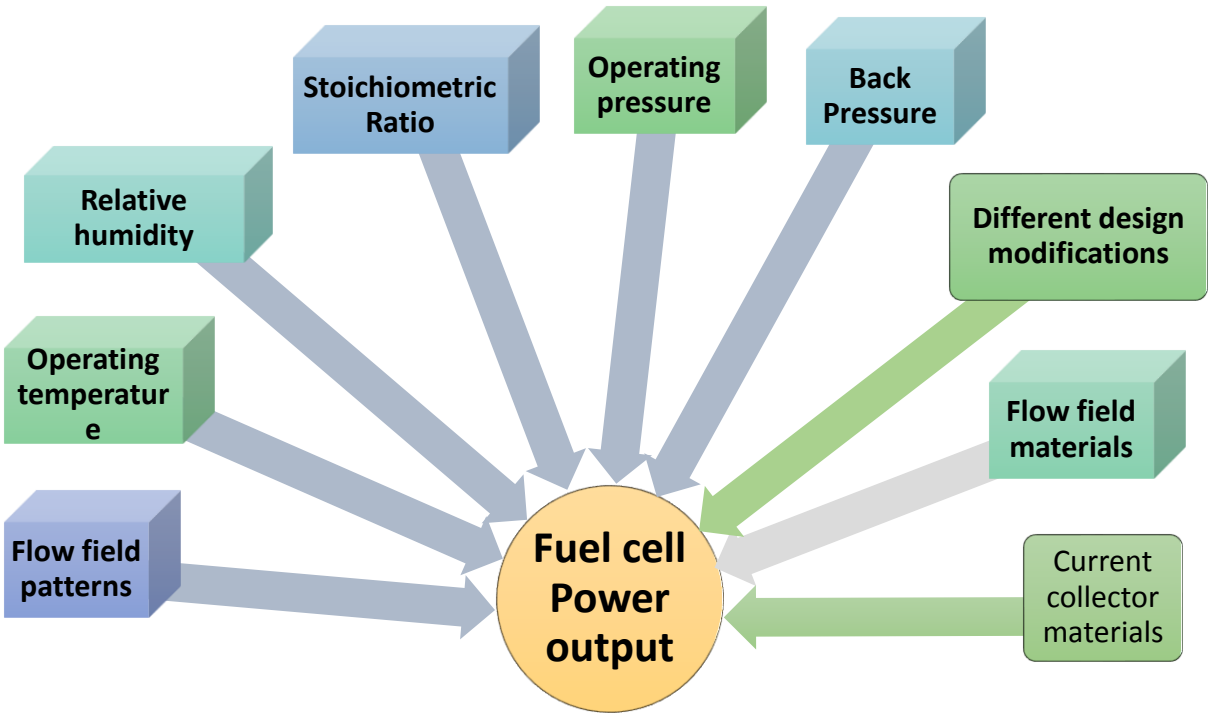

Fig. 2.1 Factors affecting the fuel cell output

Hsieh et al. [106] experimentally examined the impact of various range of operating temperatures and backpressure on a micro PEMFC performance with three dissimilar flow channel designs (interdigitated, mesh, and serpentine) and the author reported that increase in the temperature and backpressure caused enhance the fuel cell performance. Yan et al. [107] conducted experimental studies on 198.1 cm^2 active area PEMFC with different flow channel configurations to study the effect of flow field dimensions and working parameters on fuel cell performance. It is observed from the results that decrease in the cell performance with rise in the cell temperature (from 50 to 70◦C). The authors also observed that an increase in cathode humidification and cathode gas flow rate increase the FC performance. Owejan et al. [108] adopted neutron radiography imaging process for investigating the reactants distribution in the channels and the water accumulation in the gas diffusion layer (GDL). It was observed that both the surface property of the GDL and the channel design have considerable effect on the collected water volume and the water droplets surface morphology, which is retained in the channels. Water accumulation level in the flow channel was reduced by using Poly Tetra Fluoro Ethylene (PTFE) coating on the GDL.

Amirinejad et al. [109] conducted experiments on a 5 cm^2 active area PEMFC by varying operating conditions to study their influence on cell performance. The results indicated that temperature, pressure, and reactant humidity could drop mass transport limitations and increase the performance of FC. Yu et al. [110] carried out parametric analysis for a 25 cm^2 PEMFC performance using design of experiments (DOE). The study revealed that the operating pressure, operating temperature, and interaction between these two parameters have a noteworthy influence on FC performance. Yan et al. [111] conducted experiments with Core 5621 and Core 57 MEAs for a 256 cm^2 PEMFC to investigate the effect of operating temperature on FC performance. The authors found that the FC performance improved with an increase in cell temperature when the FC temperature is less than humidification temperature. On the other hand when the cell temperature is higher than humidification temperature, the FC performance decreased with increase in cell temperature.

Tohidi et al. [112] developed a 1-D, steady state and isothermal PEMFC model to investigate the influence of different parameters such as relative humidity, temperature, pressure, membrane thickness, and stoichiometric flow ratio of anode and cathode on FC performance. The authors reported that the cell performance improves with increase of operating pressure, temperature, anode and cathode stoichiometric flow ratio. The performance of FC can decrease by decreasing the relative humidity of inlet gases and increasing the membrane thickness. Wang et al. [113] designed two types of novel biometric flow channels and carried out simulation studies at various operating conditions. They found that biometric flow channels have better performance than parallel flow channels and serpentine flow channels due to novel biometric flow channels with high uniformity low distribution and strong ability to remove liquid. Guo at al. [114] designed a bio-inspired flow channel configuration for the fuel cell and observed that the designed flow field gives high power density when compared to conventional fuel cell designs. Changxing et al. [115] implemented the 3-step procedure for MEA activation of PEMFC. The temperatures were changed in a systematic process, and it led to enhance the cell performance.

Ting et al. [116] built a PEMFC using Au-coated Ni-foam as bipolar plate and studied the influence of operating parameters on cell performance. Among the operating parameters, the effect on cell performance, from most significant to least, is as follows: cell operating

temperature, cathode humidification temperature, cathode-gas stoichiometric ratio. Platinum (Pt) is a rare and costly metal; therefore reducing its loading without losing performance has always been the main goal. Both the electron transfer coefficient and exchange current density are platinum loading dependent. Chen et al. [117] numerically analyzed the impact of various bend angles and channel widths on the performance of PEMFC. The authors reported that the fuel cell with 60 deg and 120 deg bend angle combination attained peak performance due to the maximum utilization of reactants, specifically at low potential region.

Zahari & Aziz [118] studied the performance of PEMFC at different catalyst loadings (0.3, 0.35,0.40, 045 and 0.50 mg/cm^2). The authors obtained best fuel cell performance at 0.50 mg/cm^2 platinum loading in both anode and cathode. Okafor & Mogbo [119] also studied the performance of 50 cm^2 PEMFC at 0.5 mg/cm^2 and 1.0 mg/cm^2Pt loadings. The authors found that MEAs with 1 mg/cm^2Pt loading offered lower ohmic resistance, activation resistance, and total cell resistance than MEAs with of 0.5mg/cm^2Pt loading. Arvay et al. [120] carried out experimental work on PEMFC using nature inspired flow channel designs. It was identified that the performance of nature inspired flow channel was enhanced when compared to conventional designs because of uniform gas dissemination and uniform pressure. Karthikeyan et al. [121] proposed a numerical simulation model over 1-channel flow field with the help of COMSOL 4.2 software package. The influence of various operating parameters and geometric properties on performance of PEM fuel cell was studied. The outcomes revealed that the back pressure exerts extreme influence and at the same time the rib thickness also shows minimum influence on fuel cell performance. Guo et al. [122] designed a bio-inspired flow field configuration for the fuel cell. From the results it was noted that the bio-inspired channel design gave higher power density when compared with conventional channel designs.

Zenyuk et al [123] studied the influence of micro-porous layer on PEMFC performance. It was noticed that the water removal increases due to the presence of micro porous layer, which improves overall performance. Nannan Guo et al. [124] fabricated a bipolar plate using selective laser sintering technic, which reduces the fabricated cost and time due to great flexibility in design. They compared bio-inspired designs with parallel in series design, where the bio-inspired design enhances performance by 20%-25% at room

temperature. Meng et al. [125] studied the effect cathode platinum loading (0.1, 0.2 and 0.4 mg/cm^2) and backpressure (100, 150 and 200 kPa) on PEMFC performance. The results revealed that increase of Pt loading decreased the transport losses under the equivalent backpressure. They also reported that increase in the backpressure enhanced the cell performance, and this improvement in performance is more noticeable at a low Pt loading. Takalloo et al. [126] experimentally and numerically studied the influence of inlet gas humidification and inlet gas flow rate on the power density of a PEMFC. The presented results revealed that the power output of the PEMFC was enhanced with increase of reactants humidity at inlet due to reduced ionic resistance in the membrane. The fuel cell generated more power output with increase in the reactants flow rate at inlet to a particular level due to increase of diffusion capability of the reactants. Dilek et al. [127] performed an experimental analysis to examine the influence of working conditions on PEMFC performance. Their results indicated that the enhancement in the fuel cell performance was higher when the gas supplied on cathode side was humidified; similarly the PEMFC performance improved significantly with increase in the operating temperature and the gas inlet temperature.

Gazdzicki et al. [128] examined the impact of Pt loading on the performance and degradation of 19 cell PEMFC rainbow stack by varying the platinum in the range of 0.05–0.20 mg/cm^2 on anode and 0.15–0.40 mg/cm^2 on cathode. The study concluded that the cell performance is independent of anodic Pt loading for current densities up to 1.4 A/cm^2 and the performance drops significantly for cathodic Pt-loadings < 0.2–0.25 mg/cm^2 and for current densities ≥ 1.0 A/cm^2. Chowdhury et al. [129] developed a convergent-divergent type single serpentine flow channel and studied the effect of channel depth by means of inclination from inlet to outlet of the flow channel. The results exhibited that the power output of the cell improved by the addition of novel convergent serpentine channel in a bipolar plate.

Diankai et al. [130] introduced the fabrication process of metallic bipolar plates and investigated the effect of forming quality of a metallic bipolar plates with micro channels on performance of PEMFC. It was noticed that stamping force increases with increase in depth of a channel in a nonlinear manner and blank holder is needed to avoid wrinkles of a sheet in the forming process. Bin et al. [131] prepared various types of polytetrafluoroethylene(PTFE) layers and studied the influence of hydrophilic and hydrophobic layers on the performance of

the cell. It is noticed from the results that the fuel cell power output was enhanced by installing PTFE layers on the cathode catalyst layers. The PTFE layers plays a critical role for improving fuel cell power output; especially at low voltage region. Chowdhury and Bora [132] studied experimentally the effect of convergent and divergent flow channel configuration on fuel cell performance. From the results it can be shown that the design gives superior fuel cell power output due to uniform distribution of reactants.

Liu et al. [133] proposed a micro distributor for parallel flow channels to enhance the power output of the fuel cell and also maintain uniform distribution of reactants. The authors examined the effect of the size of micro distributor on the output of the fuel cell and also clearly analyzed pressure drop across flow channels. It is noticed from the results that the output of the fuel cell enhanced from minimizing the size of micro-distributor; The results of the fuel cell with modified parallel flow channel configuration with micro-distributor was compared with the fuel cell with single serpentine flow channel design; both designs gave almost the same performance. Venkateswarlu et al [134] conducted experiments as well as numerical simulation on conventional channels. The results show that 1-S flow channel design gives better performance compared with 2-S and 3-S flow channel designs under low flow rate conditions.

Ghanbarian et al. [135] investigated the impact of various design variables of a parallel serpentine flow channel such as channel width, channel height, rib thickness, number of turns and number of parallel channels on the fuel cell performance. Based on the pressure drop, even distribution of reactants and performance of a PEMFC, the authors gave a rank to all the designs. **González-Gutiérrez et. al** [136] studied the effect of aluminum AA6061 bipolar plates coated with electroless Ni-P on the performance of PEMFC. The electrochemical results indicated a higher resistance to corrosion and better performance in Ni-P/AA6061 samples with triple zincating when the solution was bubbled with H2. Tafel curve showed that for both environments (H_2 and O_2) the anodic slopes correspond to Ni oxidation and the cathodic slopes depend on the bubbling gas. An increase of current density and potential was observed when O_2 is used. Min et al. [137] proposed modified serially linked serpentine flow channel configurations for PEM fuel cells and analyzed numerically the effect of segment number and channel path number on fuel cell performance. It is noticed from the results that

the fuel cell with modified channel configuration generated more output power when compared with parallel serpentine channel configuration. Zhang et al. [138] studied the influence of land width and reactants flow rates on cell performance. The results have shown that PEMFC performance increases with decrease of land width and increase of inlet flow rates of reactants.

2.5 Research gaps identified from the literature review

- From the literature it is noticed that most of the researchers have concentrated on various conventional type flow channel configurations, optimization of various operating parameters and orientation of flow.
- Limited work is available on the optimization of flow channel width to land width ratio.
- Detailed analysis of optimization of rib thickness and channel width is a challenging task to improve the PEMFC performance and durability of the fuel cell.
- Most of the researchers have focused their attention on conventional flow field designs. Limited work is available on bio-inspired channel design of bipolar plate.
- Many of the researchers have focused on graphite bipolar plates with conventional designs. Few researchers attempted the PEMFC fitted with metal flow filed plates, but no work is find on graphene coated metal flow filed plates.

2.6 Objectives of the present research work

The objectives of the present work are

- To investigate the effect of land and channel widths of serpentine flow field on the performance of PEM Fuel Cell by using CFD analysis.
- To analyse the performance of PEM Fuel Cell using leaf, lung, bio-channel and compared with single serpentine flow field plates.
- To evaluate the effect of interdigitated, non-interdigitated, interdigitated with curved edges, and Murray' designs of leaf channel bipolar plates on fuel cell performance.
- To investigate the effect of bio-inspired metal flow field plates with different carbon based coatings on the performance of PEM Fuel Cell.

2.7 Novelty and highlights of the proposed work:

Novelty:

- Experimentally investigated the effect of bio-inspired flow field design on the performance of PEMFC at various ranges of operating parameters. Very little work is found in the literature on bio-inspired flow field design.

Highlights:

- Experimental study was carried out to analyse the performance of PEMFC with four different design modifications of a leaf channel, viz., Non-Interdigitated leaf channel design (NILCD), Interdigitated leaf channel design (ILCD), Interdigitated leaf channel design with curved edges (ILCDWCE) and Murray's design, under optimum operating conditions.

- Fuel cell with Murray's design channel gave the best performance among four modifications of the leaf channel, i.e., NILCD, ILCD, ILCDWCE and Murray's Design.

Chapter – 3

Methodology

3.1 Introduction

Dimensions of the flow channel design play an active role on the performance of a proton exchange membrane fuel cell (PEMFC). The main objective of the present study is to evaluate the PEM fuel cell performance by employing single serpentine flow channel with different land and channel widths on cathode side. Parametric study was done for the fuel cell with four channel dimensions by changing the operating temperature and flow rate of reactants on cathode. A complete three-dimensional PEMFC model was developed using ANSYS FLUENT-15.0 and simulations were carried out at 100% humidity conditions. The detailed description of the modelling equations and solution strategies along with the computational domains are discussed in this chapter.

3.2 Computational methodology

The design for proton exchange membrane fuel cell (PEMFC) is complex, since many input parameters influence the fuel cell performance, including: flow channel configuration, size of active membrane area, flow channel geometry, thickness of each component, and the material of gas diffusion layers, catalyst and membranes. In addition, the main physical and electrochemical processes taking place such as diffusion of input gases through gas flow channels, gas diffusion backing layers to catalyst layers deposited on Nafion membranes, electrochemical reactions that take place on catalysts, conductivity of protons (in the form of hydronium) through Nafion membrane, formation and removal of product water on oxygen side electrode, and the conduction of electrons through endplates and bipolar plates, and gas diffusion backing layers - all require many equations to describe theoretically. These equations usually can only be solved using numerical methods. Hence it is essential to have a multi-component computer simulation model, incorporating all the necessary theoretical equations, to model PEM cell performance.

Since lots of variable parameters need to be considered when developing PEM fuel cell designs, the effect of each parameter should be studied in order to develop the most suitable design to meet the demand. It would be prohibitively time-consuming and expensive to use experiments to test every possible design variation. Hence using numerical computer simulation models to simulate the performance of the fuel cell under a variety of input assumptions is of great benefit, and much more efficient in terms of time and costs.

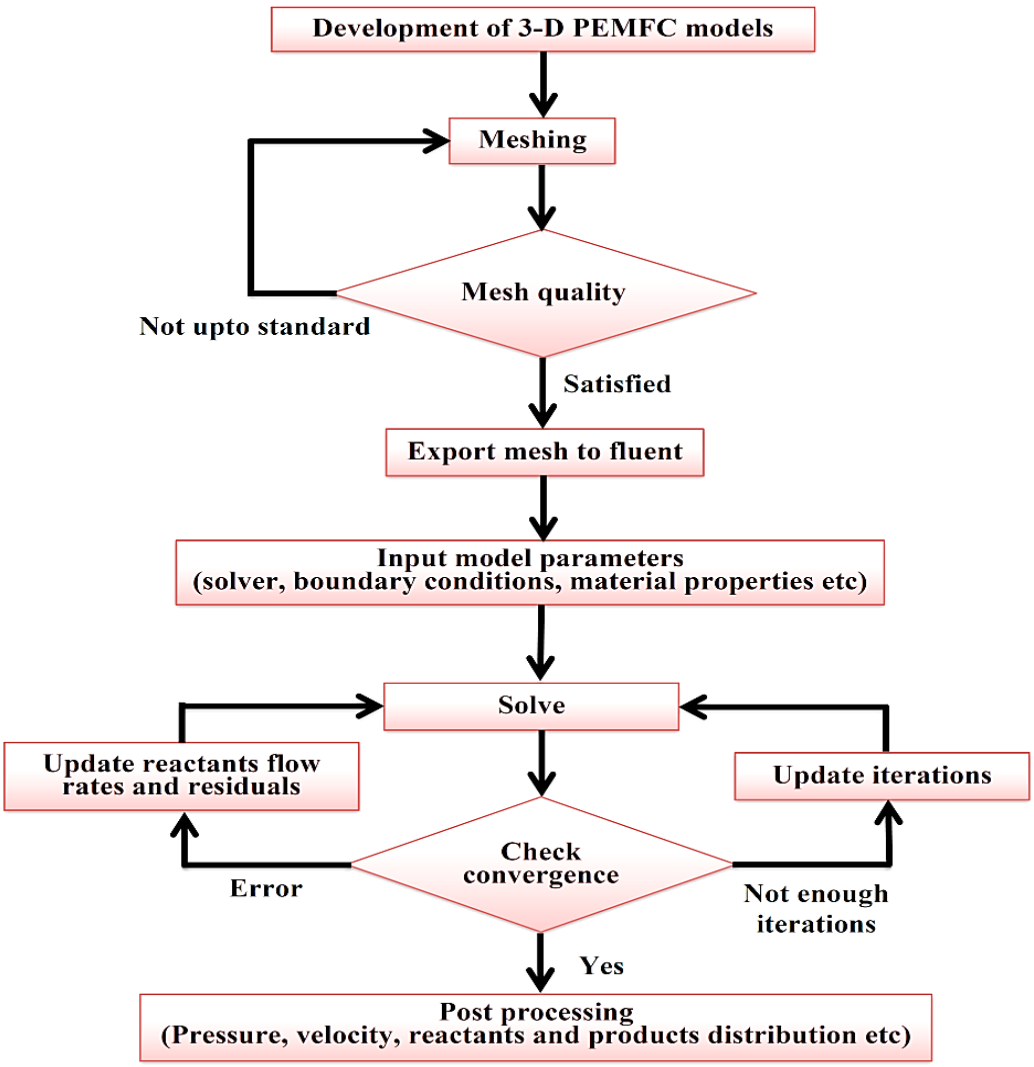

Fig. 3.1 Flow chart of computational methodology

Computational evaluation of a PEMFC performance comprises three major steps. First one is modeling the geometry of PEMFC by means of design software. The created geometrical model is the basis for creating a computational mesh. Second step is the generation of mesh for the created geometry. In order to solve the numerous governing equations associated with the PEM fuel cell simulations, the entire geometry is split into finite number of discrete volume elements or computational cells. The appropriate modelling equations are then solved in each single cell and then integrated over the computational domain to provide a solution for the entire cell domain. Generating a good mesh is one of the challenging steps. It needs a careful balance of generating adequate computational cells to capture geometry without exceeding the computational resources of the meshing computer.

The third and final step involves entering the various physical properties and operating parameters for the simulation. Some of these include electrical and thermal properties of the different cell parts, operating pressures and temperatures, open circuit voltage, inlet gas flow rates, porosity, and reactant humidification among many others. The flow chart of the computational methodology can be seen in Fig. 3.1.

3.2.1 Modeling assumptions

The flowing assumptions are made in this study:

1. The PEMFC is operating under steady state condition and its temperature is maintained at the operating temperature.
2. The pure form of hydrogen and air are used for the simulation and these gasses follow the ideal gas law.
3. Both the reactant gases flow in the laminar region in flow channels
4. They are incompressible due to low pressure gradients and small velocities.
5. Catalyst layers, gas diffusion layers and membrane are homogeneous and isotropic materials.
6. The membrane is impermeable to gasses i.e., there is no leakage current.
7. There are negligible contact resistance and minimum swelling of the membrane.
8. The products from the reaction are assumed to be in vapor phase.
9. The ohmic potential drop is very low in electrically conductive parts like bipolar plates, catalyst layers and gas diffusion layers.
10. The mass flow rate is constant at the inlet of the channel and channel outlet is at constant pressure.
11. In the gas flow channels, the liquid water droplets are assumed in fine mist form and hence liquid water velocity is equivalent to the gas velocity inside the gas channel.

3.2.2 Development PEM fuel cell models

The first step in the development of fuel cell model is modeling of individual parts of the fuel cell such as bipolar plate with different flow channel configurations, gas diffusion layer (for anode and cathode), catalyst layer (for anode and cathode) and a membrane (Nafion) by using SOLIDWORKS 2010. These parts have been assembled to get the complete

fuel cell assembly. The created geometry is imported to Design Modeler 15.0 for the generation of computational domain. The geometric dimensions of these components have been given in Table 3.1. The exploded view of PEMFC with proposed serpentine flow fields is shown in Figure. 3.2.

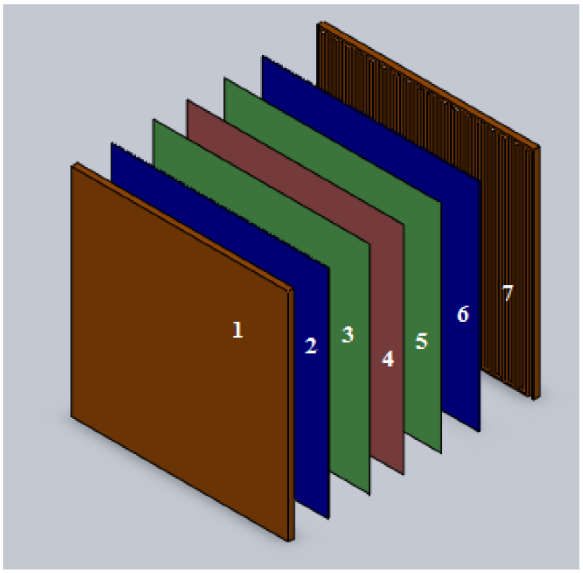

1. Anode flow field
2. Anode gas diffusion layer
3. Anode catalyst layer
4. Membrane
5. Cathode catalyst layer
6. Cathode gas diffusion layer
7. Cathode flow field

Fig. 3.2 Exploded view of three active area PEMFCs with serpentine flow fields

Table 3.1 Geometric dimensions of three PEM fuel cells

Cell	**Part**	**Length (mm)**	**Width (mm)**	**Height (mm)**
PEMFC 1 (70x70 mm^2)	Gas diffusion layers (GDL)	70	70	0.38[139]
	Catalyst Layer (CL)	70	70	0.05[139]
	Membrane	70	70	0.0175[140]
	Channels	70	1	1[141]
	Rib	--	1	1[140]
Single serpentine flow channel with four different land widths			1	0.5
			1	1
			1	1.5
			1	2
Single serpentine flow channel with four different land widths			0.5	1
			1	1
			1.5	1
			2	1

3.2.3 Computational mesh generation:

The second step is generating high quality mesh using ANSYS MESHER. The total fuel cell is divided into a number of mesh elements as shown in Fig. 3.3. Boundary conditions of the mesh are defined by named selections and naming conventions used are detailed in Table 3.2. The accuracy of the simulation results are greatly influenced by the mesh. Grid independence test is essential in CFD based simulations to optimize grid size and also to reduce the computational time as well as to save computer memory without compromising the solution reliability. In the current study, the test was conducted at 0.5 V and a set of operating conditions such as operating pressure of 1.5 bar, mass flow rates of hydrogen on the anode and oxygen on the cathode being 4.287 e-7 kg/s and 0.001429 kg/s, operating temperature of 70 ^{o}C and relative humidity (RH) of the reactants being set at 100 % were considered.

Table 3.2 Naming conventions for the boundaries

Surface function		**Named surface**
Anode flow channel	Outlet	Pressure_outlet_a
	Inlet	Mass_flow_inlet_a
Cathode flow channel	Outlet	Pressure_outlet_c
	Inlet	Mass_flow_inlet_c
Cathode side electrical contact		Terminal_c
Anode side electrical contact		Terminal_a

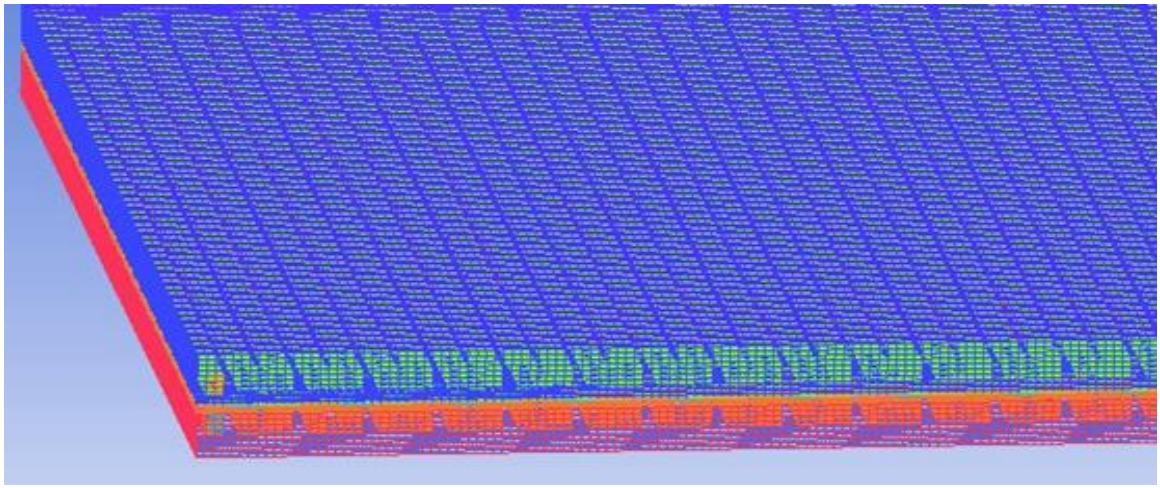

Fig. 3.3 Computational mesh of 2-S PEMFC

3.2.4 Grid independence test:

Three different mesh sizes such as 0.41 million, 1.58 million and 2.85 million were selected for this test. It is observed from fig. 3.6 that the difference in power density is about 13.5 % when the grid size is increased from 0.41 million elements to 1.58 million elements, whereas the variation in power density is only 0.8 % when the grid size is increased from 1.58 million elements to 2.85 million elements. This reveals that the simulation results do not vary much when the number of elements is increased beyond 1.58 million. So in order to reduce computational time, the mesh with 1.58 million elements was chosen for the rest of simulations in the current work.

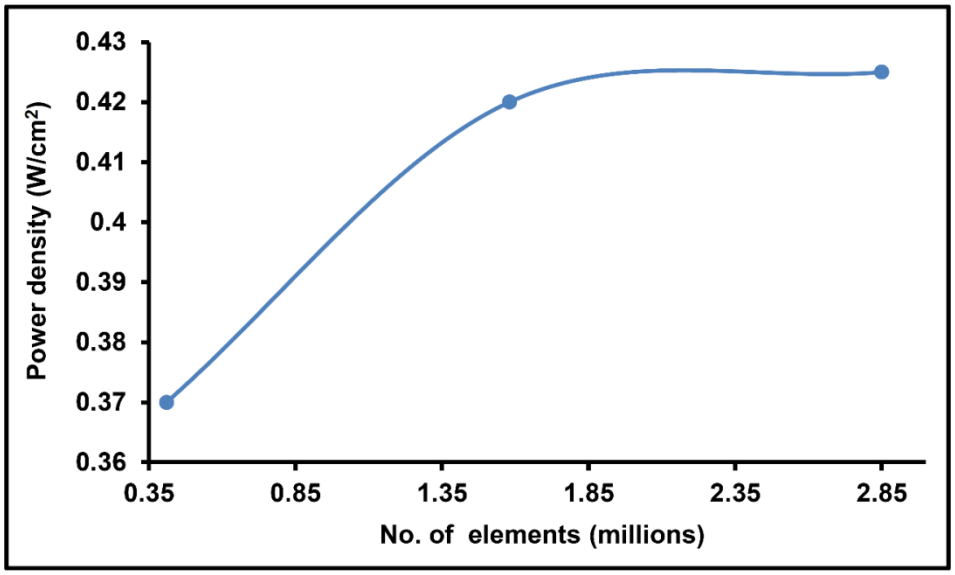

Fig. 3.4 Grid independence test

The third step is to define the boundary parameters with thermo-physical properties and operating conditions of the PEM fuel cell for solving the reaction kinetics. Some of these include operating pressures and temperatures, heat flux rates, reactant flow rates, resistances and load. These parameters are not fixed and these will be changed with the type of simulation and the materials used. The various modelling options incorporated in the simulation include reaction heating, joule heating, Butler-Volmer rate, electrochemistry sources, multiphase, membrane water transport, multi-component diffusion and anisotropic e-conductivity in porous electrode. A detailed computational procedure is given below.

3.2.5 Solver

The PEM fuel cell comprises of different physics involving coupled phenomena, which include mass transport of species such as hydrogen, oxygen, water and nitrogen, heat transfer, electrochemical reactions and fluid flow. These phenomena are modelled as partial differential equations describing species, energy, mass conservation, electrical charges and momentum. A three dimensional, multi-phase, multi-component, laminar flow through the computational domain containing different parts of the PEM fuel cell is studied using an inbuilt fuel cell module in ANSYS® 15.0 to analyse the cell performance. A rigorous 3-D computational fluid dynamic modelling methodology, which solves species transport equations, Navier-Stokes equations, mass and energy conservation equations and electrical potential equations coupled with the Butler–Volmer (BV) equations to define electro-chemical reactions on the surface of catalyst is used in this study [142]. The effect of various operating parameters on the cell performance is studied. The effect of pressure drop is also realized in present work to make the results more relevant to actual operating conditions.

Serial processing and double precision were chosen for the present model. The simulations were performed using a High-End workstation (64 GB RAM and 3.10 GHz CPU).

Governing equations

The following steady state transport equations are solved in this computational study:

- **Continuity equation**

The continuity equation with source term is given by:

$$\nabla . (\rho \vec{v}) = S_m \quad (3.1)$$

$\vec{v}$ represents the fluid velocity vector; and S_m represents the species source term

- **Momentum equation**

The momentum equation with source term is given by:

$$\nabla.(\rho \vec{v} \vec{v}) = -\nabla p + \nabla.(\mu^{eff} \nabla \vec{v}) + S_p \quad (3.2)$$

μ represents the viscosity, p represents pressure and ρ represents density.

S_p is the source term

$$S_p = -\left(\frac{\mu}{k}\right) \vec{v} \quad (3.3)$$

Where k represents the permeability of CL and GDL, and μ represents the viscosity

- **Energy equation**

The steady state energy equation is expressed by

$$\nabla.[\vec{v}(\rho E + \mathrm{p})] = \nabla.\left(k_{eff}\nabla \mathrm{T} - \sum_i h_i \vec{J}_i\right) \quad (3.4)$$

Where E indicates total energy, k_{eff} indicates effective conductivity, and $\vec{J}_i$ represents the flux diffusion of the species.

- **Species equation**

The species equation for mass fraction of each species y_i is given by:

$$\nabla.(\rho\vec{v}y_i) = -\nabla.\vec{J}_i + \mathrm{Si}. \quad (3.5)$$

Si indicates the source term and $\vec{J}_i$ indicates the flux diffusion.

Flux diffusion is obtained by:

$$\vec{J}_i = -\rho \mathrm{D_i}\nabla.y_i \quad (3.6)$$

Where D_i is the diffusion coefficient

Electrochemical equation

The electro chemical equations are applied by enabling the fuel cell add-on module available in ANSYS software. The equation governing the electron transfer between CL & GDL and between MEA & CL is given by equation (3.7) and (3.8) respectively

$$\nabla.(\sigma_{sol}.\nabla\phi_{sol}) + R_{sol} = 0 \quad (3.7)$$

$$\nabla.(\sigma_{mem}.\nabla\phi_{mem}) + R_{mem} = 0 \quad (3.8)$$

Where, σ—indicates ionic conductivity (ohm−1 m−1), ϕ represents cell voltage (V), and R indicates transfer current (A).

The current density generated on the electrode surface is obtained by using Butler- Volmer equation and can be expressed as follows:

$$R_{an} = J_{an}^{ref}\left(\frac{H_2}{H_{2,ref}}\right)^{\gamma_{an}}\left[exp\left(\frac{\alpha_{anF}\eta_{an}}{\bar{R}T}\right) - exp\left(\frac{\alpha_{caF}\eta_{an}}{\bar{R}T}\right)\right] \quad (3.9)$$

$$R_{ca} = J_{an}^{ref}\frac{O_2}{O_{2,ref}}^{\gamma_{ca}}\left[-exp\frac{\alpha_{anF}\eta_{ca}}{\bar{R}T} + exp\frac{-\alpha_{caF}\eta_{ca}}{\bar{R}T}\right] \quad (3.10)$$

$$\eta_{an} = \phi_{sol} - \phi_{mem} \quad (3.11)$$

$$\eta_{ca} = \phi_{sol} - \phi_{mem} - V_{OC} \quad (3.12)$$

Where J_{ref} represents exchange current density (A/cm2), H2/H2, ref indicates local species concentration, γ represents concentration coefficient, α indicates transfer coefficient, η

represents the activation losses, F represents Faraday's constant (96, 485 C mol−1), and R represents the universal gas constant 8.314 kJ/kg mol K.

Liquid water transport equation

The operating temperature of a PEM fuel cell is below 100°C. At high current densities, the tendency of the produced water vapour to condense and form liquid water is highly predominant. The formation of liquid water during the electrochemical reaction is obtained by the governing equation[143].

$$\frac{\partial(\varepsilon\rho_l S)}{\partial t} + \nabla\left[\rho_l \vec{V}_{lS}\right] = r_w \quad (3.13)$$

Where, r_w represents the condensation rate, and lis the liquid water.

$$r_w = c_r\left(\left[(1-s)\frac{P_{wv}-P_{sat}}{RT}M_w H_2 o\right] - S_{\rho_l}\right) \quad (3.14)$$

Membrane model

The proton conductivity (σ_{mem}) through the porous electrolyte due to electro-osmotic drag is a function of membrane water content (λ) and is evaluated by using the correlations provided by Springer et al.[144].

$$\sigma_{mem} = (0.00514\lambda - 0.00326)e^{1268\left(\frac{1}{303}-\frac{1}{T}\right)} \quad (3.15)$$

$\lambda = 0.043+17.81a-39.84a2 +36a3$ for $(0< a \leq 1)$ (3.16)

$\lambda = 14 + 1.4(a-1)$ for $(a > 1)$ (3.17)

3.2.6 Computational procedure

The simulation setup is initiated by loading fuel cell module. This is accomplished by typing the following command into the Text User Interface (TUI) and pressing Enter key.**//define/models/addon-module/3.** Once the module is loaded, it is important to test the mesh with default settings first. The basic parameters have to be set first. The basic parameters used in the simulation as given in table 3.3. Operating parameters used in the simulation are given in table 3.4. Further explanation on the procedure to perform the computations is provided in Appendix – 1.

Table 3.3 General parameters used in the simulation model[145]

Model Parameter	Value	Model Parameter	Value
Reference exchange current density at anode (A/m^2)	$4.48e^5$	Equivalent weight of membrane (kg K/mol)	1100
Reference exchange current density at cathode (A/m^2)	4.48	Membrane proton conduction coefficient	1
Anode Charge transfer coefficient	1.0	Membrane proton conduction exponent	1
Cathode Charge transfer coefficient	1.0	S/V (surface to volume) ratio of a Catalyst layer (m^{-1})	$1.25e^7$
Anode Concentration exponent	0.5	GDL electric conductivity ($\Omega^{-1}m^{-1}$)	280
Cathode Concentration exponent	1.0	Gas diffusion layer porosity	0.82
Open circuit voltage	0.98	Anode GDL viscous resistance (m^{-2})	10^{12}
H_2 diffusivity (m^2/s)	$8e^{-5}$	Cathode GDL viscous resistance (m^{-2})	$3.86e^{12}$
O_2 diffusivity (m^2/s)	$2e^{-5}$	Permeability of the GDL and catalyst layer (m^{-2})	$5.68e^{10}$
H_2O diffusivity (m^2/s)	$5e^{-5}$	Electric conductivity of the bipolar plate ($\Omega^{-1}m^{-1}$)	92,600

Under the **parameters** tab, key properties given in Table 3.5 are applied. Then, under the **anode** tab, current collector, GDL and CL are assigned for the anode. Similarly, current collector, GDL and CL are for cathode, under **cathode** tab. Under the **electrolyte** tab, electrolyte (membrane) is assigned for the cell. Finally, under the **reports** tab, anode and cathode terminals are assigned. Under the same tab, electrolyte projected area in m^2 (the fuel cell active area) also given.

Table 3.4 Operating parameters used in simulation

Specifications	Value
Mass fraction ($H_2/O_2/H_2O$) on anode	**0.6029271 / 0 / 0.3970728**
Mass fraction ($H_2/O_2/H_2O$) on cathode	**0/0.9601614 / 0.03983856**
Operating pressure (Pa)	101325
Operating temperature (K)	333
Mass flow rate on anode side (cm^3/min)	300
Mass flow rate on cathode side (cm^3/min)	600

Table 3.5 Crucial properties used in the simulation

Parameter	**Value**
Reference concentration at anode and cathode	1 kmol/m^3
Reference current density at cathode	20 A/m^2
Reference current density at anode	10000 A/m^2
Membrane equivalent weight	1100 (g/mol)
Porosity of GDL	0.5
Porosity of CL	0.5

To control the solution, under-relaxation factors are also used and here in this work under-relaxation factor was adopted as 0.3 for momentum, 0.7 for pressure and 0.95 for H_2, O_2, H_2O and water saturation. The boundary conditions that must be set are the outlets for anode and cathode flow channels, inlets for anode and cathode flow channels, and anode and cathode terminals. To set inlet mass flow rate on anode and cathode, under the **momentum** tab, the inlet mass flow rate of hydrogen was fixed according to the current to be drawn. Similarly, on cathode side also, oxygen flow rate was fixed. Under the **thermal** tab, the temperature was set as 333K. This is a typical operating temperature of the fuel cell. Under the **species** tab, the species concentration on the anode side of **H_2, O_2,** and **H_2O** were set as **0.6029271, 0,** and **0.3970728**, respectively. On the cathode side **H_2, O_2** and **H_2O** were set as **0, 0.9601614** and **0.03983856**, respectively. These values correspond to a 100% humidified inlet gas. Next, pressure outlet of anode and cathode is set as shown in Appendix-1. Finally, anode electric potential (anode terminal voltage) is set as 0 V (Zero) and cathode electric potential (cathode terminal voltage) is varied from 0.1 to 0.9 V as shown in Appendix-1. The convergence criterion was set at 10^{-6} to ensure the accuracy of simulation results. The simulation work was carried out on a HP workstation having Intel Xeon processor with 32 GB of RAM and 2.40 GHz CPU clock speed, running on Windows 7 Operating System.

3.3 Experimental methodology

The PEM fuel cell with an active area of 49 cm^2 is used in the current study. All fuel cell elements with customized specifications are fabricated with the help of M/s. Vinpro Technologies, Hyderabad.

3.3.5 Materials

The main components of PEMFC include flow field plates (single serpentine channel, lung channel, Bio-channel, non-interdigitated leaf channel (NILCD), interdigitated leaf channel (ILCD), interdigitated leaf channel with curved edges (ILCDWCE), Murray's design), end plates, copper current collector plates, SS-316L current collector plates and gaskets. Thick rubber washers act as insulators, to stop electron transfer to end plates from current collectors and flow field plates. The flow field plate has one inlet and outlet. The fuel cell assembly is subjected to uniform compression by torque wrench.

Membrane Electrode Assembly (MEAs)

The membrane electrode assembly (MEA) of (Nafion™ 212) with an approximate thickness of 50 μm was used in the experimentation. Platinum was used as catalyst, as it can be coated on both sides of membrane with a loading of 0.4 mg/cm^2 on anode side 0.6 mg/cm^2 on cathode side which is demonstrated in Fig. 3.5. The carbon paper having has a thickness of 230 μm acts as gas diffusion layer which is coated with 30% PTFE by weight.

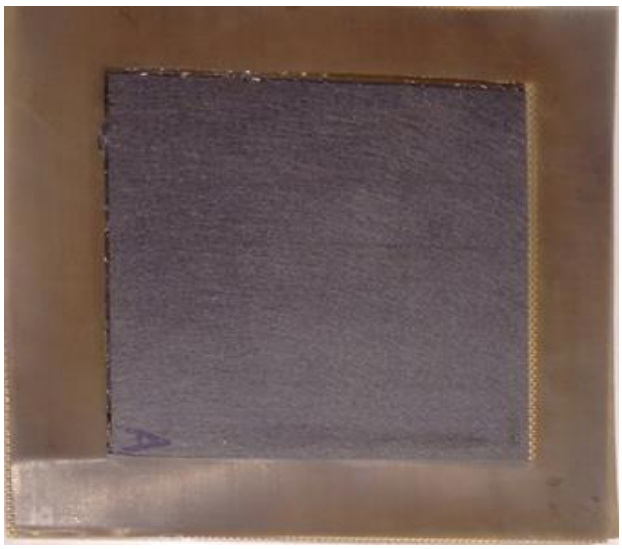

Fig. 3.5 Membrane electrode assembly (MEA)

End plates

Aluminum end plates were used in this study as shown in fig. 3.6. Holes were provided to end plates, which are identical to those in flow field plates and current collector plates. The thickness of the end plate should be adequate to with stand the shear stress at the bolts without deflecting the plate, because excess deflection of the end plates will result in poor sealing of the cell. The desired physical properties of the end plate are as follows: excellent electrochemical stability, low density, high electrical insulation, high mechanical strength, easy to machine and stiffness. Therefore, Aluminum alloy 6061 was used to meet the functional requirements of the endplates, because of its high thermal conductivity (180 W/m.K), high strength (125 MPa tensile strength), and its affordability cheap when compared to other aluminum alloys. The most commonly used materials are titanium, aluminum, and stainless steel alloys.

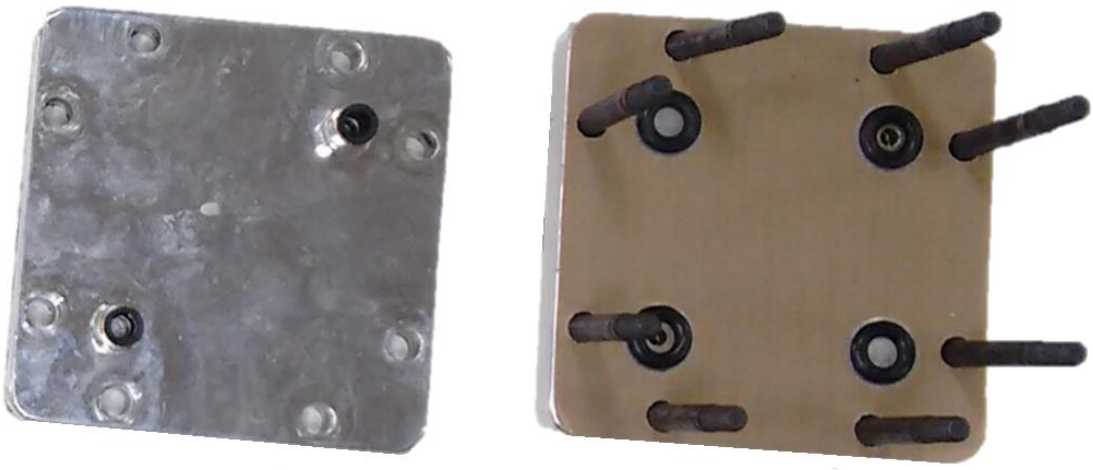

Fig. 3.6 End plates of the fuel cell

Flow Field Plate

Different types of flow field plates (FFPs) such as single serpentine flow channel design (SSFCD), lung channel design, bio channel design, Non-Interdigitated leaf channel design (NILCD), Interdigitated Leaf Channel Design (ILCD), Interdigitated Leaf Channel Design With Curved Edges (ILCDWCE) and Murrey's design are used in this study and these FFPs are made of graphite. The figures corresponding to these flow fields and the dimensional details are provided in the respective chapters. Due to desirable properties of the graphite material it is selected even though it is brittle.

Current Collector

Copper electrical/current collector plates used in this study is shown in Fig. 3.7. The plates are designed in house and fabricated in Engineering Machine Shop. It is made from C15720 copper, which contains 99.6 wt% (weight) copper. Copper provides both excellent thermal and electrical conductivities with 353 W/m.K and 89 S/m at 20 ^{o}C, respectively. The current collector is secured to the endplate via thick sheet of rubber. The rubber gasket is applied between these two plates to insulate the plates while providing proper sealing for the inlet and outlet flow reactants. Rings of silicon were used to seal the reactant flow between the current collector and the flow field plate. Two holes are drilled on opposite corners for the reactant supply, and four small holes were drilled for locating dowel pins.

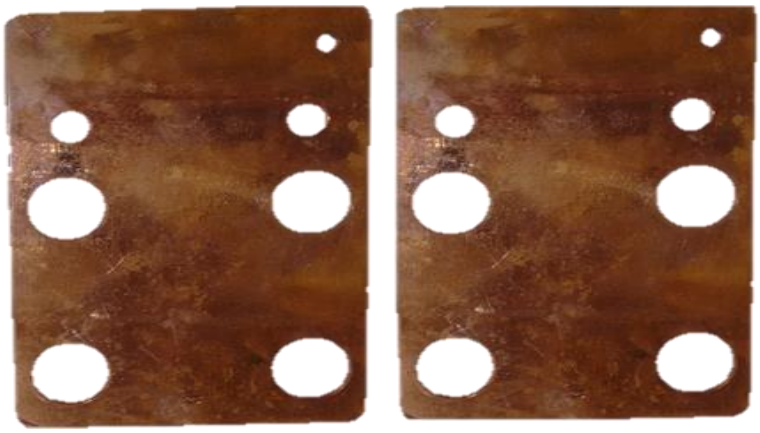

Fig. 3.7 Current collectors

PEM fuel cell test station

The experimental investigations are carried out on single PEM fuel cell with the help of programmable SMART2 Fuel Cell Test Station (make WonATech Co Ltd, Korea) which is available in the Centre of Excellence (CoE) at the Department of Mechanical Engineering, NIT Warangal. The fuel cell test station has the provision to vary the reactants mass flow rate, FC & humidification temperatures and back pressure on both the anode and cathode sides. Back-pressures are controlled using backpressure regulators. This test station is equipped with data acquisition system and computer-based control. The mass flow rates, humidification temperatures and cell temperature are set at desired value and which are read through the software called WFTS™. The FC polarization curves are obtained from this system in

conjunction with the Electric Load on the cell, which measures the voltage against the current response. The schematic of the SMART2 Fuel Cell Test Station is shown Figures 3.8.

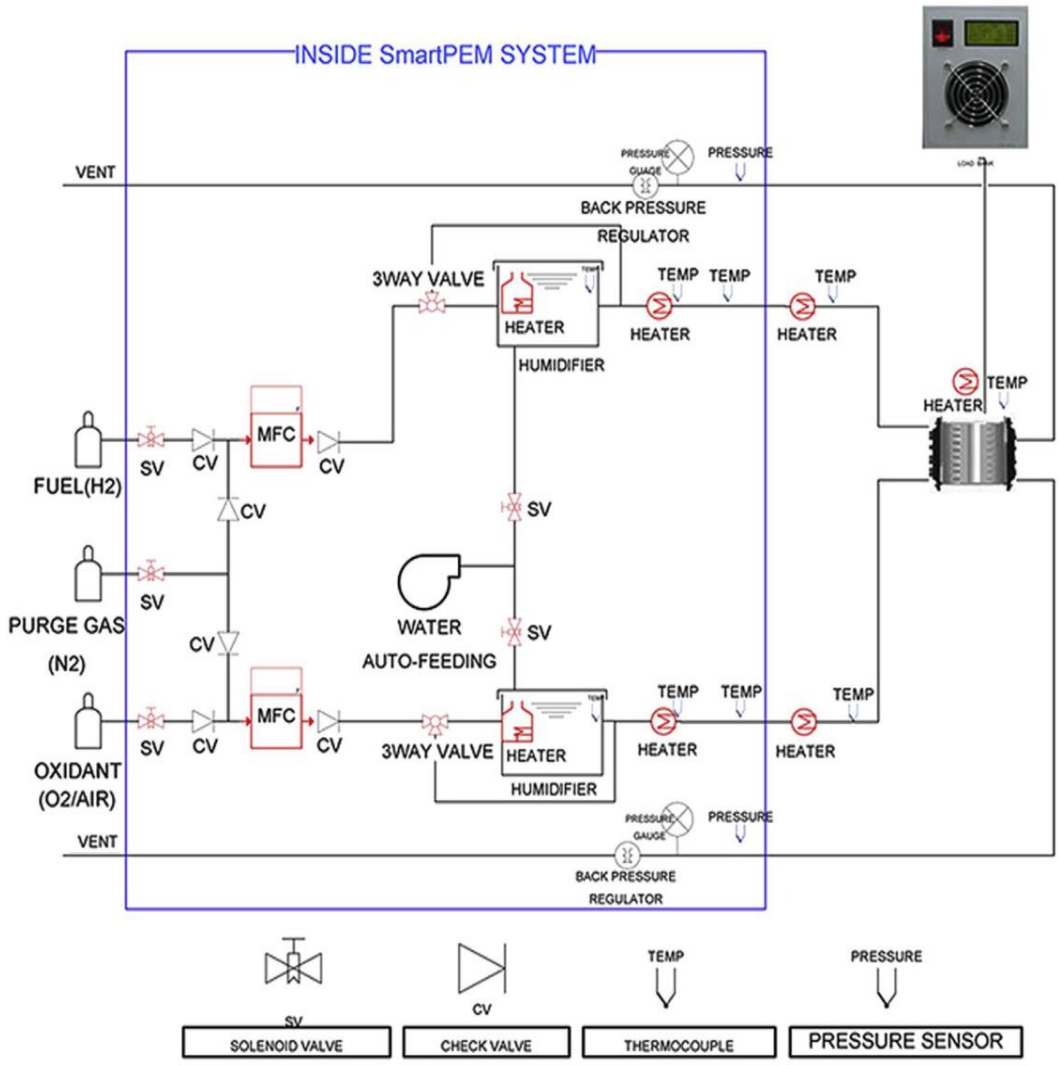

Fig. 3.8 Schematic of PEMFC test station

3.3.6 Activation of MEAs

Prior to conduct the experiments on the cell, the MEAs of fuel cell need to be activated. Activation of MEAs is carried out at cell temperature of 70^{o}C. Hydrogen and oxygen humidification temperatures also set at 70°C. During the activation, the fuel cell performance is recorded for every 30 minutes. When no further increase in performance is observed, it indicates that, the MEA is activated.

3.3.7 Experimental procedure:

The procedure for the experimentation on the fuel cell is given below:

- The Test Station is switched on and the gas cylinders valves are turned on in such a way that they release hydrogen, nitrogen and oxygen.
- The distilled water level in the storage tank of the test station is checked for better humidification.
- Prior to the experiments, the cathode and the anode of the fuel cell are purged of impurities by supplying nitrogen gas.
- The operating parameters such as the mass flow rate of the reactants, humidification temperatures of the cathode and the anode, the fuel cell temperature and the back pressure are adjusted by using the inbuilt software of the FCTS interface. The procedure to set mass flow rate and humidification temperature via FCTS interface is provided in Appendix -1.
- The voltage limit and stepwise increment of voltage in the test software interface are set.
- The time delay is to be set between every two data points in a polarization curve in the software interface. The appropriate delay between every two data points is chosen to ensure that at each point, the voltage and current is obtained when the fuel cell reaches a relatively steady state.
- Start the computer program to automatically control the experiments and collect the data.

The fuel cell is disconnected from the test station and dismantled. Again PEM fuel cell is reassembled by changing flow field design. The above experimental procedure is repeated for all the configurations.

Uncertainty analysis

There will be certain level of uncertainty with in the experimental results due to uncertainty in the measurements. Hence, uncertainty analysis is reported along with the experimental results. A detailed analysis of possible uncertainty for the FCTS was provided by the manufacturer [24] given in the Table. 3.

Table 3.6 Summery of parameter uncertainty for SMART2 fuel cell test station

Parameter	Range	Uncertainty
MFC (sccm)	10-20000	± 1.00% full scale
Voltage (V)	0-10	± 0.5 %
Temperature (^{o}C)	-200 to 1300	± 0.75 %
Current (A)	0-100	± 0.5 %
Pressure (Kpa)	0-350	± 3 Kpa

Experimental studies require performing uncertainty analysis to investigate the usual propagation of errors in the instrumentation. To estimate the uncertainties on the dependent variables such as current density (i) and power density (P_d) a propagation of error method is employed (uma et.al.2019). The application of this approach for estimating uncertainties of the dependent variables is explained below.

$$\text{Current Density, } i = \frac{I}{A} \tag{3.18}$$

Where I: current (A) and A : Active area of the fuel cell (cm^2)

Uncertainty pertaining to current, I = $\pm$0.5 %

Uncertainty pertaining to active area, A = $\pm$1 %

Uncertainty of the current density (∂i) is expressed as

$$\frac{\partial i}{i} = \left[\left(\frac{\partial i}{\partial I}\omega_I\right)^2 + \left(\frac{\partial i}{\partial A}\omega_A\right)^2\right]^{1/2} \tag{3.19}$$

Where ω_I: uncertainty of the current and ω_A: uncertainty of the active area of the fuel cell

Power Density, $P_d = \frac{V\,I}{A}$ (3.20)

Uncertainty pertaining to voltage, V = $\pm$0.5 %

Uncertainty pertaining to current, I = $\pm$0.5 %

Uncertainty pertaining to area, A = $\pm$1 %

Uncertainty of the power density (∂P_d) is expressed as

$$\frac{\partial P_d}{P_d} = \left[\left(\frac{\partial P_d}{\partial V}\omega_V\right)^2 + \left(\frac{\partial P_d}{\partial I}\omega_I\right)^2 + \left(\frac{\partial P_d}{\partial A}\omega_A\right)^2\right]^{1/2} \quad (3.21)$$

Where ω_V: uncertainty of the voltage

Chapter - 4

Simulation Results and discussion

Effect of land and channel widths of serpentine flow field on the performance of PEM Fuel Cell by using CFD analysis

4.1 Introduction

Dimensions of the flow channel design play an active role on the performance of a proton exchange membrane fuel cell (PEMFC). In this study, a single serpentine flow channel with four different channel widths and four different rib thickness was selected to evaluate the effect on the performance of PEMFC. A complete three-dimensional PEMFC model was developed using ANSYS FLUENT-15.0 and simulations were carried out at 100% humidity conditions. Parametric study was done for the fuel cell with four channel dimensions by changing the operating temperature and flow rate of reactants on cathode.

4.2 Results and discussion

Fuel cell performance depends mainly on rib thickness and width of the flow field design. Optimum flow channel dimensions improve mass transport of reactants and enable better water removal from reaction sites. Similarly, optimum rib thickness enhances electric conduction. Thinner land width restricts electron transport whereas wider land enhances electron transport and also heat transfer in the fuel cell [18], [19].

4.2.1 Effect of rib thickness / land width on the performance of PEMFC

The single serpentine flow channel with different Land width configurations is shown in Fig. 4.1. Simulations were done for PEMFC with different land widths at various ranges of operating temperatures and different range of flow rates of reactants. The performance of PEMFC is shown in terms of polarization curves (I-V curves) and the power curves (I-P curves) as discussed in the following sections.

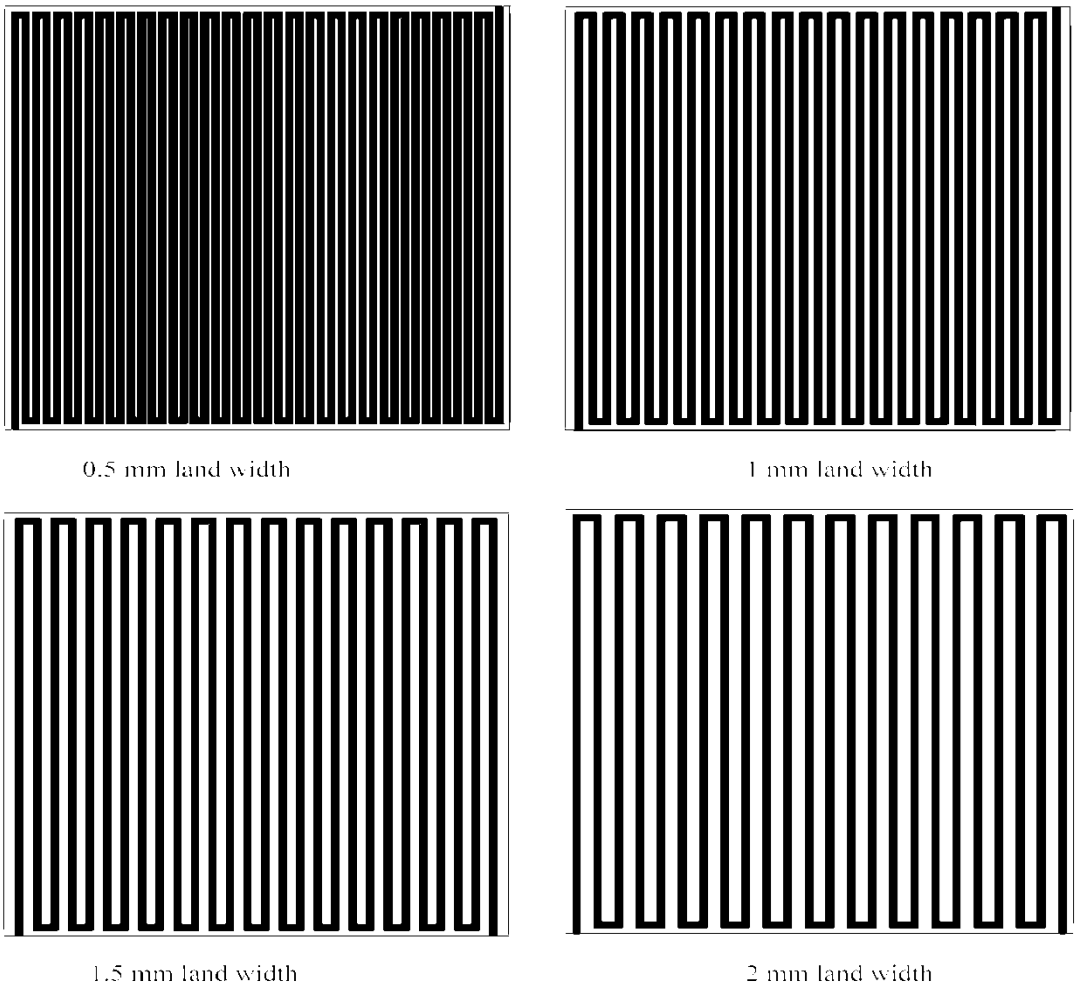

Fig. 4.1 Single serpentine flow channel with four different land widths

4.2.1.1 Effect of fuel cell operating temperature

The influence of operating temperature on the performance of PEMFC for various rib thicknesses/ land widths is shown in Fig. 4.2. The operating parameters such as oxygen and hydrogen mass flow rates were taken as 0.001429 kg/s and $4.287e^{-7}$ kg/s, operating pressure was taken as 1 bar, with 100 % humidity conditions [151] such as anode species concentration hydrogen (H_2), oxygen (O_2), and humidity (H_2O) are taken as 0.6029271, 0, and 0.3970728, and cathode species concentration hydrogen (H_2), oxygen (O_2), and humidity (H_2O) are taken as 0, 0.9601614 and 0.03983856, respectively. In the present work the rib thickness was varied from 2 mm to 0.5 mm insteps of 0.5 mm, and the channel width was kept constant at 1 mm. I-V and I-P curves of the fuel cell with various rib thickness at different fuel cell operating temperatures ranging from 323 K to 353 K are shown in Fig. 4.2.

From Fig. 4.4 (a) it is observed that the fuel cell performance was increased from minimizing the rib thickness. As the rib thickness decreases from 2 mm to 0.5 mm, the power output of the cell increased due to rise in reaction area, uniform distribution of reactants and forced convection under the rib section. But the narrow land-width having high electrical resistance during conduction of electrons. From the results it is observed that the fuel cell with 0.5 mm land width gives better performance among all the flow channel configurations without considering parasitic losses.

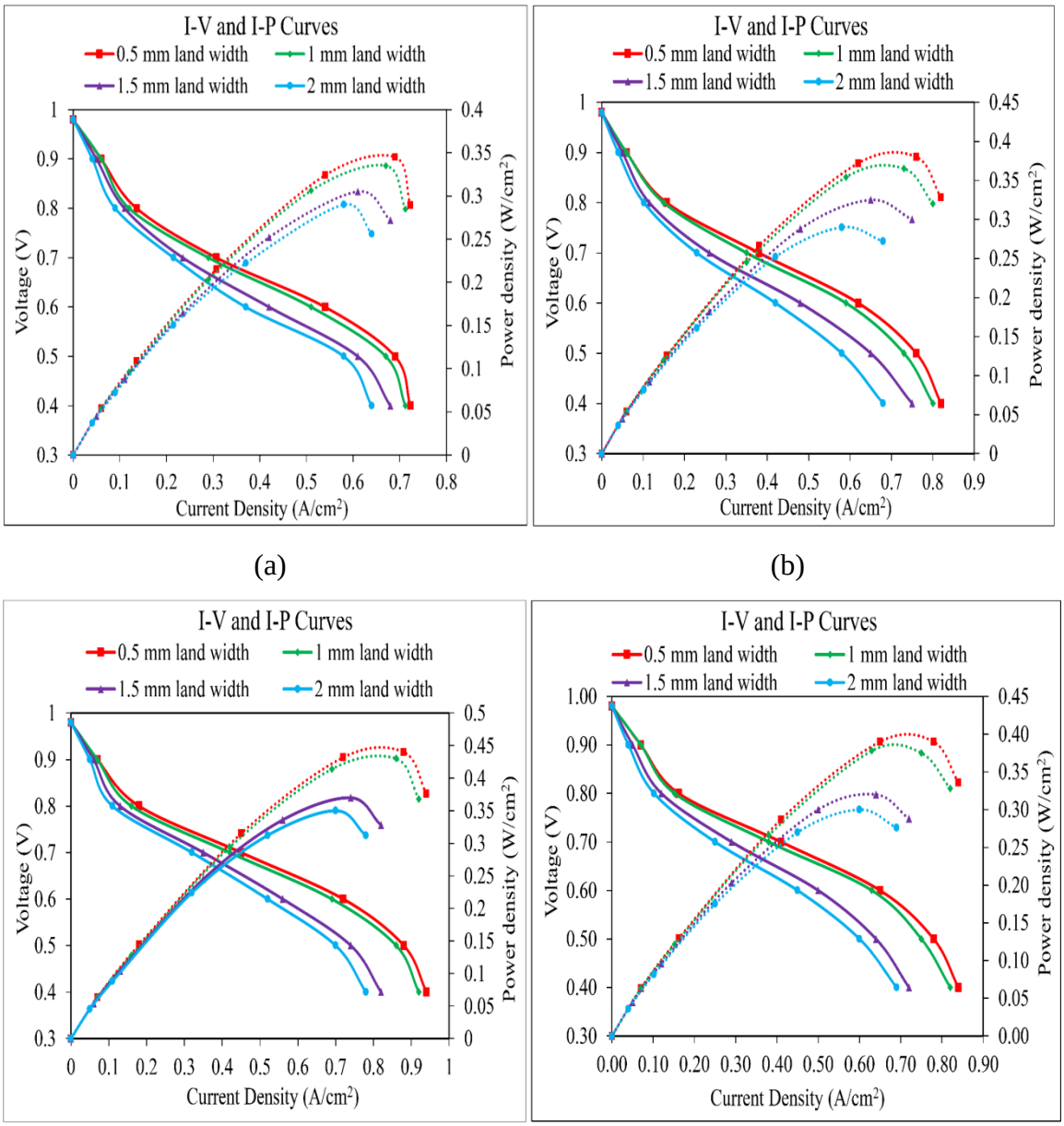

Fig. 4.2 I-V and I-P curves of different Land widths at different temperatures
(a) 323 K (b) 333 K (c) 343 K (d) 353 K

The performance of the fuel cell improved as the temperature increases from 323 K to 343 K; any further increase of temperature led to deterioration in performance. The same trend is obtained for all the four channel designs. It can also be witnessed that the cell performance for all the four channel designs is nearly the same at low current density region under different temperatures. With increase in temperature, the concentration losses reduce due to enhancement in diffusion of the reactants in GDL. Similarly, with increasing temperature, the Ohmic losses increase because the membrane dehydration causes a decrease in ionic conductivity. It can be explained that whenever the temperature crossed 343 K, dehydration occurs on the membrane, which causes ionic conductivity of the membrane to decrease, and hence increases Ohmic losses. Because of this, for all four flow field designs, the performance decreased whenever the temperature crossed 343 K as shown in Fig.4.3. It is observed from the figure that the peak power density observed was 0.44 W/cm^2 at 0.88 A/ cm^2 current density.

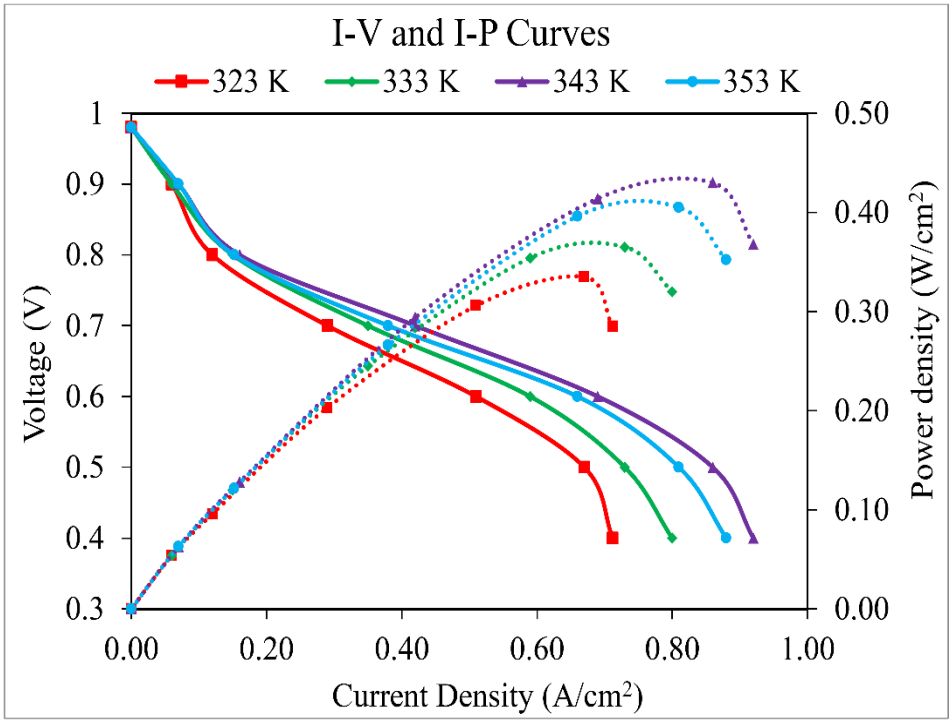

Fig. 4.3 I-V and I-P curves of 0.5 mm Land width at different operating temperatures

4.2.1.2 Effect of reactants flow rates

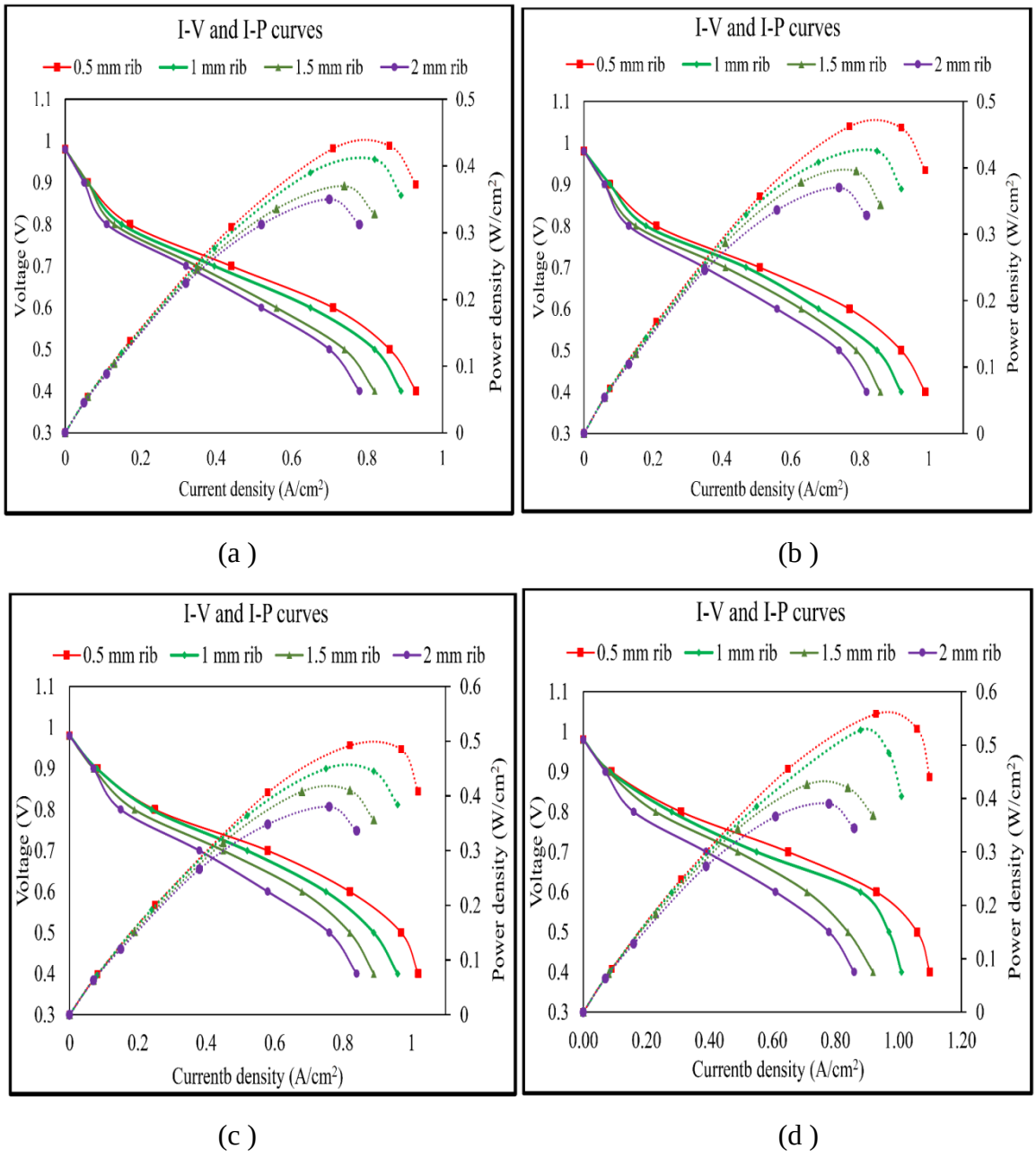

Fig. 4.4 I-V and I-P curves of different Land widths at different reactants flow rate
(a) 300 ccm (b) 400 ccm (c) 500 ccm (d) 600 ccm

The influence of reactant flow rate on the performance of PEMFC for various rib thicknesses/ land widths is shown in Fig. 4.4. The operating parameters such as fuel cell operating temperature 70 ^{o}C, operating pressure was taken as 1 bar, 100 % humidity conditions[151] such as Anode species concentration of hydrogen (H_2), oxygen (O_2), and humidity (H_2O) were taken as 0.6029271, 0, and 0.3970728, and cathode species concentration of hydrogen (H_2),

oxygen (O_2), and humidity (H_2O) were taken as 0, 0.9601614 and 0.03983856, respectively. In the present work the rib thickness was varied from 2 mm to 0.5 mm insteps of 0.5 mm, and the channel width was kept constant at 1 mm. I-V and I-P curves of the fuel cell with various rib thickness at different reactant flow rates ranging from 300 ccm to 600 ccm are shown in Fig. 4.5.As the rib thickness decreases from 2 mm to 0.5 mm, the performance of the fuel cell increase due to increase in the reaction area, uniform distribution of reactants and forced convection under the rib section. But the narrow land-width has high electrical resistance during the conduction of electrons. To overcome the resistance the reactants were supplied with different flow rates.

From Fig. 4.5 it is noticed that the PEMFC performance increased with increase in reactant flow rates for all the four land width cases. The reason is that the availability of reactant flow towards catalyst layer increases and it also easily remove the water generated from reaction sites at high flow rates. Therefore, it minimized the mass transfer losses by using higher flow rates. It is observed from the Fig. 4.4 that the flow channel configuration with 0.5 mm rib thickness generated better output among all configurations at higher flow rates. But the power consumption for supply of reactants was more in case of 0.5 mm rib thickness flow channel configuration. Peak power density was observed to be 0.43 W/cm^2 at 0.86 A/ cm^2 current density.

4.2.1.3 Net power density

Simulations were conducted for PEMFC with two types of land widths at optimum operating conditions. The parasitic losses (Wp) were calculated using the following relation given by Heidary et al. [152].

$$\mathbf{Wp} = \frac{\boldsymbol{\Delta P * A_{channel} * V}}{\boldsymbol{A_{total}}} \quad (4.1)$$

Where ΔP is drop in pressure, V is the velocity at inlet of the channel, $A_{channel}$ is the channel cross sectional area and A_{total} is the active area of the fuel cell respectively.

The net power density is calculated as shown below:

$$\boldsymbol{W_{net} = W_G - W_P} \quad (4.2)$$

Where W_{net} is net power density, W_P is the parasitic losses and $W_G$is the gross power density.

It is observed from the results that, the measured pressure drop in the fuel cell for each land width field is shown in Fig. 4.5 (a). It is noticed that the pressure drop is more for 0.5 mm land width compared to 1 mm land width due to increasing of number of channel bends in the fuel cell with 0.5 mm land width. Estimated parasitic losses are shown in Fig. 4.5 (b). The gross power density and net power density calculations are shown in Table 4.1. It is observed from Fig. 4.6 that the fuel cell with 1 mm rib thickness channel configuration performed better compared to fuel cell with 0.5 mm land width configuration. This was because more number of bend present in the flow channel configuration with 0.5 mm rib thickness and also under land flow of reactants.

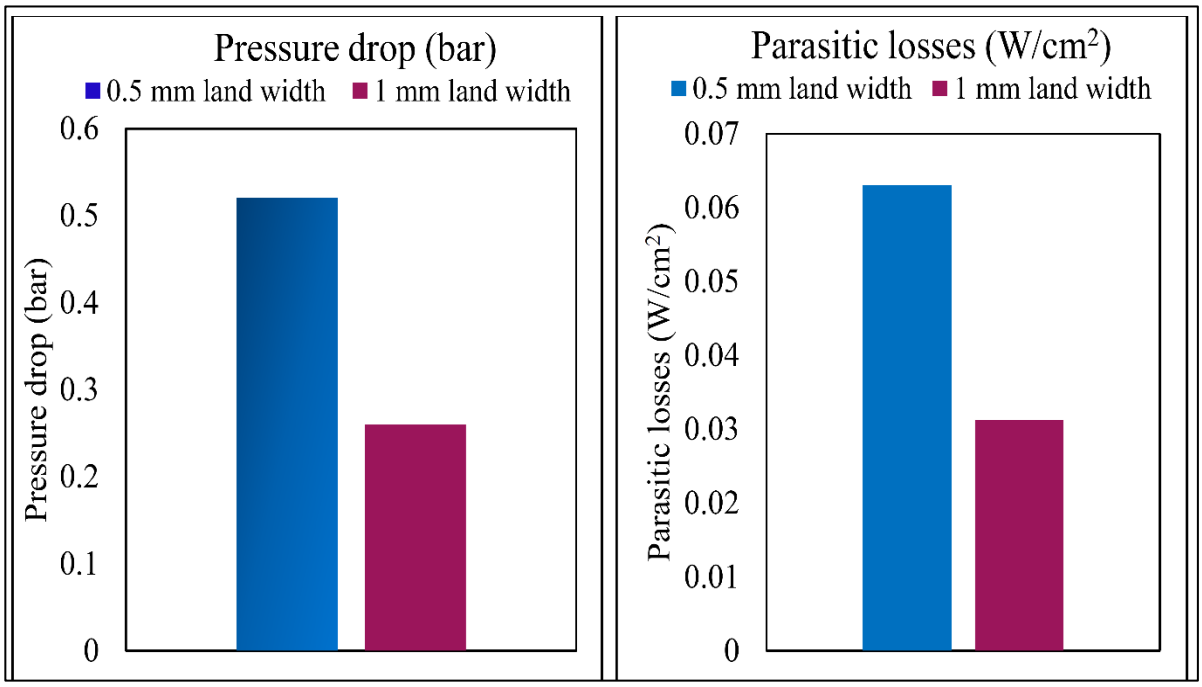

(a) (b)

Fig. 4.5 (a) Measured pressure drop in the channels (b) Estimated parasitic losses

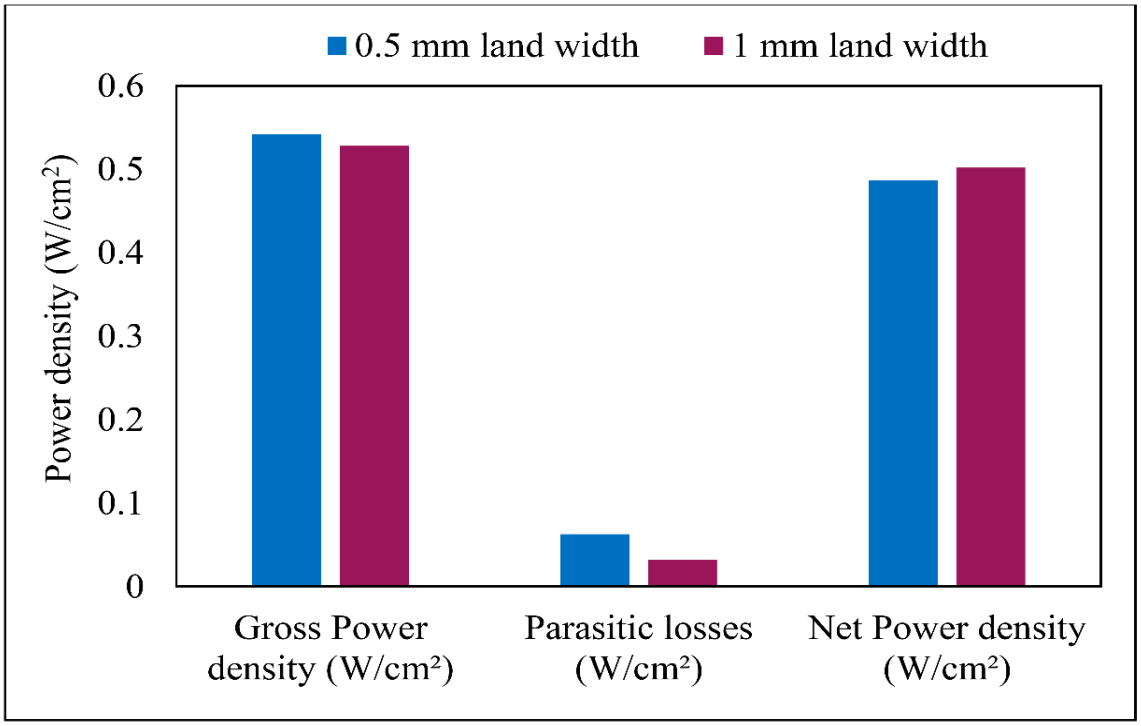

Fig. 4.6 Gross power density and net power density chart

Table 4.1 Fuel cell net power density calculations

	pressure in (bar)	**pressure out (bar)**	**pressure drop (ΔP) bar**	**parasitic power (W_p) W/cm^2)**	**Gross Power density (W_g) (W/cm^2)**	**Net Power density (W_n) ($W_n = W_g - W_p$) (W/cm^2)**
0.5 mm land width	1.5	1.05	0.45	0.055	0.542	0.487
1 mm land width	1.5	1.28	0.22	0.026	0.528	0.502

By considering the parasitic losses, it can be seen that PEMFC with 0.5 mm rib thickness channel configuration generated 0.487 W/cm^2; similarly PEMFC with 1 mm rib thickness channel configuration generated 0.502 W/cm^2 power density respectively. The PEMFC with a net power density with 1 mm rib thickness channel design was 3.08 % more when compared with PEMFC with 0.5 mm rib thickness channel configuration.

4.2.2 Effect of channel width on the PEMFC performance

The bipolar plate with different channel width configurations is as shown in Fig.4.7. Simulations were performed at different channel widths, which varied from 0.5 mm to 2 mm in steps of 0.5mm.

4.2.2.1 Effect of operating pressure

The I-V and I-P curves of the PEMFC with different channel width were drawn at different operating pressures ranging from 1 bar to 4 bar as shown in Fig. 4.8. The other working conditions such as mass flow rates of hydrogen and oxygen were taken as 4.287e-7 kg/s and 0.001429 kg/s; operating temperature was taken as 343 K, and 100% humidity conditions [151] such as Anode species concentration hydrogen (H_2), oxygen (O_2), and humidity (H_2O) were taken as 0.6029271, 0, and 0.3970728, and cathode species concentration hydrogen (H_2), oxygen (O_2), and humidity (H_2O) are taken as 0, 0.9601614 and 0.03983856, respectively.

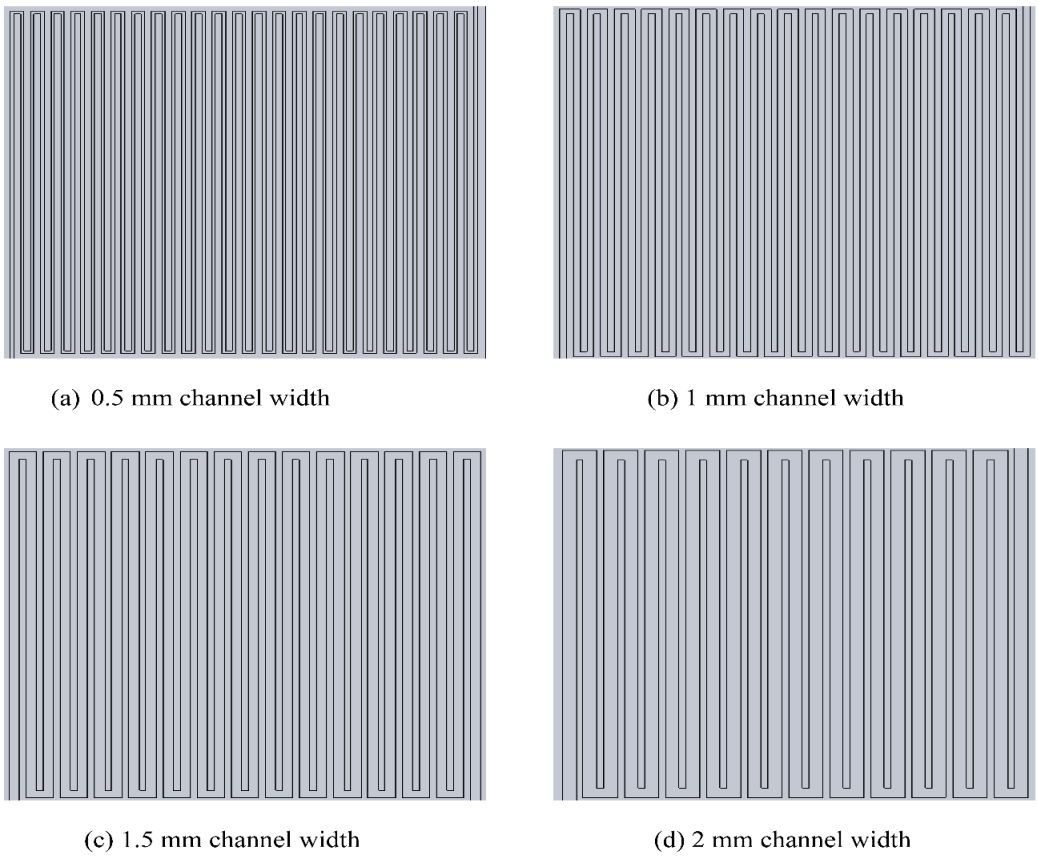

Fig.4.7 Single serpentine flow channel with four different channel width

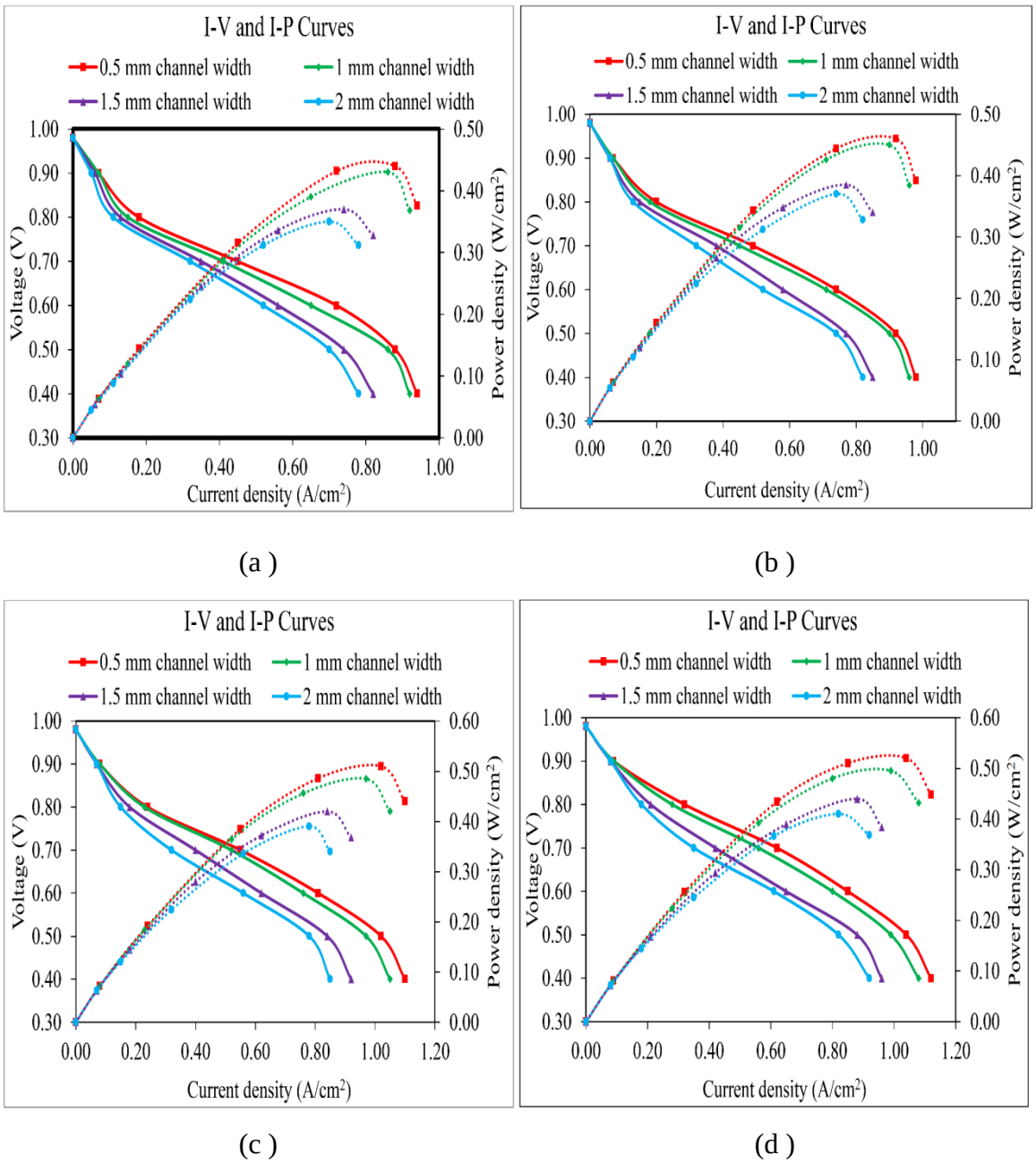

Fig. 4.8 I-V and I-P curves of different channel widths at different operating pressures (a)1 bar (b) 2 bar (c) 3 bar (d) 4 bar

Fig. 4.8 shows that I-V and I-P curves of all fuel cells with various channel sizes at various range of operating pressures and the rib width remains constant i.e. 1mm. The channel width has very small influence on the performance of PEMFC at high fuel cell potentials i.e. > 0.7 V, because at high fuel cell potentials the reaction rates are low as rate of oxygen consumption is very low and also membrane is in dehydrated state. In the present work, the effect of channel size on fuel cell performance at various range of operating pressures is

displayed in Fig. 4.8. It is perceived from the results that the performance of PEMFC was enhanced with decrease of channel width from 2 mm to 0.5 mm. At low fuel cell potential; the width of the fuel cell had a strong effect on the performance of PEMFC due to increase in reaction rates in the fuel cell.

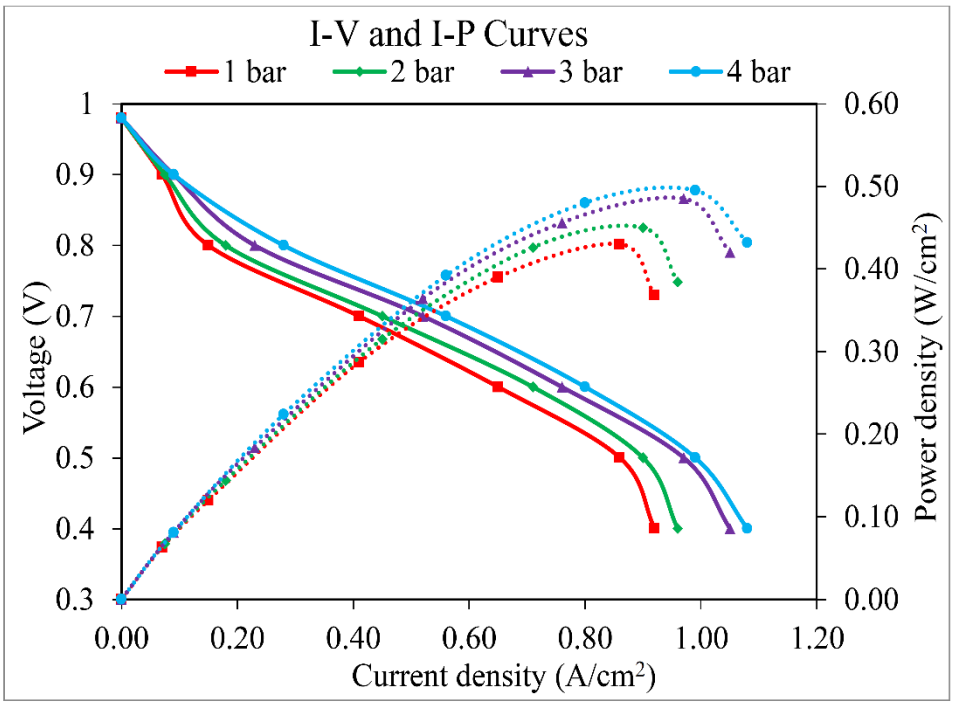

Fig. 4.9 I-V and I-P curves of 0.5 mm channel width at different operating pressures

However, at low cell potentials, the rate of reaction increases due to a large amount of reactants being consumed in the electrochemical reaction and generating more liquid water. Rate of reactant transport to the reaction sites depends on the width of channel in a PEMFC, however the reactants transport towards catalyst increases with decrease of channel width due to the forced convection in narrow channels; thus enhancing the performance. The fuel cell performance is strongly dependent on the width of the channel when it is low fuel cell potentials. In serpentine channels, the pressure variations between the neighboring channels are very high than those along the flow direction. This causes forced convection under the rib between the adjacent channels. Forced convection not only improves reactant transport to the reaction area under the rib section but also aids evacuation of water generated from the reaction zones under the ribs. The velocity of reactants increases with decrease of channel size when all the fuel cells are operating at same flow rate; this increases the performance of the

PEMFC. From the figure it a very small deviation in the performance is observed for both fuel cells with 0.5 mm and 1 mm width channel sizes.

From Fig.4.9, it is observed that the performance curves were drawn at various operating pressures for 1mm channel width. The pressure across the anode and the cathode remains constant. It can be seen from Fig. 4.9 that the performance of the fuel cell monotonically improved, with a rise in the operating pressure. The reason is that increase in the operating pressure causes increase in reactant diffusivity through the GDL, which increases the reaction rate. As a result, higher power is generated. Higher open circuit voltages at higher energies can be explained by Nernst equation. As the pressure rises, the overall polarization curve moves forward. Another reason for the improved performance is that the partial pressure of the reaction gas increases as the operating pressure increases. The peak power density 0.50 W/cm^2 is generated at 0.99 A/cm^2 current density.

4.2.2.2 Net power density

Simulations were conducted for PEMFC with two types of channel widths at optimum operating conditions. From the simulation results, the measured pressure drop in the fuel cell for each channel width field is shown in Fig. 4.10 (a).

Table 4.2 Fuel cell net power density calculations

	pressure in (bar)	**pressure out (bar)**	**pressure drop (ΔP) bar**	**parasitic power (W_p) W/cm^2)**	**Gross Power density (W_g) (W/cm^2)**	**Net Power density (W_n) ($W_n = W_g - W_p$) (W/cm^2)**
0.5 mm land width	1.5	0.98	0.52	0.063	0.51	0.447
1 mm land width	1.5	1.24	0.226	0.0312	0.5	0.468

It is observed that the pressure drop is more for 0.5 mm channel width configuration due to high gas velocity along the channel and more amount of liquid water generation. The pressure drop decreases when the channel width increases from 0.5 mm channel width to 1 mm channel width; for any further increase in channel width no significant pressure drop was observed. Estimated parasitic losses are shown in Fig. 4.10 (b). The gross power density and net power density calculations as shown in Table 4.2.It is observed from Fig. 4.11that the performance of the fuel cell with 1 mm channel width configuration is better compared to fuel cell with 0.5 mm channel width configuration.

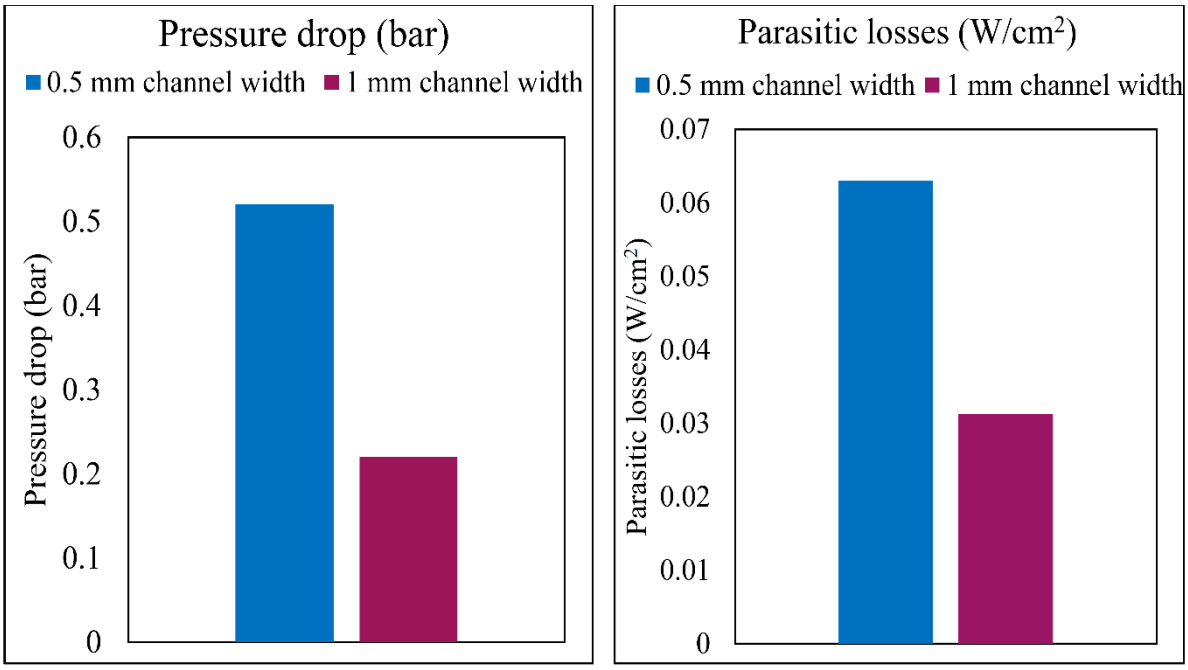

(a) (b)

Fig. 4.10 (a) Measured pressure drop in the channels (b) Estimated parasitic losses

By considering parasitic losses, it can be seen that the PEMFC with 0.5 mm channel width configuration generated 0.447 W/cm^2; similarly the PEMFC with 1 mm channel width configuration generated 0.468 W/cm^2 power density respectively. The PEMFC net power density with 1 mm channel width design was 4.69 % more when compared with PEMFC with 0.5 mm channel width configuration.

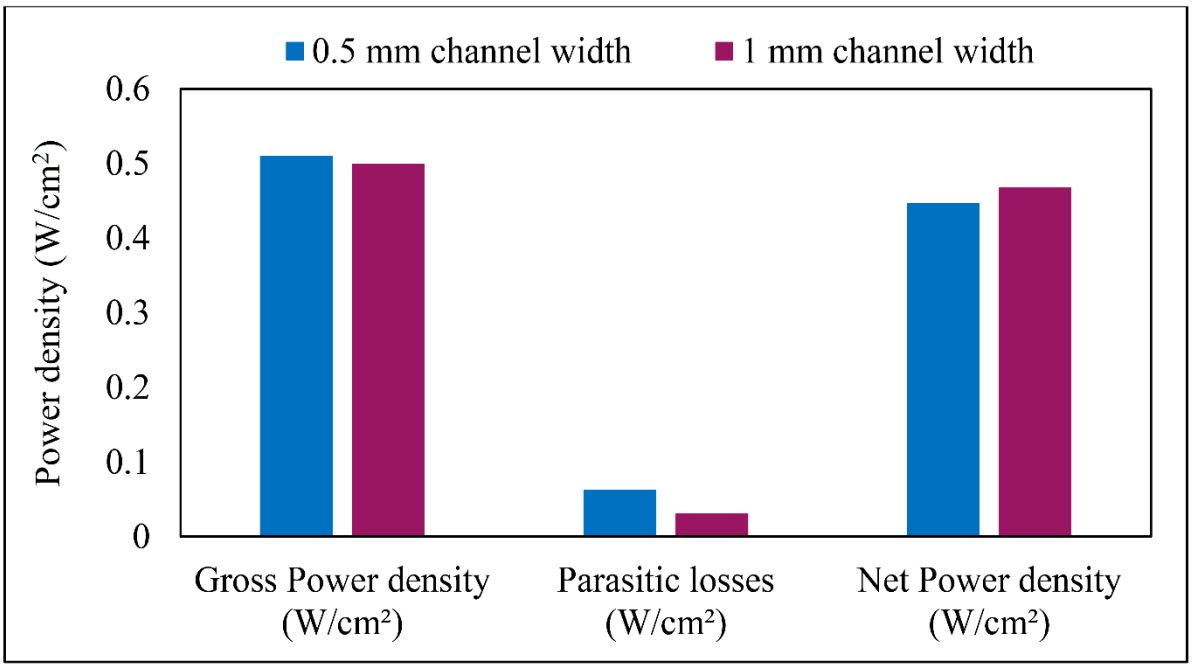

Fig. 4.11 Gross power density and net power density chart

4.2.3 Comparison of experimental and simulation results of a serpentine channel

The experiments were conducted for a single serpentine channel of 1 mm rib and channel size and the operating parameters such as mass flow rates of hydrogen and oxygen were set at $4.287e^{-7}$ kg/s and 0.001429 kg/s, operating temperature was set at 343 K, operating pressure was set at 1 bar and 100 % relative humidity respectively. Nafion 212 MEA with catalyst loading of 0.4 mg/cm^2 on anode and 0.6 mg/cm^2 on cathode was used for conducting the experiments.

The I-V and I-P curves of both simulation and experimental results of serpentine channel as shown in Fig. 4.12. It is observed from simulation data that the peak power density generated of 0.50 W/cm^2 at 0.99 A/cm^2 current density and it was observed from experimental data that the peak power density generated 0.46 W/cm^2 at 0.92 A/cm^2 current density respectively. The simulation results were slightly over predicted when compared to experimental results. Based on I-V and I-P curve it is concluded that the simulation results of serpentine flow field with optimum design parameters were compared with experimental results of the same channel, with the results in excellent agreement each other.

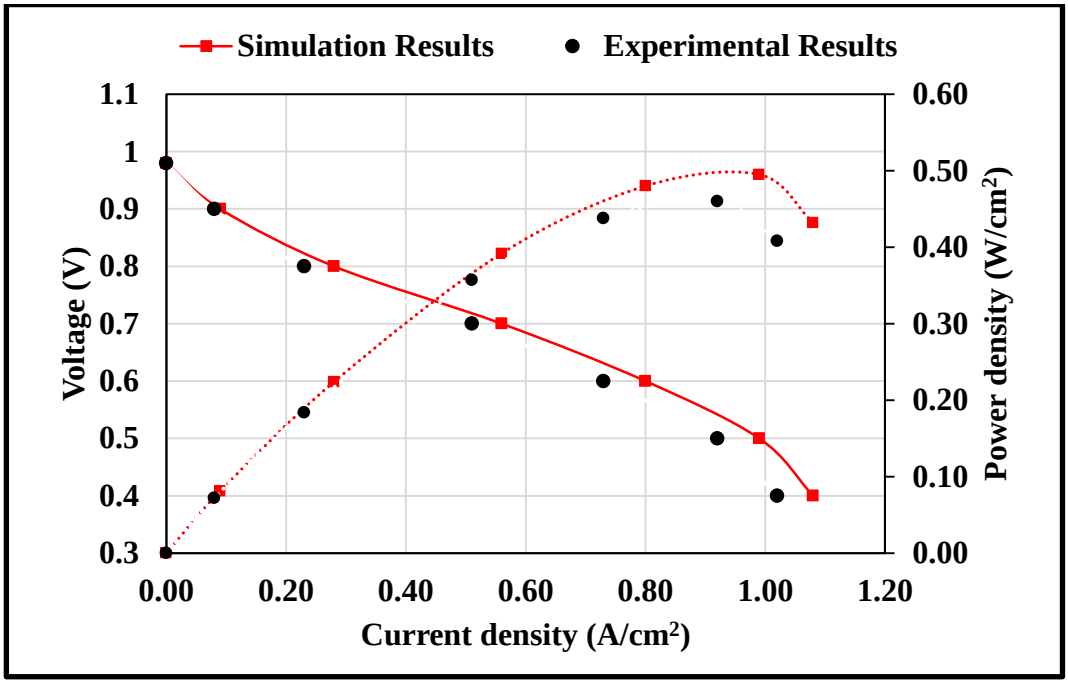

Fig. 4.12 Comparison of experimental and simulation results of single serpentine channel

4.2.4 Summary

A 3-D Model was developed to examine the influence of land width and channel width on the performance of PEMFC. The present work analyzed the effect of operating parameters such as operating temperature, flow rates on the performance of the fuel cell fitted with different rib thickness configurations and also analyzed the influence of operating pressure on the power output of the cell fitted with different channel widths configurations. The following conclusions are drawn from this study:

- The fuel cell with 1 mm land width gives the best performance when parasitic losses are considered.
- The fuel cell performance increases with increase in the flow rate of reactants.
- The fuel cell with 1 mm land width gives the best performance when it is operated with high flow rates and the performance is almost same for both the channels at low flow rate conditions.
- The performance of the fuel cell improved with rise in the operating temperature from 313 K to 343 K while the performance deteriorated beyond 343 K. At 343 K the fuel cell gives best performance.

- The fuel cell with 1 mm channel width gives the best performance when parasitic losses are considered.
- The simulation results of serpentine flow field with optimum design parameters were compared with experimental results and it is observed that the results were in good agreement.

Further, experimental study was carried out to examine the performance of PEMFC with bio-inspired channel design of bipolar plate on cathode side, viz., Lung channel, bio-channel and leaf channel designs, under different operating conditions. The performance of PEMFC with bio-inspired channels are compared with the serpentine channel (1mm land width and 1 mm channel width).

Chapter - 5
Experimental Results and discussion

Experimentally analyse the performance of PEM Fuel Cell fitted with leaf, lung, bio-channel and single serpentine flow field plates

5.1 Introduction

Performance of a Proton Exchange Membrane Fuel Cell (PEMFC) is appreciably influenced by the flow-field geometry. The branching structure of plant leaves and the human lung have efficient network to distribute the nutrients in the respective systems as shown in Fig. 5.1. The nutrients distributed in the biological branching systems have an optimum arrangement and are efficient in each part. The same nutrient transport system can be mimicked in the flow field design of a PEMFC, to aid uniform reactant distribution and better water management.

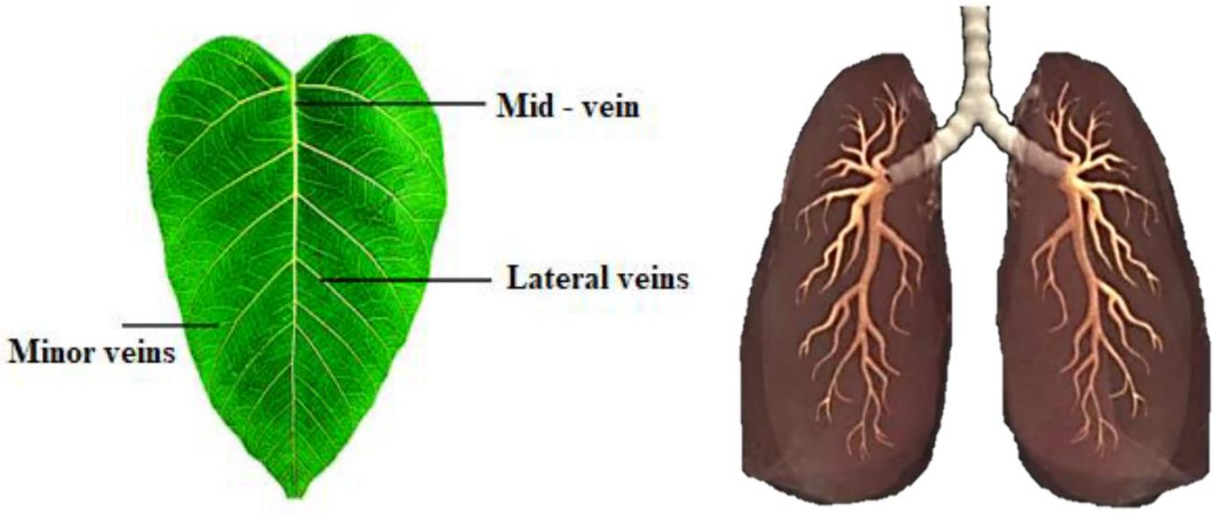

Fig. 5.1 Leaf vein system and human lung blood vessel system

5.2 The structure of a leaf

Plants are among the survivors, which can adapt to environment well and they mostly rely on the leaves to grow. The branches of vascular stems are called Veins. The vascular bundles are always distributed along the petiole in some form of special shape. The large and obvious vein, locating in the center of leaf, is called the midrib or main vein (Mid vein). And the smaller veins distributed along main vein are called the lateral veins (Lateral veins). The small veins or veinlets (Minor veins) are the smallest bundles on the leaf which are distributed all over the leaves. Those veins are the transport channel of water, salts and the output of photosynthetic products in plants. As outstanding products of nature, these different patterns of veins undoubtedly have good biological and physic-chemical properties, and they can be good at transferring material and supporting blades. These characteristics meet the

requirements of the flow channel in PEMFC which demand good circulation and mechanical properties.

5.3 Experiment

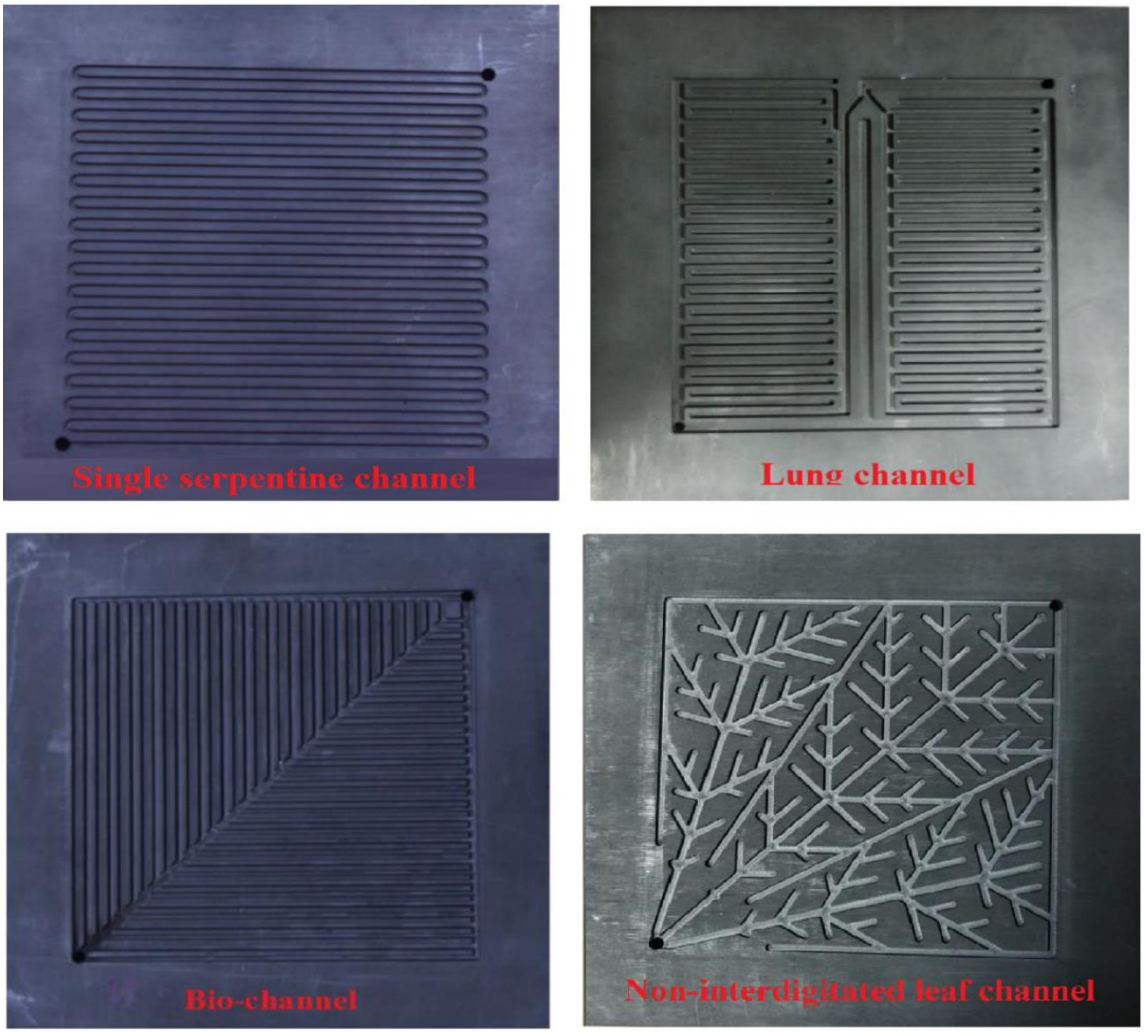

Fig. 5.2 Different Flow channel designs (Single serpentine channel, Lung channel, Bio channel, Non-Interdigitated leaf channel)

Experiments were conducted using WonATech (Korea) programmable fuel cell test station (FCTS) located at the Center for Sustainable Energy laboratory of NIT Warangal (India). Graphite plates were used as bipolar plates. Single serpentine channel design, lung channel design, bio channel design and leaf channel design bipolar plates of 49 cm^2 active area were fabricated by programmable computer numerical control machine, as shown in Fig. 5.2.The design parameters of leaf channel design are shown in Table 5.1.In this work, the effect of all

flow channel designs such as single serpentine channel, bio-channel, lung channel and leaf channel design bipolar plates on the performance of a PEMFC was examined experimentally at various range of operating conditions.

Table 5.1 Design parameters of different flow channels

S.No	Design parameter	Dimension			
		Single serpentine channel	Lung channel	Bio channel	Leaf channel
1	Active area	49 cm^2	49 cm^2	49 cm^2	49 cm^2
2	Bipolar plate thickness	10 mm	10 mm	10 mm	10 mm
3	Channel width	1 mm	1 mm	1 mm	1 mm
4	Channel depth	1 mm	1 mm	1 mm	1 mm
5	Land width	1 mm	1 mm	1 mm	1.5 mm

A membrane electrode assembly (MEA) (N212) of 49 cm^2 active area with a membrane thickness of 0.0175mm and platinum loading of 0.4 mg cm^{-2} at the anode and 0.6 mg cm^{-2} at the cathode was used. Carbon paper of thickness 0.38 mm was used as GDL, and catalyst layers of 0.05 mm thick were used on either side of the membrane. Hydrogen and oxygen were supplied through the bipolar plates. The MEA, bipolar plates and current collectors used in the experimentation were provided by Vinpro Technologies, Hyderabad. Hydrogen and oxygen were supplied through the bipolar plates. The influence of various operating parameters such as the operating temperature, operating pressure, anode humidification temperature (AHT), cathode humidification temperature (CHT) and the back pressure on the performance of fuel-cell was analyzed experimentally for the four flow channels considered.

Table 5.2. Fuel cell experimental operating conditions

Type of study	Operating temperature (^{o}C)	Relative Humidity (%)		Stoichiometric ratio (λ)		Operating Pressure (bar)	Back Pressure (bar)
		Anode	Cathode	Anode	cathode		
Temperature	**40^{o}C**	100%	100%	λ= 1	λ= 1	0	1
	50^{o}C	100%	100%	λ= 1	λ= 1	0	1
	60^{o}C	100%	100%	λ= 1	λ= 1	0	1
	70^{o}C	100%	100%	λ= 1	λ= 1	0	1
	80^{o}C	100%	100%	λ= 1	λ= 1	0	1
Relative Humidity	70^{o}C	**25%**	**25%**	λ= 1	λ= 1	0	1
	70 ^{o}C	**50%**	**50%**	λ= 1	λ= 1	0	1
	70 ^{o}C	**75%**	**75%**	λ= 1	λ= 1	0	1
	70 ^{o}C	**100%**	**100%**	λ= 1	λ= 1	0	1
Stoichiometric ratio (λ)	70 ^{o}C	100%	100%	**λ= 1**	**λ= 1**	0	1
	70 ^{o}C	100%	100%	**λ= 1**	**λ= 1.5**	0	1
	70 ^{o}C	100%	100%	**λ= 1**	**λ= 2**	0	1
	70 ^{o}C	100%	100%	**λ= 1**	**λ= 2.5**	0	1
	70 ^{o}C	100%	100%	**λ= 1**	**λ= 3**	0	1
	70 ^{o}C	100%	100%	**λ= 1**	**λ= 3.5**	0	1
	70 ^{o}C	100%	100%	**λ= 1**	**λ= 4**	0	1
Operating Pressure	70 ^{o}C	100%	100%	λ= 1	λ= 3	**1**	1
	70 ^{o}C	100%	100%	λ= 1	λ= 3	**2**	1
	70 ^{o}C	100%	100%	λ= 1	λ= 3	**3**	1
Back pressure	70 ^{o}C	100%	100%	λ= 1	λ= 3	3	**0**
	70 ^{o}C	100%	100%	λ= 1	λ= 3	3	**1**
	70 ^{o}C	100%	100%	λ= 1	λ= 3	3	**2**
	70 ^{o}C	100%	100%	λ= 1	λ= 3	3	**3**

5.4 Results and Discussion

5.4.1 Influence of fuel cell operating temperature

The influence of fuel cell operating temperature on the performance of PEMFC for various flow field designs is shown in Fig.5.3. In these experiments, the operating temperature of PEMFC was varied from 40 ^{o}C to 80 ^{o}C with an increment of 10 ^{o}C, while RH was kept constant at 100 %, the operating pressure was set at 1 bar, and back pressure was maintained at ambient pressure. It can be understood from the figure that the performance of PEMFC increased as the operating temperature increased from 40 ^{o}C to 70 ^{o}C due to improvement in catalytic activity, and as a result, the chemical reaction rate increased. Also increasing the cell temperature facilitates reactant transfer in the electrodes. However, the fuel cell performance deteriorated when the fuel cell operating temperature increased from 70^{o}C to 80^{o}C due to membrane dehydration (extreme evaporation of liquid water in the cell), which significantly increases Ohmic resistance of membrane (the active catalyst surface area may also reduce). This is mostly because of increase in exchange current density with temperature.

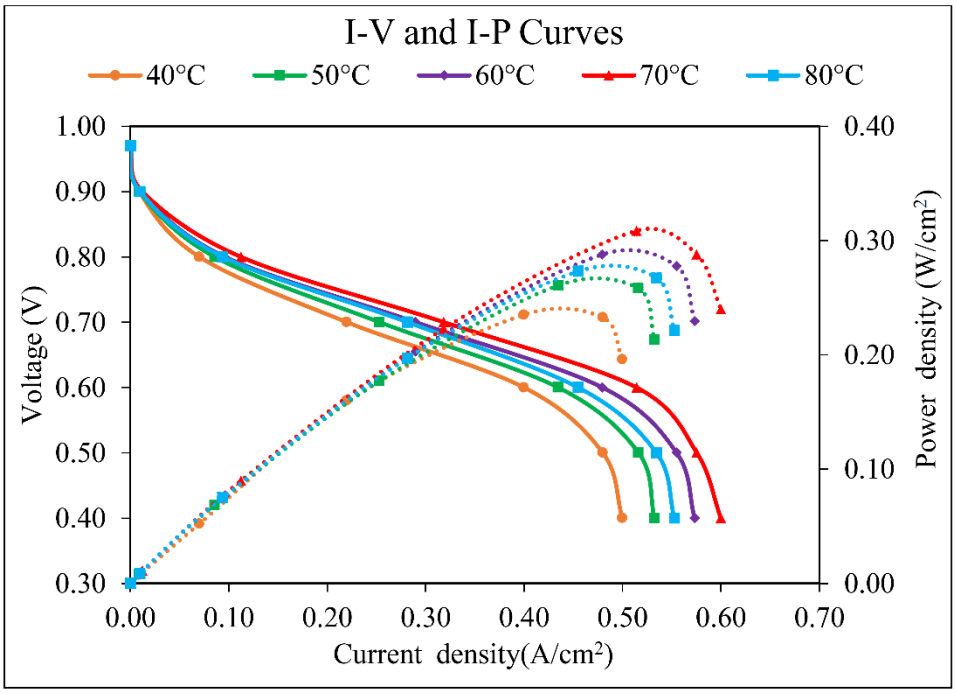

(a) Single serpentine

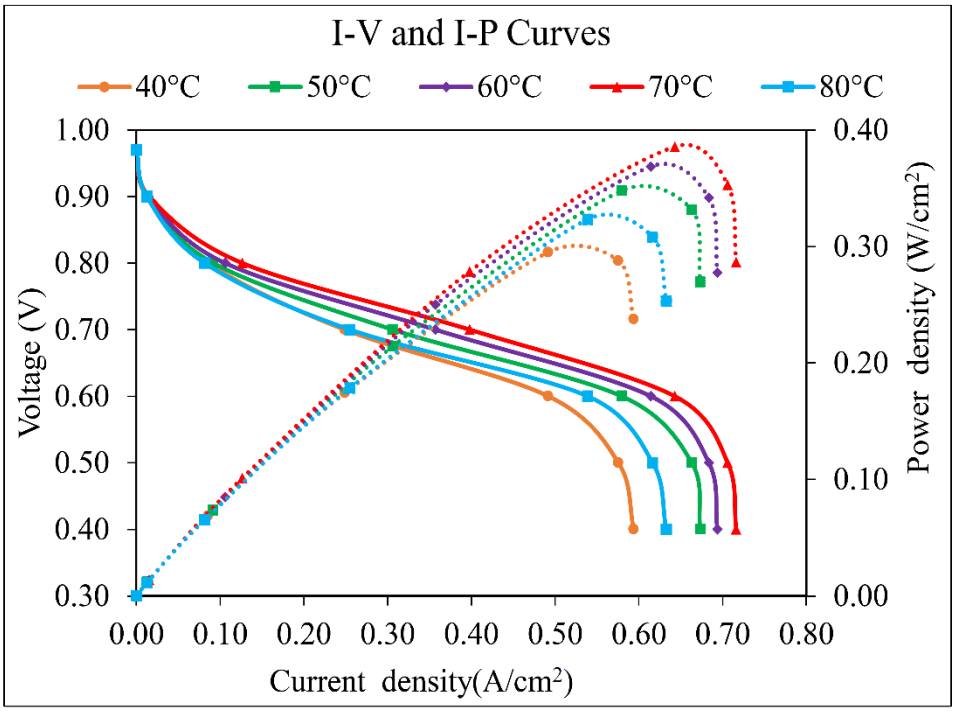

(b) Lung Channel

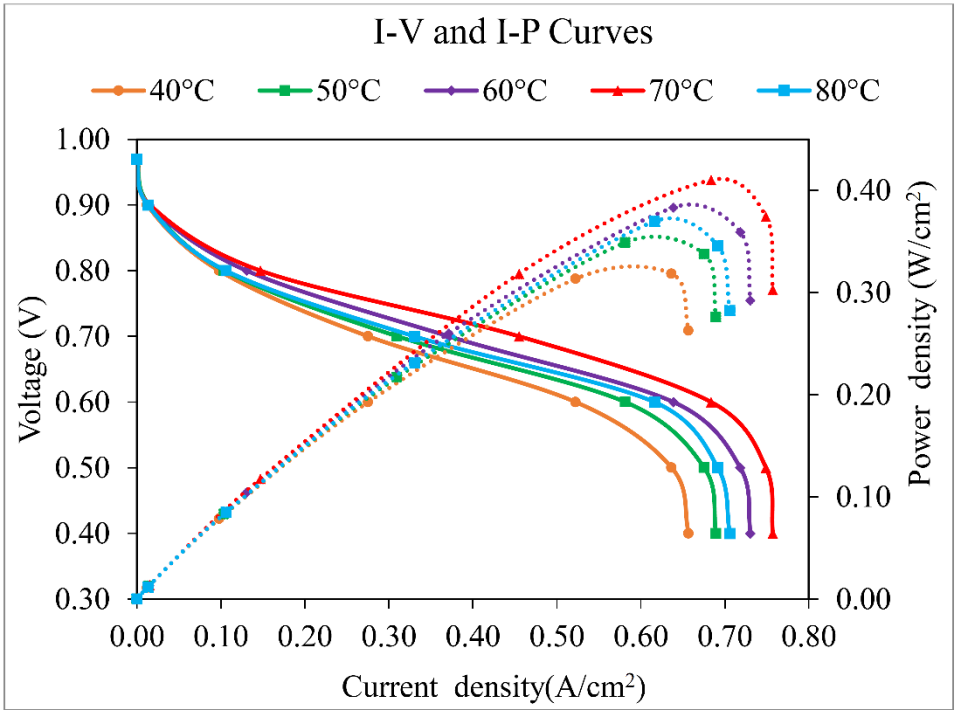

(c) Bio-channel

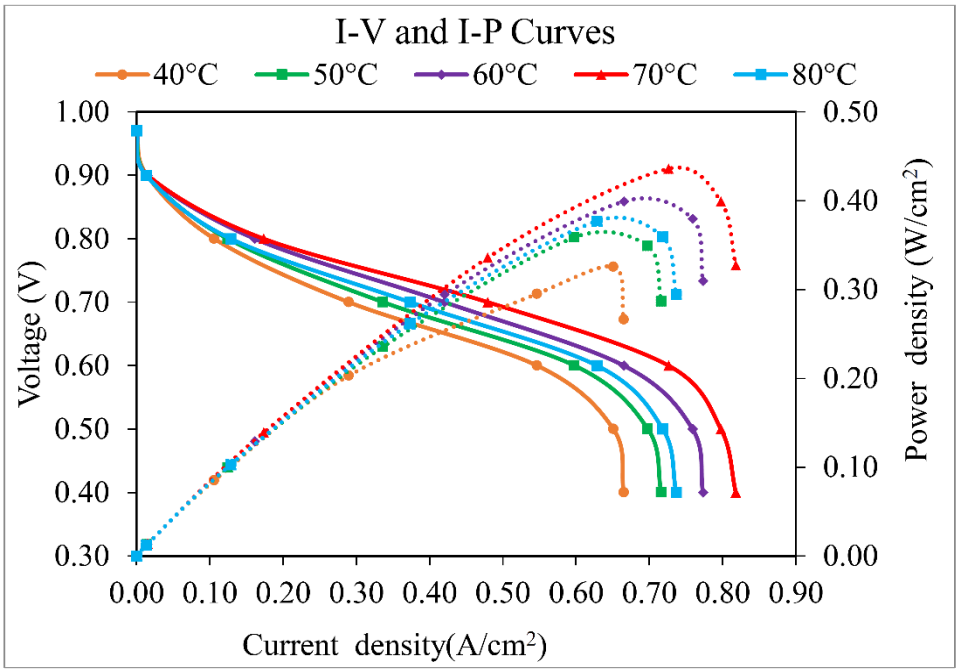

(d) Leaf Channel

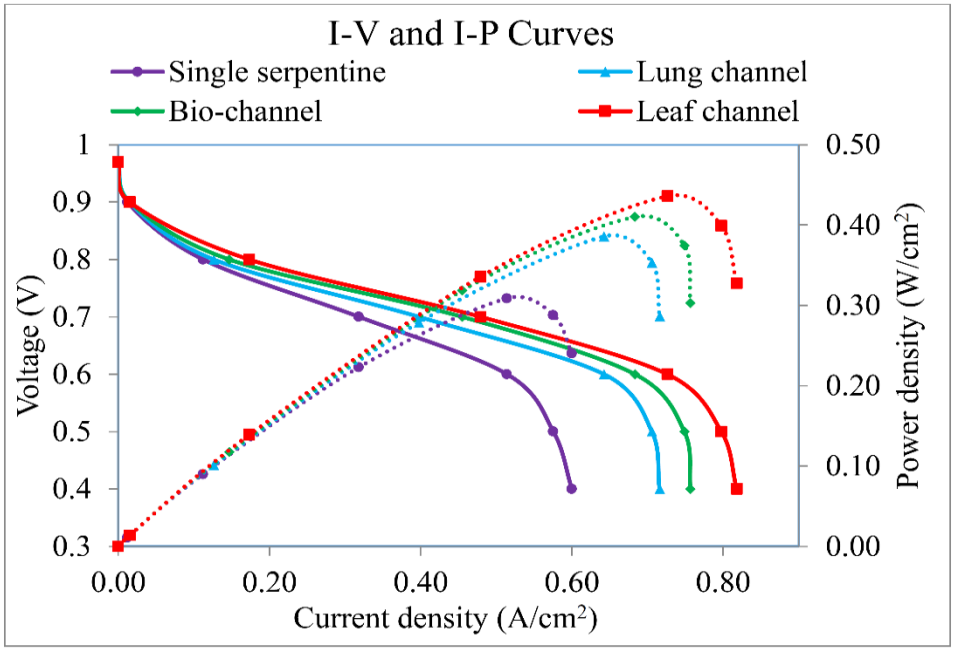

(e)

Fig. 5.3 Effect of operating temperature on the performance of the fuel cell
(a) Single serpentine flow channel (b) Lung channel (c) Bio channel (d) Leaf channel
(e) Comparison of three channels at optimum temperature (70°C)

The effect of fuel cell temperature is more significant in the high current region. At low current region, the cell performance does not change much with increase in cell temperature. The same trend is obtained for all four channel designs. It can also be witnessed that the fuel

cell performance for all the four channel designs is nearly same at low current density region under different temperatures. This is due to the balance between the positive effect of decreased activation losses and negative effect of decreased thermodynamic voltage at low current densities. With increase in temperature, the concentration losses reduce due to enhancement in diffusion of the reactants in GDL. Similarly, with increasing temperature, the Ohmic losses increase because the membrane dehydration causes a decrease in its ionic conductivity.

It can be explained that whenever temperature crossed 70 ^{o}C, dehydration occurs on the membrane, which causes ionic conductivity of the membrane to decrease, and hence increases ohmic losses. Because of this, for all the four flow channel designs, the performance decreased whenever temperature crossed 70 ^{o}C. For all the four flow channel designs, the maximum performance occurred at 70 ^{o}C as shown in Fig. 5.3(a),(b),(c),(d). The polarization curves such as I-V curves and I-P curves drawn for four channels at operating temperature 70 ^{o}C are shown in Fig 5.3(e). Among the four flow field designs, leaf channel design exhibited better performance of 0.44 W/cm^2 at 0.73 A/cm^2.

5.4.2 Influence of the relative humidity of the reactants

The influence of relative humidity (RH) on fuel cell performance is shown in Fig.5.4 for four different types of flow channel designs. During these experiments the operating temperature was set as 70 ^{o}C, the operating pressure was set as 1 bar, the flow rates of oxygen and hydrogen were kept at 700 ccm and 350 ccm, and back pressure was maintained at ambient pressure (0 bar) respectively. The back pressure is equal to zero which means that the inlet and outlet pressure of the fuel cell are the same. The RH was varied from 25% to 100% insteps of 25%, and it was varied simultaneously at the anode and the cathode. It can be observed from the polarization curves that all four flow channel designs show similar trend. From Fig. 5.4(a), (b), (c), (d) it is also evident that PEMFC performance in terms of voltage and power enhanced with increase in the RH (from 25% to 100%).

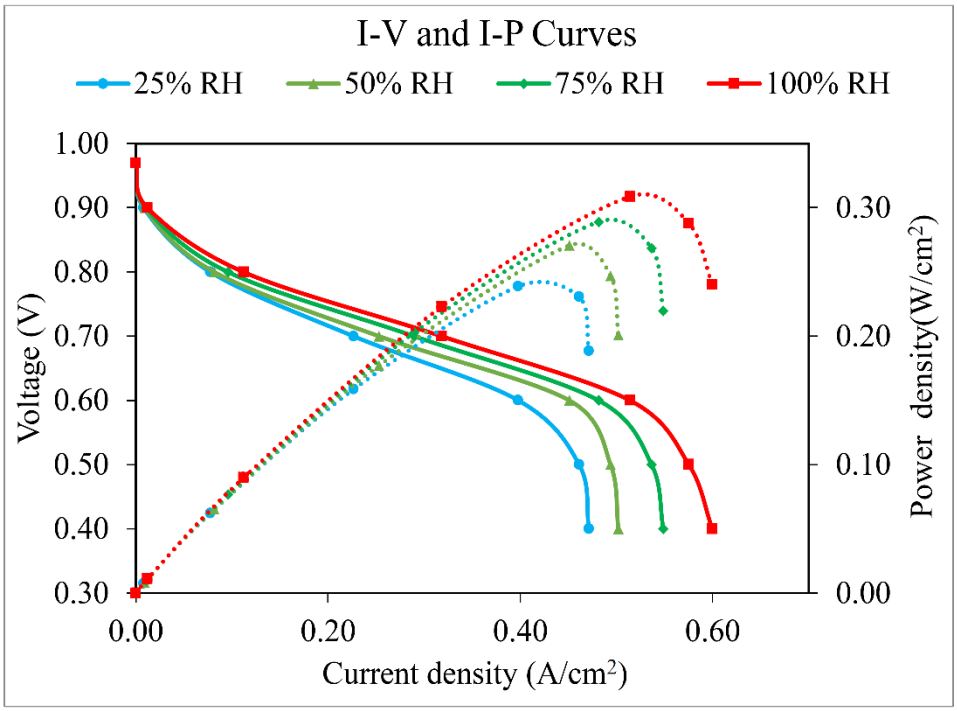

(a) Single serpentine channel

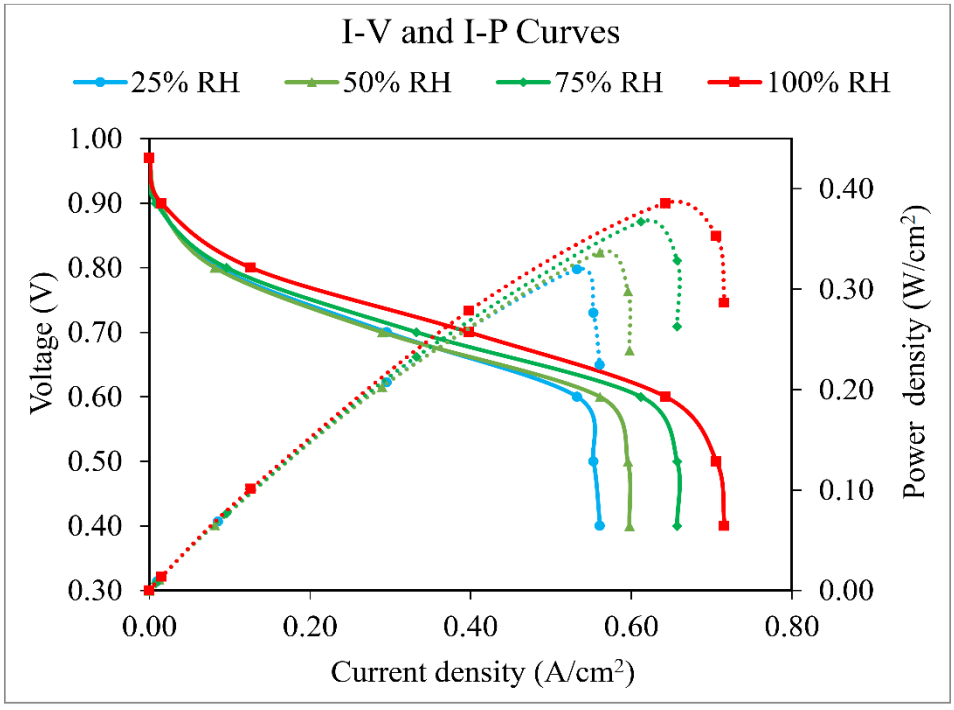

(b) Lung Channel

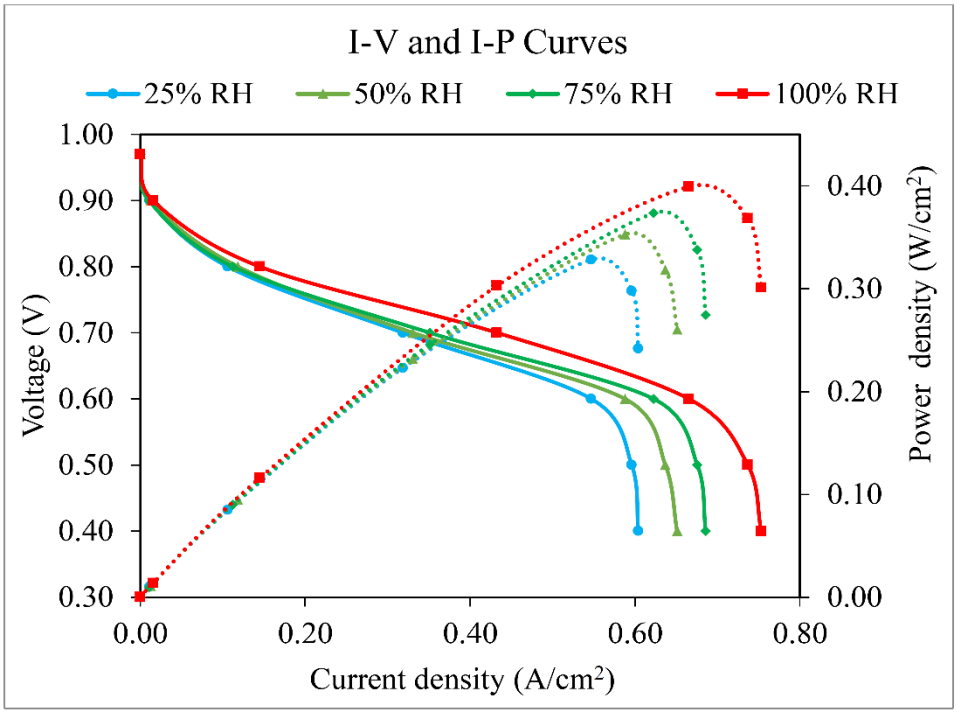

(c) Bio channel

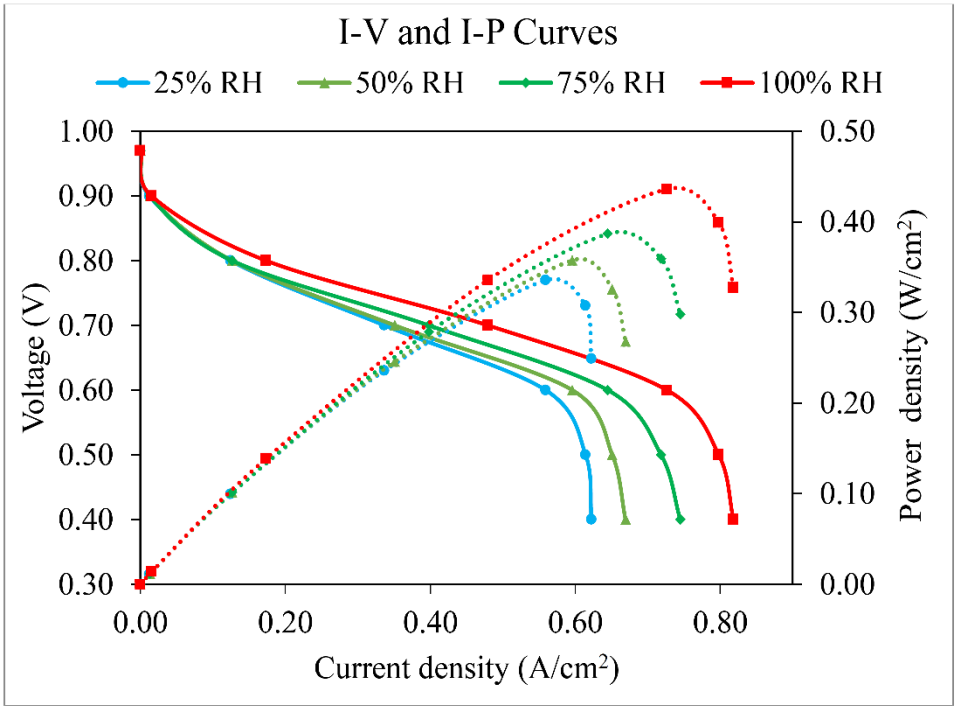

(d) Leaf channel

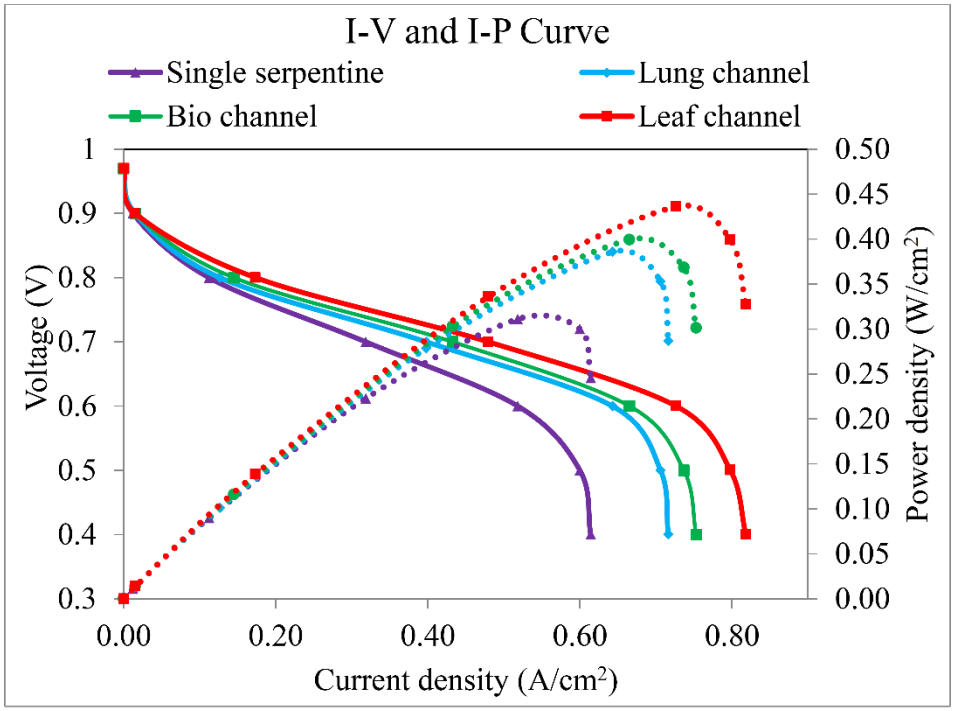

(e)

Fig. 5.4 Effect of relative humidity on the performance of the fuel cell

(a) Triple serpentine flow channel (b) Lung channel (c) Bio channel (d) Leaf channel (e) Comparison of four flow channel designs at optimum RH (100%)

This is because the proton conductivity capability of the membrane is mainly dependent on the percentage of water vapor present in the membrane. Increase in water quantity in the membrane improves the conductivity of the Nafion membrane. When the membrane is fully hydrated, the ohmic losses reduce, and finally the performance would increase significantly because of the drop in ohmic losses. The polarization curves such as I-V and I-P curves drawn for three channels at RH of 100% are shown in Fig. 5.4(e). Among the four flow field designs considered, the leaf channel design exhibited better performance of 0.44 W/cm^2 at 0.73 A/cm^2.

5.4.3 Influence of flow rates in terms of stoichiometric ratio (λ)

Stoichiometric ratio (λ) is the ratio between the actual flow rate of reactants at the fuel cell inlet and the consumption rate of reactants at reaction sites.

$$\lambda = \frac{\dot{N}_{act}}{\dot{N}_{conc}} = \frac{\dot{m}_{act}}{\dot{m}_{conc}} = \frac{\dot{V}_{act}}{\dot{V}_{conc}} \qquad (5.1)$$

Where$\dot{N}_{act}$is the actual flow of reactants at inlet of the fuel cell

N_{conc} is the consumption rate of reactants

$\dot{m}_{act}$ is the mass flow rates of reactants at inlet of the fuel cell

$m_{conc}$is the mass flow rates of the reactants consumption

V_{act} is the volumetric flow rates of reactants at inlet of the fuel cell

V_{conc} is the volumetric flow rates of reactants consumption

The reactant flow rate at the inlet of a fuel cell must be equal to or higher than the rate at which those reactants are being consumed in the fuel cell. The flow rates (mol/sec) at which hydrogen and oxygen are consumed and water is generated are determined by Faraday's law:

$$\dot{N}_{H_2} = \frac{I}{2F} \quad (5.2)$$

$$\dot{N}_{O_2} = \frac{I}{2F} \quad (5.3)$$

$$\dot{N}_{H_2O} = \frac{I}{2F} \quad (5.4)$$

Where $\dot{N}$ = consumption rate (mol/sec)

I = Current (A)

F = Faradays constant (C/mol) = 96.485 C/mol

The mass flow rates of reactants consumption (g/sec)

$$\dot{m}_{H_2} = \frac{I}{2F} \quad (5.5)$$

$$\dot{m}_{O_2} = \frac{I}{2F} \quad (5.6)$$

The mass flow rates of water generation (g/sec)

$$\dot{m}_{H_2O} = \frac{I}{2F} \quad (5.7)$$

Fig. 5.5 depicts the influence of stoichiometric ratio on fuel cell performance for various flow channel designs. The flow rates on cathode side is varied by keeping the flow rate of anode side fixed as λ_a =1. The other parameters such as operating temperature was set at 70 ^{o}C, operating temperature of the fuel cell was set at 1 bar, relative humidity was set as 100%

and the back pressure was maintained at ambient pressure respectively. The flow rates on cathode side are varied from the stoichiometric ratio of λ_c=1 to λ_c=4 with an increment factor of 0.5 for all the flow channel designs. It is evident that the performance of the fuel cell enhanced as the stoichiometric ratios were increased from λ_c=1 to λ_c=3; any further increase of stoichiometric ratios gave the same performance or slightly decreased performance.

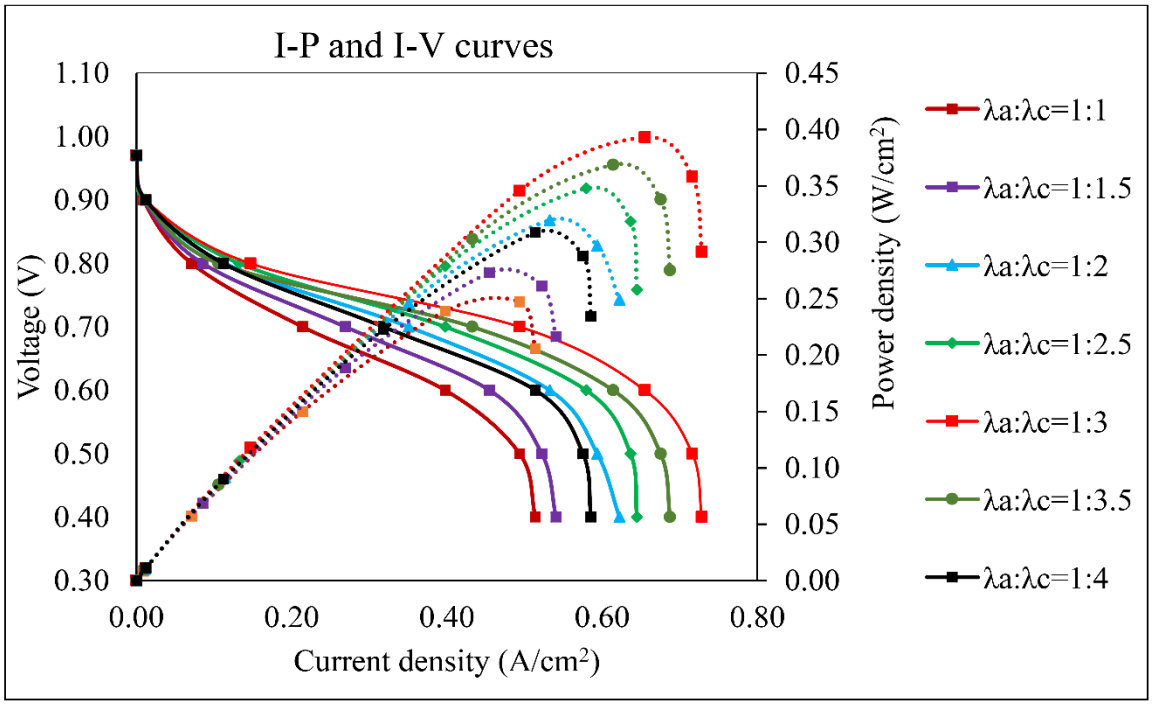

(a) Single serpentine channel

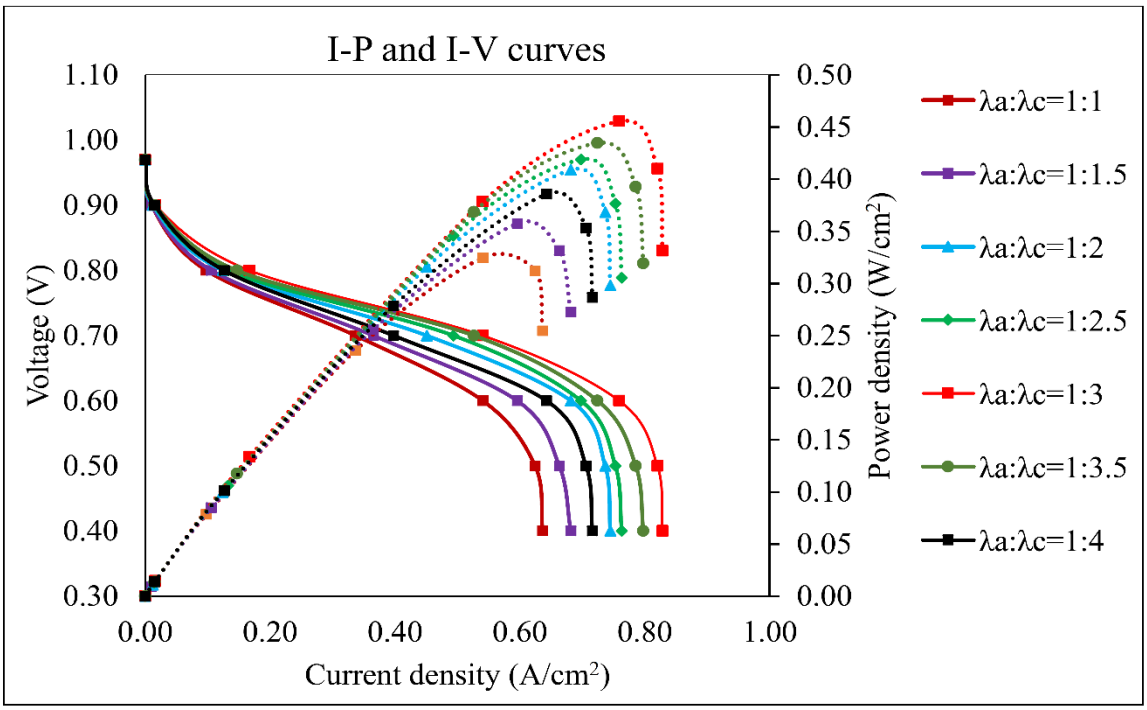

(b) Lung channel

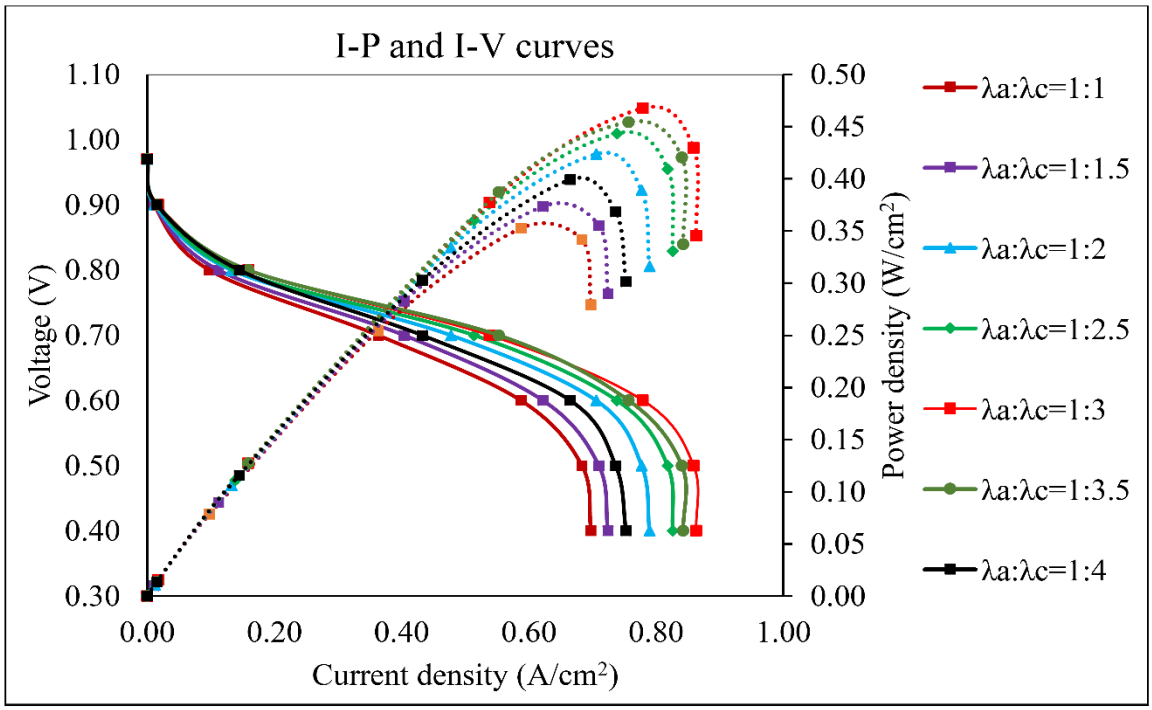

(c) Bio channel

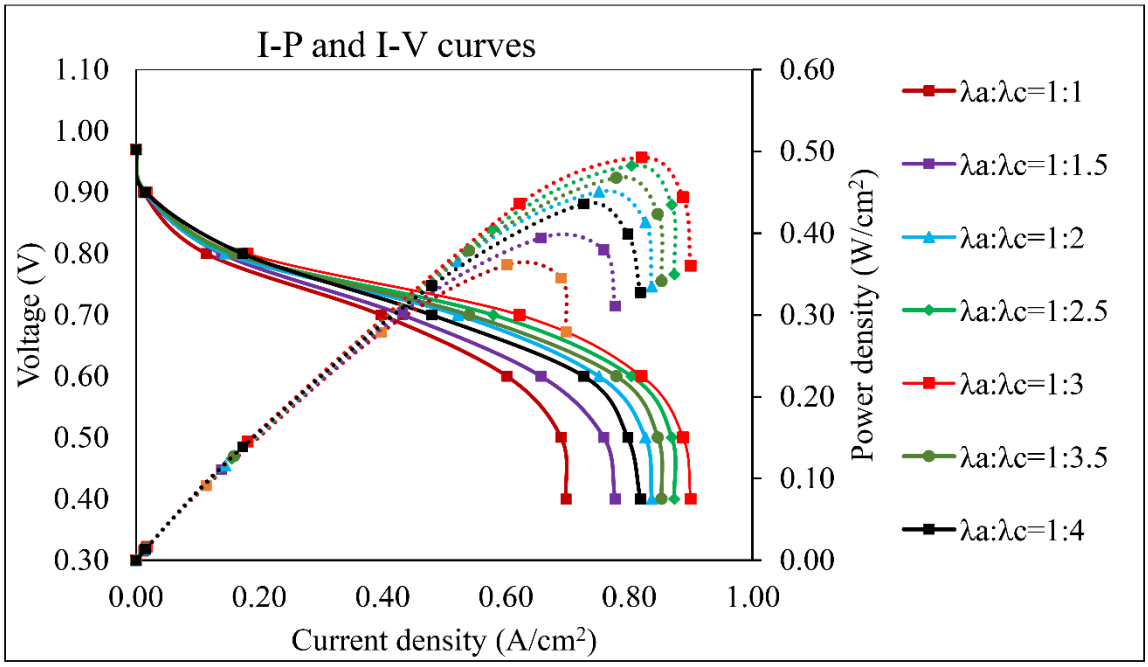

(d) Leaf channel

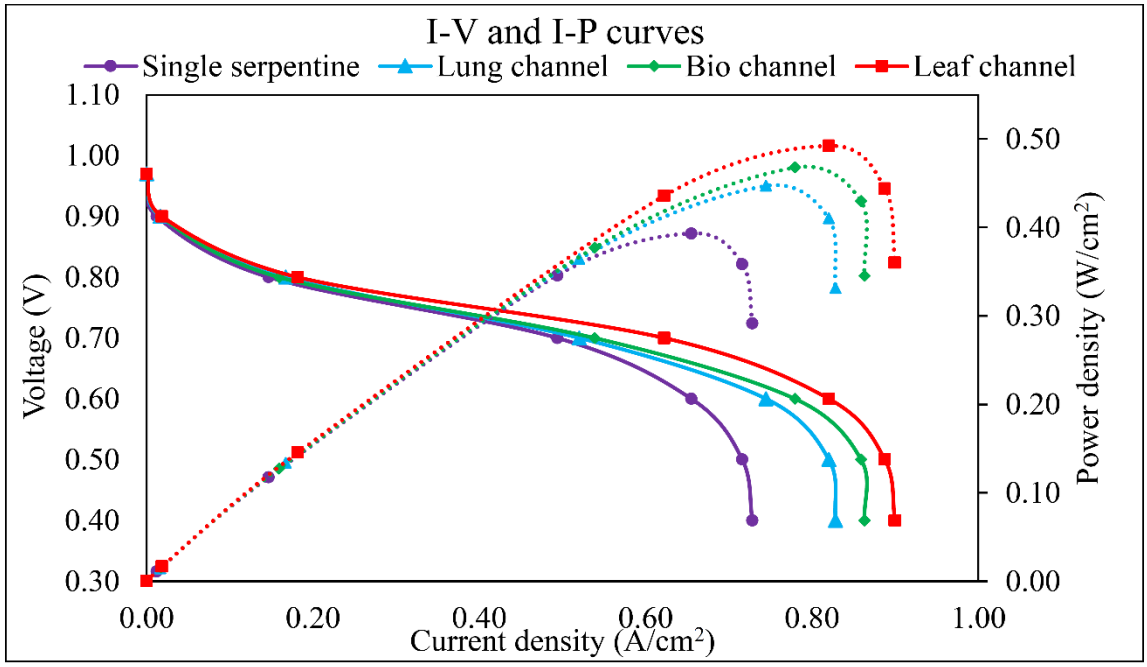

(e)

Fig. 5.5 Effect of flow rates interns of stoichiometric ratios on the performance of the fuel cell (a) Single serpentine flow channel (b) Lung channel (c) Bio channel (d) Leaf channel (e) Comparison of all the channels at 1:3 stoichiometric ratios

This is because oxygen release at the inlet of the fuel cell increases with increase in stoichiometric ratio on cathode, which provides more oxygen to catalyst layer for electrical reaction and also helps to remove water from the reaction area. With further increase in

stoichiometric ratio, the velocity of the reactants increases and the reactants may not have sufficient time to participate in reaction because of which they simply leave the cell without reaching the reaction zones. It is observed from Fig. 5.5 (e) that among the four flow field designs considered, the leaf channel design exhibited better performance of 0.57 W/cm^2 at 0.95 A/cm^2.

5.4.4 Influence of operating pressure

The performance characteristics of the fuel cell for four different flow channel designs at various operating pressures are indicated in Fig.5.6. The fuel cell operating pressure was varied from 1 bar to 3 bar with an interval of 1bar while other parameters were kept constant, i.e., the operating temperature was set at 70 ^{o}C, RH was set at 100%, back pressure was set at ambient pressure and the flow rates in terms of stoichiometric ratios was set at λ_a :λ_c = 1:3 respectively. The operating pressure of the fuel cell across anode and cathode remains constant. It can be observed that the polarization curves for all the four designs are similar in low current density. However, in the high current density region, the fuel cell performance steeply deteriorated with increase in the operating pressure.

The performance of the fuel cell was enhanced, with increase in operating pressure. The reason is that increase in operating pressure causes increase in reactant diffusivity through GDL, which increases the reaction rate. As a result, higher power is generated. Higher open circuit voltages at higher energies can be explained by Nernst equation. As the pressure rises, the overall polarization curve moves forward. Another reason for improved performance is that the partial pressure of the reaction gas increases as the operating pressure increases. Among the four flow channel designs considered, the leaf channel design exhibited better performance of 0.53 W/cm^2 at 0.88 A/cm^2.

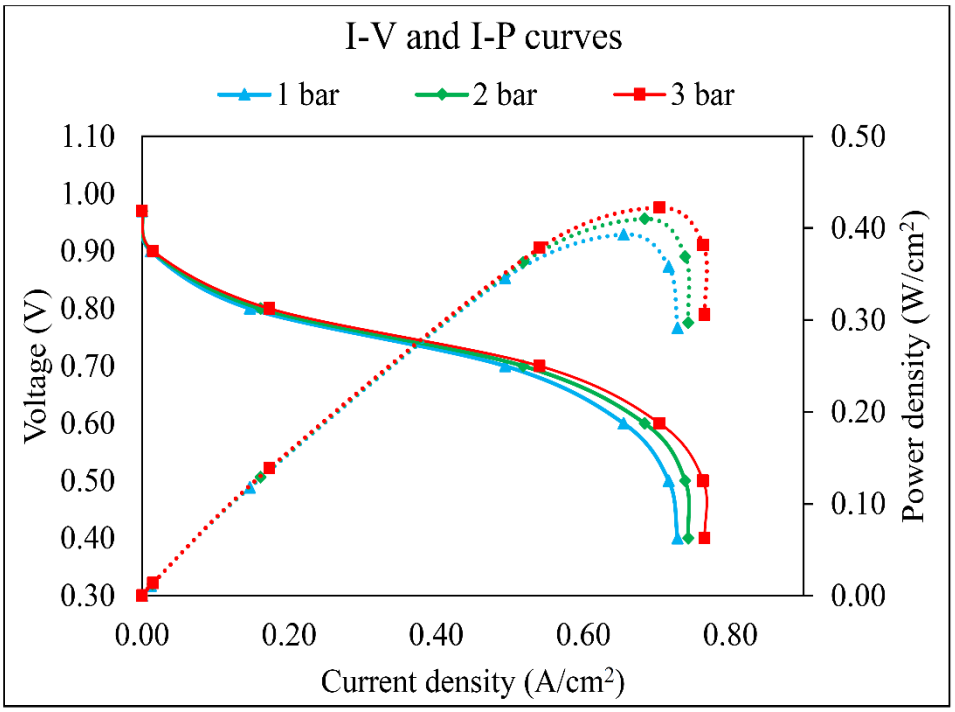

(a) Single serpentine channel

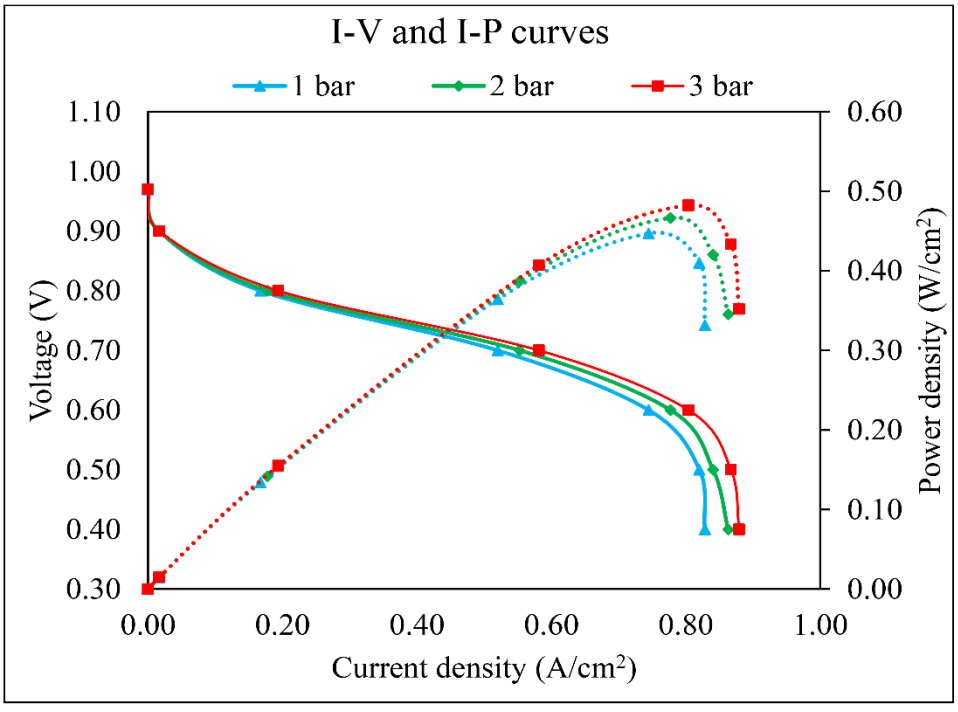

(b) Lung channel

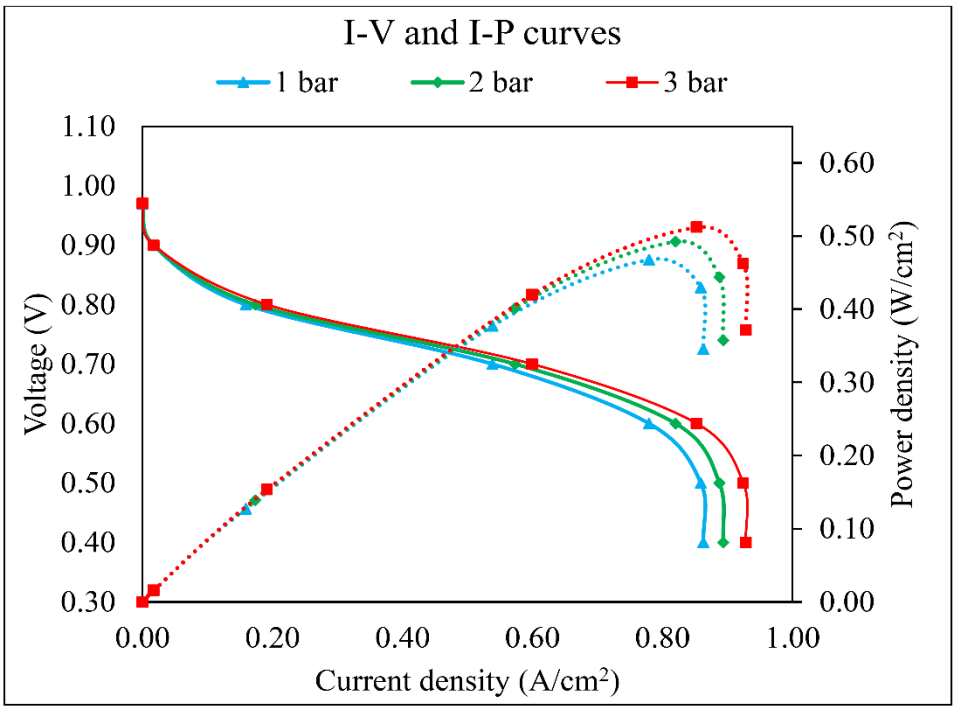

(c) Bio channel

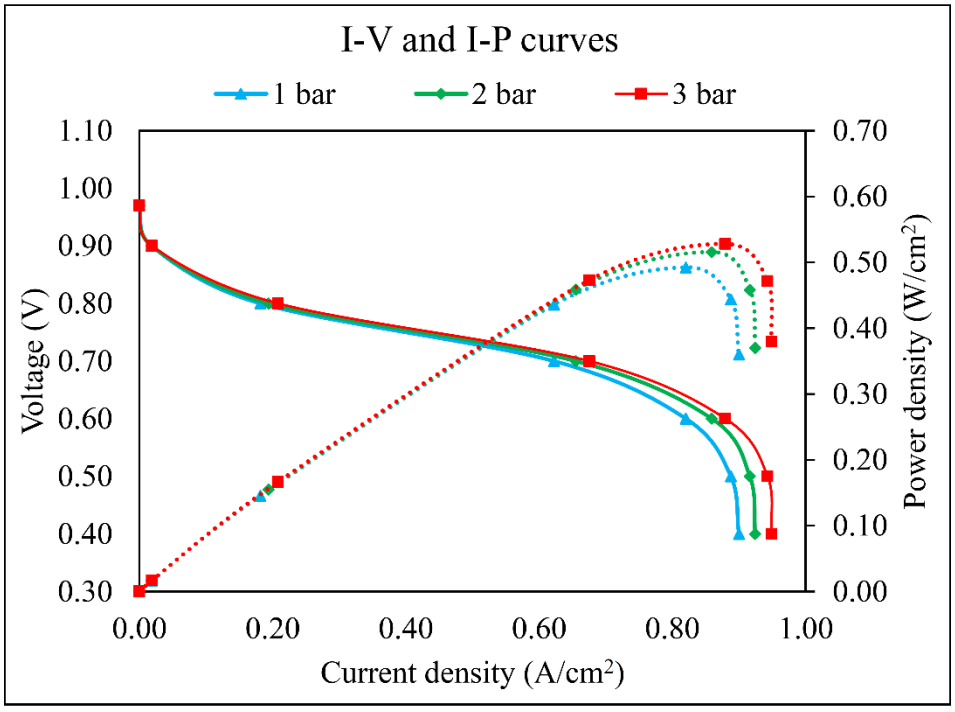

(d) Leaf channel

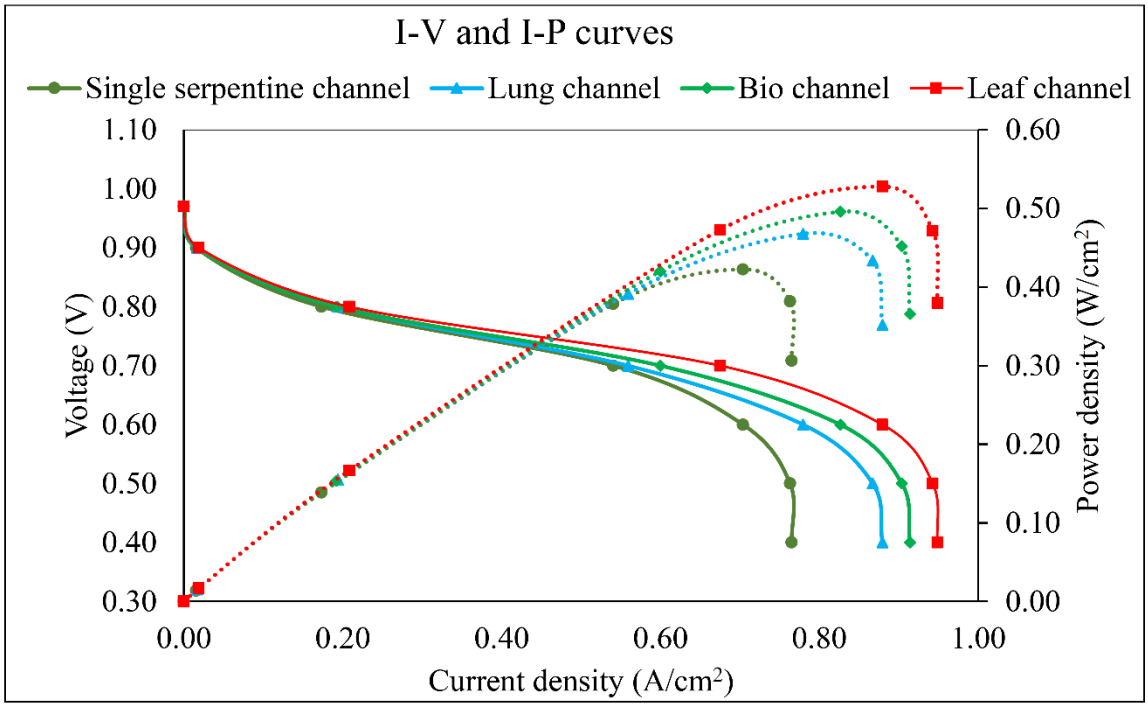

(e)

Fig. 5.6 Effect of operating pressure on the performance of the fuel cell
(a) Single serpentine flow channel (b) Lung channel (c) Bio channel (d) Leaf channel
(e) Comparison of four flow channel designs at 3 bar operating pressure

5.4.5 Influence of back pressure

The polarization and power curves of PEMFC at different back pressures for four different flow channel designs are shown in Fig. 5.7. The back pressures across anode and cathode remain the same. In these experiments, the back pressure was varied from 0 bar to 3 bar with an increment of 1 bar, while the other parameters such as operating temperature, RH, flow rates interns of stoichiometric ratios and operating pressure were set as 70 ^{o}C, 100%, $\lambda_a : \lambda_c$ = 1:3 and 3 bar respectively. The back pressure was equal to zero which means that the inlet and outlet pressure of the fuel cell are the same. The performance of PEMFC enhanced with increase in back pressure as shown in the Fig. 5.7for all four flow field designs.

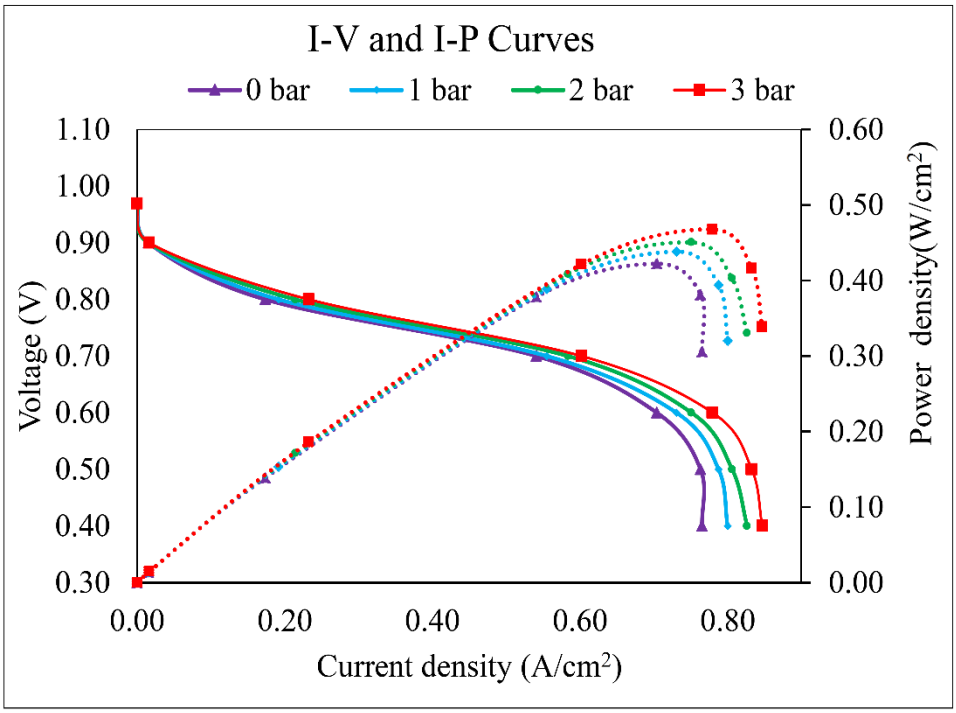

(a) Single serpentine channel

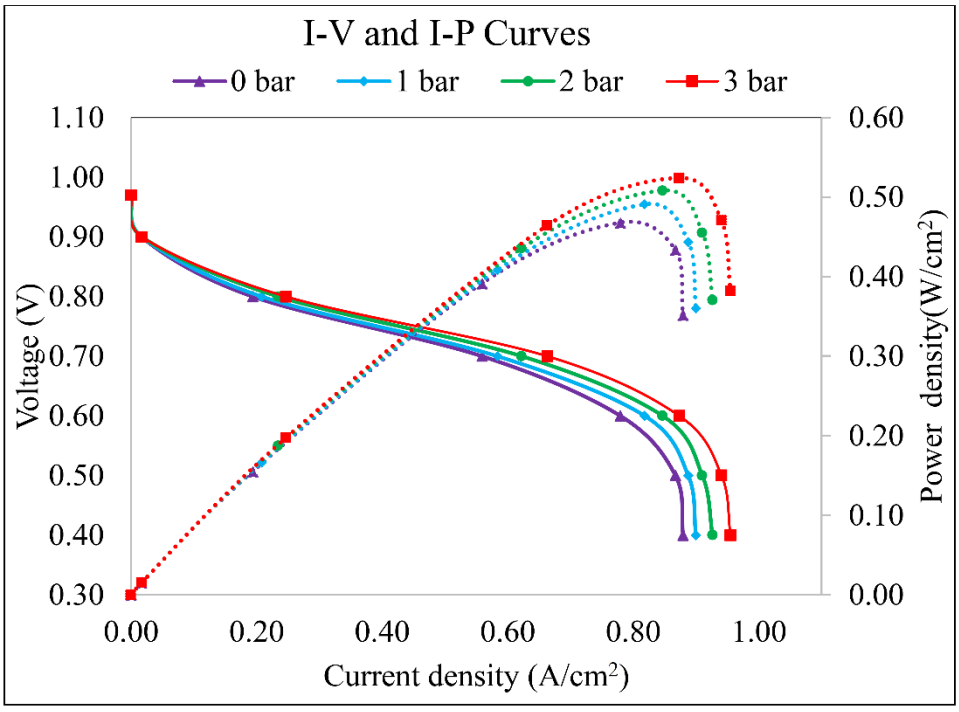

(b) Lung Channel

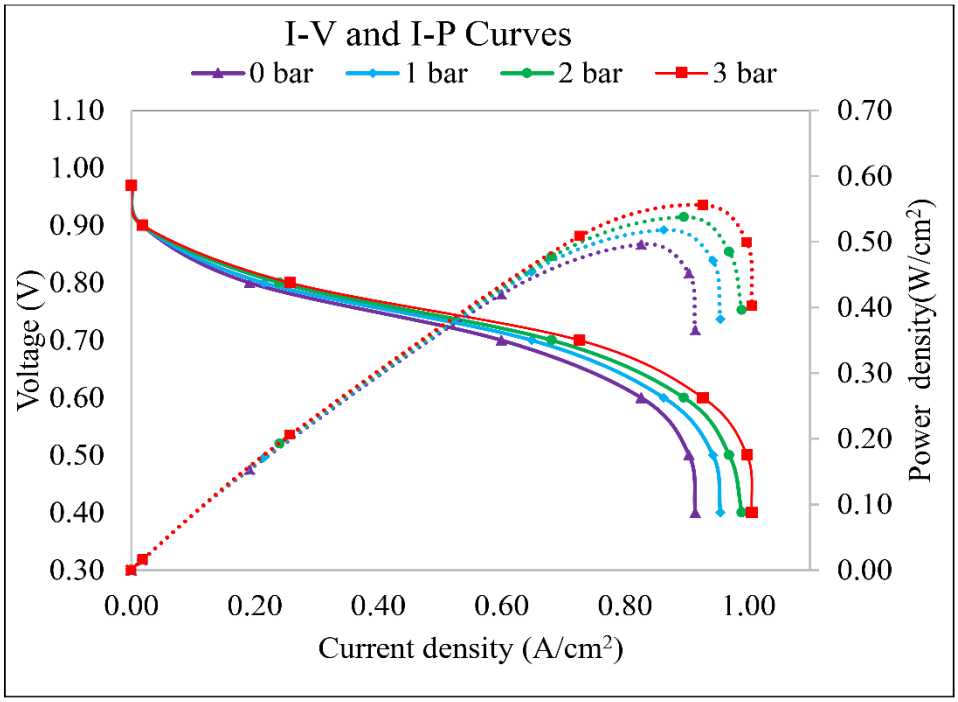

(c) Bio channel

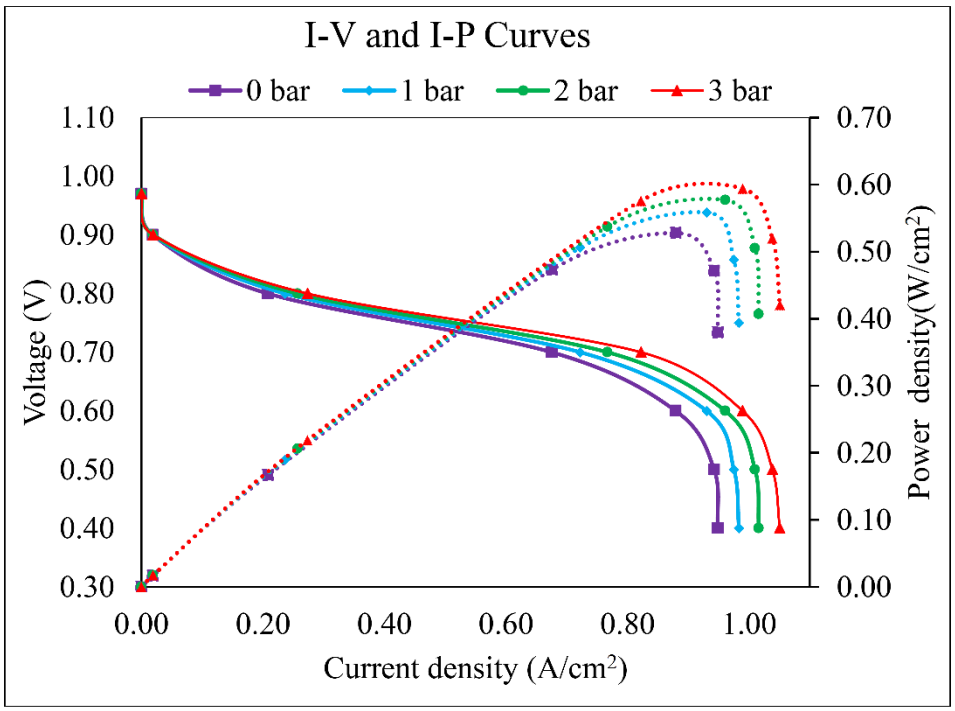

(d) Leaf Channel

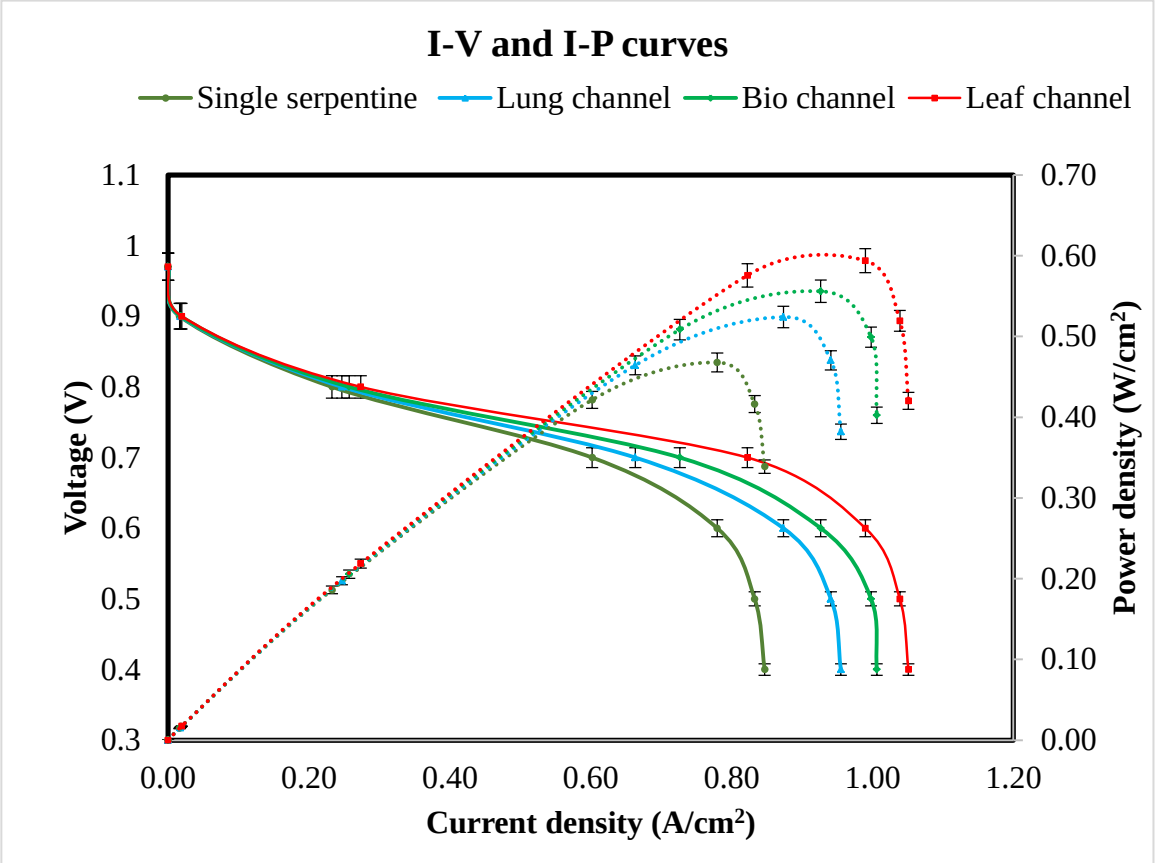

(e)

Fig. 5.7 Effect of back pressure on the performance of the fuel cell
(a) Triple serpentine flow channel (b) Lung channel (c) Bio channel (d) Leaf channel
(e) Comparison of four channels at 3 bar pressure

Back pressure has the following effects on PEMFC performance; (i) Increasing the back pressure would increase the absolute pressure of reactants within the porous electrode; which increases the diffusion rate of reactants across GDL; this in turn increases the reaction rate improving the performance. (ii) Reduction of activation losses due to increase in the activity of molecules. The polarization curves such as I-V curves and I-P curves drawn for four channels at the back pressure of 3 bar are shown in Fig. 5.7(e). Among the four flow channel designs considered, the leaf channel design exhibited better performance of power density 0.59 W/cm^2 at a current density of 0.99A/cm^2. Error bars has been implemented in the above graph using error analysis.

5.4.6 Net power density

Experiments were conducted for four flow fields at optimum operating conditions. From the experimental results, the measured pressure drop in the fuel cell for each flow field is shown in Fig. 5.8 (a). It is observed that the pressure drop is more for leaf channel design compared to other channel channels due to the disconnected inlet and outlet channels of the leaf design. It causes a large pressure drop across the discontinuity. The pressure differential between the inlet and outlet of the leaf channel design enhanced mass transport of reactants through GDL under the lands that facilitating quicker water removal.

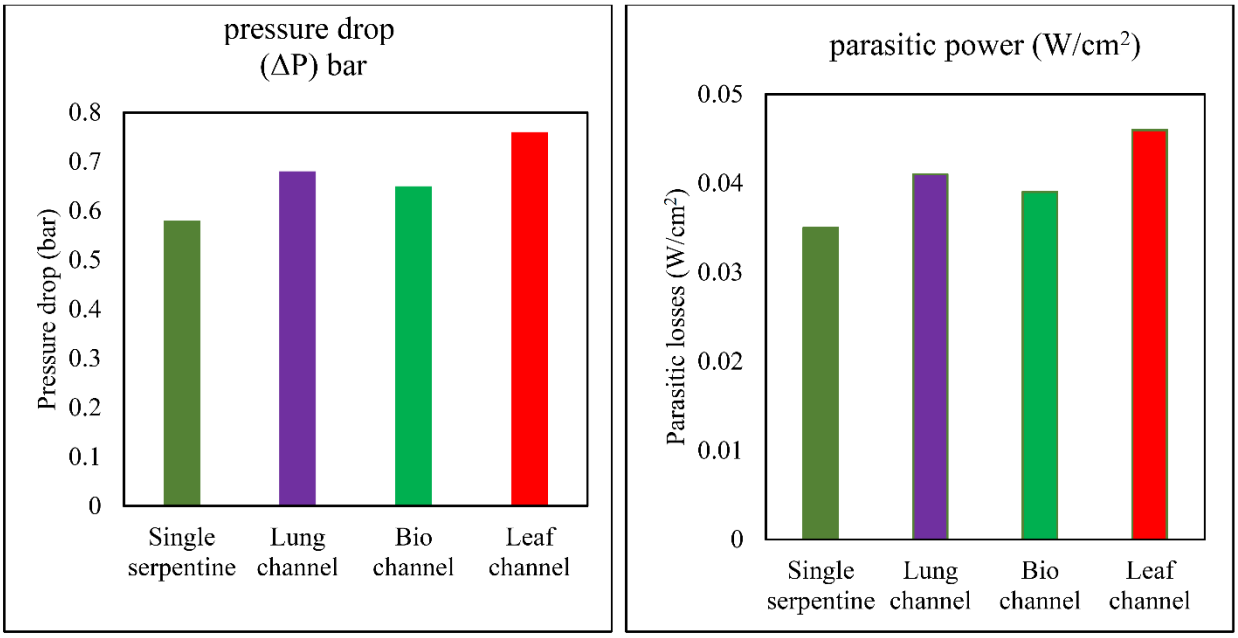

(a) (b)

Fig.5.8 (a) Measured pressure drop in the channels (b) Estimated parasitic losses

The parasitic losses (Wp) were calculated using the following relation given by Heidary et al. [152].

$$\mathbf{Wp} = \frac{\boldsymbol{\Delta P * A_{channel} * V}}{\boldsymbol{A_{total}}} \qquad (5.8)$$

Where ΔP is the pressure drop, V is the velocity at inlet of the channel, $A_{channel}$ is the channel cross sectional area and A_{total} is the active area of the fuel cell respectively.

The net power density is calculated as shown below:

$$W_{net} = W_G - W_P \quad (5.9)$$

Where W_{net} is the net power density, W_P is the parasitic losses and W_G is the gross power density.

Table 5.3 Fuel cell net power density calculations

Type of channel	pressure in (bar)	pressure out (bar)	pressure drop (ΔP) bar	parasitic power (W_p) (W/cm^2)	Gross Power density (W_g) (W/cm^2)	Net Power density (W_n) ($W_n = W_g - W_p$) (W/cm^2)
Single serpentine	3	2.42	0.58	0.035	0.47	0.434
Lung channel	3	2.32	0.68	0.041	0.52	0.478
Bio channel	3	2.35	0.65	0.039	0.56	0.521
Leaf channel	3	2.24	0.76	0.046	0.59	0.544

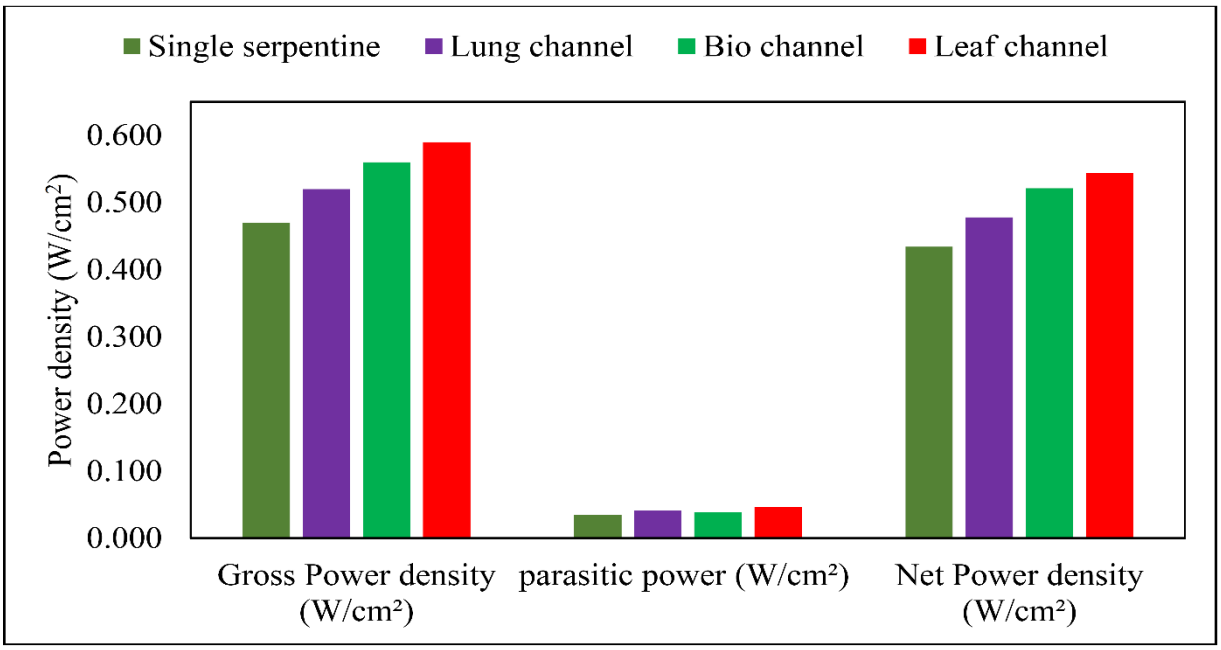

Fig. 5.9 Gross power density and net power density chart

From Fig. 5.9 it is observed that the performance of the leaf channel designs is better compared to single serpentine channel design. Because the lack of a direct connection increased the pressure differential between the inlet and outlet that, in turn, increased the average velocity and reactant concentration within the GDL, both of which helped with higher performance in bio-inspired designs. The performance of serpentine channels is low, due to reactants being transported by diffusion only. Diffusion is a relatively slow process. The calculations of parasitic losses and net power density are shown in Table 5.3.

By considering parasitic losses, it can be seen that PEMFC with the single serpentine channel design generated 0.433 W/cm^2; similarly PEMFC with lung channel design, bio channel design and non-interdigitated leaf channel design generated 0.471 W/cm^2, 0.514 W/cm^2, 0.527 W/cm^2 net power density respectively. The PEMFC net power density with leaf channel design was 25.3 % more when compared with single serpentine channel design, 13.8 % more when compared with lung channel design, and 4.41 % more when compared with bio-channel design respectively.

5.4.7 Summary

In the present work, an experimental study was carried out to analyse the performance of the PEMFC with four different flow fields, viz., single serpentine flow channel, Lung channel, bio-channel and leaf channel designs, under different operating conditions. This study analyzed the influence of the operating parameters such as operating temperature, RH of the reactants, flow rates in terms of stoichiometric ratios, operating pressure and back pressures on the performance of the fuel cell fitted with different channel designs. The following conclusions are drawn from the present study:

- The fuel cell performance enhanced, when the operating temperature increases from 40 ^{o}C to 70 ^{o}C. The performance is maximum at 70 ^{o}C. However, the performance of the cell deteriorated beyond 70^{o}C operating temperature.
- Relative Humidity (RH) had considerable influence on the cell performance. Greater values of RH caused greater power output of the fuel cell.

- The performance of the fuel cell enhanced as the stoichiometric ratio is increased from λ_c=1 to λ_c=3; any further increase of stoichiometric ratio gives the same performance or slightly decreased performance.
- With the increase in cell operating pressure, the cell performance improved.
- Back pressure had a positive effect on the cell performance, i.e., the PEMFC performance enhanced with the increment of back pressure.
- It can be observed from the results that the leaf channel design performed better among the four channel designs.
- The PEMFC net power density with leaf channel design was 25.3 % more when compared with single serpentine channel design, 13.8 % more when compared with the lung channel design, and 4.41 % more when compared with the bio-channel design respectively.

From this study Leaf channel design is observed as best flow filed configuration. Further, experimental study was carried out to analyse the performance of PEMFC with four different design modifications of a leaf channel flow filed, viz., non-interdigitated leaf channel design (NILCD), interdigitated leaf channel design (ILCD), interdigitated leaf channel design with curved edges (ILCDWCE) and Murray's design, under optimum operating conditions.

Chapter - 6
Experimental results and discussion

Influence of design modifications on a leaf channel on the performance of proton exchange membrane fuel cell

6.1 Introduction

The bio-inspired design was inspired by the vein structures of leaves, which transport mass efficiently from one central source to the whole surface of a leaf, mirroring the function of bipolar plate flow fields. The developed bio-inspired "leaf" design consists of three generations of channels. At the end of all of the channels, reactants were forced to flow through the GDL and merge into the outlet. The main aim of modifications in a leaf channel design was to facilitate reducing the resistance to flow of reactants, enhance diffusion rate of reactants through gas diffusion layer (GDL) to reach reaction sites, ensure uniform distribution of reactants, aid better water removal rate from reactant sites, improve the active surface area for reaction and also minimize pressure drop without losing the strength of a bipolar plate.

6.2 Experiment

Experiments were conducted using WonATech (Korea) programmable fuel cell test station (FCTS) located at the Center for Sustainable Energy laboratory of NIT Warangal (India). The design parameters of various leaf channel designs are shown in Table 6.1. In the present work, an experimental study was carried out to analyse the performance of PEMFC with four different design modifications of a leaf channel, viz., Non Interdigitated Leaf Channel Design (NILCD), Interdigitated Leaf Channel Design (ILCD), Interdigitated Leaf Channel Design with Curved Edges (ILCDWCE) and Murray's design, under optimum operating conditions.

Membrane electrode assembly (MEA) (N212), of 49 cm^2 active area with membrane of thickness 0.0175mm with 40 % platinum loading of 0.4 mg cm^{-2} at the anode and 0.6 mg cm^{-2} at the cathode was used. Carbon paper of thickness 0.38 mm was used as the gas diffusion layer (GDL), and catalyst layers of 0.05 mm thick were used on either side of the membrane. The MEA, bipolar plates and current collectors used in the experimentation are provided by Vinpro technologies. The experimental results of non- interdigitated leaf channel design (NILCD) are compared with interdigitated leaf channel design (ILCD), interdigitated leaf channel design with curved edges (ILCDWCE) and Murray's design flow-channel at optimum operating conditions.

Table 6.1 Design parameters of different leaf channels

S. No.	Design parameter	NILCD	ILCD	ILCDWCE	Murray's design
1	Active area	49 cm^2	49 cm^2	49 cm^2	49 cm^2
2	Bipolar plate thickness	10 mm	10 mm	10 mm	10 mm
3	Channel width	1 mm	1 mm	1 mm	1 mm
4	Channel depth	1 mm	1 mm	1 mm	1 mm
5	Land width	2.5 mm	2.5 mm	2.5 mm	2.5 mm
6	Leaf angle	45^o	45^o	45^o	45^o
7	Edge radius	--	--	3mm	--

6.3 Results and discussion

6.3.1 Influence of interdigitated leaf channel design (ILCD)

The influence of interdigitated leaf channel design on PEMFC performance at optimum operating conditions was investigated experimentally. The leaf channel design was divided into two categories based on construction i.e. non-interdigitated leaf channel design (NILCD) and interdigitated leaf channel design (ILCD) as shown in Fig. 6.1. In NILCD there is connectivity between the channel inlet channels and the outlet channels. Generally, in the non-interdigitated leaf channel design, the reactant gasses are transported to the catalyst layers from the gas channels predominantly by diffusion.

The ILCD was composed of two sets of dead-end parallel channels, one of which was connected to inlet and the other to outlet. In the ILCD lack of a direct connection between the inlet and outlet channels force water through gas diffusion layer (GDL). Due to disconnected inlet and outlet channels of the leaf design, pressure drops across the discontinuity become larger. The pressure differential between the inlet and outlet of the leaf channel design enhanced mass transport through GDL under the lands that facilitating quicker water removal, increased the average velocity and reactant concentration within the GDL, both of which helped with higher performance. This caused a convective flow through the gas diffusion layer under the rib, thus enhancing mass transport of reactant gases. In case of ILCD, the pressure drop is very large compared to NILCD because of the larger flow resistance across GDL in the interdigitated design. In the ILCD, as the reactants pass through closed channels

of the flow field, they are forced to flow through the GDL in reaching the catalyst layer. Thus, the combined effect of diffusive mass transfer and forced convection mass transfer in ILCD results in increased power output of the fuel cell.

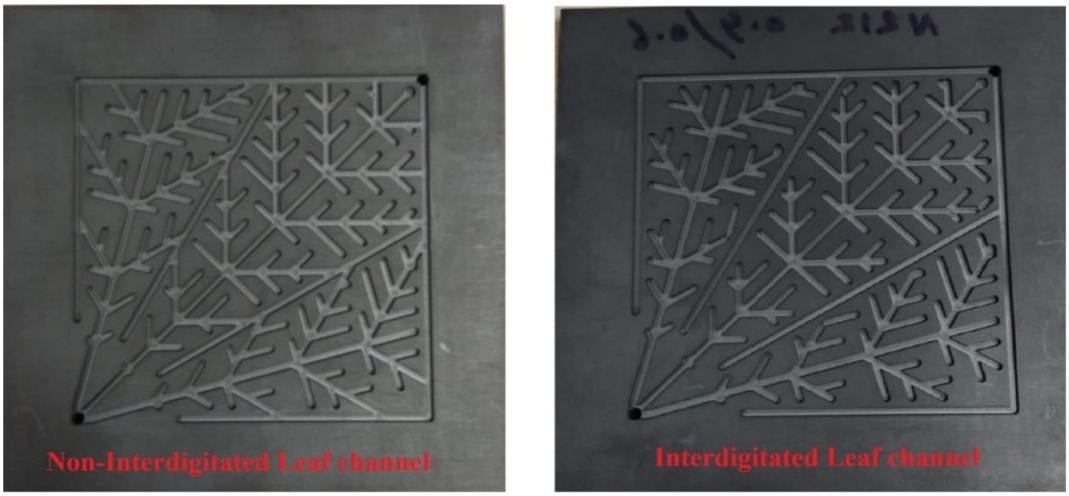

(a) (b)

Fig. 6.1Configurations of different leaf channel designs (a) NILCD (b) ILCD

The performance characteristics of the fuel cell with non-interdigitated leaf channel design and interdigitated leaf channel design bipolar plates are shown in Fig 6.2. These experiments were conducted at optimum values of the operating parameters. These optimum operating parameters, as explained in the earlier sections are: operating temperature of the fuel cell is 70 ^{o}C, RH of the reactants is 100 %, back pressure is 3 bar and operating pressure is 3 bar. The flow rate of hydrogen on anode was set at 350 ccm (λ=1) and the flow rate of oxygen on cathode was set at 525 ccm (λ=3), respectively. From the figure, it can be seen that PEMFC with non-interdigitated leaf channel generated 0.57 W/cm^2 power density at 0.95 A/cm^2 current density, while the cell with interdigitated channel design generated 0.61 W/cm^2 power density at 1.02 A/cm^2 current density; thus, it generates 7.01% more power density for ILCD than for NILCD. In the interdigitated leaf channel design, as the reactants pass through the closed channels of the flow field, they are forced to flow through GDL in reaching the catalyst layer. Thus, the combined effect of diffusive mass transfer and forced convection mass transfer in the interdigitated flow channel results in increased power output of the fuel cell.

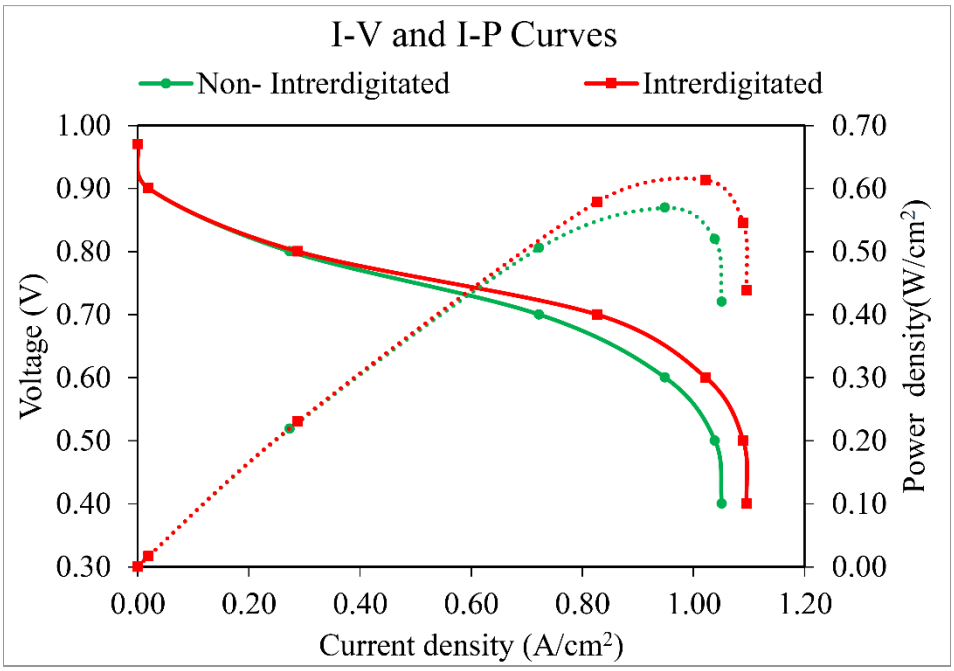

Fig. 6.2 I-V and I-P curves of NILCD and ILCD

6.3.2 Influence of interdigitated leaf channel design with curved edges (ILCDWCE)

The influence of inter digitated leaf channel design with curved edges (ILCDWCE) on the PEMFC performance at optimum operating conditions was investigated experimentally. The configurations of NILCD and ILCDWCE are shown in Fig. 6.3. The ILCDWCE has the following advantages: the reaction area increases slightly, the flow is smooth and uniform, resistance to flow decreases, and water can be removed easily from the reaction area and this also minimizes the pressure drop. The performance characteristics of the fuel cell with NILCD and ILCDWCE are shown in Fig 6.4. Experiments were conducted at optimum values of operating parameters. These optimum operating parameters, as explained in earlier sections are: operating temperature of the fuel cell is 70 ^{o}C, RH of the reactants is 100 %, back pressure is 3 bar and operating pressure is 3 bar. The flow rate of hydrogen on anode was set at 350 ccm (λ=1) and the flow rate of oxygen on cathode was set at 525 ccm (λ=3), respectively.

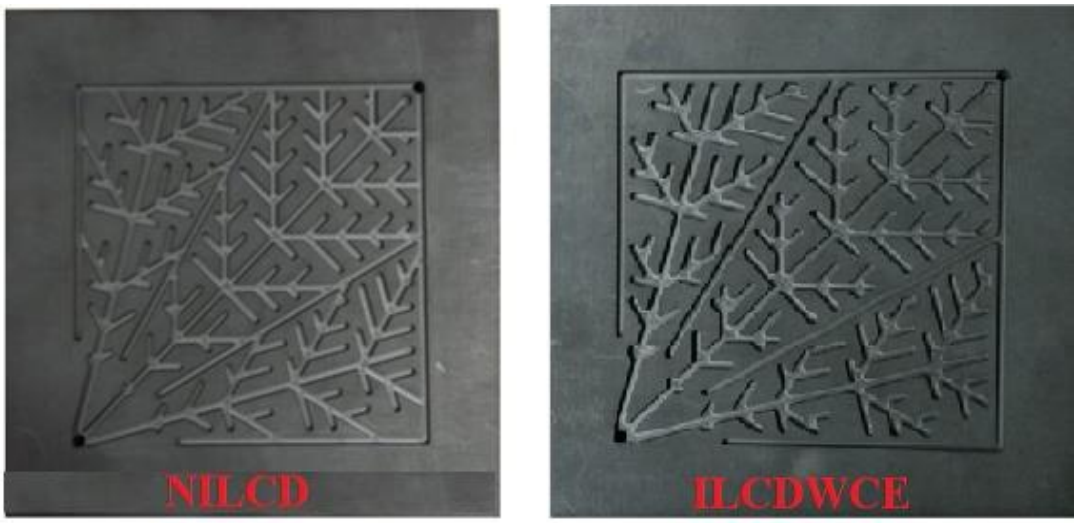

Fig.6.3 Configurations of different leaf channel designs (a) NILCD (b) ILCDWC

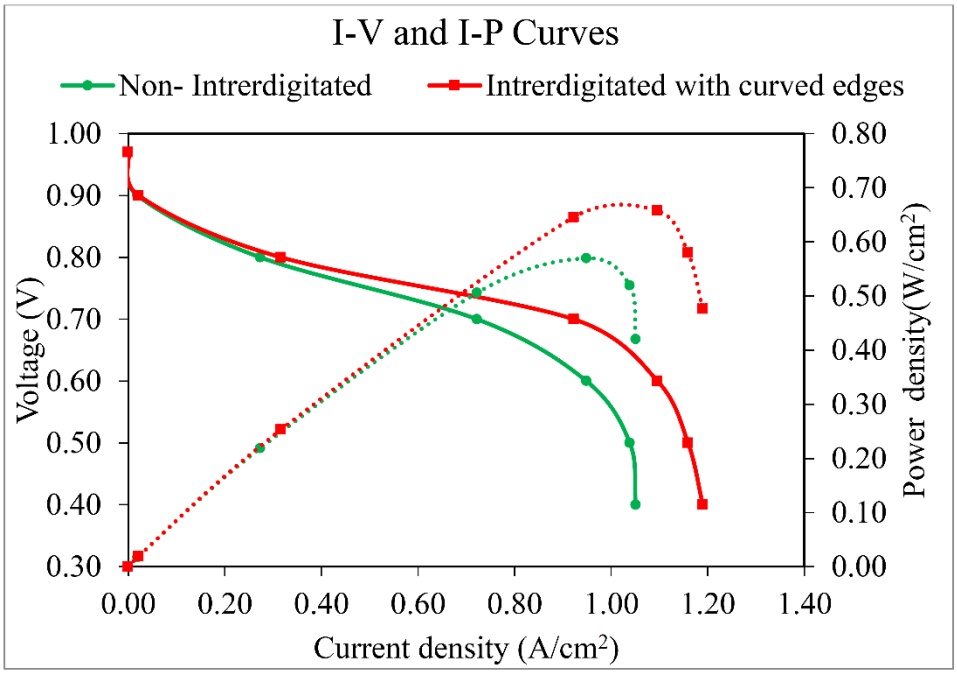

Fig. 6.4. I-V and I-P curves of NILCD and ILCDWC

It is observed from the results that PEMFC with the NILCD generated 0.57 W/cm^2 power density at 0.95 A/cm^2 current density, while the fuel cell with ILCDWCE design generated 0.66 W/cm2 power density at 1.10 A/cm2 current density; thus, it is 15.7% more power density for ILCDWCE than for NILCD. This is because ILCDWCE has the following advantages: the reaction area increases slightly, the flow is smooth and uniform, resistance to

flow decreases, and water can be removed easily from the reaction area and also minimizes the pressure drop.

6.3.3 Effect of Murray's design leaf channel

Murray's law is derived based on the distribution of mass in the biological structure with minimum energy consumption and also to maintain metabolic processes. The advantage of Murray's law is to minimize the resistance to flow in the branching system. A bio-inspired leaf flow field pattern was designed by mimicking the hierarchical structures of leaf veins. The whole flow field was divided into three sub-areas, and each sub-area had one hierarchical structure (branch) to supply reactants. The left branch and the right branch were taken to be identical. To reduce design complexity, the hierarchical structures were restricted to three generations, i.e., primary, secondary and tertiary generations. The angles between different channels were 45^{o}. The NILCD and the Murray's channel design are shown in Fig. 6.5.

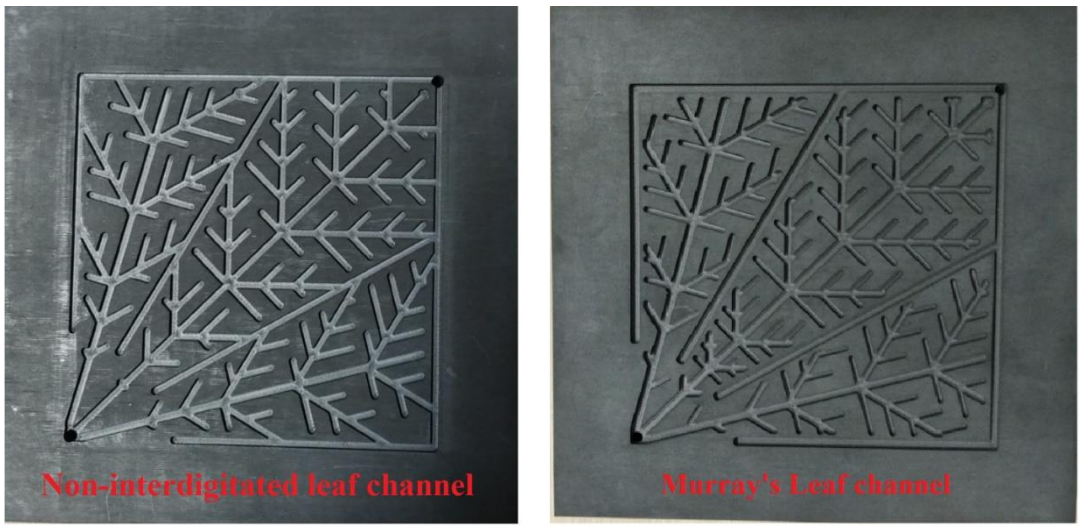

Fig. 6.5 Configurations of different leaf channel designs (a) Non-interdigitated (b) Interdigitated

Channel width is constant (i.e. 1mm) for all generations of a flow channel in case of NILCD and ILCD and the channel width is variable in case of Murray's design. The tertiary. Secondary and primary generations of channel widths were taken as 1.0 mm, 1.2 mm and 1.5 mm respectively. The dimensions of different generations of channels are given in Table 6.2. Murray's law, which is known as an optimum configuration found in biological circulatory systems, is used to determine the flow channel widths of different generations.

Table: 6.2 Channel widths of the bio-inspired leaf flow field design determined by Murray's law.

Branches	Generation	Channel width (mm)	Hydraulic diameter (mm)
Right, middle & left branches	1st	1.5	1.2
	2nd	1.2	1.02
	3rd	1.0	1

The hydraulic diameter for a rectangular channel is calculated using equation 6.1.

$$d^H = \frac{4A_c}{P} = \frac{2WD}{W+D} \tag{6.1}$$

Here, A_c is the channel's cross-sectional area, P is the perimeter, W is the channel width, and D is the channel depth. As long as the hydraulic diameter is the same, the flow resistance in the channels is also the same irrespective of variation of width and depth.

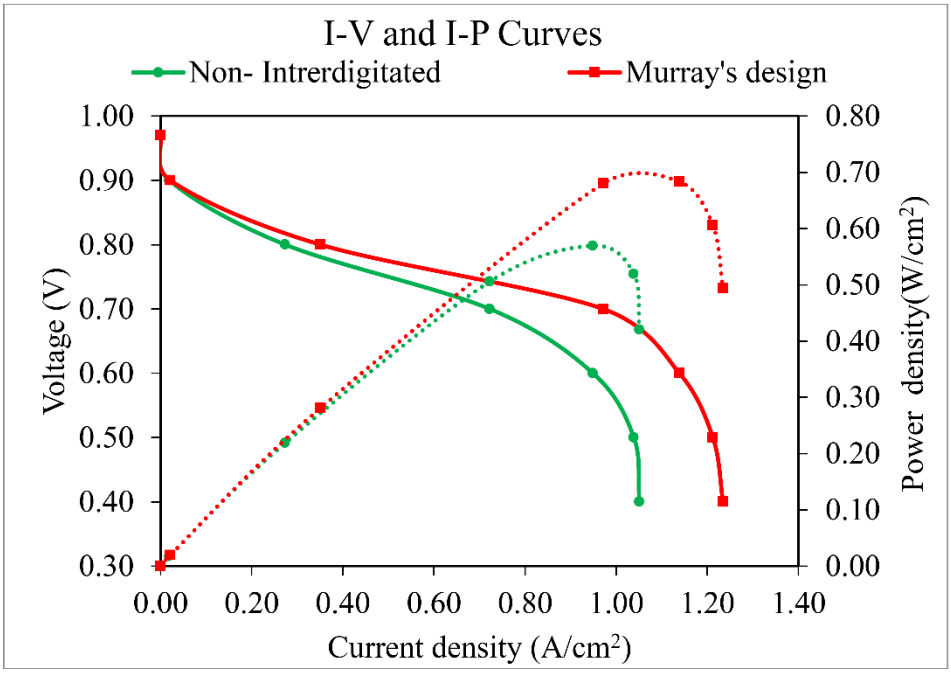

Fig. 6.6 I-V and I-P curves of NILCD and Murray's design

Experimental results of PEM fuel cells using different flow channel designs at the optimum values of the operating parameters are shown in Fig. 6.6. These optimum operating parameters, as explained in the earlier sections are: operating temperature of the fuel cell is 70

^{o}C, RH of the reactants is 100 %, back pressure is 3 bar and operating pressure is 3 bar. The flow rate of hydrogen on anode was set at 350 ccm (λ=1) and the flow rate of oxygen on cathode was set at 525 ccm (λ=3), respectively. The bio-inspired design using Murray's law is compared to a design with constant channel width.

From the figure, it is noticed that PEMFC with NILCD generated 0.57 W/cm^2 power density at 0.95 A/cm^2 current density, while the cell with Murray's design generated 0.68 W/cm^2 power density at 1.14 A/cm^2 current density; thus, it is 19.29% more power density for the interdigitated flow channel design than for non-interdigitated leaf channel design. This is due to better distribution of reactants and also enhancement of oxygen concentration at tertiary channels. The Flow channel with Murray's design minimized the energy consumption for supply of reactants, facilitate uniform distribution of reactants through GDL and also minimised the flow resistance.

6.3.4 Comparison of different types of leaf channel designs with Single Serpentine Channel

The PEMFC with NILCD, ILCD, ILCDWCE and Murray's design are considered for comparison as shown in Fig. 6.7. Using bio-inspired structures, the reactants can be effectively carried from central position to the entire surface of the channels as in the case of leaves. The bio-inspired leaf structure comprises three channel groups and at the finishing point of the flow channels, the reactants are passed through a porous layer of the GDL and join at exit flow channels. The water generated is passed through GDL with force because of higher pressure difference between inlet and exit flow channels and this pressure difference was exists due to the dis-connectivity between the channels. The transportation of reactants across GDL is enhanced by the leaf channel design, which ultimately leads to faster removal of generated water in the channels. The average velocity as well as reactant concentration at reaction sites is enhanced because of high pressure drop[153].

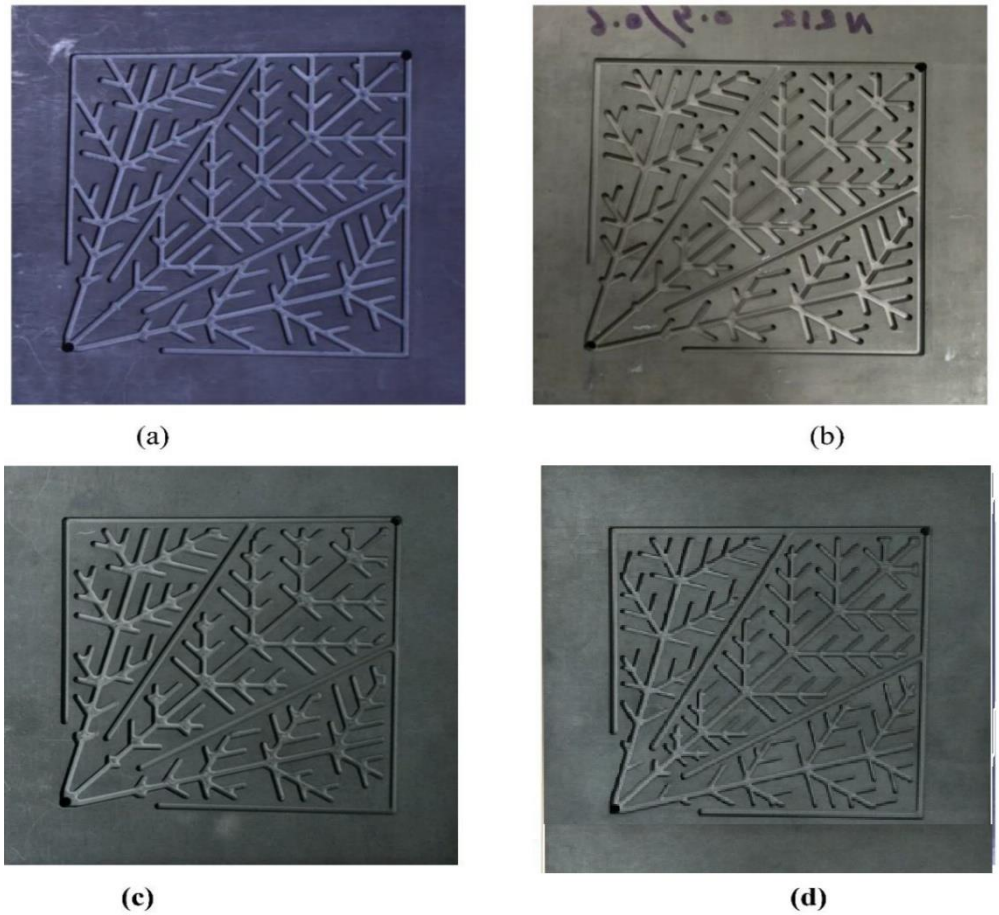

Fig. 6.7 Configurations of different leaf channel designs (a) NILCD, (b) ILCD, (c) ILCDWCE, (d) Murray's design

The leaf channel design with curved edges has the following advantages: reaction area increases slightly, the flow is smooth and uniform, resistance to flow decreases, and water can be removed easily from the reaction area and it also minimizes the pressure drop. The Murray's law design has following advantages such as enhance the oxygen concentration at tertiary channels, minimized the energy consumption for supply of reactants, facilitate uniform distribution of reactants through GDL and also minimised the flow resistance.

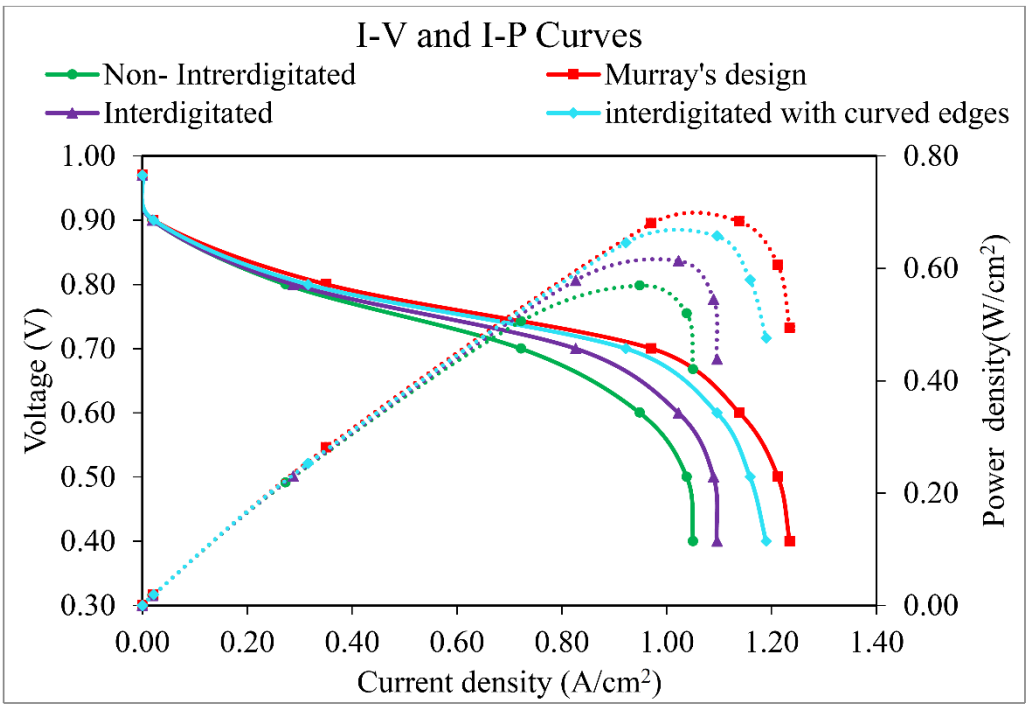

Fig. 6.8 I-V and I-P curves of different flow channels

I-V curves and I-P curves of the fuel cell fitted with NILCD, ILCD, ILCDWCE and Murray's design at optimized values of working parameters are shown in Fig. 6.8. Fuel cell operating temperature was set at 70^{o}C, AHT and RH of the reactants is 100 %, respectively and the flow rates were set at 350 ccm on anode and 525 ccm on cathode respectively. Similarly, the fuel cell working pressure and the back pressure were set at 3 bar and 3 bar respectively. From Fig. 6.8, it is observed that PEMFC with Murray's design developed maximum power density of 0.68 W/cm^2 at a current density of 1.14 A/cm^2. Similarly, ILCDWCE developed a peak power density of 0.66 W/cm^2 at a current density of 1.10 A/cm^2, ILCD generated a peak power density of 0.62 W/cm^2 at a current density of 1.02 A/cm^{2}and NILCD developed a peak power density of 0.57 W/cm^2 at a current density of 0.95 A/cm^2 respectively. The fuel cell with Murray's design is 19.29 % more efficient than the fuel cell with NILCD; ILCDWCE is 15.7 % more efficient than PEMFC with NILCD and the fuel cell with ILCD is 7.01 % more efficient than fuel cell with NILCD. This is due to better reactant distribution and minimum pressure difference in PEMFC with Murray's design when compared with other designs. A comparison is made between the different flow channel designs as shown in Table 6.3.

Table 6.3 Output values of different flow channels

S. No	Type of flow channel	Power density (W/cm^2)	Current density (A/cm^2)
1	PEMFC with Murray's design	0.68	1.14
2	PEMFC with ILCDWCE	0.66	1.10
3	PEMFC with ILCD	0.62	1.02
4	PEMFC with NILCD	0.57	0.95

6.3.5 Net power density

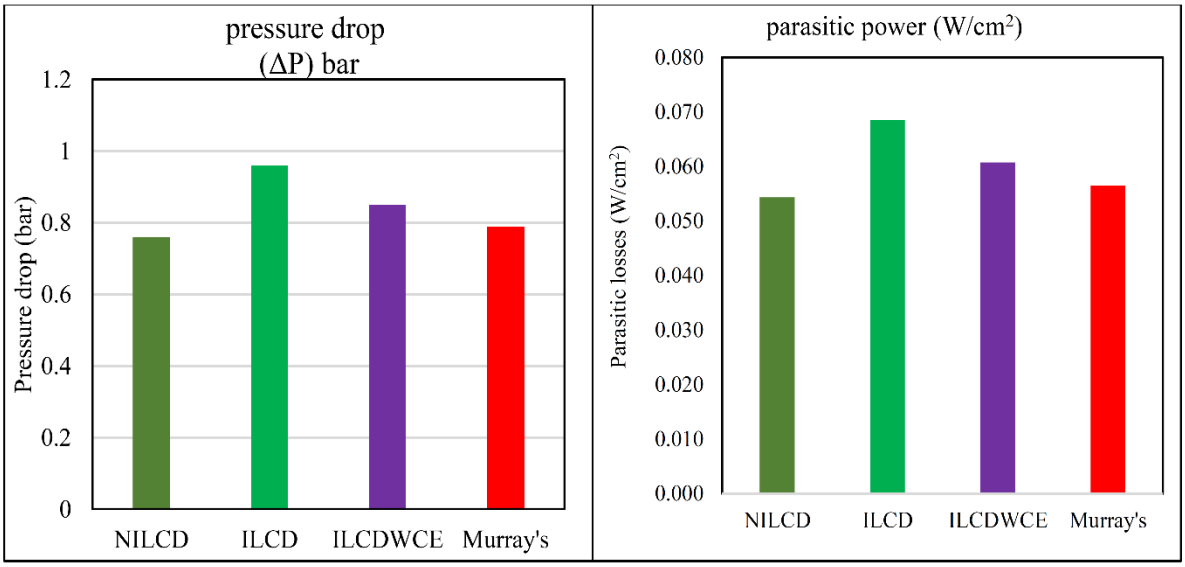

(a) (b)

Fig. 6.9 (a) Measured pressure drop in the channels (b) Estimated parasitic losses

Experiments were conducted for four different design modifications of leaf channel design at optimum operating conditions. From the experimental results, the pressure drop in the fuel cell for each flow field configurations is shown in Fig.6.9. It is observed that the pressure drop is more for interdigitated leaf channel design compared to other leaf channel configurations due to lack of direct connectivity between inlet and outlet channels of the interdigitated leaf design. It causes a large pressure drop across the disconnected ends. The pressure differential between the inlet and outlet of the leaf channel design enhanced the mass transport of reactants through GDL under the lands that facilitating quicker water removal. The reactants supplied to reaction sites

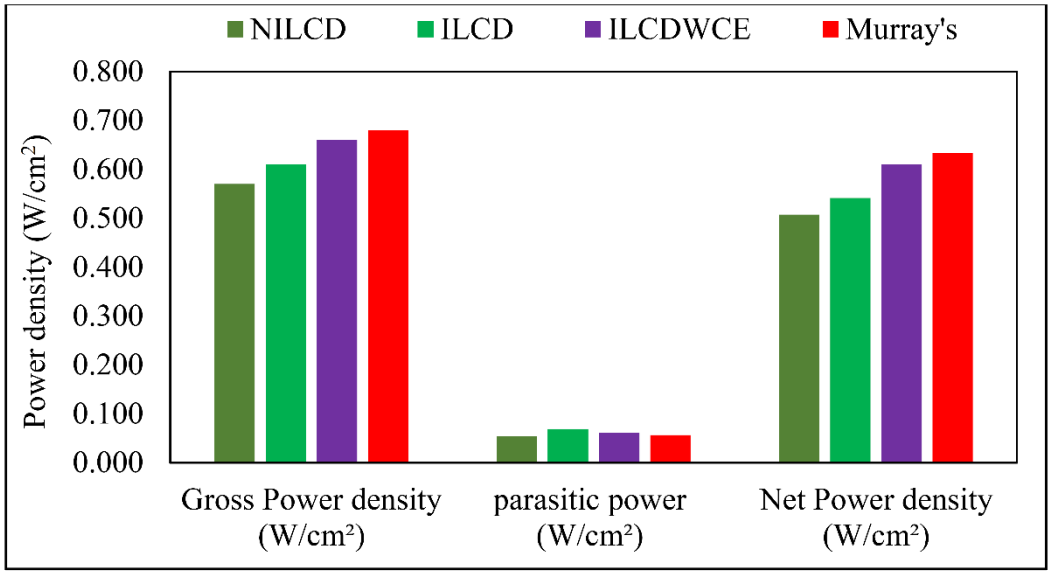

Fig.6.10 Gross power density and net power density chart

From Fig.6.10 it is observed that the performance of the Murray's design is better compared to other three designs i.e. NILCD, ILCD and ILCDWCE. This is due to better distribution of reactants and also enhance oxygen concentration at tertiary channels. The Flow channel with Murray's design minimized the energy consumption for supply of reactants, facilitated uniform distribution of reactants through GDL and also minimised the flow resistance. A comparison is made between different flow channel designs as shown in Table 6.4. By considering parasitic losses, it can be seen that PEMFC with Murray's design generated 0.624 W/cm^2; similarly PEMFC with ILCDWCE, ILCD and NILCD generated 0.599 W/cm^2, 0.541 W/cm^2, 0.516 W/cm^2 net power density respectively. The PEMFC net power density with Murray's design was 20.93 % more when compared with NILCD, 15.34 % more when compared with ILCD, and 4.17 % more when compared with ILCDWCE respectively.

Table 6.4 Net power density of a different flow channel configurations

Type of flow channel	**pressure in (bar)**	**pressure out (bar)**	**pressure drop (ΔP) bar**	**parasitic power (W_p) (W/cm2)**	**Gross Power density (W_g) (W/cm2)**	**Net Power density ($W_n = W_g - W_p$) (W/cm2)**
NILCD	3	2.24	0.76	0.054	0.570	0.516
ILCD	3	2.04	0.96	0.069	0.610	0.541
ILCDWCE	3	2.15	0.85	0.061	0.660	0.599
Murray's	3	2.21	0.79	0.056	0.680	0.624

6.3.6 Summary

In the present work, an experimental study was carried out to analyse the performance of PEMFC with four different design modifications of a leaf channel, viz., NILCD, ILCD, ILCDWCE and Murray's design, under optimum operating conditions. The following conclusions are drawn from the present study:

- The fuel cell with ILCD is 7.01 % more efficient than the fuel cell with NILCD.
- The fuel cell with ILCDWCE is 15.7 % more efficient than PEMFC with NILCD.
- The fuel cell with Murray's design is 19.29 % more efficient than the fuel cell with NILCD.
- Thus the fuel cell with Murray's design channel gave the best performance among four modifications of the leaf channel, i.e., NILCD, ILCD, ILCDWCE and Murray's Design.

CHAPTER - 7
Experimental Results and discussion

Effect of bio-inspired metal flow field plates on the performance of PEM fuel cell

7.1 Introduction

Bipolar plate is one of the important components in the fuel cell, as it collects electrons generated from reaction sites, supplies reactants to either sides of the fuel cell and also removes product gasses from reaction sites. Metallic bipolar plates have superior manufacturability and are cost effective, have higher levels of power density, and high mechanical strength, and have been regarded as an alternative to graphite bipolar plates. Surface coatings are essential to metallic BPPs because they enhance corrosion resistance and electrical conductivity. Carbon-based coatings have attracted considerable attention from both academia and industry owing to their high performance and low cost. In this study the preparation of graphene oxide and graphene has been presented. The effect of titanium metallic bipolar plates with bio inspired flow channel design was analyzed experimentally. Also analyzed the effect of metallic bipolar plates with carbon based coatings such as graphite, graphene oxide and graphene on performance of PEMFC.

7.2 Experiment

Experiments were conducted using WonATech (Korea) programmable fuel cell test station (FCTS) located at the Center for Sustainable Energy laboratory of NIT Warangal (India). Metal bipolar plates were stable in PEMFC environment with generally low pH values, caused by passivation for good corrosion characteristics and also both metals have excellent mechanical strength. Due to the following merits, Ti bipolar plates were used for experimentation. Titanium bipolar plates with interdigitated leaf type configuration were fabricated using CNC machine. A Nafion (N 212) membrane electrode assembly (MEA) of 49 cm^2 reaction area with membrane thickness 0.0165 mm with catalyst (Pt/c) loading of 0.4 mg cm^{-2} on anode side and 0.6 mg cm^{-2} on cathode side was used to enhance the reaction. Carbon paper is porous in nature, is used as gas diffusion layer (GDL) for better distribution of reactants and carbon paper of 0.36 mm thickness was used on both sides of the membrane followed by catalyst layer. In case of fuel cell with graphite bipolar plates current collectors were used for collecting electron from reaction but in case of fuel cell with metal bipolar plates, the bipolar plate itself act as a current collector. Hydrogen gas and oxygen gas were supplied to reaction area through flow channels of bipolar plates.In the present work, an experimental study was carried out to investigate the performance of PEMFC with metal

bipolar plates and we also studied the effect of different coatings i.e. graphite, graphene oxide and graphene on the performance of PEMFC under optimum operating conditions.

7.3 Synthesis of Graphene oxide (GO)

GO was synthesized from modified Hummers method as reported in the literature [22]. In brief, 2 g graphite nanopowder was added slowly to ice cold 40 mL conc. H_2SO_4 under constant stirring. It was maintained in ice bath with the addition of $NaNO_3$. Further, $KMnO_4$ was added slowly to the above reaction mixture and the temperature was maintained at 20 ºC. Thereafter, the temperature was raised to 60 ºC, and the contents were stirred vigorously for 4 h. After the stipulated time, temperature was raised to 90 ºC for 15 – 20 min with the addition of 100 mL water slowly. A change in the solution color to bright yellow with effervescence was observed with the addition of 200 mL warm water and 20 mL 30% H_2O_2 to the reaction mixture. The solid product formed was centrifuged and washed multiple times with aq. 5 % HCl and water, and finally the solid product was collected and dried in hot air oven at 50 ºC for 10 h.

7.4 Synthesis of graphene

Graphene oxide powder was dispersed in deionized water (1 mg/ml) using ultrasonication for 1 h followed by intermittent stirring. Subsequently, the required amount of reducing agent (ascorbic acid) was added to the GO suspension under vigorous stirring. The mixture was heated to 95 ºC and maintained for 6 h. The precipitation extracted from solution using centrifuge (5 min, 12000 rpm) was washed three times with DI water and ethanol and, finally, dried in hot air oven at 70 °C overnight. The prepared graphene with ascorbic acid was further used in application.

7.5 Results and discussion

7.5.1 XRD analysis

XRD was carried out, to characterize the interlayer spacing and atomic structures of GO and graphene; the results are shown in Fig. 7. 1. The graphite nanopowder shows a strong and characteristic diffraction peak at 26.6° ($d_{spacing}$ = 0.325 nm) with a basal reflection (002). After oxidation, the GO diffraction peak shifts to a lower value of 12.2° ($d_{spacing}$ = 0.719 nm).

Then, after reduction with ascorbic acid, in the case of graphene, the diffraction peak at 12.2° weakens out while a broad peak appearing at 25° ($d_{spacing}$ = 0.349 nm) was noticed. The $d_{spacing}$ of GO is relatively larger than that of Nano graphite due to the formation of oxygen functionalities and the intercalation of water molecules between layers of nano graphite. Nevertheless, the $d_{spacing}$of graphene appreciably decreased after reduction, indicating the removal of oxygen functionalities. XRD analysis confirms the successful formation of GO and graphene.

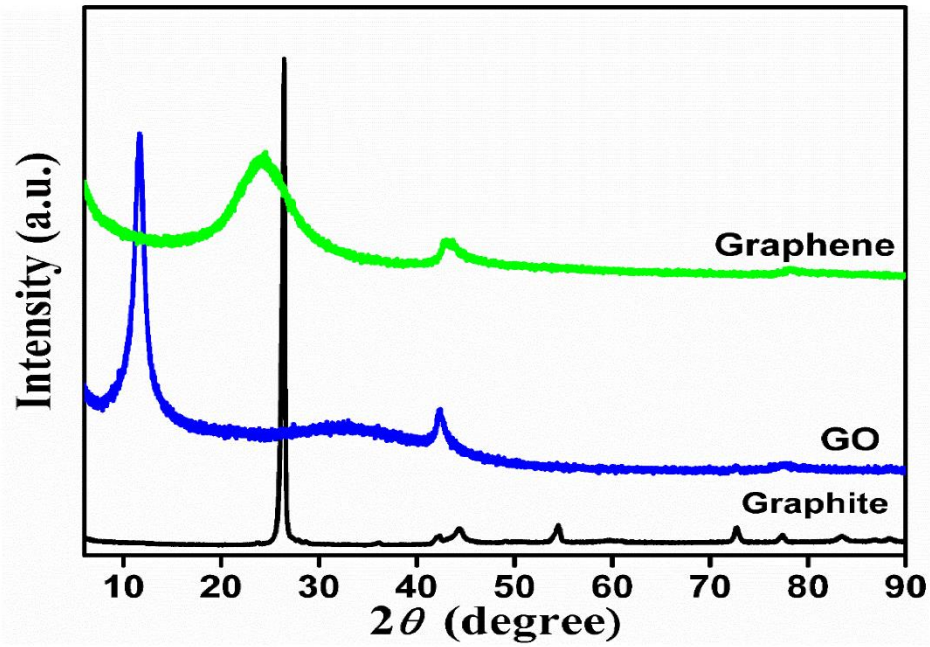

Fig. 7. 1. XRD pattern of Graphite, Graphene oxide (GO) and Graphene (rGO).

7.5.2 Transmission Electron Microscopy (TEM) analysis

High resolution TEM analysis of synthesized graphene was carried out to know the morphological characteristics feature, it is observed that a sheet like structure with a separation between the exfoliated layers and stack of graphene layers was observed at some places as shown in Fig. 7.2**.**

7.5.3 Preparation of coatings

The ink was prepared by dispersing 5 mg carbon based powders such as graphite, GO and graphene with adequate amount of polyvinylidenedifluoride (PVDF) binder and anhydrous N-methylpyrrolidone (NMP) solvent by intermittent stirring and sonication for 1h. Before being

used, these inks were ultrasonicated for at least 30 min for homogeneity. The prepared ink was coated on the metal bipolar plate by spraying method.

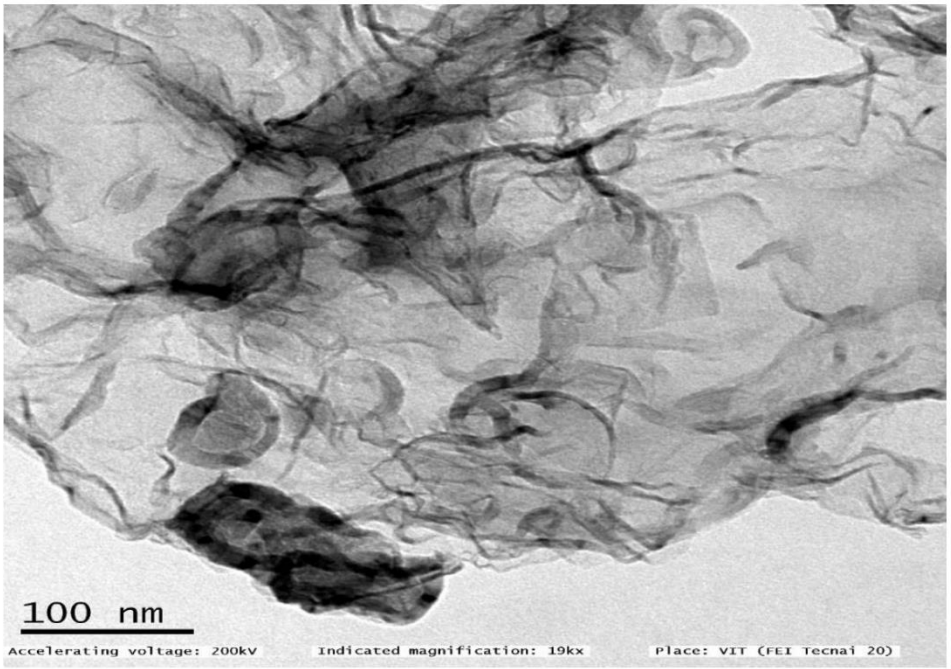

Fig. 7. 2 HRTEM image of graphene

7.5.4 Effect of Ti-metal bipolar plate with different types of carbon based coating on performance of the PEMFC.

The Graphite bipolar plate with Murray's type leaf channel design, Ti-metal bipolar plate with Murray's type leaf channel design without coatings and Ti bipolar plates with different types of carbon based coatings as shown in Fig.7.3.

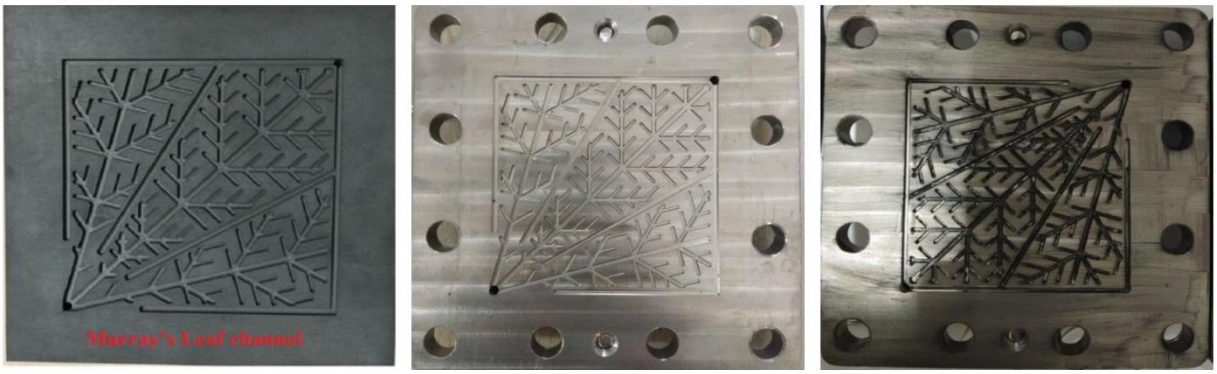

(a) (b) (c)

Fig.7.3 (a) Graphite bipolar plate with Murray's design (b) Ti metal bipolar plate (c) Ti metal bipolar plate with carbon based coatings

The graphite, GO and graphene carbon based coatings have been employed in order to study the effect of coatings on the performance of PEMFC. It was well known from the literature that the conductivity of graphene was high rather than GO and graphite. Graphene has strong adhesion property, excellent electrical and thermal conductivity, and is highly resistant to corrosion. In the literature we found that graphene coated Ti plate gave high performance because of decrease in corrosion current and interfacial contact resistance with the aid of graphene[154]. In order to improve the performance of PEM fuel cell, Ti-metal bipolar plate were used and studied the results.

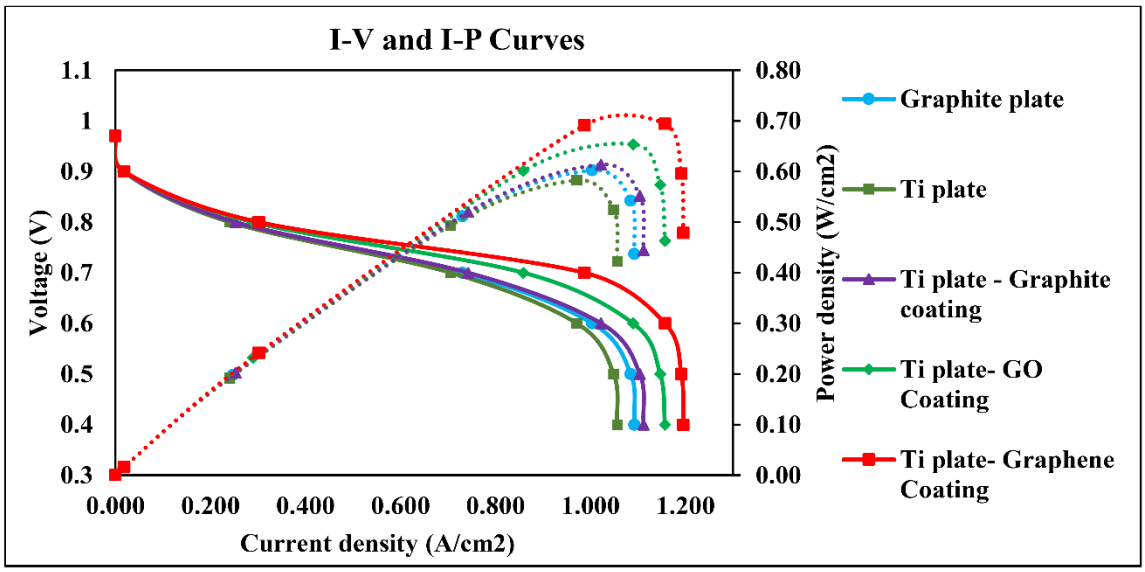

Fig. 7.4 Polarizations curves of metal bipolar plates with different coatings

Experimental results of Ti bipolar plate with different types of coatings at optimum values of the operating parameters as shown in Fig. 7.4. These optimum operating parameters, as explained in the earlier sections are: operating temperature of the fuel cell is 70 ^{o}C, RH of the reactants is 100 % and operating pressure is 3 bar. The flow rate of hydrogen on anode was set at 350 ccm (λ=1) and the flow rate of oxygen on cathode was set at 525 ccm (λ=3), respectively. It was observed from the results that graphene coated Ti-metal bipolar plate showed enhanced performance compared with bipolar plate with other coatings. Because graphene has high electrical conductivity and thermal stability among all the coatings, it has good corrosion resistance and mechanical strength compared with other coatings. It is noticed that graphene coated Ti metal bipolar plate developed 0.69 W/cm^2 power density at 1.16 A/cm^2 current density, similarly the GO coated Ti metal bipolar plate developed a peak power

density of 0.65 W/cm^2 at a current density of 1.09 A/cm^2; the graphite coated Ti metal bipolar plate developed a peak power density of 0.61 W/cm^2 at a current density of 1.02 A/cm^2, the non-coated Ti metal bipolar plate developed a peak power density of 0.58 W/cm^2 at current density of 0.97 A/cm^2 and graphite bipolar developed a peak power density of 0.60 W/cm^2 at current density of 0.99 A/cm^2 respectively. The graphene coated Ti metal bipolar plate is 18.96% more efficient than non-coated Ti metal bipolar plate, GO coated Ti metal bipolar plate is 12.06 % more efficient than non-coated Ti metal bipolar plate, and the graphite coated Ti metal bipolar plate is 5.17 % more efficient than non-coated Ti metal bipolar plate.

7.5.5 Summary

In the present work, as experimental study was carried out to analyse the performance of the PEMFC with Ti metal bipolar plate with different types of coatings, viz., graphite, graphene oxide and graphene under optimum operating conditions**.**

- **From the studies on the metal bipolar plates with different coatings, the following conclusions are drawn:**

  - The performance of PEMFC with graphite coated Ti bipolar plate generated 5.17 % more power density when compared with non-coated Ti bipolar plate.

  - The performance of PEMFC with graphene oxide coated Ti bipolar plate generated 12.06 % more power density when compared with non-coated Ti bipolar plate.

  - The performance of PEMFC with reduced graphene oxide (graphene) coated Ti bipolar plate generated 18.96 % more power density when compared with non-coated Ti bipolar plate. Thus, the Fuel cell with graphene coated metal (Ti) bipolar plate gave the best performance among the three coatings.

CHAPTER –8

Conclusions and Scope for future work

8.1 Conclusions

➢ Simulation study

A 3-D Model was developed to study the effect of land width and channel width on the performance of PEMFC. The following conclusions are drawn from the study:

- The fuel cell with 1 mm land width gives the best performance when parasitic losses are considered.
- The fuel cell performance increases with increase in the flow rate of reactants.
- The fuel cell with 1 mm land width gives the best performance when it is operated with high flow rates and the performance is almost same for both the channels at low flow rate conditions.
- The fuel cell performance enhanced with increase in operating temperature from 313 K to 343 K while the performance deteriorated beyond 343 K. At 343 K the fuel cell gives the best performance.
- The **fuel cell with 1 mm channel width** gives the best performance when parasitic losses are considered.
- The simulation results of serpentine flow field with optimum design parameters were compared with experimental results and it was observed that the results were in good agreement.

➢ Experimental study:

Experimental studies were carried out to investigate the effect of **bio-inspired flow field design** on the performance of PEMFC at various ranges of operating parameters. The following conclusions are drawn:

- The fuel cell performance enhanced, when the operating temperature increases from 40 ^{o}C to 70 ^{o}C. This performance is maximum at 70 ^{o}C. However, the performance of the cell deteriorated beyond 70^{o}C operating temperature.
- Relative Humidity (RH) had considerable influence on the cell performance. Greater values of RH caused greater power output of the fuel cell.
- The performance of the fuel cell enhanced as the stoichiometric ratio was increased from λ_c=1 to λ_c=3; any further increase of stoichiometric ratio gives the same performance or slightly decreased performance.

- With increase in the fuel cell operating pressure, the cell performance improved.
- Back pressure had a positive effect on the cell performance, i.e., the PEMFC performance enhanced with increment in back pressure.
- It can be observed from the results that the leaf channel design performed better among four channel designs considered, i.e., Single serpentine channel, Lung channel, Bio channel and Leaf channel.
- The **leaf channel flow field design yields 25.53% more power** when compared to single serpentine flow channel design.

➢ **Comparison of the performance of the fuel cell with different modifications in the leaf channel design revealed the following:**

- The fuel cell with ILCD generated 7.01 % more power density, ILCDWCE generated 15.7 % more power density and Murray's design generated 19.2 % more power density when compared with NILCD. Thus the fuel cell with Murray's design channel gave the best performance among the four modifications of the leaf channel, i.e., NILCD, ILCD, ILCDWCE and Murray's Design.

➢ **From the studies on metal bipolar plates with different coatings, the following conclusions are drawn:**

- The performance of PEMFC with graphite coated Ti bipolar plate generated 4.5 % more power density when compared with non-coated Ti bipolar plate.
- The performance of PEMFC with graphene oxide coated Ti bipolar plate generated 6.5 % more power density when compared with non-coated Ti bipolar plate.
- The performance of PEMFC with reduced graphene oxide (graphene) coated Ti bipolar plate generated 13.1 % more power density when compared with non-coated Ti bipolar plate. Thus, the Fuel cell with graphene coated metal (Ti) bipolar plate gave the best performance.

8.2 Scope for future work

- To investigate experimentally and numerically the effect of channel width and depth of the bio inspired channel designs on the performance of the fuel cell.
- To investigate experimentally and numerically the effect of GDL porosity on the performance of PEMFC.
- To study the performance of the PEMFC in the low voltage region by introducing water cooling.
- To study the effect of different catalyst materials such as Pt/graphene, Pt/carbon-black on the performance of the PEMFC.
- To study the effect of different membranes such as Polybenzimidazole (PBI) and sulfonated polyetheretherketone (SPEEK) on the performance of PEMFC.

References

[1] X. Li and I. Sabir, “Review of bipolar plates in PEM fuel cells: Flow-field designs,” *Int. J. Hydrogen Energy*, vol. 30, no. 4, pp. 359–371, 2005.

[2] A. Beicha and R. Zaamouche, “Electrochemical model for proton exchange membrane fuel cells systems,” *J. Power Technol.*, vol. 93, no. 1, pp. 27–36, 2013.

[3] J. Larminie and A. Dicks, *Fuel Cell Systems Explained*, vol. 2nd ed. 2003.

[4] D. D. Boettner, G. Paganelli, Y. G. Guezennec, G. Rizzoni, and M. J. Moran, “Proton Exchange Membrane Fuel Cell System Model for Automotive Vehicle Simulation and Control,” *J. Energy Resour. Technol.*, vol. 124, no. 1, p. 20, 2002.

[5] H. Zhao and A. F. Burke, “Optimization of fuel cell system operating conditions for fuel cell vehicles,” *J. Power Sources*, vol. 186, no. 2, pp. 408–416, 2009.

[6] R. K. Ahluwalia, X. Wang, J. Kwon, A. Rousseau, J. Kalinoski, B. James, and J. Marcinkoski, “Performance and cost of automotive fuel cell systems with ultra-low platinum loadings,” *J. Power Sources*, vol. 196, no. 10, pp. 4619–4630, 2011.

[7] K. Inman, Z. Ahmad, Z. Shi, and X. Wang, “News and Views Design of a proton exchange membrane portable fuel cell system for the 1st international association for hydrogen energy design competition,” *Int. J. Hydrogen Energy*, vol. 36, no. 21, pp. 13868–13874, 2011.

[8] S. H. Ahn, S. Jeon, H. Y. Park, S. K. Kim, H. J. Kim, E. Cho, D. Henkensmeier, S. J. Yoo, S. W. Nam, T. H. Lim, and J. H. Jang, “Effects of platinum loading on the performance of proton exchange membrane fuel cells with high ionomer content in catalyst layers,” *Int. J. Hydrogen Energy*, vol. 38, no. 23, pp. 9826–9834, 2013.

[9] N. Akhtar and P. J. A. M. Kerkhof, “Effect of channel and rib width on transport phenomena within the cathode of a proton exchange membrane fuel cell,” *Int. J. Hydrogen Energy*, vol. 36, no. 9, pp. 5536–5549, 2011.

[10] M. Shichun, W. Xiaoen, T. Haolin, L. Peigang, L. Ming, P. Mu, and Y. RunZhang, “A Self-Humidifying Composite Membrane with Self-Assembled Pt Nanoparticles for Polymer Electrolyte Membrane Fuel Cells,” *J. Electrochem. Soc.*, vol. 153, no. 10, p. A1868, 2006.

[11] P. K. Das, X. Li, and Z. S. Liu, “A three-dimensional agglomerate model for the cathode catalyst layer of PEM fuel cells,” *J. Power Sources*, vol. 179, no. 1, pp. 186–199, 2008.

[12] C. Lim and C. Y. Wang, “Effects of hydrophobic polymer content in GDL on power performance of a PEM fuel cell,” *Electrochim. Acta*, vol. 49, no. 24, pp. 4149–4156, 2004.

[13] P. Choopanya and A, “Computational Fluid Dynamics Modelling of a Polymer Electrolyte Membrane Fuel Cell under Transient Automotive Operations,” *PhD Thesis Univ. Sussex*, 2015.

[14] F. B. P. Ryan O’hare, Suk-Won Cha, Whitney G. Colella, *Fuel Cell Fundamentals*. .

[15] J. T. Pukrushpan, H. Peng, and A. G. Stefanopoulou, “Control-Oriented Modeling and Analysis for Automotive Fuel Cell Systems,” *Trans. ASME*, vol. 126, no. March 2004, pp. 14–25, 2004.

[16] F. Barbir, “PEM Fuel Cells: Theory and Practice,” *Elsevier Inc*, 2013.

[17] D. M. Bernardi and M. W. Verbrugge, “A Mathematical Model of the Solid-Polymer-Electrolyte Fuel Cell,” *J. Electrochem. Soc.*, vol. 139, no. 9, pp. 2477–2491, 1992.

[18] S. S. and C. E. C. Junbom Kim, Seong-Min Lee, “Modeling of Proton Exchange Membrane Fuel Cell Performance with an Empirical Equation,” *J. Electrochem. Soc.*, vol. 142, no. 8, pp. 2670–2674, 1995.

[19] A. Kazim, H. T. Liu, and P. Forges, “Modelling of performance of PEM fuel cells with conventional and interdigitated flow fields,” *J. Appl. Electrochem.*, vol. 29, no. 12, pp. 1409–1416, 1999.

[20] R. F. Mann, J. C. Amphlett, M. a. I. Hooper, H. M. Jensen, B. a. Peppley, and P. R. Roberge, “Development and application of a generalised steady-state electrochemical model for a PEM fuel cell,” *J. Power Sources*, vol. 86, no. 1–2, pp. 173–180, 2000.

[21] V. Gurau, F. Barbir, and H. Liu, “An Analytical Solution of a Half-Cell Model for PEM Fuel Cells,” *J. Electrochem. Soc.*, vol. 147, no. 7, p. 2468, 2000.

[22] M. W. Fowler, R. F. Mann, J. C. Amphlett, B. A. Peppley, and P. R. Roberge,

"Incorporation of voltage degradation into a generalised steady state electrochemical model for a PEM fuel cell," *J. Power Sources*, vol. 106, no. 1–2, pp. 274–283, 2002.

[23] T. Berning, D. M. Lu, and N. Djilali, "Three-dimensional computational analysis of transport phenomena in a PEM fuel cell," *J. Power Sources*, vol. 106, no. 1, pp. 284–294, 2002.

[24] A. Kumar and R. G. Reddy, "Effect of channel dimensions and shape in the flow-field distributor on the performance of polymer electrolyte membrane fuel cells," vol. 113, pp. 11–18, 2003.

[25] Q. Wang, D. Song, T. Navessin, S. Holdcroft, and Z. Liu, "A mathematical model and optimization of the cathode catalyst layer structure in PEM fuel cells," *Electrochim. Acta*, vol. 50, no. 2–3 SPEC. ISS., pp. 725–730, 2004.

[26] P. T. Nguyen, T. Berning, and N. Djilali, "Computational model of a PEM fuel cell with serpentine gas flow channels," *J. Power Sources*, vol. 130, no. 1–2, pp. 149–157, 2004.

[27] K. W. Lum and J. J. McGuirk, "Three-dimensional model of a complete polymer electrolyte membrane fuel cell - Model formulation, validation and parametric studies," *J. Power Sources*, vol. 143, no. 1–2, pp. 103–124, 2005.

[28] Y. Lin and S. B. Beale, "Numerical predictions of transport phenomena in a proton exchange membrane fuel cell," *J. Fuel Cell Sci. Technol.*, vol. 2, no. 4, pp. 213–218, 2005.

[29] W.-M. Yan, H.-Y. Li, and W.-C. Tsai, "Three-Dimensional Analysis of PEMFCs with Different Flow Channel Designs," *J. Electrochem. Soc.*, vol. 153, no. 10, p. A1984, 2006.

[30] L. Sun, P. H. Oosthuizen, and K. B. McAuley, "A numerical study of channel-to-channel flow cross-over through the gas diffusion layer in a PEM-fuel-cell flow system using a serpentine channel with a trapezoidal cross-sectional shape{star, open}{star, open}A preliminary version of this paper was prese," *Int. J. Therm. Sci.*, vol. 45, no. 10, pp. 1021–1026, 2006.

[31] S. Shimpalee, S. Greenway, and J. W. Van Zee, "The impact of channel path length on

PEMFC flow-field design," *J. Power Sources*, vol. 160, no. 1, pp. 398–406, 2006.

[32] X. Liu, W. Tao, Z. Li, and Y. He, "Three-dimensional transport model of PEM fuel cell with straight flow channels," *J. Power Sources*, vol. 158, no. 1, pp. 25–35, 2006.

[33] W. M. Yan, H. C. Liu, C. Y. Soong, F. Chen, and C. H. Cheng, "Numerical study on cell performance and local transport phenomena of PEM fuel cells with novel flow field designs," *J. Power Sources*, vol. 161, no. 2, pp. 907–919, 2006.

[34] X. D. Wang, Y. Y. Duan, W. M. Yan, and X. F. Peng, "Local transport phenomena and cell performance of PEM fuel cells with various serpentine flow field designs," *J. Power Sources*, vol. 175, no. 1, pp. 397–407, 2008.

[35] J.-H. Jang, W.-M. Yan, H.-Y. Li, and W.-C. Tsai, "Three-dimensional numerical study on cell performance and transport phenomena of PEM fuel cells with conventional flow fields," *Int. J. Hydrogen Energy*, vol. 33, no. 1, pp. 156–164, 2008.

[36] M. A. R. Sadiq Al-Baghdadi, "Three-dimensional computational fluid dynamics model of a tubular-shaped PEM fuel cell," *Renew. Energy*, vol. 33, no. 6, pp. 1334–1345, 2008.

[37] X.-D. D. Wang, Y.-Y. Y. Duan, W.-M. M. Yan, and F.-B. B. Weng, "Effects of flow channel geometry on cell performance for PEM fuel cells with parallel and interdigitated flow fields," *Electrochim. Acta J.*, vol. 53, pp. 5334–5343, Jan. 2008.

[38] J. H. Jang, W. M. Yan, H. Y. Li, and W. C. Tsai, "Three-dimensional numerical study on cell performance and transport phenomena of PEM fuel cells with conventional flow fields," *Int. J. Hydrogen Energy*, vol. 33, no. 1, pp. 156–164, 2008.

[39] M. H. Akbari and B. Rismanchi, "Numerical investigation of flow field configuration and contact resistance for PEM fuel cell performance," *Renew. Energy*, vol. 33, no. 8, pp. 1775–1783, 2008.

[40] W.-C. Weng, W.-M. Yan, H.-Y. Li, and X.-D. Wang, "Numerical Simulation of Cell Performance in Proton Exchange Membrane Fuel Cells with Contracted Flow Field Design," *J. Electrochem. Soc.*, vol. 155, no. 9, p. B877, 2008.

[41] B. Rismanchi and M. H. Akbari, "Performance prediction of proton exchange membrane fuel cells using a three-dimensional model," *Int. J. Hydrogen Energy*, vol.

33, no. 1, pp. 439–448, 2008.

[42] A. Iranzo, M. Muñoz, E. López, J. Pino, and F. Rosa, "Experimental fuel cell performance analysis under different operating conditions and bipolar plate designs," *Int. J. Hydrogen Energy*, vol. 35, no. 20, pp. 11437–11447, 2010.

[43] A. S. Bansode, T. Sundararajan, and S. K. Das, "Computational and Experimental Studies on the Effect of Flow-Distributors on the Performance of PEMFC," *J. Fuel Cell Sci. Technol.*, vol. 7, no. 5, p. 51014, 2010.

[44] X. D. Wang, W. M. Yan, Y. Y. Duan, F. B. Weng, G. Bin Jung, and C. Y. Lee, "Numerical study on channel size effect for proton exchange membrane fuel cell with serpentine flow field," *Energy Convers. Manag.*, vol. 51, no. 5, pp. 959–968, 2010.

[45] X.-D. Wang, X.-X. Zhang, T. Liu, Y.-Y. Duan, W.-M. Yan, and D.-J. Lee, "Channel Geometry Effect for Proton Exchange Membrane Fuel Cell With Serpentine Flow Field Using a Three-Dimensional Two-Phase Model," *J. Fuel Cell Sci. Technol.*, vol. 7, no. 5, p. 51019, 2010.

[46] A. P. Manso, F. F. Marzo, M. G. Mujika, J. Barranco, and A. Lorenzo, "Numerical analysis of the influence of the channel cross-section aspect ratio on the performance of a PEM fuel cell with serpentine flow field design," *Int. J. Hydrogen Energy*, vol. 36, no. 11, pp. 6795–6808, 2011.

[47] D. Juarez-Robles, A. Hernandez-Guerrero, B. Ramos-Alvarado, F. Elizalde-Blancas, and C. E. Damian-Ascencio, "Multiple concentric spirals for the flow field of a proton exchange membrane fuel cell," *J. Power Sources*, vol. 196, no. 19, pp. 8019–8030, 2011.

[48] K. S. Choi, H. M. Kim, and S. M. Moon, "Numerical studies on the geometrical characterization of serpentine flow-field for efficient PEMFC," *Int. J. Hydrogen Energy*, vol. 36, no. 2, pp. 1613–1627, 2011.

[49] É. Fontana, E. Mancusi, A. Da Silva, V. C. Mariani, A. A. Ulson De Souza, and S. M. A. G. Ulson De Souza, "Study of the effects of flow channel with non-uniform cross-sectional area on PEMFC species and heat transfer," *Int. J. Heat Mass Transf.*, vol. 54, no. 21–22, pp. 4462–4472, 2011.

[50] F. Hashemi, S. Rowshanzamir, and M. Rezakazemi, “CFD simulation of PEM fuel cell performance: Effect of straight and serpentine flow fields,” *Math. Comput. Model.*, vol. 55, no. 3–4, pp. 1540–1557, 2012.

[51] I. Khazaee and M. Ghazikhani, “Three-Dimensional Modeling and Development of the New Geometry PEM Fuel Cell,” *Arab. J. Sci. Eng.*, vol. 38, no. 6, pp. 1551–1564, 2013.

[52] J. M. Sierra, S. J. Figueroa-Ram??rez, S. E. D??az, J. Vargas, P. J. Sebastian, S. J. Figueroa-Ramírez, S. E. Díaz, J. Vargas, P. J. Sebastian, S. J. Figueroa-Ram??rez, S. E. D??az, J. Vargas, and P. J. Sebastian, “Numerical evaluation of a PEM fuel cell with conventional flow fields adapted to tubular plates,” *Int. J. Hydrogen Energy*, vol. 9, no. 29, pp. 1–12, 2014.

[53] S. H. Han, N. H. Choi, and Y. D. Choi, “Performance and flow characteristics of large-sized PEM fuel cell having branch channel,” *Int. J. Hydrogen Energy*, vol. 40, no. 14, pp. 4819–4829, 2015.

[54] N. Limjeerajarus and P. Charoen-Amornkitt, “Effect of different flow field designs and number of channels on performance of a small PEFC,” *Int. J. Hydrogen Energy*, vol. 40, no. 22, pp. 7144–7158, 2015.

[55] L. Rostami, P. Mohamad Gholy Nejad, and A. Vatani, “A numerical investigation of serpentine flow channel with different bend sizes in polymer electrolyte membrane fuel cells,” *Energy*, vol. 97, pp. 400–410, 2016.

[56] E. G. Karvelas, D. G. Koubogiannis, A. Hatziapostolou, and I. E. Sarris, “The effect of anode bed geometry on the hydraulic behaviour of PEM fuel cells,” *Renew. Energy*, vol. 93, pp. 269–279, 2016.

[57] S. Arun Saco, R. Thundil Karuppa Raj, and P. Karthikeyan, “A study on scaled up proton exchange membrane fuel cell with various flow channels for optimizing power output by effective water management using numerical technique,” *Energy*, vol. 113, pp. 558–573, 2016.

[58] M. Tamerabet, B. M. Hocine, S. Youcef, and M. Abdallah, “Unsteady three-dimensional numerical study of mass transfer in PEM fuel cell with spiral flow field,”

Int. J. Hydrogen Energy, vol. 42, no. 2, pp. 1237–1251, 2017.

[59] A. L. R. Paulino, E. F. Cunha, E. Robalinho, M. Linardi, I. Korkischko, and E. I. Santiago, "CFD Analysis of PEMFC Flow Channel Cross Sections," *Fuel Cells*, vol. 17, no. 1, pp. 27–36, 2017.

[60] C. E. Damian-Ascencio, A. Saldaña-Robles, A. Hernandez-Guerrero, and S. Cano-Andrade, "Numerical modeling of a proton exchange membrane fuel cell with tree-like flow field channels based on an entropy generation analysis," *Energy*, vol. 133, pp. 306–316, 2017.

[61] M. Ziauddin, O. Genc, and S. Toros, "ScienceDirect Numerical optimization of channel to land width ratio for PEM fuel cell," *Int. J. Hydrogen Energy*, vol. 43, no. 23, pp. 10798–10809, 2018.

[62] M. S. Moosa Ashrafi, Homayoon Kanani, "numerical and experimental study of two-phase flow uniformity in channels of parallel PEM fuel cells with modified Z-type flow fields," *Energy*, vol. 147, no. 317–328, pp. 1–12, 2018.

[63] Z. Wan, W. Quan, C. Yang, H. Yan, X. Chen, T. Huang, X. Wang, and S. Chan, "Optimal design of a novel M-like channel in bipolar plates of proton exchange membrane fuel cell based on minimum entropy generation," *Energy Convers. Manag.*, vol. 205, no. September 2019, p. 112386, 2020.

[64] abdulla shaik and P. V. suresh, "Detailed analysis of polymer electrolyte membrane fuel cell with enhanced cross - flow split serpentine flow field design," *Int. J. energy Res.*, no. November 2018, pp. 1–15, 2019.

[65] S. Abdulla, M. M. Seepana, and V. S. Patnaikuni, "Performance Comparison of PEM Fuel Cell with Enhanced Cross-Flow Split Serpentine and Single Serpentine Flow Field Designs," *Arab. J. Sci. Eng.*, vol. 45, no. 9, pp. 7691–7703, 2020.

[66] X. Wang, Y. Qin, S. Wu, X. Shangguan, J. Zhang, and Y. Yin, "Numerical and experimental investigation of baffle plate arrangement on proton exchange membrane fuel cell performance," *J. Power Sources*, vol. 457, no. September 2019, p. 228034, 2020.

[67] T. V Nguyen, "A gas distributor design for proton-exchange-membrane fuel cells," *J.*

Electrochem. Soc., vol. 143, no. 5, pp. L103–L105, 1996.

[68] A. Kazim, P. Forges, and H. T. Liu, "Effects of cathode operating conditions on performance of a PEM fuel cell with interdigitated flow fields," *Int. J. Energy Res.*, vol. 27, no. 4, pp. 401–414, 2003.

[69] G. Hu, J. Fan, S. Chen, Y. Liu, and K. Cen, "Three-dimensional numerical analysis of proton exchange membrane fuel cells (PEMFCs) with conventional and interdigitated flow fields," *J. Power Sources*, vol. 136, no. 1, pp. 1–9, 2004.

[70] A. Kumar and R. G. Reddy, "Effect of gas flow-field design in the bipolar/end plates on the steady and transient state performance of polymer electrolyte membrane fuel cells," *J. Power Sources*, vol. 155, no. 2, pp. 264–271, 2006.

[71] A. Su, F.-B. Weng, P.-H. Chi, S.-M. Lu, G.-B. Jung, C. H. Tu, and Y.-M. Ferng, "Effect of channel step-depth on the performance of proton exchange membrane fuel cells," *Proc. Inst. Mech. Eng. Part A J. Power Energy*, vol. 221, pp. 617–625, 2007.

[72] K. Hongthong, K. Pruksathorn, P. Piumsomboon, and P. Sripakagorn, "Effect of the geometry and pattern of the flow channel on the performance of polymer electrolyte membrane fuel cell," vol. 24, no. 4, pp. 612–617, 2007.

[73] M. A. R. S. Al-Baghdadi and H. A. K. S. Al-Janabi, "Numerical analysis of a proton exchange membrane fuel cell. Part 2: Parametric study," *Proc. Inst. Mech. Eng. Part A J. Power Energy*, vol. 221, no. 7, pp. 931–939, 2007.

[74] Y. M. Ferng and A. Su, "A three-dimensional full-cell CFD model used to investigate the effects of different flow channel designs on PEMFC performance," *Int. J. Hydrogen Energy*, vol. 32, no. 17, pp. 4466–4476, 2007.

[75] D. H. Jeon, S. Greenway, S. Shimpalee, and J. W. Van Zee, "The effect of serpentine flow-field designs on PEM fuel cell performance," *Int. J. Hydrogen Energy*, vol. 33, no. 3, pp. 1052–1066, 2008.

[76] W. M. Yan, H. Y. Li, P. C. Chiu, and X. D. Wang, "Effects of serpentine flow field with outlet channel contraction on cell performance of proton exchange membrane fuel cells," *J. Power Sources*, vol. 178, no. 1, pp. 174–180, 2008.

[77] C.-H. Min, "Performance of a proton exchange membrane fuel cell with a stepped flow

field design," *J. Power Sources*, vol. 186, no. 2, pp. 370–376, 2009.

[78] J. G. Carton and A. G. Olabi, "Design of experiment study of the parameters that affect performance of three flow plate configurations of a proton exchange membrane fuel cell," *Energy*, vol. 35, no. 7, pp. 2796–2806, 2010.

[79] C.-Y. L. Xiao-Dong Wang, Wei-Mon Yan, Yuan-Yuan Duan, Fang-Bor Weng, Guo-Bin Jung, "Numerical study on channel size effect for proton exchange membrane fuel cell with serpentine flow field," *Energy Convers. Manag.*, vol. 51, no. 5, pp. 959–968, 2010.

[80] W.-M. Yan, X.-D. Wang, D.-J. Lee, X.-X. Zhang, Y.-F. Guo, and A. Su, "Experimental study of commercial size proton exchange membrane fuel cell performance," *Appl. Energy*, vol. 88, pp. 392–396, 2011.

[81] P. V. Suresh, S. Jayanti, A. P. Deshpande, and P. Haridoss, "An improved serpentine flow field with enhanced cross-flow for fuel cell applications," *Int. J. Hydrogen Energy*, vol. 36, no. 10, pp. 6067–6072, 2011.

[82] P. V. Suresh, S. Jayanti, A. P. Deshpande, and P. Haridoss, "An improved serpentine flow field with enhanced cross-flow for fuel cell applications," *Int. J. Hydrogen Energy*, vol. 36, no. 10, pp. 6067–6072, 2011.

[83] A. P. Manso, F. F. Marzo, M. G. Mujika, J. Barranco, and A. Lorenzo, "Numerical analysis of the influence of the channel cross-section aspect ratio on the performance of a PEM fuel cell with serpentine flow field design," *Int. J. Hydrogen Energy*, vol. 36, no. 11, pp. 6795–6808, 2011.

[84] H.-C. Chiu, J.-H. Jang, W.-M. Yan, H.-Y. Li, and C.-C. Liao, "A three-dimensional modeling of transport phenomena of proton exchange membrane fuel cells with various flow fields," *Appl. Energy*, vol. 96, pp. 359–370, 2012.

[85] J. Y. Jang, C. H. Cheng, W. T. Liao, Y. X. Huang, and Y. C. Tsai, "Experimental and numerical study of proton exchange membrane fuel cell with spiral flow channels," *Appl. Energy*, vol. 99, pp. 67–79, 2012.

[86] N. B, Sreenivasulu, G, Vasu, V, Dharma Rao, SV, "Effect of Back Pressure and Flow Geometry on PEM Fuel Cell Performance-An Experimental Study," *Int. J. Appl. Sci.*

Eng., vol. 11, no. 1, pp. 1–11, 2013.

[87] H. Liu, P. Li, D. Juarez-Robles, K. Wang, and A. Hernandez-Guerrero, "Experimental Study and Comparison of Various Designs of Gas Flow Fields to PEM Fuel Cells and Cell Stack Performance," *Front. Energy Res.*, vol. 2, no. January, pp. 1–8, 2014.

[88] I. Khazaee, "Experimental investigation and numerical comparison of the performance of a proton exchange membrane fuel cell at different channel geometry," *Heat Mass Transf. und Stoffuebertragung*, vol. 51, no. 8, pp. 1177–1187, 2015.

[89] A. Torkavannejad, H. Sadeghifar, N. Pourmahmoud, and F. Ramin, "Novel architectures of polymer electrolyte membrane fuel cells: Efficiency enhancement and cost reduction," *Int. J. Hydrogen Energy*, vol. 40, no. 36, pp. 12466–12477, 2015.

[90] A. Iranzo, J. Biesdorf, M. Cochet, A. Salva, P. Boillat, and F. Rosa, "Effect of Serpentine Multi-pass Flow Field Channel Orientation in the Liquid Water Distributions and Cell Performance," *Fuel Cells*, vol. 16, no. 6, pp. 777–783, 2016.

[91] F. Cells, "Comparison of Numerical and Experimental Studies for Flow-Field Optimization Based on Under-Rib," pp. 1–17, 2016.

[92] W. Li, Q. Zhang, C. Wang, X. Yan, S. Shen, G. Xia, F. Zhu, and J. Zhang, "Experimental and numerical analysis of a three-dimensional flow field for PEMFCs," *Appl. Energy*, vol. 195, pp. 278–288, 2017.

[93] J. Mahmoudimehr and A. Daryadel, "ScienceDirect Influences of feeding conditions and objective function on the optimal design of gas flow channel of a PEM fuel cell," *Int. J. Hydrogen Energy*, pp. 1–19, 2017.

[94] N. Ahmadi, A. Dadvand, I. Mirzaei, and S. Rezazadeh, "Modeling of polymer electrolyte membrane fuel cell with circular and elliptical cross-section gas channels: A novel procedure," *Int. J. Energy Res.*, vol. 42, no. 8, pp. 2805–2822, 2018.

[95] P. Liang, D. Qiu, L. Peng, P. Yi, X. Lai, and J. Ni, "Contact resistance prediction of proton exchange membrane fuel cell considering fabrication characteristics of metallic bipolar plates," *Energy Convers. Manag.*, vol. 169, no. February, pp. 334–344, 2018.

[96] H. Sadeghifar, A. Torkavannejad, and N. Pourmahmoud, "A novel, net-shape polymer electrolyte fuel cell: Higher power density, smaller stack size and less bipolar plate

required," *Int. J. Heat Mass Transf.*, vol. 117, pp. 1099–1106, 2018.

[97] D. hui Wen, L. zhi Yin, Z. yu Piao, C. da Lu, G. Li, and Q. hui Leng, "Performance investigation of proton exchange membrane fuel cell with intersectant flow field," *Int. J. Heat Mass Transf.*, vol. 121, pp. 775–787, 2018.

[98] A. A. Ebrahimzadeh, I. Khazaee, and A. Fasihfar, "Experimental and numerical investigation of obstacle effect on the performance of PEM fuel cell," *Int. J. Heat Mass Transf.*, vol. 141, pp. 891–904, 2019.

[99] E. E. Kahveci and I. Taymaz, "Experimental study on performance evaluation of PEM fuel cell by coating bipolar plate with materials having different contact angle," *Fuel*, vol. 253, no. March, pp. 1274–1281, 2019.

[100] V. Velisala and N. S. Golagani, "Computational Fluid Dynamics Study of Serpentine Flow Field Proton Exchange Membrane Fuel Cell Performance Computational Fluid Dynamics Study of Serpentine Flow Field Proton Exchange Membrane Fuel Cell Performance," *Heat Transf. Eng.*, vol. 0, no. 0, pp. 1–15, 2019.

[101] A. Azarafza, M. S. Ismail, M. Rezakazemi, and M. Pourkashanian, "Comparative study of conventional and unconventional designs of cathode flow fields in PEM fuel cell," *Renew. Sustain. Energy Rev.*, vol. 116, no. September, p. 109420, 2019.

[102] Z. Qi and A. Kaufman, "Activation of low temperature PEM fuel cells," vol. 111, pp. 181–184, 2002.

[103] T. Berning and N. Djilali, "Three-dimensional computational analysis of transport phenomena in a PEM fuel cell - A parametric study," *J. Power Sources*, vol. 124, no. 2, pp. 440–452, 2003.

[104] L. Wang, A. Husar, T. Zhou, and H. Liu, "A parametric study of PEM fuel cell performances," *Int. J. Hydrogen Energy*, vol. 28, no. 11, pp. 1263–1272, 2003.

[105] L. Wang and H. Liu, "Performance studies of PEM fuel cells with interdigitated flow fields," *J. Power Sources*, vol. 134, no. 2, pp. 185–196, 2004.

[106] S. Hsieh, S. Yang, J. Kuo, C. Huang, and H. Tsai, "Study of operational parameters on the performance of micro PEMFCs with different flow fields," *Energy Convers. Manag.*, vol. 47, pp. 1868–1878, 2006.

[107] W.-M. Yan, C.-H. Yang, C.-Y. Soong, F. Chen, and S.-C. Mei, “Experimental studies on optimal operating conditions for different flow field designs of PEM fuel cells,” *J. Power Sources*, vol. 160, no. 1, pp. 284–292, 2006.

[108] J. P. Owejan, T. A. Trabold, D. L. Jacobson, M. Arif, and S. G. Kandlikar, “Effects of flow field and diffusion layer properties on water accumulation in a PEM fuel cell,” *Int. J. Hydrogen Energy*, vol. 32, no. 17, pp. 4489–4502, 2007.

[109] M. Amirinejad, S. Rowshanzamir, and M. H. Eikani, “Effects of operating parameters on performance of a proton exchange membrane fuel cell,” *J. Power Sources*, vol. 161, no. 2, pp. 872–875, 2006.

[110] W. YU, S. WU, and S. SHIAH, “Parametric analysis of the proton exchange membrane fuel cell performance using design of experiments,” *Int. J. Hydrogen Energy*, vol. 33, no. 9, pp. 2311–2322, 2008.

[111] W. M. Yan, X. D. Wang, S. S. Mei, X. F. Peng, Y. F. Guo, and A. Su, “Effects of operating temperatures on performance and pressure drops for a 256 cm2proton exchange membrane fuel cell: An experimental study,” *J. Power Sources*, vol. 185, no. 2, pp. 1040–1048, 2008.

[112] M. Tohidi, S. H. Mansouri, and H. Amiri, “Effect of primary parameters on the performance of PEM fuel cell,” *Int. J. Hydrogen Energy*, vol. 35, no. 17, pp. 9338–9348, 2010.

[113] C. T. Wang, Y. C. Hu, and P. L. Zheng, “Novel biometric flow slab design for improvement of PEMFC performance,” *Appl. Energy*, vol. 87, no. 4, pp. 1366–1375, 2010.

[114] N. Guo, M. Leu, and M. Wu, “Bio-inspired design of bipolar plate flow fields for polymer electrolyte membrane fuel cells,” *Proc. Solid Free. …*, pp. 607–623, 2011.

[115] C. Yang, M. Hu, C. Wang, and G. Cao, “A three-step activation method for proton exchange membrane fuel cells,” *J. Power Sources*, vol. 197, pp. 180–185, 2012.

[116] F. Ting, C. Hsieh, W. Weng, and J. Lin, “Effect of operational parameters on the performance of PEMFC assembled with Au-coated Ni-foam,” *Int. J. Hydrogen Energy*, vol. 37, no. 18, pp. 13696–13703, 2012.

[117] C.-H. C.-H. Chen, C.-H. C.-H. Chen, and T.-Y. Chen, “The Numerical Study of Geometric Influence of Flow Channel Patterns on Performance of Proton Exchange Membrane Fuel Cells,” *J. Fuel Cell Sci. Technol.*, vol. 9, no. 2, p. 21015, 2012.

[118] N. M. Zahari and A. A. Aziz, “Effect of platinum catalyst loading on membrane electrode assembly (MEA) in proton exchange membrane fuel cell (PEMFC),” *2012 10th IEEE Int. Conf. Semicond. Electron. ICSE 2012 - Proc.*, pp. 669–673, 2012.

[119] A. C. Okafor and H.-M. Mogbo, “EFFECTS OF GAS FLOW RATE AND CATALYST LOADING ON POLYMER ELECTROLYTE MEMBRANE (PEM) FUEL CELL PERFORMANCE AND DEGRADATION,” *Proc. ASME 2010 Eighth Int. Fuel Cell Sci. Eng. Technol. Conf. FuelCell2010 June 14-16, 2010, Brooklyn, New York, USA*, pp. 1–11.

[120] A. Arvay, J. French, J. C. Wang, X. H. Peng, and A. M. Kannan, “Nature inspired flow field designs for proton exchange membrane fuel cell,” *Int. J. Hydrogen Energy*, vol. 38, no. 9, pp. 3717–3726, 2013.

[121] P. Karthikeyan, M. Muthukumar, S. V. Shanmugam, P. P. Kumar, S. Murali, and A. P. S. Kumar, “Optimization of operating and design parameters on proton exchange membrane fuel cell by using Taguchi method,” *Procedia Eng.*, vol. 64, pp. 409–418, 2013.

[122] N. Guo, M. C. Leu, and U. O. Koylu, “Bio-inspired flow field designs for polymer electrolyte membrane fuel cells,” *Int. J. Hydrogen Energy*, vol. 39, no. 36, pp. 21185–21195, 2014.

[123] I. V. Zenyuk, R. Taspinar, A. R. Kalidindi, E. C. Kumbur, and S. Litster, “Computational and Experimental Analysis of Water Transport at Component Interfaces in Polymer Electrolyte Fuel Cells,” *J. Electrochem. Soc.*, vol. 161, no. 11, pp. F3091–F3103, 2014.

[124] N. Guo and M. C. Leu, “Performance Investigation of Polymer Electrolyte Membrane Fuel Cells Using Graphite Composite Plates Fabricated by Selective Laser Sintering,” *J. Fuel Cell Sci. Technol.*, vol. 11, no. February 2014, pp. 1–8, 2014.

[125] Y.-Q. MENG, C. WANG, Q.-L. ZHANG, S.-Y. SHEN, Z. Feng-Juan, Y. Hong, and J.-

L. ZHANG, “The Effects of Cathode Platinum Loading and Operating Backpressure on PEMFC Performance,” *Acta Phys. -Chim. Sin.*, vol. 32, no. 6, pp. 1460–1466, 2016.

[126] P. K. Takalloo, E. S. Nia, and M. Ghazikhani, “Numerical and experimental investigation on effects of inlet humidity and fuel flow rate and oxidant on the performance on polymer fuel cell,” *Energy Convers. Manag.*, vol. 114, pp. 290–302, 2016.

[127] D. N. Ozen, B. Timurkutluk, and K. Altinisik, “Effects of operation temperature and reactant gas humidity levels on performance of PEM fuel cells,” *Renew. Sustain. Energy Rev.*, vol. 59, pp. 1298–1306, 2016.

[128] P. Gazdzicki, J. Mitzel, A. M. Dreizler, M. Schulze, and K. A. Friedrich, “Impact of Platinum Loading on Performance and Degradation of Polymer Electrolyte Fuel Cell Electrodes Studied in a Rainbow Stack,” *Fuel Cells*, no. 0, pp. 1–9, 2017.

[129] M. Z. Chowdhury and Y. E. Akansu, “Novel convergent-divergent serpentine flow fields effect on PEM fuel cell performance,” *Int. J. Hydrogen Energy*, vol. 42, no. 40, pp. 25686–25694, 2017.

[130] D. Qiu, L. Peng, P. Yi, X. Lai, and W. Lehnert, “Flow channel design for metallic bipolar plates in proton exchange membrane fuel cells : Experiments,” *Energy Convers. Manag.*, vol. 174, no. August, pp. 814–823, 2018.

[131] J. R. Bin CHi, Sanying Hou, Guangzhi LIu, Yijie Deng, Jianghuang, Huiyu Song, Shijun Liao, “Turning hydrophobic-hydrophilic balance of cathode catalyst layer to improve cell performance of proton exchange membrane fuel cell (PEMFC) by mixing polytetrafluoroethylene (PTFE),” *Electrochim. Acta*, vol. 277, no. 110–115, pp. 5–10, 2018.

[132] M. Ziauddin and B. Timurkutluk, “Transport phenomena of convergent and divergent serpentine fl ow fi elds for PEMFC,” *Energy*, vol. 161, pp. 104–117, 2018.

[133] H. Liu, W. Yang, J. Tan, Y. An, and L. Cheng, “Numerical analysis of parallel fl ow fi elds improved by micro-distributor in proton exchange membrane fuel cells,” vol. 176, no. September, pp. 99–109, 2018.

[134] V. Velisala, G. Naga, and G. N. Srinivasulu, “Numerical Simulation and Experimental

Comparison of Single, Double and Triple Serpentine Flow Channel Configuration on Performance of a PEM Fuel Cell," *Arab. J. Sci. Eng.*, vol. 43, no. 3, pp. 1225–1234, 2018.

[135] A. Ghanbarian, M. J. Kermani, J. Scholta, and M. Abdollahzadeh, "Polymer electrolyte membrane fuel cell fl ow fi eld design criteria – Application to parallel serpentine fl ow patterns," vol. 166, no. April, pp. 281–296, 2018.

[136] A. G. González-Gutiérrez, M. A. Pech-Canul, G. Chan-Rosado, and P. J. Sebastian, "Studies on the physical and electrochemical properties of Ni-P coating on commercial aluminum as bipolar plate in PEMFC," *Fuel*, vol. 235, no. August 2018, pp. 1361–1367, 2019.

[137] xuguang yang chunhua min, jing he, kun wang, liyao xie, "A comprehensive analysis of secondary flow effects on the performance of PEMFCs with modified serpentine flow fields," *Energy Convers. Manag.*, vol. 1217–1224, pp. 1–8, 2019.

[138] C. Cloth, "Experimental Studies of Effect of Land Width in PEM Fuel Cells with Serpentine Flow Field and," 2019.

[139] S. Shimpalee and J. W. Van Zee, "Numerical studies on rib & channel dimension of flow-field on PEMFC performance," *Int. J. Hydrogen Energy*, vol. 32, no. 7, pp. 842–856, 2007.

[140] A. Iranzo, M. Muñoz, F. Rosa, and J. Pino, "Numerical model for the performance prediction of a PEM fuel cell. Model results and experimental validation," *Int. J. Hydrogen Energy*, vol. 35, no. 20, pp. 11533–11550, 2010.

[141] A. Iranzo, F. Rosa, and J. Pino, "A simulation tool for geometrical analysis and optimization of fuel cell bipolar plates: Development, validation and results," *Energies*, vol. 2, no. 3, pp. 582–594, 2009.

[142] S. E. Dı, C. Carmen, and C. P. Campeche, "ScienceDirect Numerical evaluation of a PEM fuel cell with conventional flow fields adapted to tubular plates," vol. 9, pp. 1–12, 2014.

[143] G. Radica, F. Barbir, S. Ni, and R. Bo, "ScienceDirect Coolant induced variable temperature flow field for improved performance of proton exchange membrane fuel

cells," vol. 4, 2018.

[144] J. E. Soc, A. The, E. Society, T. E. Springer, T. A. Zawodzinski, and S. Gottesfeld, "Polymer Electrolyte Fuel Cell Model," vol. 138, no. 8, pp. 2334–2342, 1993.

[145] N. Guo, M. C. Leu, and U. O. Koylu, "Optimization of parallel and serpentine configurations for polymer electrolyte membrane fuel cells," *Fuel Cells*, vol. 14, no. 6, pp. 876–885, 2014.

[146] Wonatech, "Smart2 PEM Fuel Cell Test System," Korea, 2018.

[147] "DataManager 4." .

[148] "wfcts4." .

[149] G. Uma Maheswararao, A. Majumadar, T. Niphadkar, and D. Jaya Krishna, "An image processing algorithm to estimate the melt fraction and energy storage of a PCM enclosed in a spherical capsule," *Int. J. Energy Res.*, vol. 43, pp. 5535–5547, 2019.

[150] M. M. A. Khan, N. I. Ibrahim, R. Saidur, I. M. Mahbubul, and F. A. Al-Sulaiman, "Performance assessment of a solar powered ammonia–water absorption refrigeration system with storage units," *Energy Convers. Manag.*, vol. 126, pp. 316–328, 2016.

[151] I. khazaee and H. Sabadbafan, "Effect of humidity content and direction of the flow of reactant gases on water management in the 4-serpentine and 1-serpentine flow channel in a PEM (proton exchange membrane) fuel cell," *Energy*, vol. 101, pp. 252–265, 2016.

[152] A. K. P. Hadi Heidary, Mohammad j. kermani, Suresh G. Advani, "Experimental investigation of in-line and staggered blockages in parallel flowfield channels of PEM fuel cells," *Int. J. Hydrogen Energy*, vol. 41, no. 6885–6893, pp. 1–9, 2016.

[153] N. Guo, "Experimental and Computational Evaluation of Performance and Water Management Characteristics of a Bio-Inspired Proton Exchange Membrane Fuel Cell," *Thesis*, 2013.

[154] J. Wang, L. Min, F. Fang, W. Zhang, and Y. Wang, "ScienceDirect Electrodeposition of graphene nano-thick coating for highly enhanced performance of titanium bipolar plates in fuel cells," *Int. J. Hydrogen Energy*, vol. 44, no. 31, pp. 16909–16917, 2019.

Appendix-I

Computational procedure

The window of the Fuel Cells & Electrolysis – PEMFC module

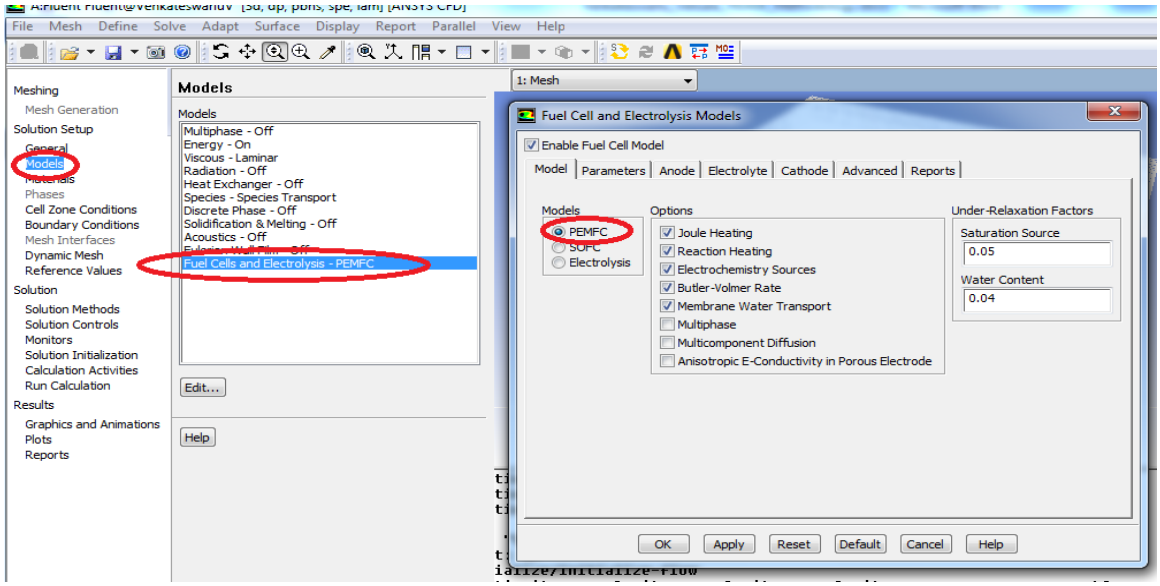

Fig. A-I. 1 Opening the fuel cell module and setting the fuel cell zones

The following steps explained the input conditions given to fuel cell simulation.

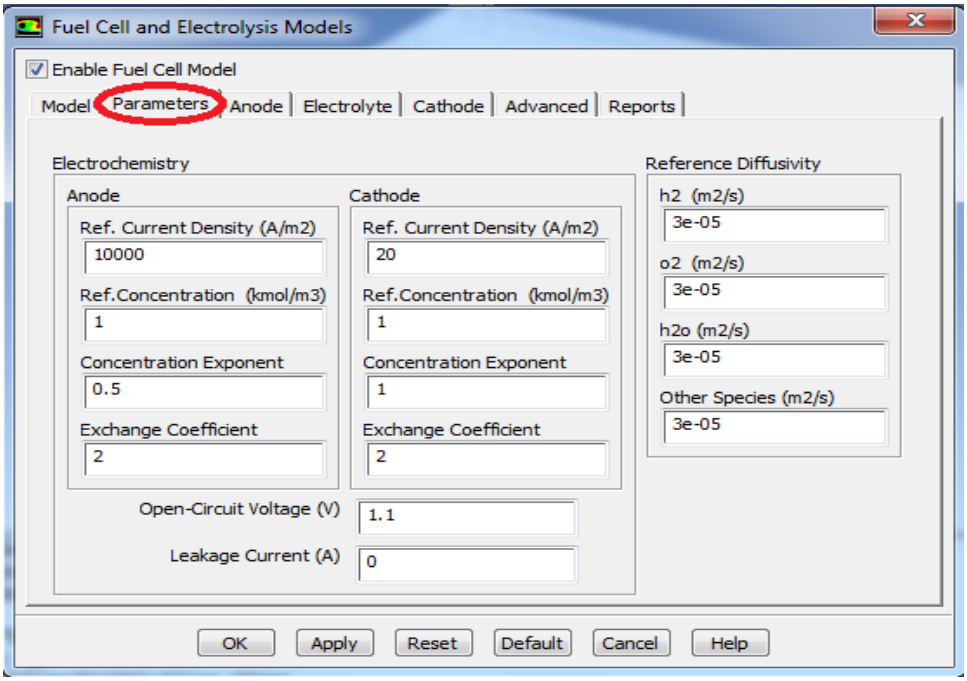

Fig. A-I. 2 setting of model parameters

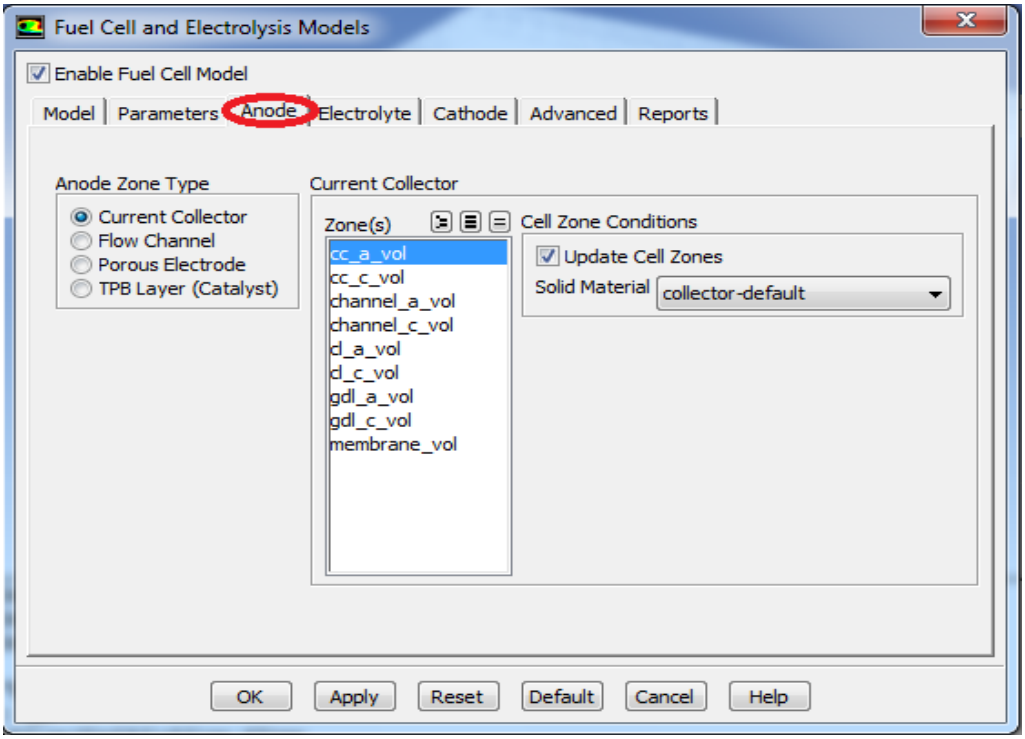

Fig. A-I. 3 Setting of anode electrode parameters

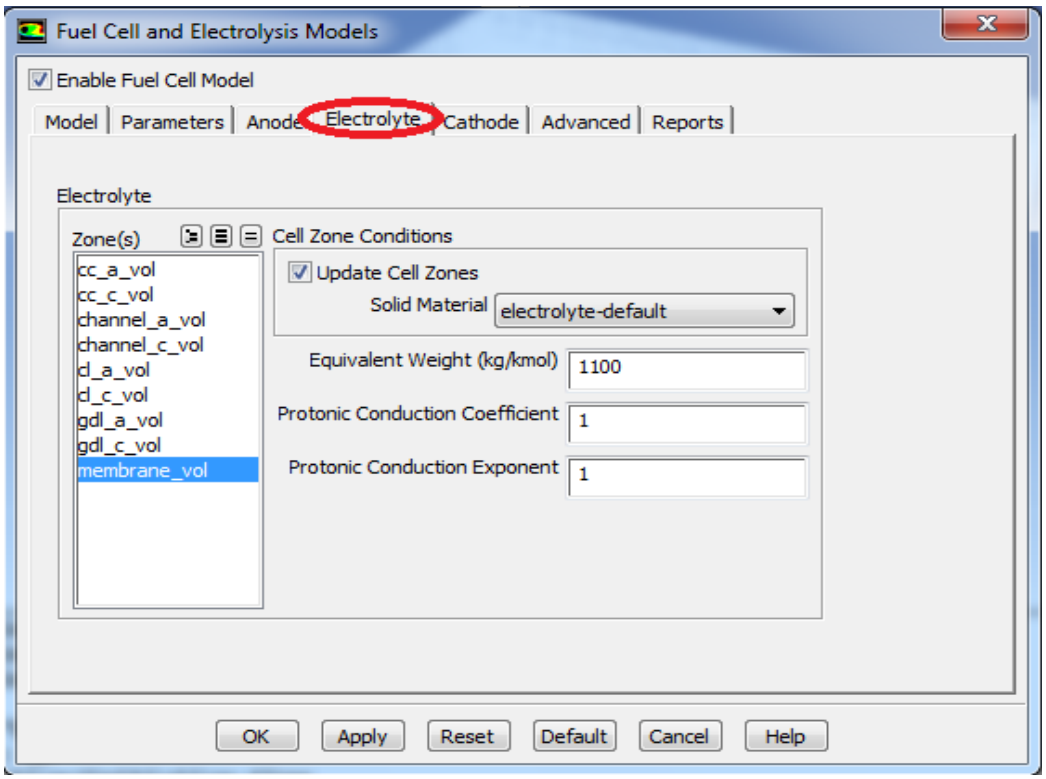

Fig. A-I. 4 Setting of membrane parameters

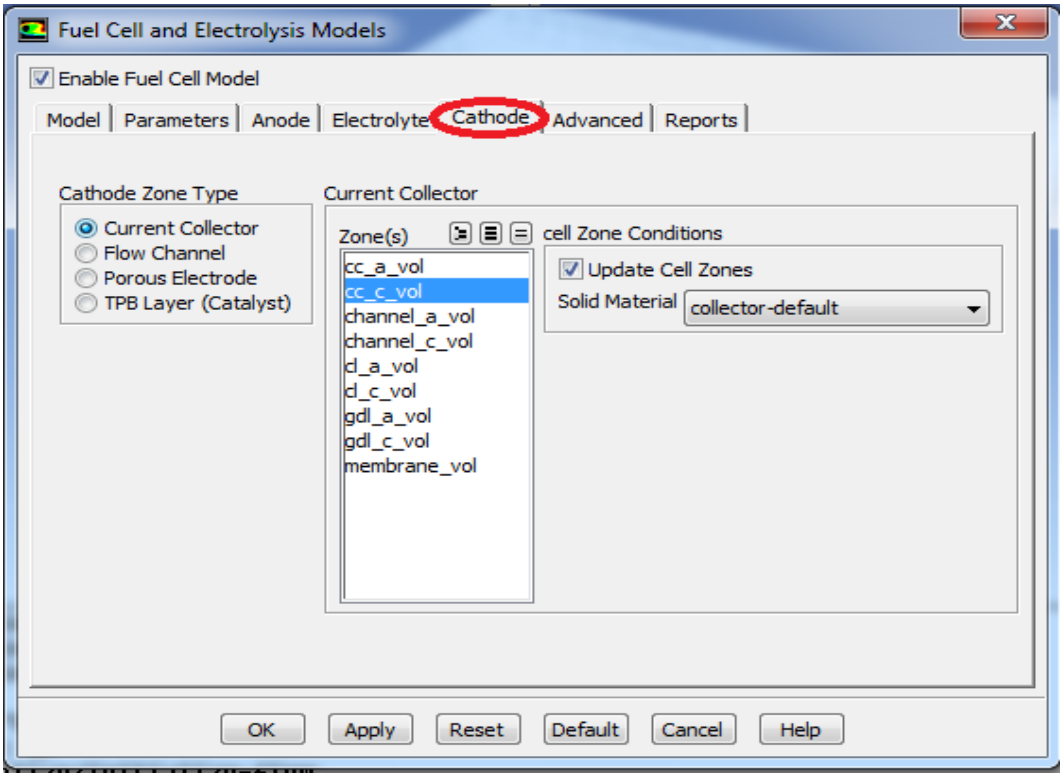

Fig. A-I. 5 Setting of cathode electrode parameters

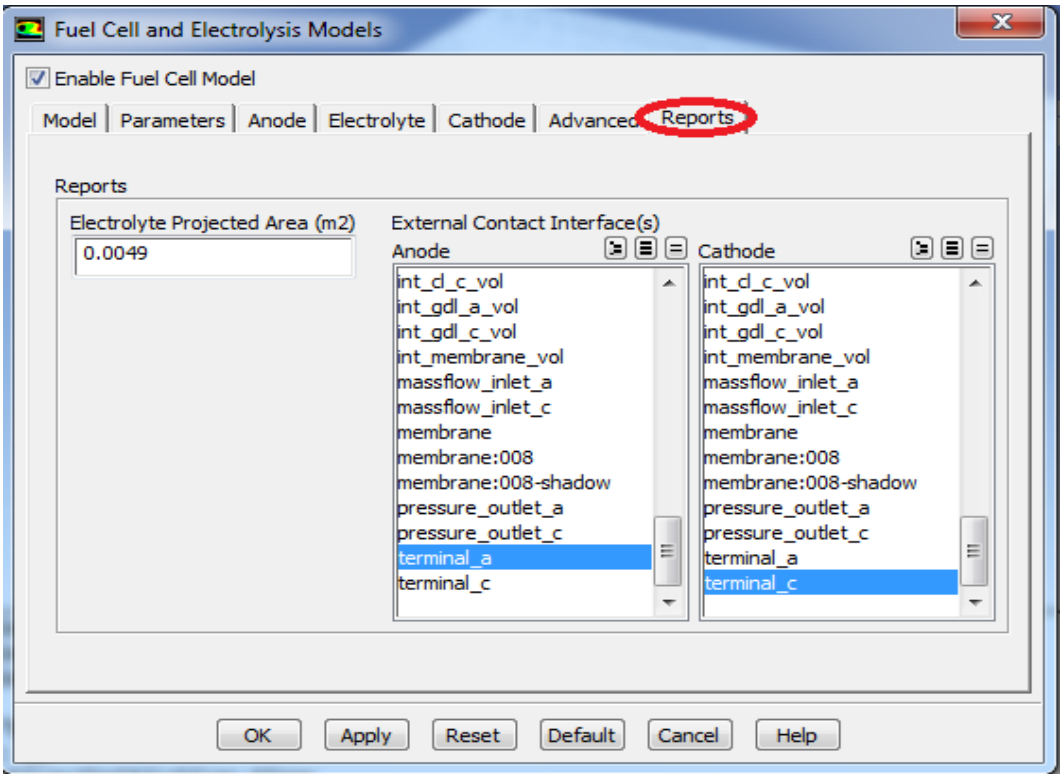

Fig. A-I. 6 Assigning of anode and cathode terminals

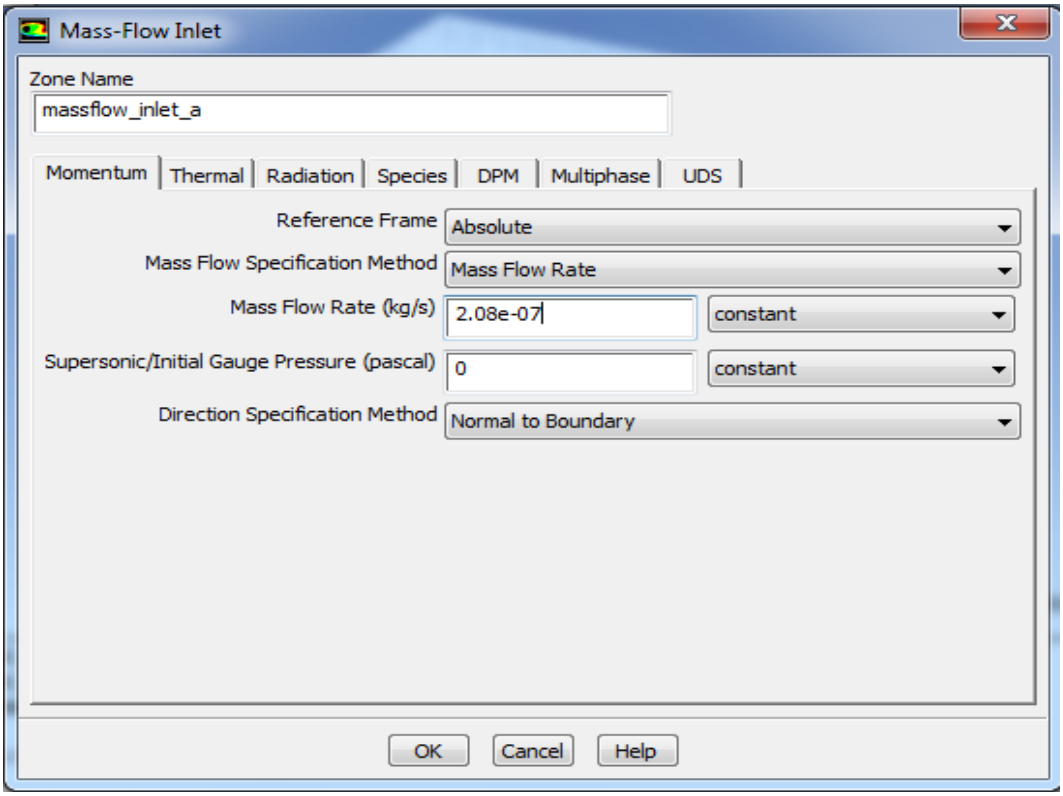

Fig. A-I. 7 Setting of anode mass flow inlet

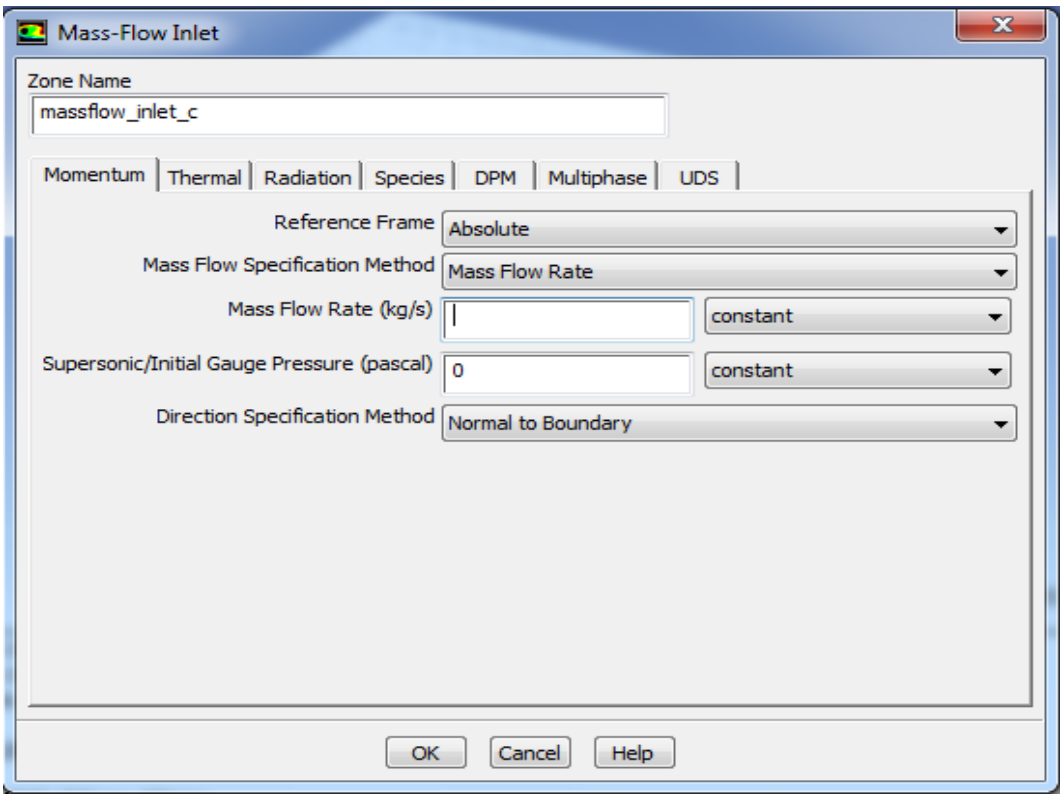

Fig. A-I. 8 Setting of cathode mass flow inlet

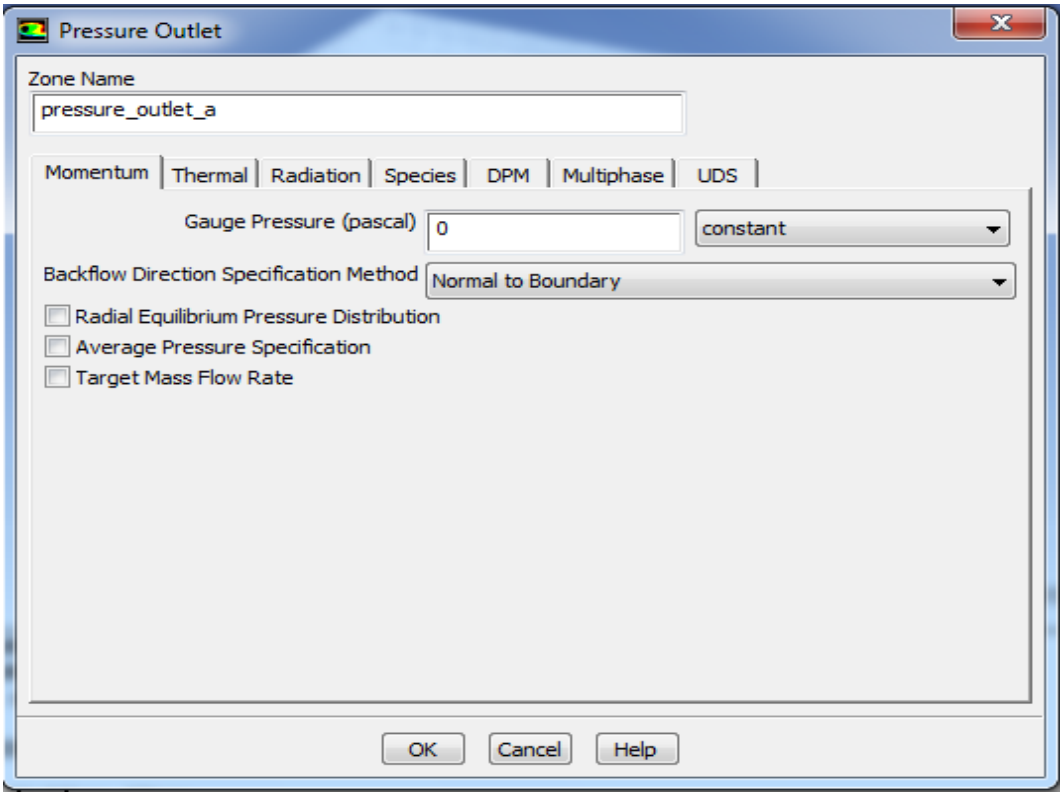

Fig. A-I. 9 Setting of anode outlet

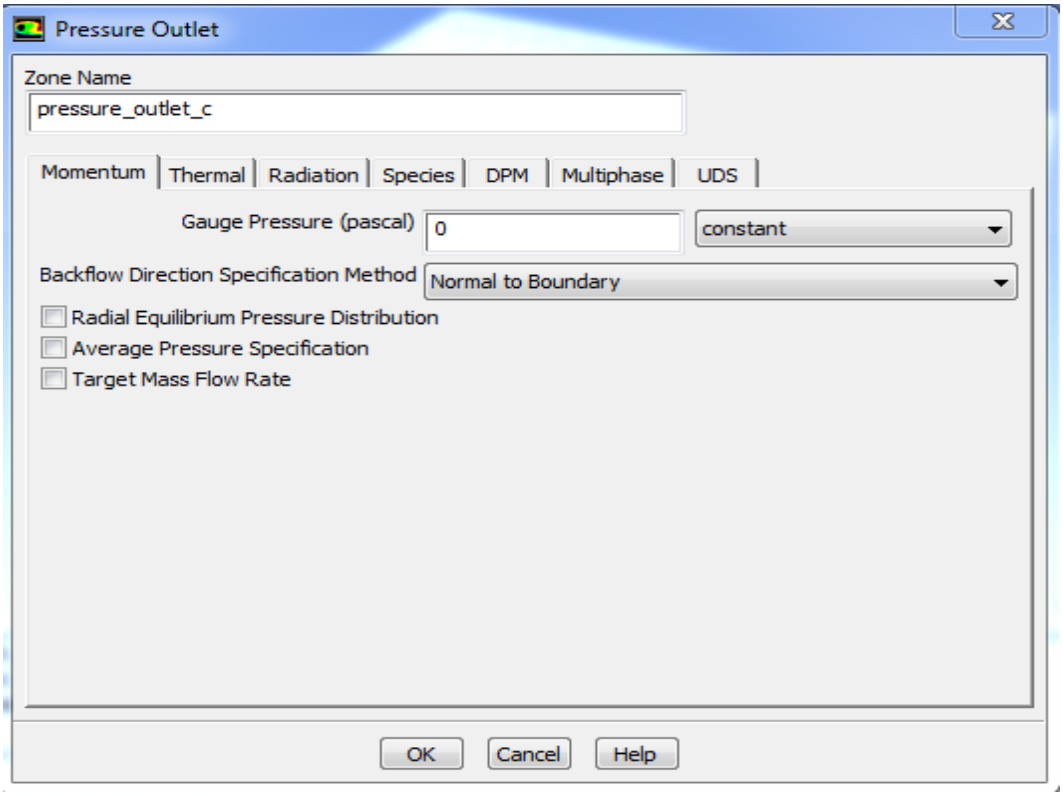

Fig. A-I. 10 Setting of cathode outlet

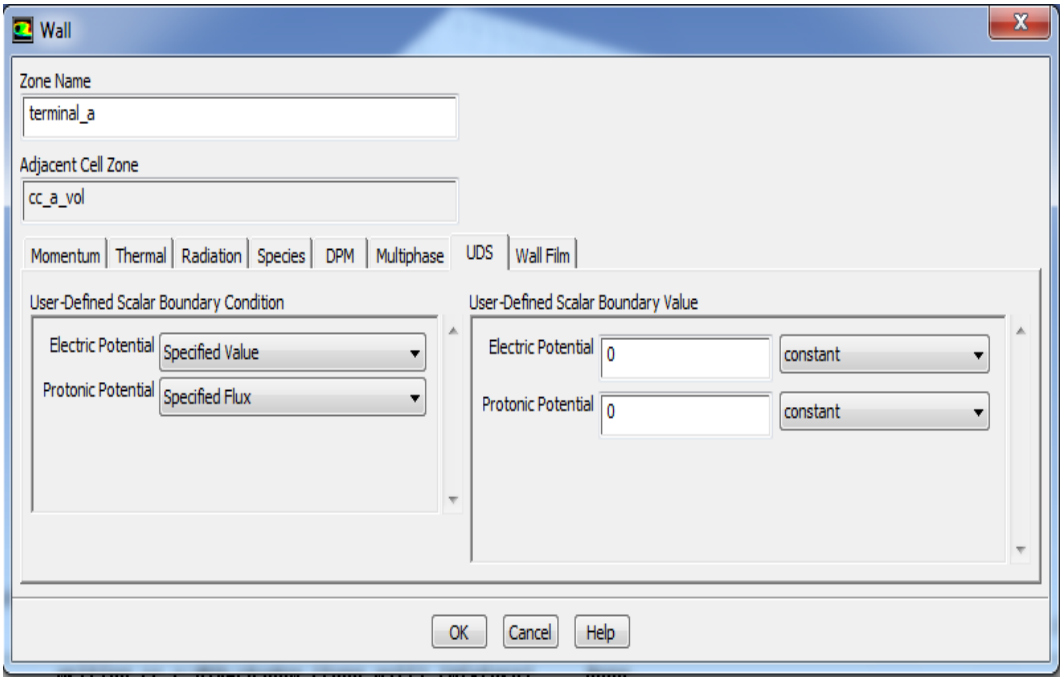

Fig. A-I. 11 Setting of anode terminal voltage

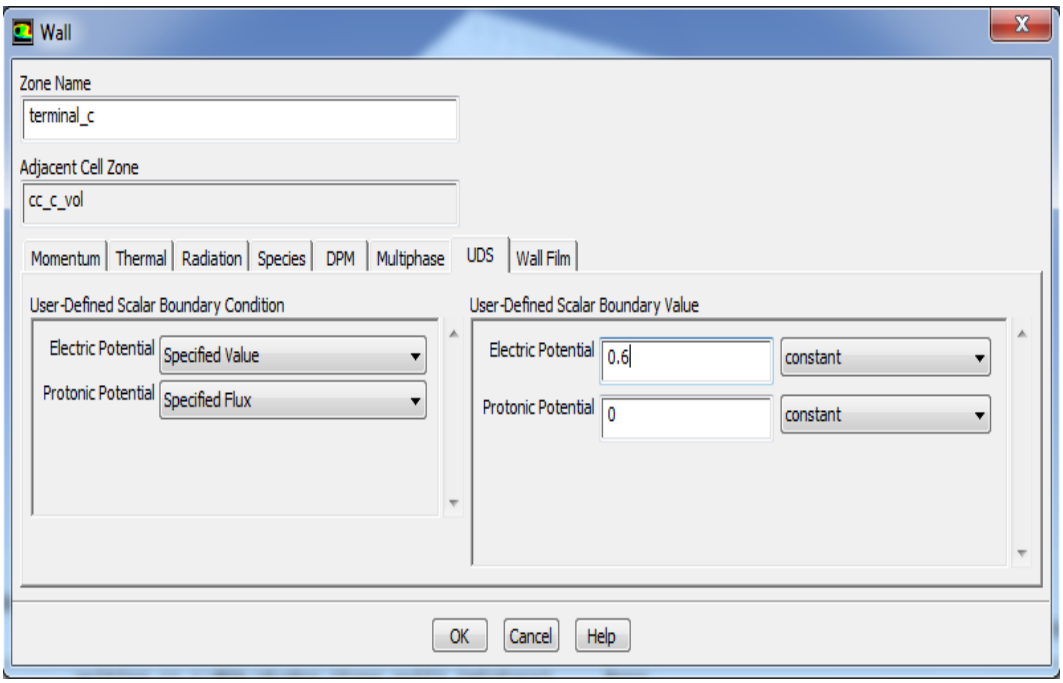

Fig. A-I.12 Setting of cathode terminal voltage

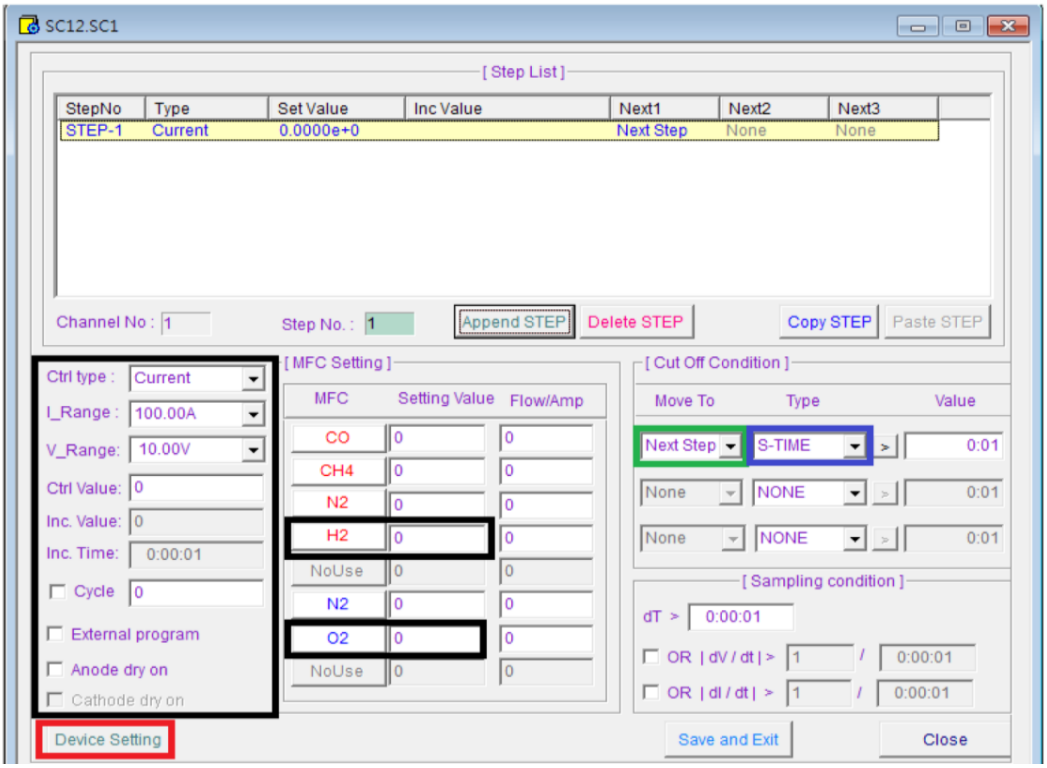

Fig. A-I. 13 Setting inlet mass flow rates in through software interface

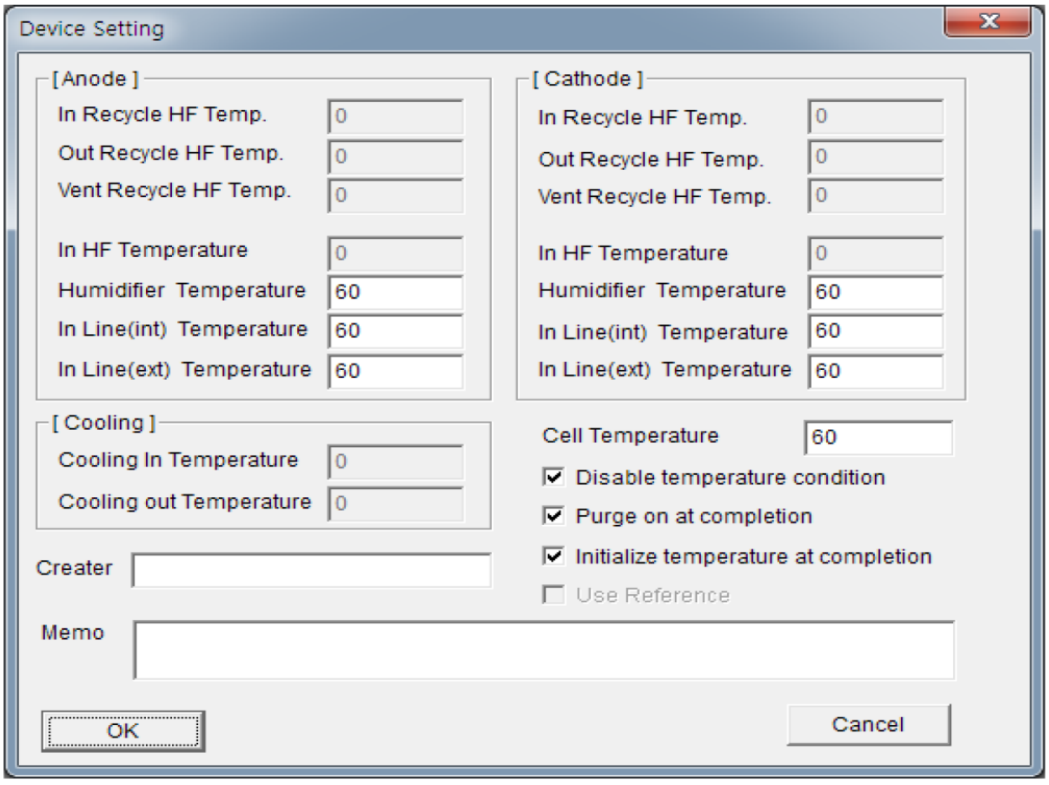

Fig. A-I. 14 Setting of cell and humidification temperatures through software interface

Appendix:II

Effect of land and channel widths of serpentine flow field on the performance of PEM Fuel Cell by using CFD analysis

Effect of operating temperature:

At 323 K

		0.5 mm Rib thickness		1 mm Rib thickness	
S.No	Voltage	Current Density (A/cm2)	Power Density (W/cm2)	Current Density (A/cm2)	Power Density (W/cm2)
1	0.4	0.723	0.2892	0.71	0.2848
2	0.5	0.69	0.345	0.67	0.335
3	0.6	0.54	0.324	0.51	0.306
4	0.7	0.307	0.2149	0.29	0.203
5	0.8	0.136	0.1088	0.12	0.096
6	0.9	0.06	0.054	0.06	0.054
7	0.98	0	0	0.00	0

1.5 mm Rib thickness		2 mm Rib thickness	
Current Density (A/cm2)	Power Density (W/cm2)	Current Density (A/cm2)	Power Density (W/cm2)
0.68	0.272	0.64	0.256
0.61	0.305	0.58	0.29
0.42	0.252	0.37	0.222
0.235	0.1645	0.215	0.1505
0.11	0.088	0.09	0.072
0.05	0.045	0.041	0.0369
0	0	0	0

333 K

		0.5 mm Rib thickness		1 mm Rib thickness	
S.No	Voltage	Current Density (A/cm2)	Power Density (W/cm2)	Current Density (A/cm2)	Power Density (W/cm2)
1	0.4	0.82	0.328	0.80	0.32
2	0.5	0.76	0.38	0.73	0.365
3	0.6	0.62	0.372	0.59	0.354
4	0.7	0.38	0.266	0.35	0.245
5	0.8	0.157	0.1256	0.15	0.12
6	0.9	0.06	0.054	0.06	0.054
7	0.98	0	0	0.00	0

1.5 mm Rib thickness		2 mm Rib thickness	
Current Density (A/cm2)	Power Density (W/cm2)	Current Density (A/cm2)	Power Density (W/cm2)
0.75	0.3	0.68	0.272
0.65	0.325	0.58	0.29
0.48	0.288	0.42	0.252
0.26	0.182	0.23	0.161
0.115	0.092	0.102	0.0816
0.05	0.045	0.04	0.036
0	0	0	0

343K

		0.5 mm Rib thickness		1 mm Rib thickness	
S.No	Voltage	Current Density (A/cm2)	Power Density (W/cm2)	Current Density (A/cm2)	Power Density (W/cm2)
1	0.4	0.94	0.376	0.92	0.368
2	0.5	0.88	0.44	0.86	0.43
3	0.6	0.72	0.432	0.69	0.414
4	0.7	0.45	0.315	0.42	0.294
5	0.8	0.18	0.144	0.16	0.128
6	0.9	0.07	0.063	0.07	0.063
7	0.98	0	0	0.00	0

1.5 mm Rib thickness		2 mm Rib thickness	
Current Density (A/cm2)	Power Density (W/cm2)	Current Density (A/cm2)	Power Density (W/cm2)
0.82	0.328	0.78	0.312
0.74	0.37	0.7	0.35
0.56	0.336	0.52	0.312
0.35	0.245	0.32	0.224
0.13	0.104	0.11	0.088
0.06	0.054	0.05	0.045
0	0	0	0

353 K

		0.5 mm Rib thickness		1 mm Rib thickness	
S.No	Voltage	Current Density (A/cm2)	Power Density (W/cm2)	Current Density (A/cm2)	Power Density (W/cm2)
1	0.40	0.84	0.34	0.82	0.33
2	0.50	0.78	0.39	0.75	0.38
3	0.60	0.65	0.39	0.63	0.38
4	0.70	0.41	0.29	0.38	0.27
5	0.80	0.16	0.13	0.15	0.12
6	0.90	0.07	0.06	0.07	0.06
7	0.98	0.00	0.00	0.00	0.00

1.5 mm Rib thickness		2 mm Rib thickness	
Current Density (A/cm2)	Power Density (W/cm2)	Current Density (A/cm2)	Power Density (W/cm2)
0.72	0.29	0.69	0.28
0.64	0.32	0.60	0.30
0.50	0.30	0.45	0.27
0.29	0.20	0.25	0.18
0.12	0.10	0.10	0.08
0.05	0.05	0.04	0.04
0.00	0.00	0.00	0.00

Land width at different operating temperatures

S.No.	Voltage	323 K		333 K		343 K		353 K	
		Current Density (A/cm2)	Power Density (W/cm2)	Current Density (A/cm2)	Power Density (W/cm2)	Current Density (A/cm2)	Power Density (W/cm2)	Current Density (A/cm2)	Power Density (W/cm2)
1	0.4	0.71	0.28	0.80	0.32	0.92	0.37	0.88	0.35
2	0.5	0.67	0.34	0.73	0.37	0.86	0.43	0.81	0.41
3	0.6	0.51	0.31	0.59	0.35	0.69	0.41	0.66	0.40
4	0.7	0.29	0.20	0.35	0.25	0.42	0.29	0.38	0.27
5	0.8	0.12	0.10	0.15	0.12	0.16	0.13	0.15	0.12
6	0.9	0.06	0.05	0.06	0.05	0.07	0.06	0.07	0.06
7	0.98	0.00	0.00	0.00	0.00	0.00	0.00	0.00	0.00

Effect of reactant flow rates:

300 ccm

		0.5 mm Rib thickness		1 mm Rib thickness		1.5 mm Rib thickness		2 mm Rib thickness	
S.No	Voltage	Current Density (A/cm2)	Power Density (W/cm2)	Current Density (A/cm2)	Power Density (W/cm2)	Current Density (A/cm2)	Power Density (W/cm2)	Current Density (A/cm2)	Power Density (W/cm2)
1	0.4	0.93	0.372	0.89	0.356	0.82	0.328	0.78	0.312
2	0.5	0.86	0.43	0.82	0.41	0.74	0.37	0.7	0.35
3	0.6	0.71	0.426	0.65	0.39	0.56	0.336	0.52	0.312
4	0.7	0.44	0.308	0.40	0.2765	0.35	0.245	0.32	0.224
5	0.8	0.172	0.1376	0.15	0.12	0.13	0.104	0.11	0.088
6	0.9	0.06	0.054	0.06	0.054	0.06	0.054	0.05	0.045
7	0.98	0	0	0.00	0	0	0	0	0

400 ccm

		0.5 mm Rib thickness		1 mm Rib thickness		1.5 mm Rib thickness		2 mm Rib thickness	
S.No	Voltage	Current Density (A/cm2)	Power Density (W/cm2)	Current Density (A/cm2)	Power Density (W/cm2)	Current Density (A/cm2)	Power Density (W/cm2)	Current Density (A/cm2)	Power Density (W/cm2)
1	0.4	0.99	0.396	0.92	0.368	0.86	0.344	0.82	0.328
2	0.5	0.92	0.46	0.85	0.425	0.79	0.395	0.74	0.37
3	0.6	0.77	0.462	0.68	0.408	0.63	0.378	0.56	0.336
4	0.7	0.51	0.357	0.47	0.329	0.41	0.287	0.35	0.245
5	0.8	0.21	0.168	0.18	0.144	0.15	0.12	0.13	0.104
6	0.9	0.075	0.0675	0.08	0.0675	0.06	0.054	0.06	0.054
7	0.98	0	0	0.00	0	0	0	0	0

500 ccm

		0.5 mm Rib thickness		1 mm Rib thickness		1.5 mm Rib thickness		2 mm Rib thickness	
S.No	Voltage	Current Density (A/cm2)	Power Density (W/cm2)	Current Density (A/cm2)	Power Density (W/cm2)	Current Density (A/cm2)	Power Density (W/cm2)	Current Density (A/cm2)	Power Density (W/cm2)
1	0.4	1.02	0.408	0.96	0.384	0.89	0.356	0.84	0.336
2	0.5	0.97	0.485	0.89	0.445	0.82	0.41	0.76	0.38
3	0.6	0.82	0.492	0.75	0.45	0.68	0.408	0.58	0.348
4	0.7	0.58	0.406	0.52	0.364	0.45	0.315	0.38	0.266
5	0.8	0.25	0.2	0.24	0.192	0.19	0.152	0.15	0.12
6	0.9	0.082	0.0738	0.08	0.072	0.07	0.063	0.07	0.063
7	0.98	0	0	0.00	0	0	0	0	0

600 ccm

S.No	Voltage	Current Density (A/cm2)	Power Density (W/cm2)	Current Density (A/cm2)	Power Density (W/cm2)	Current Density (A/cm2)	Power Density (W/cm2)	Current Density (A/cm2)	Power Density (W/cm2)
1	0.4	1.10	0.44	1.01	0.404	0.92	0.368	0.86	0.344
2	0.5	1.06	0.53	0.97	0.485	0.84	0.42	0.78	0.39
3	0.6	0.93	0.558	0.88	0.528	0.71	0.426	0.61	0.366
4	0.7	0.65	0.455	0.55	0.385	0.49	0.343	0.39	0.273
5	0.8	0.31	0.248	0.28	0.224	0.23	0.184	0.16	0.128
6	0.9	0.09	0.081	0.085	0.0765	0.08	0.072	0.07	0.063
7	0.98	0.00	0	0	0	0	0	0	0

Effect of channel width on the PEMFC performance:

1 bar operating pressure

S.No	Voltage	0.5 mm channel width		1 mm channel width		1.5 mm channel width		2 mm channel width	
		Current Density (A/cm2)	Power Density (W/cm2)	Current Density (A/cm2)	Power Density (W/cm2)	Current Density (A/cm2)	Power Density (W/cm2)	Current Density (A/cm2)	Power Density (W/cm2)
1	0.40	0.94	0.38	0.92	0.37	0.82	0.33	0.78	0.31
2	0.50	0.88	0.44	0.86	0.43	0.74	0.37	0.70	0.35
3	0.60	0.72	0.43	0.65	0.39	0.56	0.34	0.52	0.31
4	0.70	0.45	0.32	0.41	0.29	0.35	0.25	0.32	0.22
5	0.80	0.18	0.14	0.15	0.12	0.13	0.10	0.11	0.09
6	0.90	0.07	0.06	0.07	0.06	0.06	0.05	0.05	0.05
7	0.98	0.00	0.00	0.00	0.00	0.00	0.00	0.00	0.00

2 bar operating pressure

S.No	Voltage	0.5 mm channel width		1 mm channel width		1.5 mm channel width		2 mm channel width	
		Current Density (A/cm2)	Power Density (W/cm2)	Current Density (A/cm2)	Power Density (W/cm2)	Current Density (A/cm2)	Power Density (W/cm2)	Current Density (A/cm2)	Power Density (W/cm2)
1	0.40	0.98	0.39	0.96	0.38	0.85	0.34	0.82	0.33
2	0.50	0.92	0.46	0.90	0.45	0.77	0.39	0.74	0.37
3	0.60	0.74	0.44	0.71	0.43	0.58	0.35	0.52	0.31
4	0.70	0.49	0.34	0.45	0.32	0.38	0.27	0.32	0.22
5	0.80	0.20	0.16	0.18	0.14	0.15	0.12	0.13	0.10
6	0.90	0.07	0.06	0.07	0.06	0.06	0.05	0.06	0.05
7	0.98	0.00	0.00	0.00	0.00	0.00	0.00	0.00	0.00

3 bar operating pressure

S.No	Voltage	0.5 mm channel width		1 mm channel width		1.5 mm channel width		2 mm channel width	
		Current Density (A/cm2)	Power Density (W/cm2)	Current Density (A/cm2)	Power Density (W/cm2)	Current Density (A/cm2)	Power Density (W/cm2)	Current Density (A/cm2)	Power Density (W/cm2)
1	0.40	1.10	0.44	1.05	0.42	0.92	0.37	0.85	0.34
2	0.50	1.02	0.51	0.97	0.49	0.84	0.42	0.78	0.39
3	0.60	0.81	0.49	0.76	0.46	0.62	0.37	0.56	0.34
4	0.70	0.55	0.39	0.52	0.36	0.40	0.28	0.32	0.22
5	0.80	0.24	0.19	0.23	0.18	0.18	0.14	0.15	0.12
6	0.90	0.08	0.07	0.08	0.07	0.07	0.06	0.07	0.06
7	0.98	0.00	0.00	0.00	0.00	0.00	0.00	0.00	0.00

4 bar operating pressure

S.No	Voltage	0.5 mm channel width		1 mm channel width		1.5 mm channel width		2 mm channel width	
		Current Density (A/cm2)	Power Density (W/cm2)	Current Density (A/cm2)	Power Density (W/cm2)	Current Density (A/cm2)	Power Density (W/cm2)	Current Density (A/cm2)	Power Density (W/cm2)
1	0.40	1.12	0.45	1.08	0.43	0.96	0.38	0.92	0.37
2	0.50	1.04	0.52	0.99	0.50	0.88	0.44	0.82	0.41
3	0.60	0.85	0.51	0.80	0.48	0.65	0.39	0.61	0.37
4	0.70	0.62	0.43	0.56	0.39	0.42	0.29	0.35	0.25
5	0.80	0.32	0.26	0.28	0.22	0.21	0.17	0.18	0.14
6	0.90	0.09	0.08	0.09	0.08	0.08	0.07	0.08	0.07
7	0.98	0.00	0.00	0.00	0.00	0.00	0.00	0.00	0.00

channel width at different operating pressures

S.No.	Voltage	1 bar operating pressure		2 bar operating pressure		3 bar operating pressure		4 bar operating pressure	
		Current Density (A/cm2)	Power Density (W/cm2)	Current Density (A/cm2)	Power Density (W/cm2)	Current Density (A/cm2)	Power Density (W/cm2)	Current Density (A/cm2)	Power Density (W/cm2)
1	0.4	0.92	0.37	0.96	0.38	1.05	0.42	1.08	0.43
2	0.5	0.86	0.43	0.90	0.45	0.97	0.49	0.99	0.50
3	0.6	0.65	0.39	0.71	0.43	0.76	0.46	0.80	0.48
4	0.7	0.41	0.29	0.45	0.32	0.52	0.36	0.56	0.39
5	0.8	0.15	0.12	0.18	0.14	0.23	0.18	0.28	0.22
6	0.9	0.07	0.06	0.08	0.07	0.09	0.08	0.09	0.08
7	0.98	0.00	0.00	0.00	0.00	0.00	0.00	0.00	0.00

Experimentally analyse the performance of PEM Fuel Cell fitted with leaf, lung, bio-channel and single serpentine flow field plates

Effect of operating temperature:

Single serpentine flow channel

Tc	40°C					50°C			
S.No	Voltage	Current	Current Density	Power	Power Density	Current	Current Density	Power	Power Density
1	0.97	0.00	0.00	0.00	0.00	0.00	0.00	0.00	0.00
2	0.90	0.48	0.01	0.43	0.01	0.52	0.01	0.47	0.01
3	0.80	4.30	0.09	3.44	0.07	4.80	0.10	3.84	0.08
4	0.70	14.30	0.29	10.01	0.20	16.50	0.34	11.55	0.24
5	0.60	22.10	0.45	13.26	0.27	24.20	0.49	14.52	0.30
6	0.50	26.20	0.53	13.10	0.27	28.20	0.58	14.10	0.29
7	0.40	27.20	0.56	10.88	0.22	29.30	0.60	11.72	0.24

60°C				70°C				80°C			
Current	Current Density	Power	Power Density	Current	Current Density	Power	Power Density	Current	Current Density	Power	Power Density
0.00	0.00	0.00	0.00	0.00	0.00	0.00	0.00	0.00	0.00	0.00	0.00
0.60	0.01	0.54	0.01	0.65	0.01	0.59	0.01	0.50	0.01	0.45	0.01
5.20	0.11	4.16	0.08	5.50	0.11	4.40	0.09	5.10	0.10	4.08	0.08
18.50	0.38	12.95	0.26	22.30	0.46	15.61	0.32	17.20	0.35	12.04	0.25
29.50	0.60	17.70	0.36	33.20	0.68	19.92	0.41	26.50	0.54	15.90	0.32
34.20	0.70	17.10	0.35	37.60	0.77	18.80	0.38	30.50	0.62	15.25	0.31
36.20	0.74	14.48	0.30	38.50	0.79	15.40	0.31	32.20	0.66	12.88	0.26

Lung channel

Tc	40°C					50°C			
S.No	Voltage	Current	Current Density	Power	Power Density	Current	Current Density	Power	Power Density
1	0.97	0.00	0.00	0.00	0.00	0.00	0.00	0.00	0.00
2	0.90	0.60	0.01	0.54	0.01	0.67	0.01	0.60	0.01
3	0.80	4.20	0.09	3.36	0.07	4.50	0.09	3.60	0.07
4	0.70	12.20	0.25	8.54	0.17	15.00	0.31	10.50	0.21
5	0.60	24.10	0.49	14.46	0.30	28.40	0.58	17.04	0.35
6	0.50	28.20	0.58	14.10	0.29	32.50	0.66	16.25	0.33
7	0.40	29.10	0.59	11.64	0.24	33.00	0.67	13.20	0.27

60°C				70°C				80°C			
Current	Current Density	Power	Power Density	Current	Current Density	Power	Power Density	Current	Current Density	Power	Power Density
0.00	0.00	0.00	0.00	0.00	0.00	0.00	0.00	0.00	0.00	0.00	0.00
0.70	0.01	0.63	0.01	0.75	0.02	0.68	0.01	0.62	0.01	0.56	0.01
5.20	0.11	4.16	0.08	6.20	0.13	4.96	0.10	4.00	0.08	3.20	0.07
17.50	0.36	12.25	0.25	19.50	0.40	13.65	0.28	12.50	0.26	8.75	0.18
30.10	0.61	18.06	0.37	31.50	0.64	18.90	0.39	26.40	0.54	15.84	0.32
33.50	0.68	16.75	0.34	34.60	0.71	17.30	0.35	30.20	0.62	15.10	0.31
34.00	0.69	13.60	0.28	35.10	0.72	14.04	0.29	31.00	0.63	12.40	0.25

Bio channel

Tc	40°C					50°C			
S.No	Voltage	Current	Current Density	Power	Power Density	Current	Current Density	Power	Power Density
1	0.97	0.00	0.00	0.00	0.00	0.00	0.00	0.00	0.00
2	0.90	0.60	0.01	0.54	0.01	0.70	0.01	0.63	0.01
3	0.80	4.80	0.10	3.84	0.08	5.10	0.10	4.08	0.08
4	0.70	13.50	0.28	9.45	0.19	15.20	0.31	10.64	0.22
5	0.60	25.60	0.52	15.36	0.31	28.50	0.58	17.10	0.35
6	0.50	31.20	0.64	15.60	0.32	33.10	0.68	16.55	0.34
7	0.40	32.20	0.66	12.88	0.26	33.80	0.69	13.52	0.28

60°C				70°C				80°C			
Current	Current Density	Power	Power Density	Current	Current Density	Power	Power Density	Current	Current Density	Power	Power Density
0.00	0.00	0.00	0.00	0.00	0.00	0.00	0.00	0.00	0.00	0.00	0.00
0.72	0.01	0.65	0.01	0.75	0.02	0.68	0.01	0.65	0.01	0.59	0.01
6.40	0.13	5.12	0.10	7.20	0.15	5.76	0.12	5.20	0.11	4.16	0.08
18.20	0.37	12.74	0.26	22.30	0.46	15.61	0.32	16.20	0.33	11.34	0.23
31.30	0.64	18.78	0.38	33.50	0.68	20.10	0.41	30.20	0.62	18.12	0.37
35.20	0.72	17.60	0.36	36.70	0.75	18.35	0.37	33.90	0.69	16.95	0.35
35.80	0.73	14.32	0.29	37.10	0.76	14.84	0.30	34.60	0.71	13.84	0.28

Leaf channel

Tc	40°C					50°C			
S.No	Voltage	Current	Current Density	Power	Power Density	Current	Current Density	Power	Power Density
1	0.97	0.00	0.00	0.00	0.00	0.00	0.00	0.00	0.00
2	0.90	0.70	0.01	0.63	0.01	0.70	0.01	0.63	0.01
3	0.80	5.20	0.11	4.16	0.08	6.10	0.12	4.88	0.10
4	0.70	14.20	0.29	9.94	0.20	16.50	0.34	11.55	0.24
5	0.60	26.80	0.55	14.46	0.30	29.30	0.60	17.58	0.36
6	0.50	31.90	0.65	15.95	0.33	34.20	0.70	17.10	0.35
7	0.40	32.60	0.67	13.04	0.27	35.10	0.72	14.04	0.29

60°C				70°C				80°C			
Current	Current Density	Power	Power Density	Current	Current Density	Power	Power Density	Current	Current Density	Power	Power Density
0.00	0.00	0.00	0.00	0.00	0.00	0.00	0.00	0.00	0.00	0.00	0.00
0.72	0.01	0.65	0.01	0.75	0.02	0.68	0.01	0.65	0.01	0.59	0.01
7.90	0.16	6.32	0.13	8.50	0.17	6.80	0.14	6.30	0.13	5.04	0.10
20.60	0.42	14.42	0.29	23.50	0.48	16.45	0.34	18.30	0.37	12.81	0.26
32.60	0.67	19.56	0.40	35.60	0.73	21.36	0.44	30.80	0.63	18.48	0.38
37.20	0.76	18.60	0.38	39.10	0.80	19.55	0.40	35.20	0.72	17.60	0.36
37.90	0.77	15.16	0.31	40.10	0.82	16.04	0.33	36.10	0.74	14.44	0.29

Comparison of four channels at optimum operating temperature (70 ^{o}C)

	Single serpentine			**Lung channel**		**Bio-channel**		**Leaf channel**	
S.No	**Voltage**	**CD**	**PD**	**CD**	**PD**	**CD**	**PD**	**CD**	**PD**
1	0.97	0.00	0.00	0.00	0.00	0.00	0.00	0.00	0.00
2	0.9	0.01	0.01	0.02	0.01	0.02	0.01	0.02	0.01
3	0.8	0.11	0.09	0.13	0.10	0.15	0.12	0.17	0.14
4	0.7	0.32	0.22	0.40	0.28	0.46	0.32	0.48	0.34
5	0.6	0.51	0.31	0.64	0.39	0.68	0.41	0.73	0.44
6	0.5	0.58	0.29	0.71	0.35	0.75	0.37	0.80	0.40
7	0.4	0.60	0.24	0.72	0.29	0.76	0.30	0.82	0.33

Influence of the relative humidity of the reactants

Single serpentine channel

	25%					50%		
S.No	Voltage	Current	Current density (A/cm2)	Power	Power density (W/cm2)	Current	Current density (A/cm2)	Power
1	0.97	0.00	0.00	0.00	0.00	0.00	0.00	0.00
2	0.90	0.40	0.01	0.36	0.01	0.45	0.01	0.41
3	0.80	3.80	0.08	3.04	0.06	4.00	0.08	3.20
4	0.70	11.10	0.23	7.77	0.16	12.40	0.25	8.68
5	0.60	19.50	0.40	11.70	0.24	22.10	0.45	13.26
6	0.50	22.60	0.46	11.30	0.23	24.20	0.49	12.10
7	0.40	23.10	0.47	9.24	0.19	24.60	0.50	9.84

	75%				100%			
Power density (W/cm2)	Current	Current density (A/cm2)	Power	Power density (W/cm2)	Current	Current density (A/cm2)	Power	Power density (W/cm2)
0.00	0.00	0.00	0.00	0.00	0.00	0.00	0.00	0.00
0.01	0.52	0.01	0.47	0.01	0.60	0.01	0.54	0.01
0.07	4.70	0.10	3.76	0.08	5.50	0.11	4.40	0.09
0.18	14.20	0.29	9.94	0.20	15.60	0.32	10.92	0.22
0.27	23.60	0.48	14.16	0.29	25.20	0.51	15.12	0.31
0.25	26.30	0.54	13.15	0.27	28.20	0.58	14.10	0.29
0.20	26.90	0.55	10.76	0.22	29.40	0.60	11.76	0.24

Lung channel

	25%					50%			
S.No	Voltage	Current	Current density (A/cm2)	Power	Power density (W/cm2)	Current	Current density (A/cm2)	Power	Power density (W/cm2)
1	0.97	0.00	0.00	0.00	0.00	0.00	0.00	0.00	0.00
2	0.90	0.50	0.01	0.45	0.01	0.60	0.01	0.54	0.01
3	0.80	4.20	0.09	3.36	0.07	4.00	0.08	3.20	0.07
4	0.70	14.50	0.30	10.15	0.21	14.20	0.29	9.94	0.20
5	0.60	26.10	0.53	15.66	0.32	27.50	0.56	16.50	0.34
6	0.50	27.10	0.55	13.55	0.28	29.20	0.60	14.60	0.30
7	0.40	27.50	0.56	11.00	0.22	29.30	0.60	11.72	0.24

75%				100%			
Current	Current density (A/cm2)	Power	Power density (W/cm2)	Current	Current density (A/cm2)	Power	Power density (W/cm2)
0.00	0.00	0.00	0.00	0.00	0.00	0.00	0.00
0.40	0.01	0.36	0.01	0.75	0.02	0.68	0.01
4.70	0.10	3.76	0.08	6.20	0.13	4.96	0.10
16.30	0.33	11.41	0.23	19.50	0.40	13.65	0.28
30.00	0.61	18.00	0.37	31.50	0.64	18.90	0.39
32.20	0.66	16.10	0.33	34.60	0.71	17.30	0.35
32.20	0.66	12.88	0.26	35.10	0.72	14.04	0.29

Bio-channel

	25%					50%			
S.No	Voltage	Current	Current density (A/cm2)	Power	Power density (W/cm2)	Current	Current density (A/cm2)	Power	Power density (W/cm2)
1	0.97	0.00	0.00	0.00	0.00	0.00	0.00	0.00	0.00
2	0.90	0.55	0.01	0.50	0.01	0.60	0.01	0.54	0.01
3	0.80	5.20	0.11	4.16	0.08	5.80	0.12	4.64	0.09
4	0.70	15.60	0.32	10.92	0.22	16.20	0.33	11.34	0.23
5	0.60	26.80	0.55	16.08	0.33	28.80	0.59	17.28	0.35
6	0.50	29.20	0.60	14.60	0.30	31.20	0.64	15.60	0.32
7	0.40	29.60	0.60	11.84	0.24	31.90	0.65	12.76	0.26

75%				100%			
Current	Current density (A/cm2)	Power	Power density (W/cm2)	Current	Current density (A/cm2)	Power	Power density (W/cm2)
0.00	0.00	0.00	0.00	0.00	0.00	0.00	0.00
0.51	0.01	0.46	0.01	0.75	0.02	0.68	0.01
5.50	0.11	4.40	0.09	7.10	0.14	5.68	0.12
17.20	0.35	12.04	0.25	21.20	0.43	14.84	0.30
30.50	0.62	18.30	0.37	32.60	0.67	19.56	0.40
33.10	0.68	16.55	0.34	36.10	0.74	18.05	0.37
33.60	0.69	13.44	0.27	36.90	0.75	14.76	0.30

Leaf channel

	25%					50%			
S.No	Voltage	Current	Current density (A/cm2)	Power	Power density (W/cm2)	Current	Current density (A/cm2)	Power	Power density (W/cm2)
1	0.97	0.00	0.00	0.00	0.00	0.00	0.00	0.00	0.00
2	0.90	0.60	0.01	0.54	0.01	0.65	0.01	0.59	0.01
3	0.80	6.10	0.12	4.88	0.10	6.20	0.13	4.96	0.10
4	0.70	16.50	0.34	11.55	0.24	17.20	0.35	12.04	0.25
5	0.60	27.40	0.56	16.44	0.34	29.20	0.60	17.52	0.36
6	0.50	30.10	0.61	15.05	0.31	31.90	0.65	15.95	0.33
7	0.40	30.50	0.62	12.20	0.25	32.80	0.67	13.12	0.27

75%				100%			
Current	Current density (A/cm2)	Power	Power density (W/cm2)	Current	Current density (A/cm2)	Power	Power density (W/cm2)
0.00	0.00	0.00	0.00	0.00	0.00	0.00	0.00
0.65	0.01	0.59	0.01	0.75	0.02	0.68	0.01
6.20	0.13	4.96	0.10	8.50	0.17	6.80	0.14
19.50	0.40	13.65	0.28	23.50	0.48	16.45	0.34
31.60	0.64	18.96	0.39	35.60	0.73	21.36	0.44
35.20	0.72	17.60	0.36	39.10	0.80	19.55	0.40
36.50	0.74	14.60	0.30	40.10	0.82	16.04	0.33

Comparison of four flow channel designs at optimum RH (100%)

	Triple serpentine			Lung channel		Leaf channel		Bio channel	
S.No	Voltage	CD	PD	CD	PD	CD	PD	CD	PD
1	0.97	0.00	0.00	0.00	0.00	0.00	0.00	0.00	0.00
2	0.9	0.01	0.01	0.02	0.01	0.02	0.01	0.02	0.01
3	0.8	0.11	0.09	0.13	0.10	0.17	0.14	0.14	0.12
4	0.7	0.32	0.22	0.40	0.28	0.48	0.34	0.43	0.30
5	0.6	0.52	0.31	0.64	0.39	0.73	0.44	0.67	0.40
6	0.5	0.60	0.30	0.71	0.35	0.80	0.40	0.74	0.37
7	0.4	0.61	0.25	0.72	0.29	0.82	0.33	0.75	0.30

Influence of flow rates in terms of stoichiometric ratio (λ)

Single serpentine channel

	λa:λc=1:1				λa:λc=1:1.5				λa:λc=1:2			
Voltage	Current	Current Density	Power	Power Density	Current	Current Density	Power	Power Density	Current	Current Density	Power	Power Density
0.97	0.00	0.00	0.00	0.00	0.00	0.00	0.00	0.00	0.00	0.00	0.00	0.00
0.9	0.60	0.01	0.54	0.01	0.65	0.01	0.59	0.01	0.75	0.02	0.68	0.01
0.8	5.60	0.11	4.48	0.09	6.80	0.14	5.44	0.11	7.10	0.14	5.68	0.12
0.7	22.60	0.46	15.82	0.32	23.50	0.48	16.45	0.34	25.60	0.52	17.92	0.37
0.6	35.60	0.73	21.36	0.44	39.50	0.81	23.70	0.48	43.20	0.88	25.92	0.53
0.5	42.20	0.86	21.10	0.43	43.20	0.88	21.60	0.44	48.20	0.98	24.10	0.49
0.4	43.20	0.88	17.28	0.35	45.80	0.93	18.32	0.37	50.60	1.03	20.24	0.41

λa:λc=1:2.5				λa:λc=1:3			
Current	Current Density	Power	Power Density	Current	Current Density	Power	Power Density
0.00	0.00	0.00	0.00	0.00	0.00	0.00	0.00
0.82	0.02	0.74	0.02	0.95	0.02	0.86	0.02
7.60	0.16	6.08	0.12	9.70	0.20	7.76	0.16
29.60	0.60	20.72	0.42	32.60	0.67	22.82	0.47
47.20	0.96	28.32	0.58	49.50	1.01	29.70	0.61
53.20	1.09	26.60	0.54	57.20	1.17	28.60	0.58
53.20	1.09	21.28	0.43	59.60	1.22	23.84	0.49

λa:λc=1:3.5(350:612.5)				λa:λc=1:4(350:700)			
λa:λc=1:3.5				λa:λc=1:4			
Current	Current Density	Power	Power Density	Current	Current Density	Power	Power Density
0.00	0.00	0.00	0.00	0.00	0.00	0.00	0.00
0.80	0.02	0.72	0.01	0.60	0.01	0.54	0.01
7.80	0.16	6.24	0.13	5.50	0.11	4.40	0.09
28.30	0.58	19.81	0.40	15.60	0.32	10.92	0.22
46.30	0.94	27.78	0.57	25.20	0.51	15.12	0.31
43.20	0.88	21.60	0.44	28.20	0.58	14.10	0.29
55.60	1.13	22.24	0.45	29.40	0.60	11.76	0.24

Lung channel

	λa:λc=1:1				λa:λc=1:1.5				λa:λc=1:2			
Voltage	Current	Current Density	Power	Power Density	Current	Current Density	Power	Power Density	Current	Current Density	Power	Power Density
0.97	0.00	0.00	0.00	0.00	0.00	0.00	0.00	0.00	0.00	0.00	0.00	0.00
0.9	0.60	0.01	0.54	0.01	0.65	0.01	0.59	0.01	0.75	0.02	0.68	0.01
0.8	5.60	0.11	4.48	0.09	6.80	0.14	5.44	0.11	7.10	0.14	5.68	0.12
0.7	22.60	0.46	15.82	0.32	23.50	0.48	16.45	0.34	25.60	0.52	17.92	0.37
0.6	35.60	0.73	21.36	0.44	39.50	0.81	23.70	0.48	43.20	0.88	25.92	0.53
0.5	42.20	0.86	21.10	0.43	43.20	0.88	21.60	0.44	48.20	0.98	24.10	0.49
0.4	43.20	0.88	17.28	0.35	45.80	0.93	18.32	0.37	50.60	1.03	20.24	0.41

λa:λc=1:2.5				λa:λc=1:3			
Current	Current Density	Power	Power Density	Current	Current Density	Power	Power Density
0.00	0.00	0.00	0.00	0.00	0.00	0.00	0.00
0.82	0.02	0.74	0.02	0.95	0.02	0.86	0.02
7.60	0.16	6.08	0.12	9.70	0.20	7.76	0.16
29.60	0.60	20.72	0.42	32.60	0.67	22.82	0.47
47.20	0.96	28.32	0.58	49.50	1.01	29.70	0.61
53.20	1.09	26.60	0.54	57.20	1.17	28.60	0.58
53.20	1.09	21.28	0.43	59.60	1.22	23.84	0.49

λa:λc=1:3.5				λa:λc=1:4			
Current	Current Density	Power	Power Density	Current	Current Density	Power	Power Density
0.00	0.00	0.00	0.00	0.00	0.00	0.00	0.00
0.80	0.02	0.72	0.01	0.75	0.02	0.68	0.01
7.80	0.16	6.24	0.13	6.20	0.13	4.96	0.10
28.30	0.58	19.81	0.40	19.50	0.40	13.65	0.28
46.30	0.94	27.78	0.57	31.50	0.64	18.90	0.39
43.20	0.88	21.60	0.44	34.60	0.71	17.30	0.35
55.60	1.13	22.24	0.45	35.10	0.72	14.04	0.29

Bio-channel

	λa:λc=1:1				λa:λc=1:1.5				λa:λc=1:2			
Voltage	Current	Current Density	Power	Power Density	Current	Current Density	Power	Power Density	Current	Current Density	Power	Power Density
0.97	0.00	0.00	0.00	0.00	0.00	0.00	0.00	0.00	0.00	0.00	0.00	0.00
0.9	0.55	0.01	0.50	0.01	0.55	0.01	0.50	0.01	0.60	0.01	0.54	0.01
0.8	4.80	0.10	3.84	0.08	5.50	0.11	4.40	0.09	6.50	0.13	5.20	0.11
0.7	17.80	0.36	12.46	0.25	19.80	0.40	13.86	0.28	24.80	0.51	17.36	0.35
0.6	28.80	0.59	17.28	0.35	30.50	0.62	18.30	0.37	35.50	0.72	21.30	0.43
0.5	33.50	0.68	16.75	0.34	34.80	0.71	17.40	0.36	39.50	0.81	19.75	0.40
0.4	34.20	0.70	13.68	0.28	35.50	0.72	14.20	0.29	41.20	0.84	16.48	0.34

λa:λc=1:2.5				λa:λc=1:3			
Current	Current Density	Power	Power Density	Current	Current Density	Power	Power Density
0.00	0.00	0.00	0.00	0.00	0.00	0.00	0.00
0.75	0.02	0.68	0.01	0.85	0.02	0.77	0.02
6.80	0.14	5.44	0.11	7.80	0.16	6.24	0.13
26.80	0.55	18.76	0.38	30.20	0.62	21.14	0.43
38.50	0.79	23.10	0.47	45.60	0.93	27.36	0.56
43.50	0.89	21.75	0.44	49.20	1.00	24.60	0.50
44.60	0.91	17.84	0.36	50.20	1.02	20.08	0.41

λa:λc=1:3.5				λa:λc=1:4			
Current	Current Density	Power	Power Density	Current	Current Density	Power	Power Density
0.00	0.00	0.00	0.00	0.00	0.00	0.00	0.00
0.75	0.02	0.68	0.01	0.75	0.02	0.68	0.01
7.80	0.16	6.24	0.13	7.10	0.14	5.68	0.12
28.50	0.58	19.95	0.41	21.20	0.43	14.84	0.30
41.50	0.85	24.90	0.51	32.60	0.67	19.56	0.40
45.60	0.93	22.80	0.47	36.10	0.74	18.05	0.37
47.30	0.97	18.92	0.39	36.90	0.75	14.76	0.30

Leaf channel

	λa:λc=1:1				λa:λc=1:1.5				λa:λc=1:2			
Voltage	Current	Current Density	Power	Power Density	Current	Current Density	Power	Power Density	Current	Current Density	Power	Power Density
0.97	0.00	0.00	0.00	0.00	0.00	0.00	0.00	0.00	0.00	0.00	0.00	0.00
0.9	0.60	0.01	0.54	0.01	0.65	0.01	0.59	0.01	0.75	0.02	0.68	0.01
0.8	5.60	0.11	4.48	0.09	6.80	0.14	5.44	0.11	7.10	0.14	5.68	0.12
0.7	19.50	0.40	13.65	0.28	21.20	0.43	14.84	0.30	25.60	0.52	17.92	0.37
0.6	29.50	0.60	17.70	0.36	32.20	0.66	19.32	0.39	43.20	0.88	25.92	0.53
0.5	34.80	0.71	17.40	0.36	37.20	0.76	18.60	0.38	48.20	0.98	24.10	0.49
0.4	35.20	0.72	14.08	0.29	38.10	0.78	15.24	0.31	50.60	1.03	20.24	0.41

λa:λc=1:2.5				λa:λc=1:3			
Current	Current Density	Power	Power Density	Current	Current Density	Power	Power Density
0.00	0.00	0.00	0.00	0.00	0.00	0.00	0.00
0.82	0.02	0.74	0.02	0.90	0.02	0.81	0.02
7.60	0.16	6.08	0.12	8.90	0.18	7.12	0.15
29.60	0.60	20.72	0.42	35.50	0.72	24.85	0.51
47.20	0.96	28.32	0.58	50.20	1.02	30.12	0.61
51.50	1.05	25.75	0.53	54.20	1.11	27.10	0.55
53.20	1.09	21.28	0.43	55.40	1.13	22.16	0.45

λa:λc=1:3.5				λa:λc=1:4			
Current	Current Density	Power	Power Density	Current	Current Density	Power	Power Density
0.00	0.00	0.00	0.00	0.00	0.00	0.00	0.00
0.80	0.02	0.72	0.01	0.75	0.02	0.68	0.01
7.80	0.16	6.24	0.13	8.50	0.17	6.80	0.14
26.50	0.54	18.55	0.38	23.50	0.48	16.45	0.34
39.20	0.80	23.52	0.48	35.60	0.73	21.36	0.44
44.50	0.91	22.25	0.45	39.10	0.80	19.55	0.40
45.60	0.93	18.24	0.37	40.10	0.82	16.04	0.33

Comparison of all the channels at 1:3 stoichiometric ratios

	Single serpentine				Lung channel			
Voltage	Current	Current Density	Power	Power Density	Current	Current Density	Power	Power Density
0.97	0.00	0.00	0.00	0.00	0.00	0.00	0.00	0.00
0.9	0.60	0.01	0.54	0.01	0.80	0.02	0.72	0.01
0.8	7.20	0.15	5.76	0.12	8.20	0.17	6.56	0.13
0.7	24.20	0.49	16.94	0.35	25.50	0.52	17.85	0.36
0.6	32.10	0.66	19.26	0.39	36.50	0.74	21.90	0.45
0.5	35.10	0.72	17.55	0.36	40.20	0.82	20.10	0.41
0.4	35.70	0.73	14.28	0.29	40.60	0.83	16.24	0.33

Bio channel				Leaf channel			
λa:λc=1:2				λa:λc=1:2.5			
Current	Current Density	Power	Power Density	Current	Current Density	Power	Power Density
0.00	0.00	0.00	0.00	0.00	0.00	0.00	0.00
0.85	0.02	0.77	0.02	0.90	0.02	0.81	0.02
7.80	0.16	6.24	0.13	8.90	0.18	7.12	0.15
26.40	0.54	18.48	0.38	30.50	0.62	21.35	0.44
38.20	0.78	22.92	0.47	40.20	0.82	24.12	0.49
42.10	0.86	21.05	0.43	43.50	0.89	21.75	0.44
42.30	0.86	16.92	0.35	44.10	0.90	17.64	0.36

Influence of operating pressure

S.No	Voltage (V)	Single serpentine channel											
		1 bar				2 bar				3 bar			
		Current (A)	Current density (A/cm2)	Power (Watts)	Power density (A/cm2)	Current (A)	Current density (A/cm2)	Power (Watts)	Power density (A/cm2)	Current (A)	Current density (A/cm2)	Power (Watts)	Power density (A/cm2)
1	0.97	0.00	0.00	0.00	0.00	0.00	0.00	0.00	0.00	0.00	0.00	0.00	0.00
2	0.90	0.60	0.01	0.54	0.01	0.70	0.01	0.63	0.01	0.75	0.02	0.68	0.01
3	0.80	7.20	0.15	5.76	0.12	7.90	0.16	6.32	0.13	8.50	0.17	6.80	0.14
4	0.70	24.20	0.49	16.94	0.35	25.40	0.52	17.78	0.36	26.50	0.54	18.55	0.38
5	0.60	32.10	0.66	19.26	0.39	33.50	0.68	20.10	0.41	34.50	0.70	20.70	0.42
6	0.50	35.10	0.72	17.55	0.36	36.20	0.74	18.10	0.37	37.40	0.76	18.70	0.38
7	0.40	35.70	0.73	14.28	0.29	36.40	0.74	14.56	0.30	37.50	0.77	15.00	0.31

S.No	Voltage (V)	Lung channel											
		1 bar				2 bar				3 bar			
		Current (A)	Current density (A/cm2)	Power (Watts)	Power density (A/cm2)	Current (A)	Current density (A/cm2)	Power (Watts)	Power density (A/cm2)	Current (A)	Current density (A/cm2)	Power (Watts)	Power density (A/cm2)
1	0.97	0.00	0.00	0.00	0.00	0.00	0.00	0.00	0.00	0.00	0.00	0.00	0.00
2	0.90	0.80	0.02	0.72	0.01	0.80	0.02	0.72	0.01	0.82	0.02	0.74	0.02
3	0.80	8.20	0.17	6.56	0.13	8.70	0.18	6.96	0.14	9.50	0.19	7.60	0.16
4	0.70	25.50	0.52	17.85	0.36	27.10	0.55	18.97	0.39	28.50	0.58	19.95	0.41
5	0.60	36.50	0.74	21.90	0.45	38.10	0.78	22.86	0.47	39.40	0.80	23.64	0.48
6	0.50	40.20	0.82	20.10	0.41	41.20	0.84	20.60	0.42	42.50	0.87	21.25	0.43
7	0.40	40.60	0.83	16.24	0.33	42.30	0.86	16.92	0.35	43.10	0.88	17.24	0.35

S.No	Voltage (V)	Bio channel											
		1 bar				2 bar				3 bar			
		Current (A)	Current density (A/cm2)	Power (Watts)	Power density (A/cm2)	Current (A)	Current density (A/cm2)	Power (Watts)	Power density (A/cm2)	Current (A)	Current density (A/cm2)	Power (Watts)	Power density (A/cm2)
1	0.97	0.00	0.00	0.00	0.00	0.00	0.00	0.00	0.00	0.00	0.00	0.00	0.00
2	0.90	0.85	0.02	0.77	0.02	0.85	0.02	0.77	0.02	0.85	0.02	0.77	0.02
3	0.80	7.80	0.16	6.24	0.13	8.50	0.17	6.80	0.14	9.40	0.19	7.52	0.15
4	0.70	26.40	0.54	18.48	0.38	28.10	0.57	19.67	0.40	29.40	0.60	20.58	0.42
5	0.60	38.20	0.78	22.92	0.47	40.20	0.82	24.12	0.49	41.80	0.85	25.08	0.51
6	0.50	42.10	0.86	21.05	0.43	43.50	0.89	21.75	0.44	45.30	0.92	22.65	0.46
7	0.40	42.30	0.86	16.92	0.35	43.80	0.89	17.52	0.36	45.50	0.93	18.20	0.37

S.No	Voltage (V)	Leaf channel											
		1 bar				2 bar				3 bar			
		Current (A)	Current density (A/cm2)	Power (Watts)	Power density (A/cm2)	Current (A)	Current density (A/cm2)	Power (Watts)	Power density (A/cm2)	Current (A)	Current density (A/cm2)	Power (Watts)	Power density (A/cm2)
1	0.97	0.00	0.00	0.00	0.00	0.00	0.00	0.00	0.00	0.00	0.00	0.00	0.00
2	0.90	0.90	0.02	0.81	0.02	0.90	0.02	0.81	0.02	0.92	0.02	0.83	0.02
3	0.80	8.90	0.18	7.12	0.15	9.50	0.19	7.60	0.16	10.20	0.21	8.16	0.17
4	0.70	30.50	0.62	21.35	0.44	32.10	0.66	22.47	0.46	33.10	0.68	23.17	0.47
5	0.60	40.20	0.82	24.12	0.49	42.10	0.86	25.26	0.52	43.10	0.88	25.86	0.53
6	0.50	43.50	0.89	21.75	0.44	44.90	0.92	22.45	0.46	46.20	0.94	23.10	0.47
7	0.40	44.10	0.90	17.64	0.36	45.30	0.92	18.12	0.37	46.50	0.95	18.60	0.38

Comparison of four flow channel designs at 3 bar operating pressure

S.No	Voltage (V)	Single serpentine channel				Lung channel			
		3 bar				3 bar			
		Current (A)	Current density (A/cm2)	Power (Watts)	Power density (A/cm2)	Current (A)	Current density (A/cm2)	Power (Watts)	Power density (A/cm2)
1	0.97	0.00	0.00	0.00	0.00	0.00	0.00	0.00	0.00
2	0.90	0.75	0.02	0.68	0.01	0.82	0.02	0.74	0.02
3	0.80	8.50	0.17	6.80	0.14	9.50	0.19	7.60	0.16
4	0.70	26.50	0.54	18.55	0.38	27.40	0.56	19.18	0.39
5	0.60	34.50	0.70	20.70	0.42	38.20	0.78	22.92	0.47
6	0.50	37.40	0.76	18.70	0.38	42.50	0.87	21.25	0.43
7	0.40	37.50	0.77	15.00	0.31	43.10	0.88	17.24	0.35

Bio channel				Leaf channel			
3 bar				3 bar			
Current (A)	Current density (A/cm2)	Power (Watts)	Power density (A/cm2)	Current (A)	Current density (A/cm2)	Power (Watts)	Power density (A/cm2)
0.00	0.00	0.00	0.00	0.00	0.00	0.00	0.00
0.85	0.02	0.77	0.02	0.92	0.02	0.83	0.02
9.40	0.19	7.52	0.15	10.20	0.21	8.16	0.17
29.40	0.60	20.58	0.42	33.10	0.68	23.17	0.47
40.50	0.83	24.30	0.50	43.10	0.88	25.86	0.53
44.30	0.90	22.15	0.45	46.20	0.94	23.10	0.47
44.80	0.91	17.92	0.37	46.50	0.95	18.60	0.38

Influence of back pressure

Single serpentine channel

S.No	Voltage (V)	0 bar				1 bar			
		Current (A)	Current density (cm2)	Power (Watts)	Power density (W/cm2)	Current (A)	Current density (cm2)	Power (Watts)	Power density (W/cm2)
1	0.97	0.00	0.00	0.00	0.00	0.00	0.00	0.00	0.00
2	0.90	0.75	0.02	0.68	0.01	0.75	0.02	0.68	0.01
3	0.80	8.50	0.17	6.80	0.14	9.40	0.19	7.52	0.15
4	0.70	26.50	0.54	18.55	0.38	27.20	0.56	19.04	0.39
5	0.60	34.50	0.70	20.70	0.42	35.80	0.73	21.48	0.44
6	0.50	37.40	0.76	18.70	0.38	38.60	0.79	19.30	0.39
7	0.40	37.50	0.77	15.00	0.31	39.20	0.80	15.68	0.32

2 bar				3 bar			
Current (A)	Current density (cm2)	Power (Watts)	Power density (W/cm2)	Current (A)	Current density (cm2)	Power (Watts)	Power density (W/cm2)
0.00	0.00	0.00	0.00	0.00	0.00	0.00	0.00
0.75	0.02	0.68	0.01	0.80	0.02	0.72	0.01
10.50	0.21	8.40	0.17	11.40	0.23	9.12	0.19
28.60	0.58	20.02	0.41	29.50	0.60	20.65	0.42
36.80	0.75	22.08	0.45	38.20	0.78	22.92	0.47
39.50	0.81	19.75	0.40	40.80	0.83	20.40	0.42
40.50	0.83	16.20	0.33	41.50	0.85	16.60	0.34

Lung channel

S.No	Voltage (V)	0 atm				1 atm			
		Current (A)	Current density (cm2)	Power (Watts)	Power density (W/cm2)	Current (A)	Current density (cm2)	Power (Watts)	Power density (W/cm2)
1	0.97	0.00	0.00	0.00	0.00	0.00	0.00	0.00	0.00
2	0.90	0.82	0.02	0.74	0.02	0.85	0.02	0.77	0.02
3	0.80	9.50	0.19	7.60	0.16	10.20	0.21	8.16	0.17
4	0.70	27.40	0.56	19.18	0.39	28.60	0.58	20.02	0.41
5	0.60	38.20	0.78	22.92	0.47	40.10	0.82	24.06	0.49
6	0.50	42.50	0.87	21.25	0.43	43.50	0.89	21.75	0.44
7	0.40	43.10	0.88	17.24	0.35	44.10	0.90	17.64	0.36

2 bar				3 bar			
Current (A)	Current density (cm2)	Power (Watts)	Power density (W/cm2)	Current (A)	Current density (cm2)	Power (Watts)	Power density (W/cm2)
0.00	0.00	0.00	0.00	0.00	0.00	0.00	0.00
0.85	0.02	0.77	0.02	0.85	0.02	0.77	0.02
11.50	0.23	9.20	0.19	12.10	0.25	9.68	0.20
30.50	0.62	21.35	0.44	32.50	0.66	22.75	0.46
41.50	0.85	24.90	0.51	42.80	0.87	25.68	0.52
44.60	0.91	22.30	0.46	46.10	0.94	23.05	0.47
45.40	0.93	18.16	0.37	46.80	0.96	18.72	0.38

Bio-channel

S.No	Voltage (V)	0 atm				1 atm			
		Current (A)	Current density (cm2)	Power (Watts)	Power density (W/cm2)	Current (A)	Current density (cm2)	Power (Watts)	Power density (W/cm2)
1	0.97	0.00	0.00	0.00	0.00	0.00	0.00	0.00	0.00
2	0.90	0.85	0.02	0.77	0.02	0.85	0.02	0.77	0.02
3	0.80	9.40	0.19	7.52	0.15	10.50	0.21	8.40	0.17
4	0.70	29.40	0.60	20.58	0.42	31.80	0.65	22.26	0.45
5	0.60	40.50	0.83	24.30	0.50	42.30	0.86	25.38	0.52
6	0.50	44.30	0.90	22.15	0.45	46.20	0.94	23.10	0.47
7	0.40	44.80	0.91	17.92	0.37	46.80	0.96	18.72	0.38

2 bar				3 bar			
Current (A)	Current density (cm2)	Power (Watts)	Power density (W/cm2)	Current (A)	Current density (cm2)	Power (Watts)	Power density (W/cm2)
0.00	0.00	0.00	0.00	0.00	0.00	0.00	0.00
0.86	0.02	0.77	0.02	0.90	0.02	0.81	0.02
11.80	0.24	9.44	0.19	12.60	0.26	10.08	0.21
33.40	0.68	23.38	0.48	35.60	0.73	24.92	0.51
43.90	0.90	26.34	0.54	45.40	0.93	27.24	0.56
47.50	0.97	23.75	0.48	48.90	1.00	24.45	0.50
48.50	0.99	19.40	0.40	49.30	1.01	19.72	0.40

Leaf channel

S.No	Voltage (V)	0 bar				1 bar			
		Current (A)	Current density (cm2)	Power (Watts)	Power density (W/cm2)	Current (A)	Current density (cm2)	Power (Watts)	Power density (W/cm2)
1	0.97	0.00	0.00	0.00	0.00	0.00	0.00	0.00	0.00
2	0.90	0.92	0.02	0.83	0.02	0.92	0.02	0.83	0.02
3	0.80	10.20	0.21	8.16	0.17	11.60	0.24	9.28	0.19
4	0.70	33.10	0.68	23.17	0.47	35.40	0.72	24.78	0.51
5	0.60	43.10	0.88	25.86	0.53	45.60	0.93	27.36	0.56
6	0.50	46.20	0.94	23.10	0.47	47.80	0.98	23.90	0.49
7	0.40	46.50	0.95	18.60	0.38	48.20	0.98	19.28	0.39

2 bar				3 bar			
Current (A)	Current density (cm2)	Power (Watts)	Power density (W/cm2)	Current (A)	Current density (cm2)	Power (Watts)	Power density (W/cm2)
0.00	0.00	0.00	0.00	0.00	0.00	0.00	0.00
0.95	0.02	0.86	0.02	0.95	0.02	0.86	0.02
12.60	0.26	10.08	0.21	13.40	0.27	10.72	0.22
37.60	0.77	26.32	0.54	40.30	0.82	28.21	0.58
47.10	0.96	28.26	0.58	48.50	0.99	29.10	0.59
49.50	1.01	24.75	0.51	50.90	1.04	25.45	0.52
49.80	1.02	19.92	0.41	51.50	1.05	20.60	0.42

Comparison of four channels at 3 bar pressure									
	Single serpentine			Lung channel		Bio channel		Leaf channel	
S.No	Voltage	CD	PD	CD	PD	CD	PD	CD	PD
1	0.97	0.00	0.00	0.00	0.00	0.00	0.00	0.00	0.00
2	0.9	0.02	0.01	0.02	0.02	0.02	0.02	0.02	0.02
3	0.8	0.23	0.19	0.25	0.20	0.26	0.21	0.27	0.22
4	0.7	0.60	0.42	0.66	0.46	0.73	0.51	0.82	0.58
5	0.6	0.78	0.47	0.87	0.52	0.93	0.56	0.99	0.59
6	0.5	0.83	0.42	0.94	0.47	1.00	0.50	1.04	0.52
7	0.4	0.85	0.34	0.96	0.38	1.01	0.40	1.05	0.42

Influence of design modifications on a leaf channel on the performance of proton exchange membrane fuel cell

Non-Interdigitated flow channel					Interdigitated flow channel			
Voltage (V)	Current (A)	Current density (A/cm2)	Power (W)	Power density (W/cm2)	Current (A)	Current density (A/cm2)	Power (W)	Power density (W/cm2)
0.97	0.00	0.00	0.00	0.00	0.00	0.00	0.00	0.00
0.90	0.95	0.02	0.86	0.02	0.95	0.02	0.86	0.02
0.80	13.40	0.27	10.72	0.22	14.10	0.29	11.28	0.23
0.70	35.40	0.72	24.78	0.51	40.50	0.83	28.35	0.58
0.60	46.50	0.95	27.90	0.57	50.10	1.02	30.06	0.61
0.50	50.90	1.04	25.45	0.52	53.40	1.09	26.70	0.54
0.40	51.50	1.05	20.60	0.42	53.70	1.10	21.48	0.44

Interdigitated flow channel with curved edges				Murray's law			
Current (A)	Current density (A/cm2)	Power (W)	Power density (W/cm2)	Current (A)	Current density (A/cm2)	Power (W)	Power density (W/cm2)
0.00	0.00	0.00	0.00	0.00	0.00	0.00	0.00
1.05	0.02	0.95	0.02	1.05	0.02	0.95	0.02
15.50	0.32	12.40	0.25	17.20	0.35	13.76	0.28
45.20	0.92	31.64	0.65	47.60	0.97	33.32	0.68
53.70	1.10	32.22	0.66	55.80	1.14	33.48	0.68
56.80	1.16	28.40	0.58	59.40	1.21	29.70	0.61
58.30	1.19	23.32	0.48	60.50	1.23	24.20	0.49

Effect of bio-inspired metal flow field plates on the performance of PEM fuel cell

	Graphite bipolar plate		Titanium bipolar plate		Titanuim bipolar plate with graphite coating	
Voltage (V)	Current density (A/cm^2)	Power density (W/cm^2)	Current density (A/cm^2)	Power density (W/cm^2)	Current density (A/cm^2)	Power density (W/cm^2)
0.97	0.00	0.00	0.00	0.00	0.00	0.00
0.9	0.02	0.02	0.02	0.01	0.02	0.02
0.8	0.27	0.22	0.24	0.19	0.26	0.21
0.7	0.72	0.51	0.63	0.44	0.69	0.48
0.6	0.88	0.53	0.76	0.46	0.83	0.50
0.5	0.93	0.46	0.81	0.40	0.88	0.44
0.4	0.94	0.38	0.82	0.33	0.90	0.36

Appendix-III

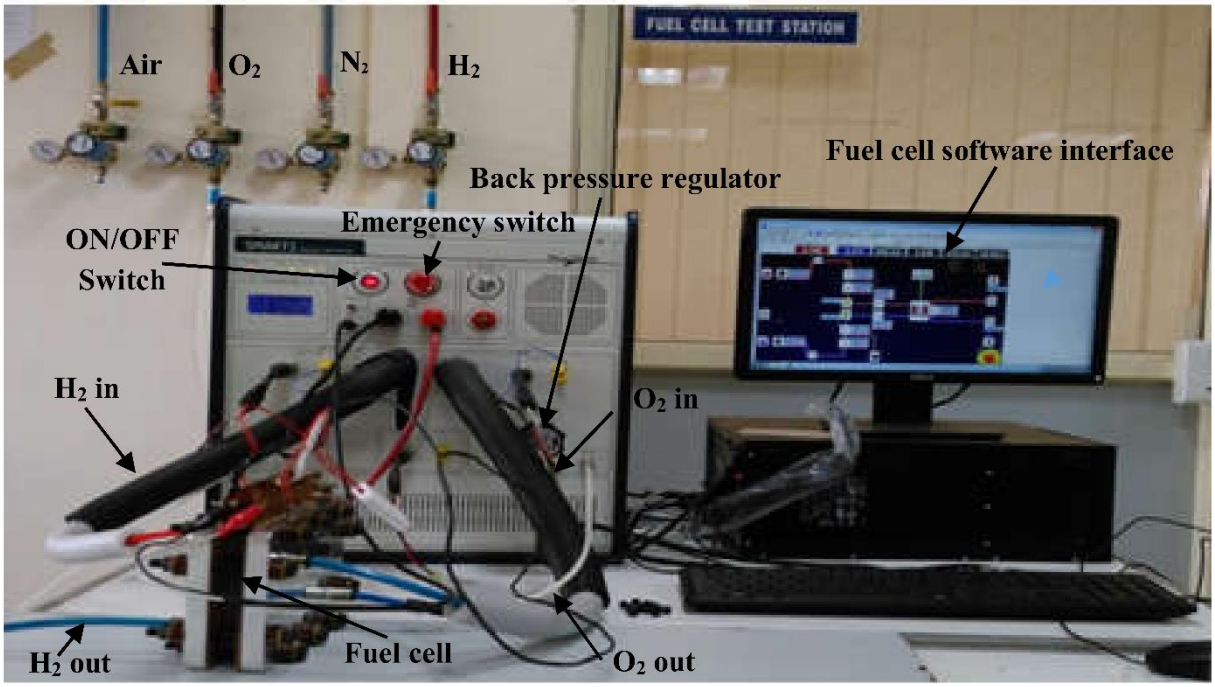

Publications on present research

Published

1. Srinivasa Reddy Badduri, G. Naga Srinivasulu, S Srinivasa Rao **"Influence of bio-inspired flow channel designs on the performance of a PEM fuel cell"** Chinese journal of chemical engineering, S1004-9541(19)30806-7, doi.org/10.1016/j.cjche.2019.07.010, (Elsevier) (SCI)
2. Srinivasa Reddy Badduri, G. Naga Srinivasulu, S Srinivasa Rao **"Experimental analysis of PEM fuel cell performance using lung channel design bipolar plate"** International journal of Green Energy, ISSN: 1543-5075 (Print) 1543-5083, doi.org/ 10.1080/15435075.2019.1677238, (Taylor & Francis) (SCI)
3. Srinivasa Reddy Badduri, G. Naga Srinivasulu, S Srinivasa Rao **"Computational fluid dynamic analysis on PEM fuel cell performance Using Bio channel"** Materials science forum,ISSN:1662-9752,Vol.969,pp524-529, (Scientific.net) (SCOPUS) doi.org/10.4028/www.scientific.net/MSF.969.524,
4. Srinivasa Reddy Badduri, G. Naga Srinivasulu, S Srinivasa Rao **"Influence of Lung channel design bipolar plate on performance of PEMFC using computational fluid dynamic analysis"** Materials Science forum, ISSN: 1662-9752, Vol. 969, pp 530-535, doi.org/10.4028 /www.scientific.net/MSF.969.530(Scientific.net) (SCOPUS)

Under review

1. Srinivasa Reddy Badduri, G. Naga Srinivasulu, S Srinivasa Rao**" Effect of design modifications of a leaf channel on performance of proton exchange membrane fuel cell"** Asia-Pacific journal of chemical engineering (Wiley) (SCI)
2. Srinivasa Reddy Badduri, G. Naga Srinivasulu, S Srinivasa Rao **"Effect of interdigitated leaf channel design bipolar plate on performance of proton exchange membrane fuel cell"** Journal of power and energy (SAGE) (SCI)
3. **S**rinivasa Reddy Badduri, G. Naga Srinivasulu, S Srinivasa Rao **"Effect of channel dimensions of a serpentine flow field on performance of proton exchange membrane fuel cell"** International journal of Ambient energy (Taylor & Francis) (ESCI)